SCUOLA NORMALE SUPERIORE

Tagging of potentiated synapses with a locally translated optogenetic reporter

Phd Thesis

Francesco Gobbo

Supervisor
Prof. Antonino Cattaneo

[This page intentionally left blank]

abstract

Increasing evidence points to the importance of dendritic spines in the formation and allocation of memories, and alterations of spine number and physiology are associated with memory and cognitive disorders. Modifications of the activity of subsets of synapses are believed to be crucial for memory establishment. Indeed, treatments or conditions that affect synaptic potentiation almost inevitably lead to an impairment in the acquisition of memories. Thus, the potentiation of synaptic transmission is a likely correlate of the acquisition of associative memories. This suggests that, in the brain, memories are formed and stored as a persistent modification of the strength of a subset of synapses within a neural circuit. To test this hypothesis, it would be necessary to re-excite such a subset of synapses and observe a behavioural response coherent with the encoded memory. A precondition for this experimental test is the ability to detect potentiated synapses during the encoding phase. However, the development of a method to directly test this hypothesis is currently lacking. Here I developed a hybrid RNA/protein approach to selectively express proteins at potentiated synapses (SynActive). To open the possibility for recalling synaptic activity, SynActive can be used to express a light-sensitive membrane channel of the Channelrhodopsin2

family (SA-Ch). After the characterization of SA-Ch using primary neuronal culture SA-Ch was expressed in the hippocampus of living mice. By controlling the timing of its expression with doxycycline, I was able to tag and identify potentiated synapses during the exposure of mice to a novel context. This allowed the identification of a candidate synaptic engram encoding the representation of the explored context. Furthermore, SA-Ch was used to map the relative distribution of potentiated synapses within and across neurons. In both the hippocampal CA1 and dentate gyrus regions, I demonstrate the presence of clusters of potentiated synapses, whose dimension (i.e. number of synapses) is increased by the behavioural task. I also highlight differences between CA1 and DG in terms of distribution of potentiated synapses between different neurons. The results provide strong experimental evidence in support of proposed models for memory acquisition and activity flow in the hippocampal circuit. The SynActive approach can then be used to map potentiated synapses in the brain and will make it possible to re-activate neurons only at previously activated synapses, testing if the activity of the identified synaptic trace is sufficient to recall the memory of the encoded representation. Furthermore, it will provide an experimental way to expand the current neuron-tagging technologies in the investigation of memory processes to the synaptic level.

" Memory is the steamstress, and a capricious one at that. […] Thus, the most ordinary movement in the world, such as sitting down at a table and pulling the inkstand towards one, may agitate a thousand odd, disconnected fragments, now bright, now dim, hanging and bobbing and dipping and flaunting, like the undelinen of a family of fourteen on a line in a gale of wind. "

– Virginia Woolf

Table of Contents

Introduction

Memory

Memory is the ability to store mental representations of past events, and enables to respond accordingly when a new situation is faced. Memories shape our interpretation of reality, and have a unifying role in the representation of our mental life (Kandel et al., 2014). There are two main forms of memory: implicit memory regulates our perceptual and motor skills ("memory of ways"), and declarative memory is involved in the representation of facts and events, people and objects ("memory of things"). The latter has such a prominent and pervasive role in our life, making sense of the fragments of reality that reach our sensation, that the loss of memory in aging and pathology shatters the life of patients.

Memory is often perceived as a collection of pieces of information and stories, which are stored in the mind, in Plato's metaphor, as if it were a block of wax, and memories were imprinted on it (Plato). Aristotle then argues that memory is a state of imagination relating as a copy to its original and that memory rests in sense-perception rather than imagination (Aristoteles). These ideas would then have a profound effect on the philosophers of memory, and to scientists embarking in the search of the mechanisms of memory.

The engram

The concept of "engram" was first introduced by early 20th century scientist Richard Wolfgang Semon to describe "... the enduring though primarily latent modification in the irritable substance produced by a stimulus..." (Semon, 1921). An intrinsically linked concept to engram in Semon's theory of mind is ecphory, which he defines as "... the influences which awaken the mnemic trace or engram out of its latent state into one of manifested activity...".

The law of Engraphy

Semon postulated that all simultaneously concurring excitations form a connected complex in the organism (Semon does not explicitly name the brain as the physical substrate for memories) leaving behind a connected trace. Such trace is what Semon calls the engram (Semon, 1921). An important tract of Semon's engram theory is its unitary nature in the formation of the excitation-complex. According to his postulate, sensations would be represented by the emergence of a unitary representation in the "active substance", which would then be maintained as if this representation is inscribed onto the substance in the form of a dormant trace (Schacter et al., 1978).

The law of Ecphory

Intrinsic in the engram definition is the ability of the memory trace to be retrieved, being reactivated from a state where the engram is present, although latent (Semon, 1921). Only part of the engram needs to be present to recall it in its entirety (Schacter et al., 1978): "resemblance, that is to say, partial coincidence between the components of an actual group of excitations and those of any previous engram-complex, causes ecphory of the latter through the former". The cuing of a stimulus, and the resulting ecphory, "does not strengthen an already existing engram, but generates a new engram, and the mnemic excitations resulting from any subsequent ecphory are in homophony" (Semon, 1921). That is, anytime an engram is reactivated, it is subject to changes and it is engraphycally stored in a modified version. The old (original) and the new engrams become associated by contiguity, in an interplay described as homophony.

One last notion that Semon introduced is the competition between engrams for ecphory. When two engram-complexes are related equally to a particular ecphoric cue, Semon argued that, in most situations, serially processing the two complexes would happen (Semon, 1923).

Where are memories stored?

"To follow [the engram] into the molecular field seems to me […] a hopeless undertaking at the present stage of our knowledge; and for my part I renounce the task"

Semon (1923)

The search for the physical location of engrams in the brain was pioneered by Karl Lashley, who systematically lesioned portions of cerebral cortex in the attempt to drive a correlation with the deterioration of the performance of the animal in solving a memory maze task (Lashley, 1950). Although establishing a cornerstone criterion to assess the involvement of a brain area in the memory, he found that no lesion could impair the memory task, and only large-scale lesions did (Josselyn et al., 2017).

The hippocampus

In search of epileptic foci in his patients, Wilder Penfield found that stimulation of the lateral temporal lobe elicited the recall of past memories in a fraction of subjects (Tonegawa et al., 2015). Brenda Milner, analysing amnesia in Penfield's patients with resected epileptic lobes, including famous patient HM, found that the hippocampal region, including the hippocampus proper and adjacent temporal

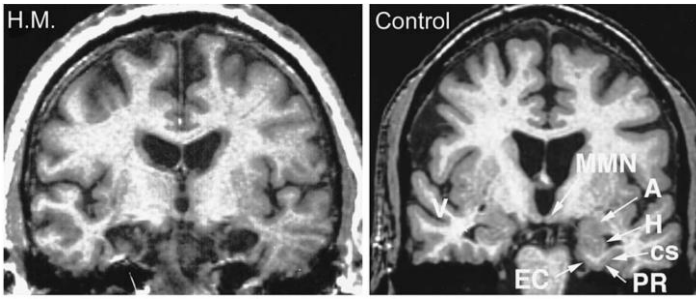

Figure 1 Coronal magnetic resonance of patient HM compared to a control who did not undergo surgery. Note the bilateral resection of the hippocampal formation (H) and damage of the enthorhynal (EC) and perirhynal cortex (PR). Reproduced from Andersen et al. (2007).

lobe structures (Figure 1), was critical for the formation of long-term memories (Scoville and Milner, 1957). Patients with surgically removed hippocampal regions could form short-term memories; however, they were not able to keep them in mind for more than a few minutes. At the same time, they lost memories formed up to 11 years before the hippocampal damage (Andersen et al., 2007). Decades of experiments have then confirmed and demonstrated the involvement of the hippocampus in the formation of new memories and, in particular, of episodic memories (Neves et al., 2008). As in the case of patient HM, lesions to the hippocampus produce severe anterograde amnesia (i.e. the impairment in forming new memories) and time-dependent retrograde amnesia (i.e. the inability to recall past

experiences) (Anagnostaras et al., 2001; Langston et al., 2010). Consistently, rodents with experimentally damaged hippocampal displayed sever deficits in learning tasks involving more complex mazes than a Y-turn (Andersen et al., 2007). Olga Vinogradova, among the first scientists performing single unit registrations in the hippocampus, later demonstrated that hippocampal neurons responded to the presentation of a novel environment. Later work also showed that the hippocampus was involved in the spatial representation of the animal location (Andersen et al., 2007).

Hippocampus anatomy

The hippocampus is a conserved structure in vertebrates characterized by a peculiar ultrastructure, with neurons prevalently disposed in single layers, and a prominent laminated segregation of inputs (Figure 2) (Andersen et al., 2007). Anatomically, the hippocampus is composed by the dentate gyrus (DG) and the cornu ammonis, which comprises areas CA1, CA2, CA3 and CA4. The main input comes from the entorhinal cortex (EC), in the parahippocampal gyrus (Figure 2), via the perforant path that synapses the dendrites of granule cells in the molecular layer (sm in figure 2b). The EC also forms synapses with apical

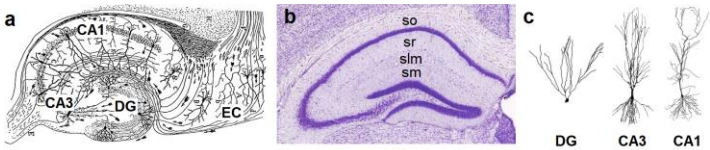

Figure 2 a 1911 drawing by Ramon y Cajal showing a rabbit hippocampus stained with the Golgi impregnation method. **b** Nissl staining of mouse hippocampus. so: stratum oriens, sr: stratum radiatum, slm: stratum lacunosum moleculare, sm: stratum moluculare. Modified from Paxinos and Franklin (2001) **c** Typical DG, CA3 and CA1 neurons showing the differences in the dendritic arbours shape.

CA1 dendrites in the stratum lacunosum moleculare (slm), distally to the soma layer. DG then forms excitatory synapses with CA3 pyramidal neurons, which then project to CA1 pyramidal neurons, particularly in the stratum radiatum (sr) containing the proximal portion of apical dendrites (Andersen et al., 2007). Pyramidal neurons in CA3 and CA1 form a single cellular layer and display both apical (in the sr and slm) and basal dendrites (in the stratum oriens, so) (Figure 2c). CA1 basal dendrites receive prevalently CA3 inputs, including a significant proportion of CA3 axons from the hippocampus in the other hemisphere (Shipton et al., 2014), as well as less characterized inputs from the other hemisphere CA1.

Other areas

The hippocampus is not the sole area involved in the formation and storage of memories. The amygdala plays a fundamental role in the encoding of the emotional valence of a memory, and some associations like the tone-shock conditioning involve inputs from the auditory cortex in a hippocampus-independent manner. Cortical areas like the prefrontal cortex are also recruited in contextual memories (Tse et al., 2007; Ben-Yakov et al., 2015), which have the tendency to become progressively independent of hippocampus (Genzel et al., 2017; Nadel and Moscovitch, 1997; Squire, 1986). However, the hippocampus remains indispensible for the formation of contextual memories, and lesions to such area cause severe and permanent retrograde amnesia (Nadel and Moscovitch, 1997).

Cell assemblies

Imagining a physical counterpart of engrams, Donald Hebb postulated groups of reciprocally interconnected cells that are simultaneously active during an event. Their interconnection produces a recurrent activity which in turn, if sustained for a long enough time, can induce metabolic changes that strengthen the interconnections between

assembly cells (neurons that fire together wire together), allowing the event to be represented in long-term memory. Because of their mutual connections, the assembly can be activated by the activity of any subset of cells (Josselyn et al., 2017).

Activity mapping

A first step towards the engram is the identification of neurons that are active during the encoding phase of a memory. Immediate Early Genes (IEGs) are a class of genes whose expression is induced as a result of neuron activation, and comprises genes like *Arc* (also known as activity regulated gene 3.1, *arg3.1*), *c-fos*, *zif268*, *Homer1a* and *cox-2* (Guzowski et al., 2001; Kubik et al., 2007). Making use of this property, Guzowski et al. (1999) pioneered the use of IEGs to map neurons activated by a specific experience. Active neurons can be therefore identified looking at either IEG transcription or translation by *in situ* hybridization or immunodetection of the resulting protein. For example, by detecting Arc transcript in the nucleus (2-15 minutes from stimulation) or in the cytoplasm (15-30 minutes) (Figure 3), Guzowski et al. (1999) were able to identify neurons activated by the exploration of a novel context. In addition, they could compare the sets of active neurons in two

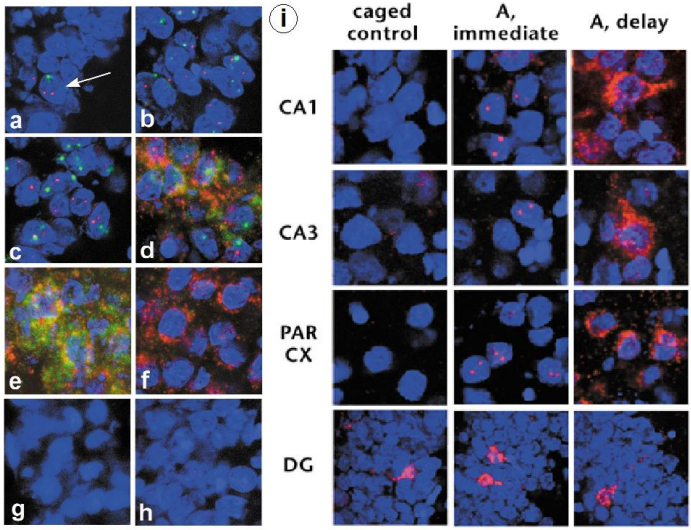

Figure 3 (**a-h**) *Arc* (green) and *zif268* (red) expression induced by electroconvulsive shock in CA1 neurons. **a** caged control **b** 2 min **c** 5 min **d** 15 min **e** 30 min and **f** 60 min after stimulation. **g** RNAse A treatment control and **h** sense riboprobe control. **i** *Arc* expression in hippocampal regions DG, CA3 and CA1, and in the parietal cortex in home caged animals (left column) and after exploration of a novel environment (central and right comuns). Modified from Guzowski et al. (1999).

different contexts separated by 20 minutes by looking at the subcellular localization of Arc signal (i.e., nuclear or cytoplasmic).

Transcription of reporters from IEG promoters – and their translation – has been since used to mark and recognize active neurons, FosGFP mice being one of the first examples (Barth et al., 2004). A major advance came through when

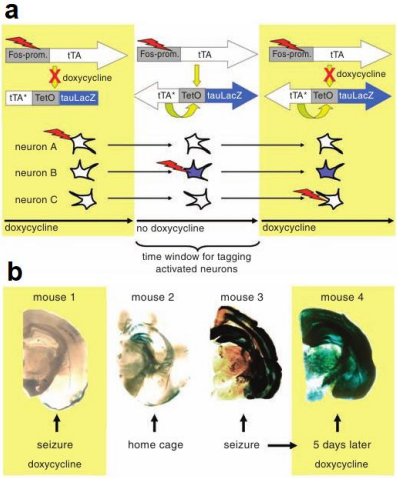

Figure 4 a scheme of TetTAG system. Transactivator tTA under the *c-fos* promoter is expressed by neuron activation. If doxycyline is removed, tTA binds bidirectional TetO promoter, which expresses lacZ and doxycycline-insensitive tTA*, allowing for the autonomous *lacZ* expression. **b** examples of home caged and seizure animals. Modified from Reijmers et al. (2007).

Reijmers et al. (2007) combined the use of IEG *c-fos* promoter with the tetracycline system to tag active neurons in a defined time window given by the removal of doxycycline repression of tTA activity. c-fos^{+} neurons can be permanently tagged because the initial activation of tTA transcription factor is converted in a self-sustaining expression loop by a bidirectional promoter driving the expression of *lacZ* and doxycycline-insensitive tTA* (Figure 4). These TetTAG mice were removed from a doxycycline diet before auditory fear conditioning or contextual fear conditioning, and active neurons were tagged by LacZ expression, then mice were put back on doxycycline diet. A few days later, mice were tested for memory recall, and active neurons during this second

exposure were identified by Zif268 expression. This demonstrated that neurons that were active during the encoding of the memory were preferentially reactivated during memory recall (Reijmers et al., 2007).

The use of the Tetracycline system is just one of the possible ways to implement the activity tagging (Gore et al., 2015). For example, activity tagging has been implemented using tamoxifen-sensitive Cre (CreER)-mediated recombination. CreER expression is driven by *Arc* promoter, and the floxed reporter is only expressed when tamoxifen is administered to the animal (Denny et al., 2014; Guenthner et al., 2013). Notably, also synthetic versions of IEG promoter have been recently started to emerge and to be implemented in the activity tagging, usually modifying existing IEG transcriptional regulatory elements to increase fold induction (Kawashima et al., 2014; Sørensen et al., 2016). A variant of this system expresses via the *c-fos* promoter a membrane protein that acts as a receptor to a modified envelope protein of a viral vector, enabling only active cells to be transduced (Sakurai et al., 2016).

An ingenious way to restrict the timing of activity tagging has been recently described, and allows tagging active neurons by combining light and calcium influx (Lee

et al., 2017; Wang et al., 2017). Making use of the M2 peptide, that binds CaMKII in presence of calcium, and a light sensitive LOV domain, both groups were able to transduce light signal in coincidence with activity-related calcium influx into the expression of a reporter. They showed the usefulness of this approach by labelling active neurons in the motor cortex during rewarded tasks, although it not exactly clear how this set is related to c-fos^{+} neurons. If proven successful, this could restrict the tagging time window with a precision that currently available activity-tagging technology cannot achieve, although more limited by the spatial dimension.

Engram cells

If tagged neurons constitute a putative engram, it is expected that manipulating their activity has a behaviour counterpart in the associated memory task. The role of specific cells in the encoding of memory was first suggested by experiments from the Mayford group: Garner et al. (2012) tagged active cells during the presentation of context A with chemogenetic, CNO-responsive activator hM_3D_q. This ensemble was then reactivated during fear conditioning in context B by CNO administration; this formed a mixed representation A/B, as upon testing the animal in context A

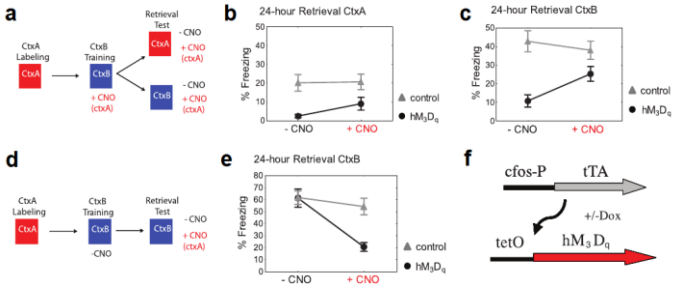

Figure 5 Generation of a synthetic memory trace **a** Outline of experiment. 'Context A' engram is labeled with DREADD expression and later reactivated by CNO in concomitance to Context B conditioning with a footshock. **b,c** Retrieval in context A (**b**) or B (**c**) for hM_3D_q and control mice shows the formation of a mixed A/B memory trace. **d,e** Reactivation of 'context A' engram competes with the recall of conditioned context B during retrieval. **f** Scheme of construct expression in engram cells. Modified from Garner et al. (2012).

alone, no freezing was observed (Figure 5b) – however, animals in context B froze significantly less if no CNO was administered (Figure 5c). The ensemble tagged by hM_3D_q represents a neutral (not feared) engram indeed, since CNO administration during retrieval of a conditioned context competed with memory recall blocking freezing, suggesting memory occlusion (Figure 5e).

The experiment described above generated a mixed, artificial engram that had a complex crosstalk with the physiological circuit, which is assumed to exist rather than proved. If an engram exists, it should recruit a number of cells which are tagged and, after the stimulation has passed,

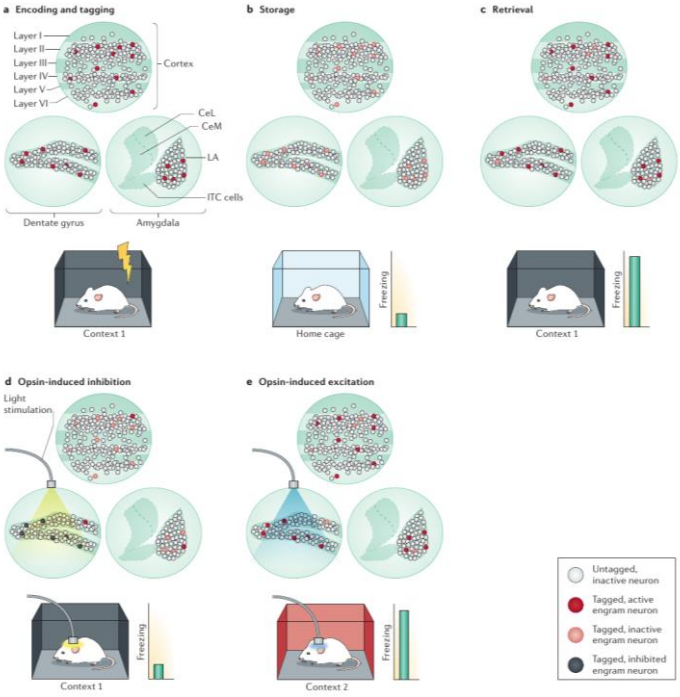

Figure 6 a During fear conditioning, a mouse is placed in context 1 and given a footshock, activating neuronal ensembles in the dentate gyrus, cortex and lateral amygdala. Neurons are tagged during the first epoch of stimulus presentation, or encoding. **b** In the home cage, the engram is consolidated, and tagged engram neurons are inactive. **c** Re-exposure to context 1 reactivates the ensemble, causing the animal to freeze. **d** If tagged neurons in the dentate gyrus are optogenetically silenced when the mouse is returned to context 1, mice show reduced conditioned fear, indicating impaired memory retrieval, which is reflected in a reduced activation of downstream areas. **e** Optogenetic activation of tagged engram neurons in the dentate gyrus alone is sufficient to act as a memory retrieval cue such that mice now freeze in a third unrelated context (context 2). Reproduced from Josselyn et al. (2015).

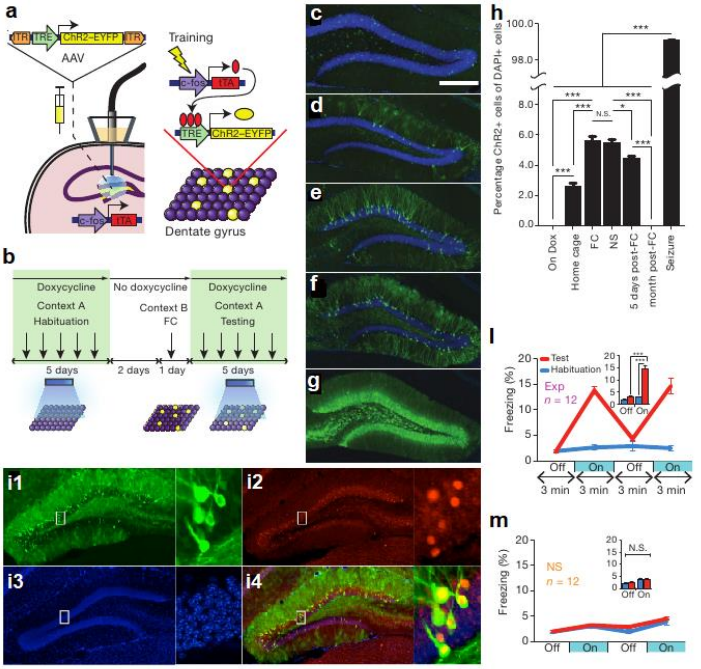

Figure 7 Optogenetic engram labeling and reactivation **a** Schema of AAV activity Tet-tagging **b** Experimental outline (**c-g**) expression of ChR2-EYFP on dox (**c**), **d** home caged animals **e** fear conditioned, **f** exposed to context, non shocked animals, **g** seizure, demonstrating dox- and activity-dependence of ChR2-EYFP expression. **h** Quantification of the fraction of ChR2-EYFP cells in **c-g**. **i** expression of ChR2-EYFP (**i1**) in DG cells strongly correlate with c-fos (**i2**) expression. **l** Reactivation of tagged DG cells with blue light illumination induced significant freezing in fear conditioned (**l**) but not in non-shocked (**m**) animals, demonstrating the reactivation of the encoded memory trace. Modified from Liu et al. (2012).

they become part of a silent trace, only to be reactivated by the later retrieval induced by a stimulus (or part of it) sufficiently close to the original one (Figure 6a-c). If a subset

of cells makes up an engram, then, it is expected that silencing their activity during the recall should block the animal response and, conversely, reactivating their activity in the absence of the original natural context should elicit that same response (Figure 6d, e).

Using Tet-tag mice, Liu et al. (2012) tagged c-fos^{+} neurons during a fear conditioning epoch while in Context B, and demonstrated the existence of such a population engram in the hippocampus DG (Figure 7): tagged cells expressed ChR2-EYFP, and their reactivation with blue-light illumination recalled the fear memory, causing the animal to freeze. This was paralleled by experiments performed by Denny et al. (2014), who confirmed the existence of such engram population in the DG (as well as in CA3) by tagging active cells in an analogous manner with inhibitory opsin Arch-GFP. Green-light illumination significantly reduced freezing with respect to control animals when exposed in a fear-conditioned context. Together, these two works demonstrate that a subset of active neurons in the DG is part of an engram representing the association of a specific context with a noxious stimulus (the shock), and that their activity is both necessary (Denny

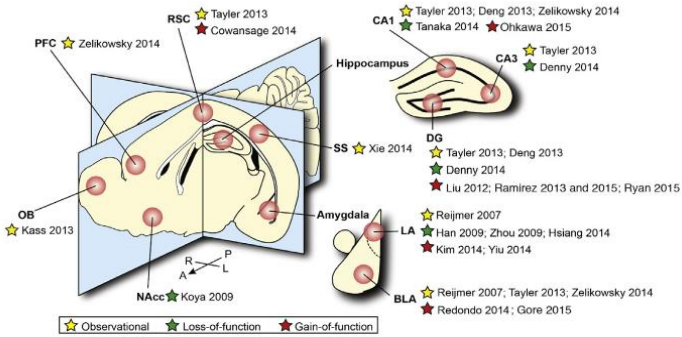

Figure 8 Non-exhaustive list of regions where engram cells have been identified. Three criteria may be used to define them: observational (e.g. calcium imaging during activity) provide the less strong evidence of the three – loss-of-function, i.e. tag-and-inactivation experiments – gain-of-function implies that cells have been reactivate to recall existing memories or create new ones. Reproduced from Tonegawa et al. (2015).

et al., 2014) and sufficient (Liu et al., 2012) to at least partially recall the original experience.

The cell tagging-and-capture described above has been since found use in many brain areas, including the amygdala (Redondo et al., 2014), ventral CA1 (Okuyama et al., 2016), the retrosplenial (Cowansage et al., 2014) and prefrontal cortex (Kitamura et al., 2017), each encoding different portions of engrams in various forms of memory (e.g. contextual, social) (Tonegawa et al., 2015). A non-exhaustive list of brain areas where engrams have been identified is presented in Figure 8. Engrams can be identified

by either of three criteria, that is (i) observational: the activity of a defined set of neurons is correlated with a specific memory task or memory retrieval, for example by means of calcium imaging (Kitamura et al., 2015; Roy et al., 2017a) or IEG expression (Deng et al., 2013; Tayler et al., 2013); (ii) loss-of function: inhibiting the activity of engram cells should result in memory impairment, that is engram cells activity is *necessary* for the recall (Figure 6d), for example in Denny et al. (2014); (iii) gain-of-function: stimulating their activity is *sufficient* to instate the memory recall (Figure 6e), as in Liu et al. (2012).

Creating new memories

Given the specialization of brain areas, a complete engram is likely to be composed by multiple components, which may be localized in distinct regions (Tonegawa et al., 2015). Each component then could convey defined information of the complete engram. It would be possible, then, to create false memories by combining multiple subtraces in a new, artificial engram. Ramirez et al. (2013) tried to associate a neutral, contextual engram with a noxious stimulus by means of optogenetic tagging-and capture technology. The active population of cells was first tagged with ChR2-Cherry during the presentation of context A (Figure 9), and after 24

hours the animal was first conditioned in context B while putative 'context A' engram was activated by blue light. The next day, animals were put back in context A, where they never experienced a shock, and tested for freezing. While DG engram reactivation could form an association of context A to an unpleasant experience, the (putative) CA1 engram could not (Figure 9). This could mean that (i) CA1 does not allocate part of the engram, (ii) CA1 engram does not represent contextual information, (iii) CA1 has no causal role in providing such information, or (iv) the putatively identified engram deviates too much from the actual one.

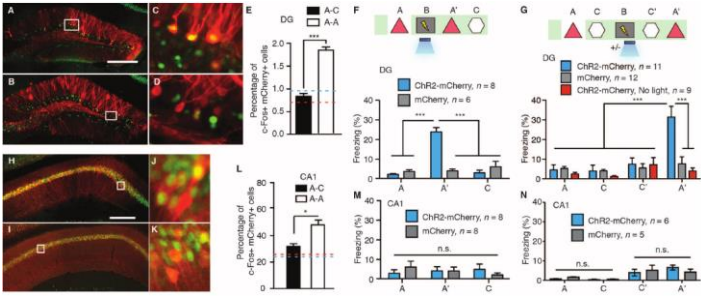

Figure 9 (**a-d**) c-fos::tTA mice injected with AAV9-TRE-ChR2-mCherry in the DG were exposed to context A while off Dox, then put back on Dox and exposed to the same context A (**a,c**) or a novel context C (**b,d**); activated cells express c-fos (green). (**f,g**) (Top) Training and testing scheme of animals injected with AAV9-TRE-ChR2-mCherry or AAV9-TRE- mCherry. (Bottom) Animals' freezing levels in context A before fear conditioning and in context A and C after fear conditioning (**h-n**) Same as in (**a-g**) except the virus injection was targeted to CA1. The lack of freezing in the test session (A') shows that the identified CA1 ensemble could not be associated with the aversive stimulus. Reproduced from Ramirez et al. (2013).

Explanation (i) can be excluded by a series of evidences that imply the presence of engram cells: first, memory-specific cells have been identified by means of IEG expression (Tayler et al., 2013). Second, optogenetic CA1 inhibition prevents contextual fear memory recall (Goshen et al., 2011; Sakaguchi et al., 2015) and third, selective silencing of c-fos^{+} cells in CA1 impaired memory retrieval in fear conditioning (Tanaka et al., 2014) and novel object recognition (Nomoto et al., 2016). Fourth, CA1 is the main area sending outputs from the hippocampus, while DG only projects to the downstream CA3 area (Basu and Siegelbaum, 2015; Cenquizca and Swanson, 2007; Paxinos, 2015). CA3 then massively projects to CA1, so CA1 is, by definition, part of the engram. Explanation (ii) is also unlikely, given the overwhelming amount of data implying CA1 as a major area processing spatial and contextual information (Barrientos and Tiznado, 2016; Jeffery, 2007; Ocampo et al., 2017). Similarly, explanation (iii) can be also excluded for the same reasons as (i); it is also difficult to imagine how CA1 contextual (sub)engram could not have a causal role in the building of the memory engram, even if it is role was only to relay the activity generated in the DG via the trisynaptic circuit. We are therefore left with explanation (iv). Indeed, a high proportion of total cells in CA1 is tagged

in Ramirez et al. (2013) and, most importantly, there is significant overlap in the engram representing two different contexts (Figure 9l). Indeed, optogenetically silencing CA1 'context A´' engram inhibits freezing during the recall of an animal trained in a similar context A (which activates an overlapping population of neurons to A´), but has little of no effect on an animal trained in a distinct context B (Tanaka et al., 2014). The vast majority of tagged cells are also expressing c-fos (Figure 7i) (Liu et al., 2012), so it must be concluded that, if an engram exists in CA1, it is either a subset of this population, or it otherwise represented within it.

From engram cells to connections

A similar proportion of cells is activity-labelled in CA1 when the animal is exposed to a new context when this is coupled to a shock and when it is not (Figure 10), further suggesting that a contextual engram is formed in the hippocampus independently from an association (Ohkawa et al., 2015). Accordingly, presentation of context B alone activity-tagged a population of cells in CA1; later, animals were shocked in a different context without giving them the time to explore it (Ohkawa et al., 2015). This was not enough

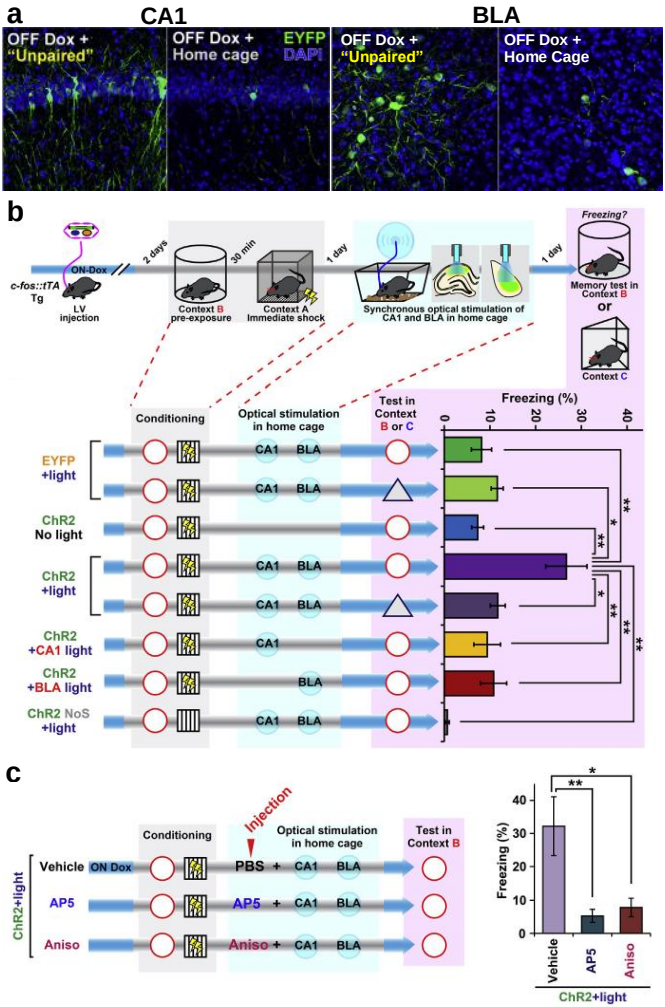

Figure 10 Artificial association of pre-stored memories **a** expression of ChR2-EYFP by context exposure or immediate shock when off-dox **b** experiment and outcome of optogenetic association of the two memories. The concomitant activation with light of the tagged amygdala and CA1 ensembles could form a meaningful association. **c** The association between the two engrams is dependent on NMDAR activation and de novo translation. Modified from Ohkawa et al. (2015).

to induce an association between the shock and context B the next day. However, optogenetically co-activating the CA1 'context B' engram and BLA 'foot shock/Ouch ouch ouch!' engram was sufficient to form an association between the two engrams in a unitary representation: when tested in context B, but not in the unrelated context C, animals froze significantly. This association was blocked if BLA and CA1 were injected with NMDAR blocker D-AP5 or translation inhibitor anisomycin, suggesting a Hebbian-like form of plasticity (Figure 10c).

Synapses and memory

Synapses, the physical connections between neuron, have always been ascribed a critical role in learning and memory processes (Rudy, 2008; Yuste, 2010). Virtually all excitatory synapses are associated with postsynaptic structures called spines. Due to their structure, spines have the ability to compartmentalize secondary signals, and to modify their responsiveness as a consequence of their past activity (Yuste, 2010). For its properties, synaptic plasticity has been long regarded as a candidate for sustaining changes that occur during memory encoding.

LTP

First described by Bliss and Lømo (1973) in the rabbit hippocampus, LTP is the long-lasting change in synaptic efficacy observed after a strong initial stimulation. LTP is usually measured as change in field potential, but is also detected in whole-cell (Nicoll, 2017). While some forms of LTP act at the presynaptic level (Castillo, 2012), most mechanisms are a modification of the postsynaptic response (Kandel et al., 2016).

A broad classification distinguish E-LTP from L-LTP, plus a series of changes in synaptic efficiency on shorter time scales (e.g. facilitation, depression…) which have more to do with biophysics than with biological regulation. Typically, LTP is induced by tetanic or theta-burst electrical stimulation, or by stimulation of the presynaptic neuron while depolarizing the postsynaptic neuron (Wigström et al., 1986). Although E- and L-LTP can be dissociated (Kelleher III et al., 2004; Park et al., 2014), generally E-LTP precedes and L-LTP is only observed if the stimulation is sufficiently strong. Weak tetanisation (one train) of the Schaffer collateral causes an increase in synaptic response that decays to pre-induction level in 1 or 2 hours. This E-LTP is not sensitive to transcription or translation inhibitors (Kelleher III et al., 2004), and is due to the

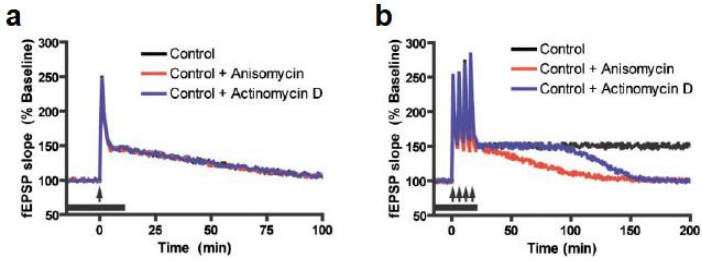

Figure 11 a Time course of E-LTP induced by a single tetanus at CA1 synapses. **b** Time course of L-LTP induced by four trains of tetanization. In red and blue, treatment with anisomycin or actinomycin D during stimulation. Reproduced from Kelleher III et al. (2004).

exposure of more AMPA-type glutamate receptors (AMPAR) which are not, generally, permeable to calcium (Kandel et al., 2016). L-LTP is induced by stronger stimulation (e.g. four trains of tetanisation) and lasts much longer, typically hours and (possibly) days (Kandel, 2012). Unlike E-LTP, L-LTP is affected by translation inhibitors like anisomycin and emetine, as well as transcription inhibitors (whose effect, however, acts on a longer timescale than translation inhibitors) (Figure 11) (Kelleher III et al., 2004).

When translation is blocked, only E-LTP is observed; thus, E-LTP and L-LTP are generally viewed as two distinct mechanisms that function in parallel from a common induction signal. Indeed, a slow rising form of L-LTP is

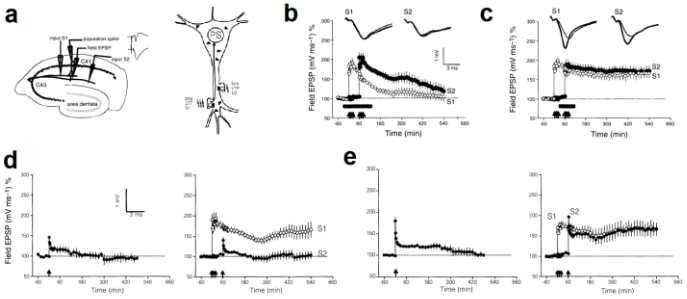

Figure 12 Synaptic capture and tag at CA3 to CA1 connections **a** Scheme of setup and possible mechanism **b** Anisomycin blocks L-LTP in 4x tetanized S1 and S2 input pathways **c** Prior 4x tetanization of S1 prevents anisomycin block of S2 L-LTP. **d** a weak tetanization of S2 cannot be converted into L-LTP by prior 4x tetanization of S1. **e** 1x strong tetanization alone produces a decaying LTP. However, if it is preceded by 4x tetanization of S1, also 1x strong tentanization of S2 produces a long lasting form of L-LTP. Modified from Frey and Morris (1997)

induced by BDNF without the induction of E-LTP (Kelleher III et al., 2004; Reymann and Frey, 2007). This is also consistent with the tag-and-capture phenomenon: single tetanisation of a pathway (S2) – which normally induces transient LTP – can be converted into a long lasting form if it is coupled by the strong tetanisation of another pathway (S1) (Figure 12). This suggests that, upon induction, a tag is created in S2 synapses that can capture effectors of LTP generated by S1 tetanisation, collectively called Plasticity Related Products (PRPs) (Frey and Morris, 1997).

LTP mechanisms

The main form of L-LTP is NMDAR-dependent LTP. NMDAR are calcium-permeant glutamate receptors found predominantly on the postsynaptic sites. Unlike AMPAR, NMDAR are normally blocked by extracellular Mg^{2+} ions that occlude the channel pore (Kandel et al., 2013). The depolarization of the postsynaptic neuron removes the Mg^{2+} block; therefore, NMDAR are detectors of coincident activity of the pre- and postsynaptic neurons (Lüscher and Malenka, 2012). Calcium influx through NMDARs activates a series of events including the recruitment of kinases like CaMKII, PKC and PKA (Mayford et al., 2012).

Selective deletion of NMDAR1 (*grin1*) in the CA1 (Tsien et al., 1996), CA3 (Nakazawa et al., 2002) and DG (McHugh et al., 2007) regions abolishes LTP induction in the corresponding pathway (respectively, EC-DG via perforant path, DG-CA3 via Mossy fibers, and CA3-CA1 via the Schaffer collateral). Downstream, αCaMKII phosphorylation and activation is also necessary for LTP induction. Inducing LTP causes a spine-specific αCaMKII activation (Lee et al., 2009) and recruitment from the surrounding regions (Otmakhov et al., 2004). LTP is abolished in acute slices in αCaMKII knock-out mice (Silva et al., 1992a). In addition, knock-in mice with non-

phosphorylable αCaMKII T286A lack LTP; similarly, phosphomimetic T286D have occluded LTP (Kandel et al., 2016; Lisman et al., 2012). NMDAR activation activates CaMKII holoenzyme via calcium/calmodulin (calcium chelators EGTA and EDTA block LTP induction), which can mediate LTP by phosphorylating a number of downstream proteins, including αCaMKII itself (Lisman et al., 2012).

LTP and local translation

As seen above (Figure 11), blocking protein synthesis with anisomycin, cycloheximide or emetine blocks L-LTP induction (Fonseca et al., 2006a). Given the temporal profile of L-LTP in presence of translation or transcription inhibitors (Figure 11), and that the sensitive period for inhibition is around the time of induction, the treatment is likely to interfere with translation from pre-existing mRNAs. Indeed, LTP can be induced even when dendrites are physically isolated from the cell body (Kang and Schuman, 1996) (Figure 13). Even so, LTP is sensitive to D-AP5 and cycloheximide; in addition, LTP is accompanied by ^{35}S-methionine incorporation, indicating novel protein translation (Vickers et al., 2005). ^{3}H-leucine is incorporated by isolated dendrites in glia-free cultures, and specific

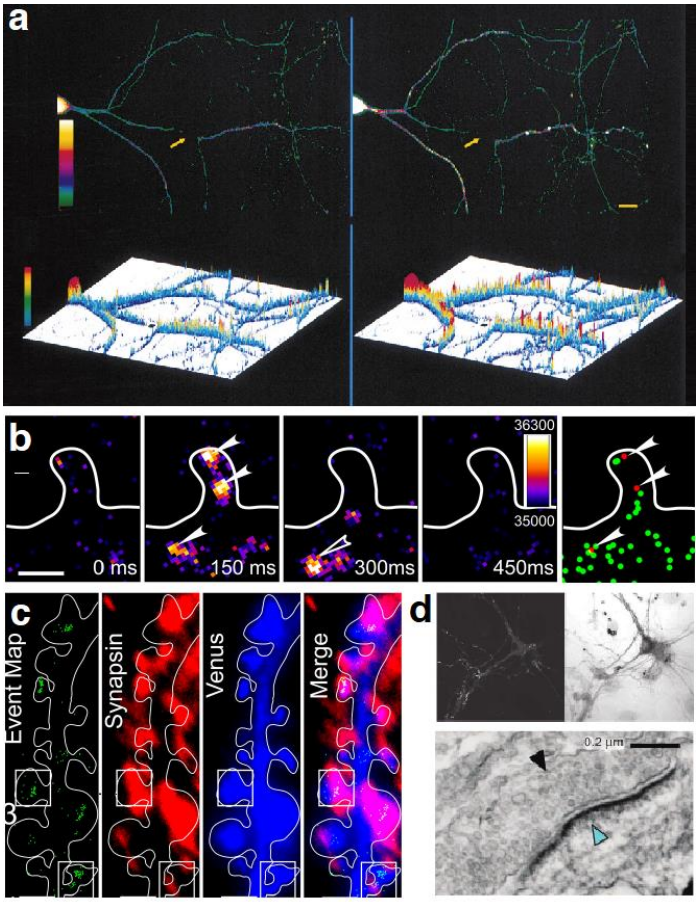

Figure 13 Translation of dendritically localized tales place in dendrites. **a** BDNF-stimulated dendrites translate a CaMKII reporter even when severed from the cell body. Reproduced from Aakalu et al. (2001). **b** Event map showing translation sites of a PSD95 reporter. **c** Translation events are predominantly confined to dendritic spines, as confirmed by association with presynaptic marker synapsin. Modified from Ifrim et al. (2015). **d** Identification of the newly translated PSD95 with TimeSTAMP. Modified from Butko et al. (2012).

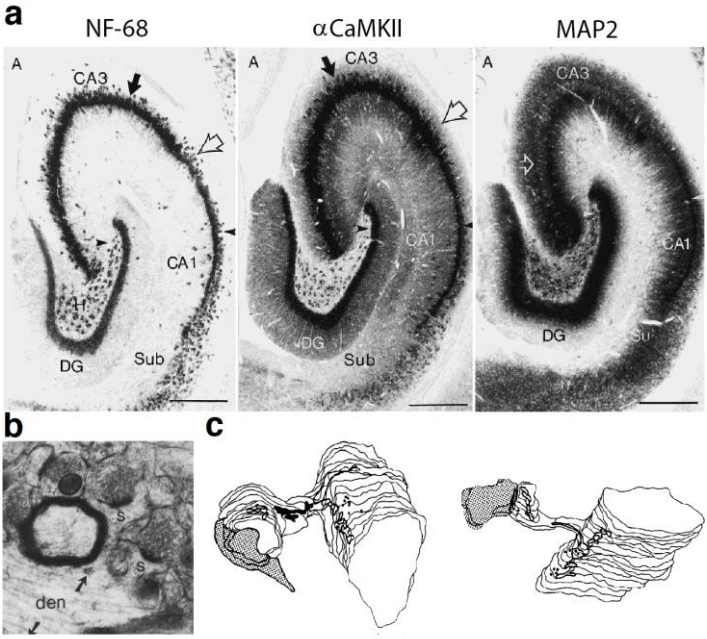

Figure 14 a A set of RNAs are present in dendrites, like αCaMKII and MAP2; for comparison, the ISH signal of soma-localized NF-68 marks the cell body and the most proximal part of the apical dendrites. Modified from Paradies and Steward (1997). **b** Ribosomes (arrowheads) are associated with dendritic spines (s) **c** Most spines have associated ribosomes in the spine head or at the dendritic junction. Furthermore, internal membrane stores known as Golgi apparatus are present in some spines. Modified from Steward and Reeves (1988).

classes of RNAs are present within dendrites (Torre and Steward, 1992).

Dendrites contain a whole set of translation and regulation machinery, including initiation and elongation

factors, ribosomes, tRNA, ncRNA and an internal membrane system (Figure 14); it is also possible that a subclass of ribosome exists, with different isoform/protein composition from somatic ribosomes (Bramham and Wells, 2007; Holt and Schuman, 2013; Muslimov et al., 1998; Sutton and Schuman, 2006). RNA translation is stimulated by neuron activity via NMDAR, TrkB or mGluR signalling, which regulate the various steps of the translation process: RNA distribution, polyadenylation, ribosome assembly, initiation and elongation complexes formation (Jung et al., 2014; Kindler and Kreienkamp, 2012; Klann and Dever, 2004).

Dendrites contain several mRNAs, which are translated locally, contributing to protein homeostasis or producing effectors to respond in a spatially confined way to incoming stimulation. Although the whole picture is still incomplete, different stimuli can induce the expression of different transcripts (or transcript classes) (Bramham and Wells, 2007). mRNAs are generally transported in a translationally repressed state either singly (Batish et al., 2012; Mikl et al., 2011) or in complexes containing multiple transcripts (Gao et al., 2008). Translation is prevented by RNA binding proteins (RBPs) like CPEB, FMRP and hRNPA2 (Kindler and Kreienkamp, 2012; Wells, 2006),

forming large (0.4-0.8μm) macromolecular complexes that travel along the cytoskeleton, known as RiboNucleic Particles (RNPs) or granules (Kindler et al., 2005). RNP assembly starts co-transcriptionally (Giorgi and Moore, 2007) and their protein content may change during transcription, granule assembly and transport progression (Fritzsche et al., 2013; Hachet and Ephrussi, 2004; Lewis and Mowry, 2007). For example, intron sequences are found in dendritically localized transcripts (Buckley et al., 2011), and dendrites have a minimal set of spliceosomal proteins to remove introns independently of the soma (Glanzer et al., 2005). Thus, for some RNAs, introns can influence mRNA transport either directly (Hachet and Ephrussi, 2004) or indirectly (Giorgi et al., 2007).

The transport of RNAs is mediated by dendritic (or axonal) targeting elements (DTEs or ATEs), instructive portions of the transcript that bind RBPs and molecular motors (Blichenberg et al., 2001). Most DTEs form secondary structures comprising one or more stem loops (Muslimov et al., 2006) or G-quadruplexes (Subramanian et al., 2011), but also linear DTEs have been described (Raju et al., 2011). Most sequences, however, are poorly characterised, and multiple DTEs generally exist in a single transcript, and could act in a cooperative or redundant

fashion; for example in the 1.6 kb αCaMKII 3'UTR, probably the first identified RNA element to confer dendritic targeting (Mayford et al., 1996), at least four distinct DTEs have been identified (Blichenberg et al., 2001; Mori et al., 2000; Raju et al., 2011; Subramanian et al., 2011). While most DTEs are localized in the 3'UTR of transcripts, DTEs and instructive sequences that can influence targeting have also been reported in the 5'UTR as well as in the coding sequence (Baj et al., 2011; Chiaruttini et al., 2009).

Plasticity related transcripts

While some dendritic transcripts may predominantly contribute to protein homeostasis (including ribosomal and mitochondrial proteins), some, if not most of the more than 2,500 transcripts encode proteins involved in synaptic plasticity. Among them there can be found kinases like αCaMKII (Figure 15a) and PKMζ, a constitutively active form of PKC (Muslimov et al., 2004), scaffold proteins like PSD95 and Shank3, and AMPAR and NMDAR subunits (Figure 15b) (Cajigas et al., 2012). For instance, abolishing αCaMKII dendritic translation in the αCaMKII 3'UTR knockout mice (while sparing somatic translation) causes impairments in LTP induction, and memory deficits in contextual and cued responses in associative fear

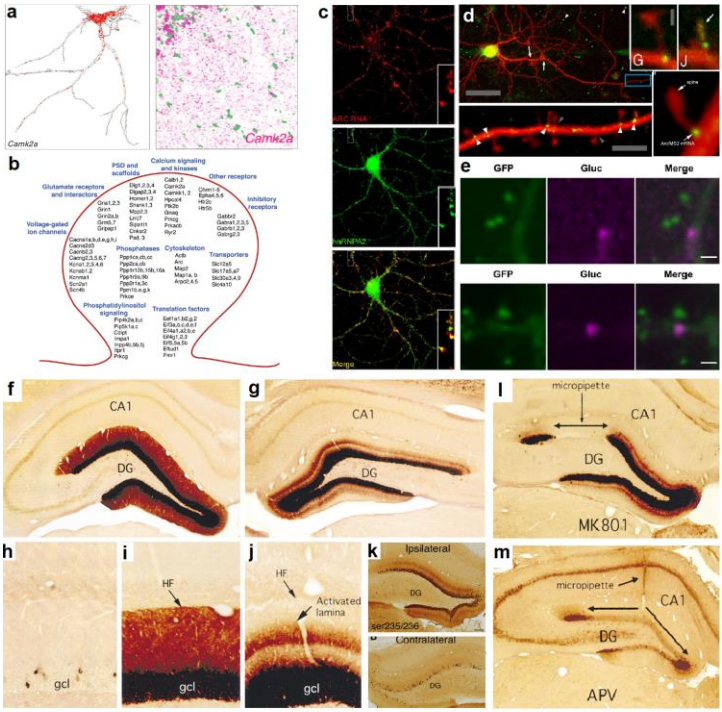

Figure 15 a αCaMKII gene is involved in synaptic plasticity and is one of the most abundant dendritic RNAs. αCaMKII smFISH in cultured neurons and hippocampal CA1 (nuclei are in green). **b** Dendritically localized RNAs include a large number of synaptic proteins including signaling, scaffold, and membrane receptor proteins. Modified from Cajigas et al. (2012) and Will et al. (2013). **c** Arc RNA is a dendritically localized RNA that predominantly exists in granules, associated with RBPs. Modified from Gao et al. (2008) **d** Live imaging of MS2-tagged Arc RNA shows that it predominantly associated with dendritic spines either at the base or with the spine head. Modified from Dynes and Steward (2012). **e** Gluc-fused Arc is translated at dendritic spines (marked with PSD95-GFP) after glutamate application. From Na et al. (2016). **f,g** (magnified in **i,j**) Dendritic localization of Arc RNA after electroconvulsive seizure in anestethized rat. Perforant path stimulation of one hemisphere (**g**) induced selective re localization of the RNA. **h** Arc expression in control animal. **k** High-frequency stimulation of the medial perforant path also induces lamina-specific ribosomal RPS6 phosphorylation. Arc expression and localization is blocked by NMDAR blockers MK-801 (**l**) and APV (**m**). Modified from Pirbhoy et al. (2016) and Steward and Worley (2001b).

conditioning, as well as in the Morris water maze (Miller et al., 2002).

Among plasticity-related transcripts, Arc (also known as Arg3.1) is particularly interesting, being at the same time an IEG and a dendritically localized transcript (Steward and Worley, 2001a). Under resting conditions, Arc RNA levels are low, and mainly present in dendrites in granules associated to RBPs that prevent translation (Figure 15c). Live imaging of the transcripts shows that Arc RNA localizes in correspondence to spines, either in the head or at the spine-dendrite junction (Figure 15d), where it is translated after glutamate stimulation in a NMDAR-dependent way (Figure 15e) (Dynes and Steward, 2012; Na et al., 2016). Furthermore, Arc translation has been reported in synaptoneurosome preparations, indicating that translation can occur, at least in part, also in spines (Yin et al., 2002). Arc 5'UTR, then, has one of the highest IRES (internal ribosome entry site) activity among dendritic mRNAs (Pinkstaff et al., 2001), a process involved in spine potentiation (Barco et al., 2008; Kindler et al., 2005)

Arc is rapidly expressed after neuron and synaptic activation by electroconvulsive seizures and perforant path (PP) high frequency stimulation that induce LTP (Figure

15f-k); the administration of the NMDAR blocker MK-801 blocks both LTP and Arc expression induction (Lyford et al., 1995). Arc RNA rapidly translocates in the dendritic layer of stimulated DG; concomitant PP stimulation induces Arc RNA accumulation to the activated lamina (Steward and Worley, 2001b). Notably, in an unbiased screen, Arc was found to be the mRNA with the greatest fold induction change in the dendritic layer after PP-HFS stimulation of the DG (de Solis et al., 2017). Dendritic targeting of Arc RNA is due to sequences in the 3'UTR, where a DTE has been identified (Kobayashi et al., 2005), although other sequences involved in targeting have been identified (Bramham et al., 2010; Gao et al., 2008).

ARC protein associates with PSD95 and synaptic proteins (Fernández et al., 2017), and has been reported to associate with AMPAR vesicles, enhancing their mobilization (Bramham et al., 2008). Novel Arc synthesis is necessary for induction and consolidation of LTP (Plath et al., 2006). Arc KO mice have impaired L-LTP, and blocking activity-dependent Arc expression with antisense oligonucleotides in rat hippocampus inhibits LTP consolidation. Furthermore, injected animals have a severe impairment in recalling the platform position in the Morris water maze (Guzowski et al., 2000). Indeed, ARC associates

with the cytoskeleton stabilizing F-actin, suggesting a possible positive feedback loop that docks novel transcribed mRNAs during the consolidation phase (Bramham et al., 2010). Consistently, F-actin stabilization with jasplakinolide prevents LTP loss due to Arc antisense oligo administration (Messaoudi et al., 2007).

Although ARC protein has been ascribed a complementary role in LTD and homeostatic scaling, *in vivo* stimulations at frequencies that induce LTD (e.g. 1 Hz) do not initiate Arc expression (Steward and Worley, 2001b), and LTD induced by NMDA-only application does not induce Arc expression and does not require ARC protein (Bramham et al., 2010). Most data come from pharmacological treatments in culture or slices, and acute Arc overexpression *in vivo* does not induce LTD (Steward et al., 2015). Recently, it has been reported that ARC may have a priming effect on synapses rather than causing LTD (Jakkamsetti et al., 2013). An intriguing possibility is that these could be synapses surrounding potentiated ones, which could explain the accumulation of ARC protein in inactive synapses following LTP-inducing BDNF administration, as reported in Okuno et al. (2012). Although ARC may play additional roles, then, most data imply a role in LTP induction and consolidation at the spine level: after the

induction of LTP, Arc mRNA is transcribed and accumulates in stimulated zones, Arc associates with synapses, and blocking Arc expression impairs LTP consolidation and memory formation.

In addition to a structural role (Zhang et al., 2015b), ARC has been recently reported to be capable of forming oligomeric particles and to transfer its own RNA to other cells, where it is competent for activity-dependent translation (Pastuzin et al., 2018). The authors ascribe this effect to the ability of ARC protein to form virus-like particles, based on the established retrotransposon origin of *Arc* gene, and the structural homology with retroviral gag protein (Zhang et al., 2015b). If observed *in vivo* in physiological situations, this would provide an interesting mechanism of neuron-to-neuron information transfer that could affect the plasticity of close cells. Also, it would be necessary to further assess the mechanism of RNA transfer observed by Pastuzin et al. (2018) to exclude the contribution of mechanisms other than the proposed encapsidation of ARC particles (e.g. exosomes, microsomes), and to evaluate whether the employed concentration in which ARC particles are formed *in vitro* are compatible with actual concentration expected in neurons.

LTP and memory

For what has been said above, LTP is an attractive candidate mechanism to be the substrate for memory. First, electrical LTP can be induced in brain structures implicated in learning and memory. It is found in amygdala preparations, and L-LTP has been described at all synapses in the hippocampus circuit (Kandel et al., 2016). Notably, NMDAR conditional deletion in postsynaptic populations DG, CA3 or CA1 selectively impairs L-LTP in the corresponding station of the trisynaptic circuit (Figure 16). Second, it is associative in nature, as it requires coincident pre- and postsynaptic activity (section "LTP mechanisms"). Third, its long-lasting nature has the right temporal scale of memory retention (section "LTP"). Fourth, it is synapse-specific (Bliss and Collingridge, 1993), and potentiation can be induced even in single spines (Bosch et al., 2014; Hill and Zito, 2013). Fifth, potentiation is observed *in vivo* in parallel to memory formation. Recordings from contextual fear conditioned rats show increased AMPAR currents in response to test stimuli in the amygdala (McKernan and Shinnick-Gallagher, 1997); similarly, training rats in contextual fear conditioning, or letting animals experience a novel context, increased fEPSP slope of CA1 response to Schaffer collateral (SC)

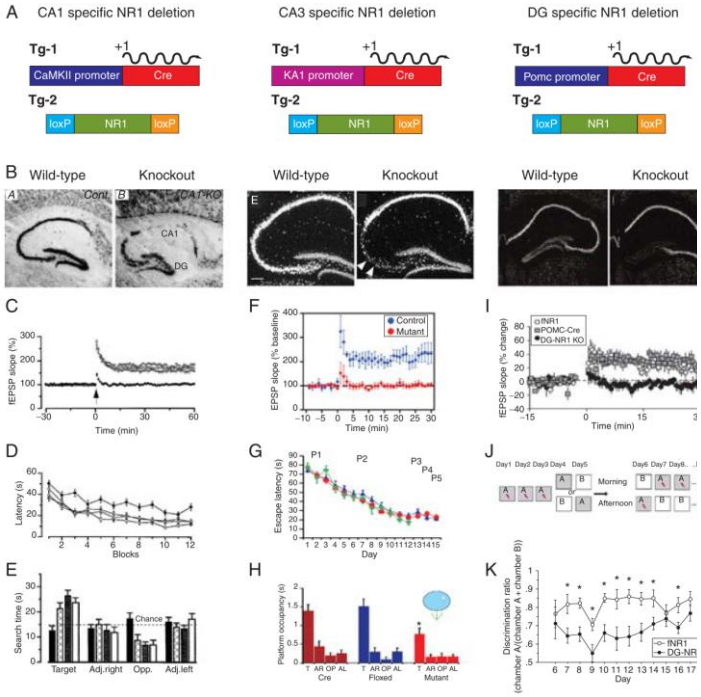

Figure 16 a Deletion of NMDA receptor NR1 subunit in specific subregions of the hippocampus can be achieved crossing floxed *nr1* mice with Cre mice under a region-specific promoter, as confirmed by ISH (**b**). **c,f,i** region-restricted deletion of the NR1 subunit impairs LTP in the corresponding pathway (**c** CA1: Schaffer collateral, **f** CA3: commissural-associative synapses, **i** DG-Perforant path). This is paralled by memory impairments: **d,e** Mice lacking NMDAR CA1 are impaired in the spatial version of the MWM. **g,h** although the training in MWM in CA3 *nr1* knockout, their performance is reduced in probe trials. **j,k** DG *nr1* KO have reduced discrimination ability between different contexts. Reproduced from Havekes and Abel (2009)

stimulation in *ex vivo* preparations (Sacchetti et al., 2001) (Figure 17a,b). Whitlock et al. (2006) recorded potentiated

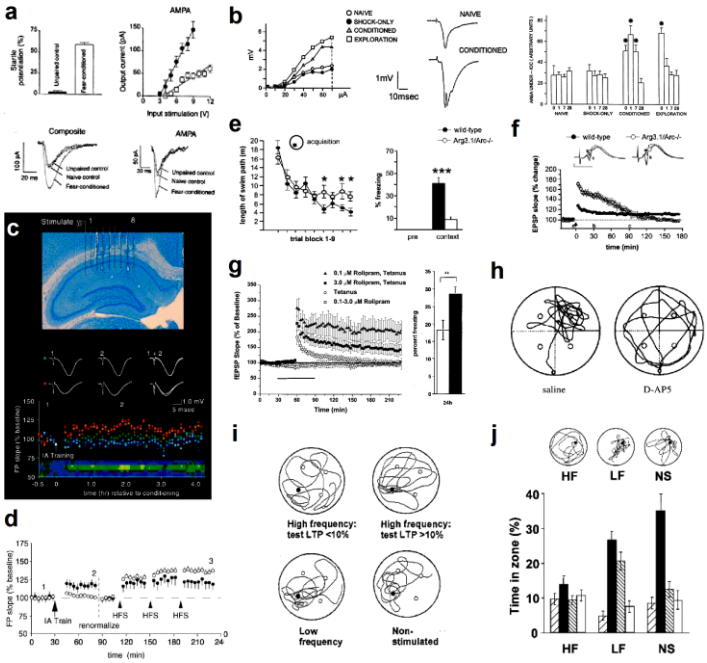

Figure 17 a Amygdala slices from fear-conditioned rats have higher EPSCs and input-output curves. From McKernan and Shinnick-Gallagher (1997). **b** Slices from fear-conditioned or context-exposed rats display higher input-output response in the Schaffer collagteral-CA1 synapses than control animals. From Sacchetti et al. (2001). **c** Potentiation of stimulus-response is observed in CA1 of rats after inhibitory avoidance learning in some recording sites. Potentiates sites display occlusion, and electrical LTP produces smaller changes in potentiated vs. non potentiated sites (**d**). Modified from Whitlock et al. (2006). **e** $Arc^{-/-}$ performance in MWM is lower than control mice, and freezing during recall of fear-conditioned $Arc^{-/-}$ mice is dramatically reduced. **f** $Arc^{-/-}$ have enhanced E-LTP but severly impaired L-LTP. Modified from Plath et al. (2006). **g** In hippocampal slices, a single tetanus, that normally induces E-LTP, induces L-LTP in presence of phosphodiesterase inhibitor rolipram. Rolipram enhances memory maintenance in cued contextual conditioning with a mild footshock. Modified from Barad et al. (1998) **h** Blocking NMDAR with D,L-AP5 during training impairs (*continue on next page*)

(*continued from previous page*) learning of platform location in MWM. From Morris et al. (1986). **i** Complete LTP electrical saturation (<10%) in PP-DG synapses prevents learning of the platform location in MWM. From Moser et al. (1998). **j** LTP saturation of PP-DG synapses after learning impairs the retrieval of platform location in MWM. From Brun et al. (2001).

responses in some electrodes in a multi-electrode array implanted in CA1 following training in the inhibitory place avoidance task (Figure 17c); importantly, occlusion of experimentally induced LTP was more prominent at potentiated electrode positions (Figure 17d). Thus, the synaptic plasticity and memory hypothesis (which posits a causal role of synaptic plasticity in the formation of memories) satisfies the principle of detectability (Martin and Morris, 2002). Sixth, pharmacological and genetic manipulations that affect LTP also affect memory, and vice versa. Arc knock-out mice have a worse performance in memory tasks like the Morris Water Maze and the contextual fear conditioning than wild type mice (Figure 17e). Analogously, L-LTP is impaired in these animals, although E-LTP is enhanced (Figure 17f) (Plath et al., 2006). This seems the rule rather than the exception: for example, mutant mice knock-out for αCaMKII have severe L-LTP deficits (Silva et al., 1992a), and spatial learning is heavily impaired in MWM and plus maze (Silva et al., 1992b). Similar results

are observed in non-phosphorylable T286A CaMKII mice (Lisman et al., 2002). Conversely, mutant mice with enhanced or facilitated L-LTP generally have a better performance in learning and memory tasks (Lee and Silva, 2009). These correlative observations suggest that synaptic plasticity and memory formation share underlying mechanisms of induction.

Experimental interventions that block L-LTP also impair learning: NMDAR inhibition during training with hippocampal infusion of D,L-AP5 blocks memory formation (Morris et al., 1986). Inhibition of protein synthesis has been often reported to impair both L-LTP and memory formation (Barrientos et al., 2002; Fonseca et al., 2006b), although the generalized block of translation can have confounding effects (Fonseca et al., 2004; Gold, 2008). Immediate pre- and peristimulation inhibition of αCaMKII activation with a light-sensitive inhibitor blocked L-LTP induction. Light inhibition of αCaMKII in the amygdala hindered learning in the place avoidance task (Murakoshi et al., 2017). Inhibition of actin polymerization with latrunculin or cytochalasin D impairs L-LTP induction (Krucker et al., 2000) and memory acquisition (Mantzur et al., 2009); thus, interfering with at least four of the main components implied in L-LTP formation (NMDAR,

CaMKII, novel protein synthesis and actin cytoskeleton reorganization) also blocks memory formation.

Saturating LTP with implanted electrodes in the DG prevents the acquisition of the platform location in rats trained in the MWM (Figure 17i). The effect was specific to LTP, since it was not observed when the DG was stimulated with a lower frequency paradigm (which does not induce LTP) (Moser et al., 1998). The same holds for pharmacological treatments that enhance memory function: for example, phosphodiesterase inhibitor rolipram facilitates L-LTP, which can be induced by a single tetanus, a stimulation that produces E-LTP only when cAMP levels are not altered. Rolipram administration to mice trained in a weak contextual fear conditioning task enhances memory and increases memory performance during recall (Barad et al., 1998).

If the memory relies on (relative) changes of synaptic strength in a subset of synapses, then inducing LTP in the complementary set of synapses should result in impairment in the ability to recall the original memory. Indeed, the artificial tetanisation of PP-DG synapses impairs memory recall in rats trained to find the exit tunnel in the Barnes maze (McNaughton et al., 1986) and the platform in the Morris

Water Maze (Brun et al., 2001) (Figure 17j). Consistently, overexpression of dominant negative αCaMKII*, or constitutively active αCaMKII impair in CA1 impair memory retention in a place-avoidance task (Rossetti et al., 2017).

While the data presented so far (and more) advocate a role for LTP as the underlying mechanism for the formation and storage of memories, they still do not provide a definitive demonstration. Most manipulations in fact affect LTP formation as well as other cellular mechanisms (Gold, 2008). The most direct evidence of causal involvement of plasticity in memory is probably the manipulations performed by Nabavi et al. (2014). First, they showed that the conditioned stimulus (tone) in cued fear conditioning could be substituted by optogenetic stimulation of axons from the auditory cortex when paired with a foot shock; the association was dependent on NMDAR and resulted in an increase AMPAR/NMDAR current ratio compared to control mice. The learned tone-shock association, then, could be reversed by optical LTD and afterwards reinstated with optical LTP. However, optical LTP could not induce any association that resulted in freezing in response to the auditory cue.

Synaptic engrams

When learning occurs, patterns of neural activity representing the occurrence of events cause changes in the strength of synaptic connections within the brain. Going back to Semon's definition, active synapses during the presentation of a stimulus apparently meet the requirements to be an engram. It is generally assumed that the reactivation of these altered connections constitutes the experience of memory for these events and for other events with which they may be associated. If this were true, then, potentiated synapses would have all the properties of an engram: (1) they are activated by the occurrence of a stimulus, (2) they undergo modifications that change their response as a consequence of stimulus presentation and (3) their reactivation should start the memory recall. However, a direct way to test this last point is still missing. Indeed, there are evidences that specific synapses are the stable representation of a given stimulus. For instance, single spines in pyramidal neurons of the auditory cortex can be repeatedly activated by a sound of their preferred tone frequency (Chen et al., 2011). Analogously, some spines in the barrel cortex were activated uniquely by single whisker stimulation (Varga et al., 2011). In the visual cortex, synapses maintain their orientation preference over at least

27 days of imaging (Chen et al., 2013). This suggests that indeed a given stimulus *can* be represented at the synaptic level. Furthermore, new synapses formed during motor learning are preferentially stabilized, and at least a subset of them is still present after four months (Xu et al., 2009; Yang et al., 2009). Notably, there appears to be a correlation between the performance and the persistence of spines formed upon learning (Yang et al., 2009). The stabilization of new synapses has also been reported for the amygdala-auditory cortex connections during cued fear conditioning (Yang et al., 2016). Therefore, possible candidates for synaptic engrams exist, i.e. synapses with a constant information content over time, and task-related synapses that are stable over time.

Synaptic vs cellular engrams

Cellular engram theory regards neurons as the unitary element constituting engrams (Figure 19a). Synaptic engram theory posits that instead of whole cells, engrams are stored in the stabilized modifications that spines undergo during memory encoding (Figure 19b) (Papoutsi et al., 2014). It is expected that a relationship between cellular and synaptic engram exists (Kaczmarek, 1992), as c-fos expression correlates with potentiation of synaptic inputs. However,

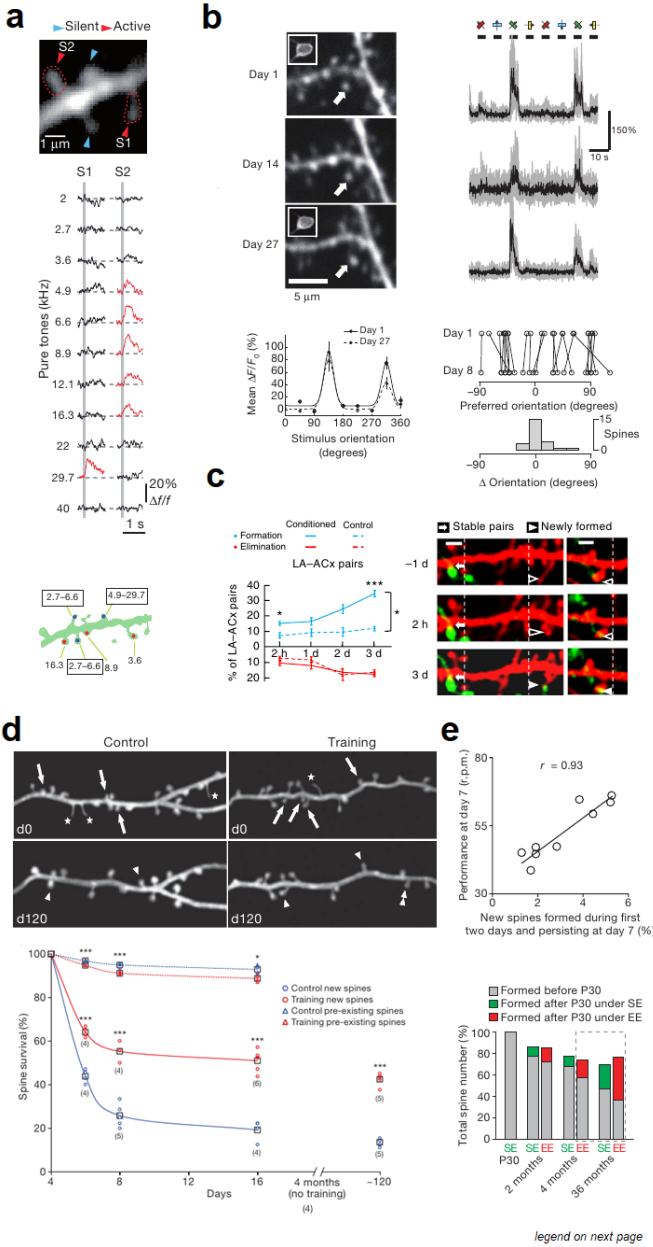

legend on next page

← **Figure 18** Synaptic correlates of candidate engrams **a** Frequency-tuned response of synapses in the auditory cortex (Chen et al., 2011). **b** Orientation tuned synapses in the visual cortex. Their response is stable over a long period of time (Chen et al., 2013). **c-e** Fear conditioning (**c**) and motor learning (**d,e**) induce the formation and selective stabilization of new spines during the formation of the memory in the auditory and motor cortex, respectively. Modified from Yang et al. (2016), Yang et al. (2009) and Xu et al. (2009).

considering the c-fos$^+$ cells ensemble as the engram neglects the different weights that presynaptic inputs have (Figure 19c,d). Cell firing is a rather downstream manifestation of efficient synaptic transmission (Grienberger et al., 2014). This could be the reason why CA1 c-fos$^+$ cells activation does not provide a contextual representation that could be associated to a foot shock (Ramirez et al., 2013) (although, apparently, CA1 c-fos$^+$ neurons activation could induce freezing when they were already part of a naturally formed contextual fear memory (Ryan et al., 2015)). The pattern of activity generated by the natural recall and by the optogenetic reactivation of the c-fos$^+$ neuron ensemble could have been too different from each other, with the result of recalling a mixed context having some features of the original one. Indeed, silencing a putative CA1 c-fos$^+$ cellular engram impaired the physiological recall of a similar, but not of a distinct, context (Tanaka et al., 2014).

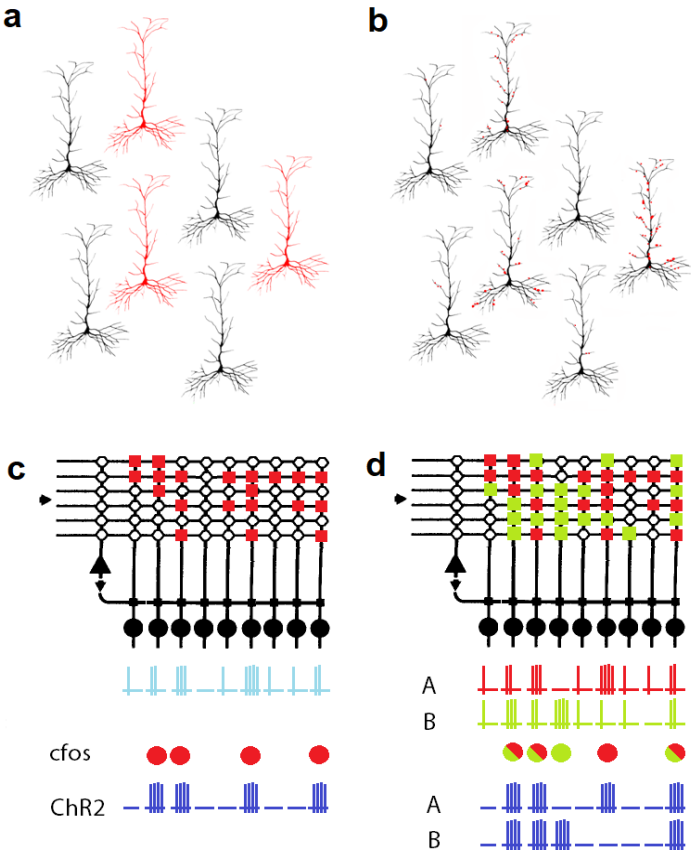

Figure 19 a cellular engrams are generally identified as c-fos⁺ neurons active during the encoding of a given representation. **b** a putative synaptic engram is expected to be the subset of synapses undergoing LTP during the encoding. **c** a set of synapses is activated during an event. This will lead to (1) potentiation of a set of active synapses and (2) c-fos activation if the activation is strong enough. A relationship between the number of potentiated synapses and c-fos activation is expected. If tagged neurons are reactivated with ChR2 and an engram-coherent response is elicited, neurons are assigned the role of engram cells. **d** If two different representations converge onto the same neuron (*continue on next page*)

(*continued from previous page*) population, two sets of synapses will become potentiated (let us assume there are no shared synapses); consistently, some neurons will express c-fos only after context A presentation, some after context B, and some will be activated by both. Having two distinct sets of synapses, natural recall will activate neurons differently, yielding different activity profile. ChR2 stimulation, however, will activate all c-fos$^+$ neurons to the same extent, giving largely overlapping activity for context A and context B.

Importantly, engram cells display many features that accompany LTP. For instance, engram cells in the DG have a higher AMPA/NMDA current ratio, and a higher spine density (Kitamura et al., 2017; Ryan et al., 2015), suggesting that they undergo synaptic plasticity upon recruitment into an engram trace. An unexpected result of the c-fos-based optogenetic tag-and-reactivate experiments is the ability of light stimulation to reinstate the engram even when the formation of the natural engram is apparently blocked by anisomycin infusion (Ryan et al., 2015) or by the pathological condition of Alzheimer's disease model (Roy et al., 2016). Not only was a consistent behaviour response elicited, but also the reactivation of a coherent subset of cells in the downstream circuit with the originally activated one was observed (Ryan et al., 2015).

While the recall observed despite anisomycin infusion apparently contrasts with a role of potentiated synapses in

the encoding of memory, it must be noted that whole-cell ChR2 stimulation can be very powerful and drive stronger synaptic transmission than the physiological one; indeed, it can also be used to induce LTP (Roy et al., 2016), and ChR2 stimulation is able to reactivate even a no longer active engram in the DG, when the memory trace has become DG-(and, possibly, hippocampal-) independent (Nadel and Moscovitch, 1997) and the newly formed spines have been lost (Kitamura et al., 2017). Consistently, optogenetic reactivation with a light power below the one inducing a saturating response was unable to reinstate the engram when anisomycin was administered in the encoding phase (Roy et al., 2017b). This suggests that the engram formation was not completely blocked, but rather hindered. Only a percentage of synapses might have been potentiated in this regime of low protein synthesis compared to untreated controls, and their number and/or degree of potentiation would not be enough to support the recall initiated by natural cues. This is supported by the finding that, while LTP is still possible upon inhibiting protein synthesis, the reduced availability of new protein products causes synapses to compete for them, and potentiation of certain pathways takes place at the expense of others (Fonseca et al., 2004). Consistently, reinstating LTP in silent CA1 engram cells by PAK1

overexpression rescues natural memory recall impaired by anisomycin (Roy et al., 2017b), in analogy to what observed in Nabavi et al. (2014).

In conclusion, there appears to be some difficulties in reconciling the long-established paradigm of synaptic plasticity as the framework mechanism for memory formation and the cellular engram model. The aim of this thesis is to address this gap by the development of a novel experimental strategy.

Aim of the thesis

To directly test the role of potentiated synapses in the encoding of memory, a suitable molecular tool is still lacking. Being able to re-excite the set of synapses that undergo potentiation during the acquisition of a memory would demonstrate their role in the encoding of the memory itself. Optogenetic and chemogenetic ion channels have been widely used to excite or silence neural activity (Yizhar et al., 2011), and constitute the standard in engram cells experiments for their ability to be activated by otherwise physiologically inert signals (Garner et al., 2012; Liu et al., 2012). Although patterned light excitation allows controlled neuron excitation with optogenetics, (Packer et al., 2013),

and single spines can be excited with two-photon laser focalization (Packer et al., 2012), it would still be required to know the identity of the spines to be excited. Expressing ChR2 (or variants) at potentiated synapses would solve this problem, as also wide field illumination would result in synapse-specific illumination.

To date, targeting sequences have been fused to opsin coding sequence to localize ChR2 to the somatodendritic compartment (Lewis et al., 2009), the axon compartment (Lewis et al., 2011) or the axon initial segment, (Grubb and Burrone, 2010), or to confine it to the soma (Baker et al., 2016). Protein localization sequences have been used for example, to simulate the centre-surround antagonism in retinal ganglion cells (Greenberg et al., 2011), and to inhibit presynaptic neurotransmitter release (Lin et al., 2013). However, it looks a demanding task for protein localization sequences to be transported and localized in activity-dependent manner to potentiated synapses, and it is unlikely that the targeting precision that could be obtained with such a protein-targeting approach would be satisfactory.

The scope of this thesis is then to develop a suitable methodology to identify and tag potentiated synapses during memory encoding, and therefore test their identity as

candidate synaptic engrams. In order to be able to reactivate tagged synapses at a later time, they ought to be tagged with a light-sensitive ion channel of the opsin family. This will enable to test their role in memory formation and storage. I will describe here the development of such an approach, based on a hybrid RNA/protein approach to express and retain ChR2 variant ChETA at potentiated synapses *in vitro* and *in vivo*. The developed system, named SynActive, relies on LTP-dependent local protein translation of normally repressed transcripts, a property conferred by Arc RNA sequences, and on posttranslational protein anchoring and localization with peptide sequences interacting with the postsynaptic density (PSD).

Materials and Methods

Constructs

palmitoyl-Cherry-MS2 sequence was generated by cloning the cDNA of Cherry encoding the palmitoylation sequence from GAP43 in N-terminal position, whereas the *ms2* sequence was derived from plasmid pSL-MS2 12X (Addgene #27119) (Zacharias et al., 2002). HA-MS2 plasmid was generated inserting ms2 sequences after the HA tag cDNA in pcDNA3-HA (Invitrogen). *Arc* DTE is nts 2035-2701 (NCBI NM_019361.1), as reported in Kobayashi et al. (2005). Reference NCBI entry NM_019361.1 [Rattus norvegicus activity-regulated cytoskeleton-associated protein (*Arc*), mRNA] bears T2130A mismatch and T2293Δ deletion, as reported by the Authors (H.Kobayashi, personal communication).

The cDNA for CaMKII DTE was derived from pNECKu1481-2708 in Blichenberg et al. (2001). The cDNA for MAP2 DTE was derived from pNEu2432-3071 in Blichenberg et al. (1999). The cDNA for IMPA1 ATE was amplified from pSC-A IMPA1L (Andreassi et al., 2010) and corresponds to IMPA1 nts 2044-2165. Sequence maps nts 1126-1249 of NCBI entry GU441530.1 [Rattus norvegicus strain Sprague-Dawley inositol (myo)-1(or 4)-monophosphatase 1 (Impa1-L) mRNA, 3' UTR].

The coding sequence for EGFP-MS2 coat protein-NLS was constructed and cloned into pcDNA3.1(+) (Invitrogen) from plasmid Cherry-MS2 coat protein-NLS (a gift from A.Marcello, ICGEB Trieste). ChETA-Cherry cDNA was PCR amplified from plasmid pAAV-CaMKII-hChR2 (E123A)-mCherry-WPRE (Gunaydin et al., 2010). ChETA-Cherry-SYN (S-Ch) was generated by oligo cloning sequence GCCGCCGCTGCTTCAATTGAAAGTGACGTGGCCGCAGCTGCCGAAACCCAGGTGTAATAA (IDT technologies) using unique site BglII site at 3' end of Cherry sequence; as a result, the sequence encoding the SYN tag (AAAASIESDVAAAAETQV) sequence is in frame with ChETA-Cherry coding sequence. A-Ch and SA-Ch constructs were generated by inserting *Arc* 5' and 3' UTRs before and after ChETA-Cherry and S-Ch cDNA, respectively. *Arc* UTRs were amplified from plasmid pCMV-ArcF encompassing whole 5'UTR and first 13 nucleotides of *Arc* CDS, where start ATG was mutated to ACG, and whole 3'UTR (Kobayashi et al., 2005). MS2 sequence was inserted downstream the STOP codon before the 3'UTR. Constructs were cloned into plasmid pcDNA3.1(+) (Invitrogen) under CMV promoter. Soluble EGFP was expressed from plasmid pN1-EGFP (Clontech).

A plasmid encoding the postsynaptic marker Homer1c-EGFP was kindly provided by D.Choquet, Institut interdisciplinaire de Neurosciences CNRS, Université Bordeaux 2. Membrane-anchored cyan protein palmitoyl-Turquoise2 was expressed from Addgene plasmid #36209. Green calcium fluorescent indicator GCaMP6s was expressed from pGP-CMV-GCaMP6s (Addgene #40753). SEP-GluA1 was expressed from Addgene plasmid #64942.
For in utero electroporation, SA-Ch sequene was inserted downstream of third generation TRE promoter (Sato et al., 2013); the plasmid also contained the minimal CK0.4 promoter driving the expression of rtTA2S-M2 transactivator. rtTA2s-M2 cDNA was amplified from the vector TMPrtTA (Barde et al., 2006), while the parental plasmid was custom synthesised by LifeTechnologies (USA). The resulting bicistronic expression plasmid was named pTRE3-SA-CK-rtTA. In in utero electroporation experiments, it was cotransfected with plasmid pCAGGS-rtTA-TRE-EGFP, which was generated by cloning rtTA2S-M2 and TRE-EGFP sequences into plasmid pCAGGS (Dal Maschio et al., 2012). The DNA encoding EGFP under the TRE promoter (TRE-EGFP) was amplified by PCR from plasmid pSIN-TRE-EGFP, provided by Dr L.Marchetti. Sequences are reported in Appendix A.

Cell culture.

SH-SY5Y (EACC) were cultured in DMEM:F12 (Gibco) with 10% FBS (Invitrogen), 100 U/ml penicillin, 0.1 mg/ml streptomycin 2 mM glutamine.

Primary cortical and hippocampal neurons were extracted from P0 B6129 mice as described in Beaudoin III et al. (2012), with modifications. Pups were decapitated, the head was sterilized in ethanol and the skull was cut open to remove the brain, which was placed in cold dissection medium (calcium-free HBSS, 100 U/ml penicillin, 0.1 mg/ml streptomycin). Cortices and hippocampi were surgically isolated and meninges were removed. Tissues were minced and triturated in cold dissection medium and digested in 0.1% trypsin (Invitrogen) at 37°C for 5-10 minutes, an equal volume of 10% FBS DMEM (Invitrogen) 100 U/ml DNase (Sigma-Aldrich) was added to inhibit trypsin. Cells were dissociated by gentle pipetting, and pelleted by centrifugation. Neurons were seeded on previously acid-washed, poly-D-lysine coated glass coverslips or plasma-treated poly-D-lysine coated Willco dishes. For initial plating, neurons were maintained in Neurobasal-A medium (Invitrogen) supplemented with 4.5

g/l D-glucose, 10% FBS, 2% B27 (Invitrogen), 1% Glutamax (Invitrogen), 1 mM pyruvate, 4 μM reduced glutathione, 12.5 μM glutamate. From the following day on, neurons were grown in Neurobasal-A medium (Invitrogen) supplemented with 2% B27 (Invitrogen) 1% Glutamax (Invitrogen) 1-10 μg/ml gentamicin. On DIV 2, 2.5 μM AraC was added to reduce glia growth. Medium was refreshed every 2-4 days. DTE expression was evaluated in DIV 12 neurons, while all other experiments employed div 17-19 neurons.

Neurons were transfected with calcium phosphate method the day before experiment. A total amount of 10μg DNA is dissolved in 100μl 250 mM $CaCl_2$, then 100μl of 2xHBS (280 mM NaCl, 50 mM HEPES, 1.4 mM Na_2HPO_4 pH 7.1) are added dropwise while vortexing. The final solution is let stand at room temperature for 20 minutes; 100μl of the resulting suspension is added to a 24-wells well. After 90 minutes, the medium is removed, cultures are thoroughly washed with 1mM $MgCl_2$ 2mM $CaCl_2$ HBSS to remove precipitate, and replenished with 1:1 conditioned:new culture medium.

All procedures involving animals respect Italian Ministery of Health as well as Italian National Research Council (CNR) guidelines.

FRET

SH-SY5Y expressing either MS2-EGFP and MS2-Cherry alone or in combination with HA-*ms2* (transfection molar ratio 1:1:0 or 1:1:6) were acquired 48 hours post-transfection with confocal microscope Leica TCS SP5 on DM6000 using oil objective HCX PL APO CS 40.0X (NA=1.25), under humidified 5% CO_2 atmosphere at 37°C. Ar 488 nm and Ar 561 nm laser lines were used for sequential acquisition. Point mCherry fluorescence bleaching in the cytoplasm was performed with 2-3 min 561 nm maximum laser power illumination until complete loss of red fluorescence. Pre- and post-bleaching 512x512 pixels images were acquired with 1 Airy unit pinhole aperture. FRET efficiency was calculated according to Roy et al. (2008) as

$$E_{FRET} = 1 + \left(\gamma \frac{I_{EGFP,488}}{F_{FRET}}\right)^{-1}$$

where: $F_{FRET} = I_{Cherry,488\ nm} - \alpha \cdot I_{EGFP,488nm} - \beta \cdot I_{Cherry,561nm}$ the FRET intensity corrected for the donor and acceptor spectral crosstalk as, with α and β estimated from independent samples expressing MS2-EGFP or MS2-Cherry alone yielding α=0.081±0.005 and β=0.108±0.005 (mean±95%CI); and

$$\gamma = \frac{\mu_{Cherry} \cdot \varphi_{Cherry}}{\mu_{EGFP} \varphi_{EGFP}} \cong \frac{F_{FRET}^{pre} - F_{FRET}^{post}}{I_{EGFP}^{post} - I_{EGFP}^{pre}}$$

where φ is the quantum yield μ is the proportionality factor between the arbitrary units in the emission channel for FP and the total number of emitted photons. For the MS2-EGFP/MS2-Cherry pair, we measured Γ=0.325±0.071 (mean±95%CI).

FLIM–FRET

SH-SY5Y cells were transfected as described above (FRET section). Cells were analysed 24 to 30 hours post transfection with the same set-up described for FRET experiments but using a HCX PL FLUOTAR 100X, NA 1.30 oil objective. Pinhole was set to 1.53 Airy units and 512x512 pixel images were acquired with a pulsed laser at wavelength at 470 nm at 40 MHz repetition rate. TCSPC photon counting and fitting were performed with the software SymphoTime integrated with the Leica LAS AF FLIM wizard. Reference EGFP-expressing cells are a SH-SY5Y derived line expressing EGFP under a doxycycline-responsive promoter (unpublished results). In a parallel set of experiments, cells were fixed at 30 hours post-transfection for 10’ in 4% formaldehyde, 5% sucrose PBS solution after

two cold PBS washes, and kept in PBS at 4°C until acquisition with the set-up described here.

Neuron treatments.

In DTE-driven translation experiments, neurons were treated for 1h with either KCl to a final concentration of 10mM or saline added to bath.

In the comparison of ChETA constructs expression, neurons were treated with (i) BDNF: hBDNF (Alomone) 100ng/ml 90'; (ii) KCl: KCl 10mM 90'; (iii) LTP: 20' in 2mM $CaCl_2$/1mM $MgCl_2$ ACSF followed by 10' in 2mM $CaCl_2$/Mg^{2+}-free ACSF 5.4mM KCl 100 µM NMDA (Sigma-Aldrich) 20 µM glycine (Sigma-Aldrich) 0.1 µM rolipram (Sigma-Aldrich) as described in Palida et al. (2015), followed by 90' in culture medium; (iv) AP5: 50 µM AP5 (Sigma-Aldrich) from transfection to analysis (17-20h). Stimulated neurons expressing SA-Ch and Homer1c-EGFP in Figure 35 are treated with 20' 2mM $CaCl_2$/1mM $MgCl_2$ ACSF followed by 5' in 2mM $CaCl_2$/Mg^{2+}-free ACSF 60mM KCl 100µM NMDA (Sigma-Aldrich) 20 µM glycine (Sigma-Aldrich) and fixed after 90'.

Immunofluorescence.

Neurons expressing A-Ch or SA-Ch were fixed in 2% formaldehyde 5% sucrose PBS and permeabilised in 0.1% Triton X-100. After PBS washing, samples were blocked in 1% BSA PBS, and primary antibodies anti-Cherry (GeneTex GTX59788, 1:500) and anti-PSD95 (Abcam ab9909, 1:600) were used in 0.5% BSA PBS. Samples were washed three times in 0.5% BSA PBS, then primary antibodies were detected with anti-rabbit-TRITC (Sigma-Aldrich T6778, 1:200) and anti-mouse-Alexa647 (Thermo Fisher A32728, 1:200) in 0.5% BSA PBS. Coverslips were mounted in Fluoroshield (Sigma-Aldrich) mounting medium.

Hippocampal neurons expressing EGFP, ChETA/EGFP, S-Ch/EGFP or SA-Ch/EGFP for 24h were processed as above. Primary antibody was 1:2500 anti-MAP2 (Abcam ab5392) and it was detected with anti-chicken-Alexa647 (Abcam ab150171, 1:250). For surface NMDAR/AMPAR immunostaining, DIV 9 neurons were transfected with plasmids encoding SA-Ch, and palmitoyl-Turquoise2, or palmitoyl-Turquoise2 alone; on the third day from transfection, neurons were fixed in 4% formaldehyde 5% sucrose PBS and washed, blocked in 5% BSA PBS and stained with 1:500 anti-GluR1-NT (Millipore MAB2263) and 1:500 anti-GluN1 (Alomone AGC-001), and followed

by 1:200 anti-mouse-Alexa488 (Thermo Fisher A32723)/1:200 anti-rabbit-Alexa647 (Thermo Fisher A32733) and mounting.

Microscopy.

512x512 pixels optical sections were acquired with a confocal microscope (Leica TCS SP5 on DM6000, equipped with MSD module) using an oil objective HCX PL APO CS 40.0X (NA=1.25), and pinhole was set to 1.47AU. Digital zoom was adjusted to correctly sample spines. For whole cell reconstruction z-stacks were acquired every 0.5 μm. Sequential illumination with HeNe 633, Ar 561, Ar 488, Ar 458, and diode (Picoquant, Berlin, Germany) 405 laser lines was used for Alexa647, TRITC and Cherry, EGFP, Turquoise2 and DAPI, respectively.

For two-photon uncaging, images were acquired using an Olympus FV1000 confocal module on an inverted IX81 microscope with immersion oil objective UPLSAPO 60X (NA=1.35), and pinhole was set to 180 μm. Digital zoom was set to 8x. I used Ar 488 and HeNe 543 laser lines for EGFP and Cherry excitation, respectively. For two-photon illumination, 720 nm line was set on a tunable Chameleon Vision II Ti:Sapphire pulsed laser (Coherent, 80MHz).

Green and red channels were acquired before 720 nm stimulation (-5' time point) and 60' after medium change (see the following two-photon uncaging section).

Two-photon uncaging.

DIV 8-10 cortical neurons were seeded on plasma-treated, poly-D-lysine coated Willco dishes and transfected the day before experiment. Neurons were maintained in Mg^{2+}-free ACSF (in mM, 136 NaCl, 2.5 KCl, 2 $CaCl_2$ 10 D-glucose, 10 HEPES, 2 pyruvate, 1 ascorbic acid, 0.5 myo-inositol) with 10 μM forskolin (Tocris BioSciences) 1 μM TTX (Tocris BioSciences) and, where indicated, 2.5 mM MNI-caged glutamate (Tocris BioSciences) for 20' before uncaging. Following EGFP and Cherry acquisition, 30 pulses (720 nm, 9-13 mW at the objective lens) of 7 ms were delivered at 0.5 Hz at 0.5-1 μm from spine head as in (Hill and Zito, 2013). After 5', medium was changed to 1mM $MgCl_2$ ACSF supplemented with 2% B27 and the same dendrite was imaged after 60'. The mock stimulation was performed in the same way except that MNI-glutamate was not added in the medium. For time course experiments, red and green channels were acquired 20' and 5' before the uncaging start. Green channel was acquired at 0.5', 1', 2',

5', 30', 60' and 90' following uncaging, and red channel was acquired at 5', 30', 60' and 90'. Throughout the whole protocols, neurons were maintained at 37°C under humidified 5% CO_2 atmosphere. In experiments with translation inhibitors, 5μM anisomycin (Sigma-Aldrich) was present in the medium all the time staring from the 20' preincubation.

Calcium imaging.

Div 7-11 cortical neurons grown on glass-bottom coverslip expressing GCaMP6s and SA-Ch were imaged using an Olympus FV1000 confocal module on an inverted IX81 microscope with immersion oil objective UPLSAPO 60X (NA=1.35). Neurons were maintained in standard ACSF containing 2mM $CaCl_2$ 1mM $MgCl_2$ at 37°C under humidified atmosphere. In a parallel sets of experiments we included (i) VGCC inhibitors nifedipine 5μM (Sigma-Aldrich), Ni^{2+} (as $NiSO_4$) 500 μM and Zn^{2+} (as $ZnCl_2$) 500μM (Büsselberg et al., 1992) or (ii) 1μM TTX (Tocris Biosciences). SA-Ch was imaged at 543nm, and GCaMP6s was excited with Chameleon Vision II Ti:Sapphire pulsed laser (Coherent, 80MHz) tuned at 990 nm (actual peak was detected at 988±2 nm) to minimize Channelrhodopsin

excitation (Paluch-Siegler et al., 2015). Selected spines were identified comparing the 543nm and the two-photon channel. A rectangular imaging region of interest (ROI) was defined on the dendrite immediately under the selected spines, whereas the excitation ROI was set on the spine. We acquired 500 frames every 20ms by exciting at 990 nm using RM690 filter; GCaMP6s fluorescence was acquired in the 500-600nm range. The size and dimension of the ROIs were maintained constant in all experiments. After 50 frames, we stimulated the spine with a 10ms pulse of the 488nm laser line in spiral scanning mode in the excitation ROI, and continued imaging. 488nm laser power was measured to be 8.9-10.7μW upon steady illumination (Schoenenberger et al., 2008), and 990 nm laser power was 2.5-3.7mW. Randomly between stimulations, trains were performed identically except the 488nm laser line was kept switched off. After dark frame subtraction, ΔF/F values were integrated for the first 200 frames following stimulation.

Culture optogenetics.

DIV 17-19 hippocampal neurons were grown on poly-D-lysine coated glass coverslips in 24wells. The day after transfection, neurons expressing SA-Ch and EGFP, ChETA-

Cherry and EGFP, or EGFP alone, were put in standard 2mM $CaCl_2$ 1mM $MgCl_2$ ACSF and illuminated with single channel PlexBright LED Module 450nm connected to an optical fiber (THORLABS, 200 μM diameter, 0.39 NA, ceramic ferrule) at 1-3 mW peak power (measured at the end of the fiber). 10 trains of 13 pulses at 100Hz were repeated at 0.5Hz; four stimulations at different positions were performed on each culture in order to evenly illuminate the whole culture area.

In a first set of experiments, neurons were pre-treated for 3 hours with 40 μM CNQX 100 μM AP5 1 μM TTX. Medium was changed to standard ACSF 2mM $CaCl_2$ 1mM $MgCl_2$ 1 μM TTX and cultures were light stimulated or maintained in the dark; 7.5 minutes after stimulation neurons were fixed for 15 minutes in 2% formaldehyde 5% sucrose PBS supplemented with 1mM Na_2VO_4 1mM NaF to inhibit phosphatases; after permeabilisation in ice-cold methanol, neurons were blocked in 5% BSA 1mM Na_2VO_4 1mM NaF PBS and subsequently incubated overnight with 1:100 mouse anti-phosphoCaMKII (Thermo Fisher MA1-047 clone 22B1) and 1:300 rabbit anti-Cherry (GeneTex GTX59788) in 2% BSA PBS. Secondary antibodies were 1:100 anti-rabbit-TRITC, 1:100 anti-mouse-Alexa647 in 2% BSA.

In the second set of experiments, neurons were light-stimulated in standard ACSF 2mM $CaCl_2$ 1mM $MgCl_2$; after stimulation, neurons were put back into culture medium; parallel cultures did not undergo such a treatment and were maintained in the dark. After one hour, cells were fixed in 2% formaldehyde 5% sucrose PBS and permeabilised in 0.5% Triton X-100; after PBS washing, cells were blocked in 4% BSA PBS for 1 hou, and incubated with 1:100 rabbit polyclonal anti c-fos (Santa Cruz sc-52) in 2% BSA 0.05% Triton X-100 PBS. Secondary antibody was anti-rabbit-Alexa647. Samples were mounted in Fluoroshield with DAPI (Sigma-Aldrich).

In utero electroporation and animal experiments.

Hippocampal in utero electroporation was performed as described in Dal Maschio et al. (2012). E15.5 timed-pregnant CD1 mice (Charles River SRL, Italy) were used. Time-pregnant matings were performed on the evening; the day after mating was defined as E0.5 and the day of birth was defined as P0. Embryos from time-pregnant mothers were electroporated unilaterally with pTRE3-SA-CK-rtTA and pCAGGS-rtTA-TRE-EGFP. Mice were P24-P26 on the day of the experiment. A first group of mice received 0.5mg

doxycycline (1mg/30g BW) in saline solution intraperitoneally once a day for two days; on third day, brains were fixed by transcardial perfusion of 4% formaldehyde. A second group of mice received an additional intraperitoneal injection (1mg/mouse) on day 3, and brains were fixed on day 4. On day 4, mice of the novel context group were put separately in a different cage (novel context). Two of the walls had visual cues (3cm black/white vertical stripes and 3x3 cm black/white dashboard); one object was put in the cage (a blue 50ml Falcon tube) (Rinaldi et al., 2010). After 3 hours, brains were fixed by 4% formaldehyde transcardial perfusion. Home cage animals were kept in their cage until perfusion. After perfusion, brains were post-fixed overnight in 4% formaldehyde in PBS, then cryoprotected in 30% sucrose PBS. Coronal sections of 60-80µm were cut with a cryostat. Slices were mounted in Vectashield or Fluoroshield with DAPI (Sigma) and native fluorescence was imaged with Leica SP5 (see above) with 1.5AU pinhole; stacks encompassing the whole section were acquired every 0.5µm. To calculate intensity profiles in CA1 large fields, immunofluorescence was performed on free floating slices. Slices were blocked 1h in 0.3% Triton X-100 in 10% normal goat serum (NGS, Sigma) PBS, then incubated overnight in 1:500 anti-GFP (Abcam

ab38689) 1:500 anti-Cherry (Abcam ab16743) in 0.3% Triton X-100 10% NGS PBS at 4°C, washed three times (10' each) and incubated in secondary antibodies (anti-mouse-Alexa488 and anti-rabbit-Alexa647) 1:200 in 0.3% Triton X-100 10% NGS for 1h. After three washes in PBS, slices were mounted in Fluoroshield with DAPI.

The immunodetection of c-fos was performed on slices from home caged animals or exposed to the new context for 1hr as follows: slices were incubated in 3.5% H_2O_2 in PBS for 30', washed in TBS 0.3% Triton (TBST), blocked in TBST FBS 10% for 1hr, then incubated with anti-c-fos (Santa Cruz sc-52) 1:1000 in TBST 10%FBS overnight at 4°C. After 3 washes in TBST, slices were incubated with biotinylated anti-rabbit 1:500 in TBST 10%FBS for 3hr, then washed thrice in TBS. Biotin was detected with avidin-HRP (ABC kit, Vector Laboratories); DAB staining with glucose oxidase was performed for 10 minutes and stopped wih TBS. Finally, slices were mounted, dehydrated with xylene and included with Mowiol mounting medium.

Animal care and experimental procedures were conducted in accordance with the Italian Institute of Technology licensing and the Italian Ministry of Health.

Data quantification.

Spine number and subclass for neurons were assigned manually based on established nomenclature. Short spines with no apparent neck are classified as stubby; elongated spines whose head and neck diameters are similar are classified as thin, and spines with a defined neck and a prominent head are classified as mushroom. Filopodia were few in number across all samples and were excluded from analysis.

For the calculation of surface AMPAR/NMDAR ratio, ROIs were defined on dendrites from expressing neurons (SA-Ch/palmitoyl-Turquoise2 or palmitoyl-Turquoise2) and mean sGluR1/Alexa488 and sGluN1/Alexa647 intensities were calculated after background subtraction. The calculated value is the ratio of the two means.

Enrichment index (EI) was calculated as the ratio between the Cherry average intensity on the spine region (identified using the EGFP channel) and the average intensity calculated on the dendritic shaft between 1 and 2 μm away from the spine junction, after background subtraction. For the EI calculation, only expressing spines were included in the analysis. Homer1c-EGFP content was quantified by integrating EGFP intensity in correspondence to the PSD, and normalized by the mean intensity on the dendrite. SEP-

GluA1 Enrichment was calculated in an analogous manner to Cherry EI; for the comparison of the two EIs, the same regions were considered in the two channels.

For two-photon stimulation experiments, spines were identified in the EGFP filler channel, Cherry fluorescence was integrated in the corresponding channel after background subtraction. Intensity was calculated for images acquired immediately before photouncaging and after 60' for stimulated and neighbouring spines. The relative change in Cherry intensity (Δ_{Ch}) at time point i was calculated as the difference, normalized for the initial intensity as

$$\Delta_{Ch} = \frac{I_c(i) - I_c(-5')}{I_c(-5')} .$$

Volume change was calculated in an analogous way as

$$\Delta V = \frac{I_{GFP}(i) - I_{GFP}(-5')}{I_{GFP}(-5')} ,$$

where I_{GFP} is the spine integrated density in the EGFP channel, normalized by the mean value in the dendrite underneath.

For the intensity profiles shown, 1024x1024, 0.5µm stacks of immunostained slices were acquired by centering the field on the CA1 region above the DG upper blade. For each channel, slices were summed to generate the projection image. After background subtraction, linear profiles of

325μm were measured starting from the stratum oriens toward the stratum lacunosum-moleculare. Profiles were aligned in the DAPI channel by setting the start of the stratum pyramidale, identified as the stratum with packed soma, at 100μm. For EGFP and Cherry channels, resulting profiles were averaged and baseline was subtracted. Baseline was evaluated in the non-electroporated hemisphere in an analogous manner. To reduce noise, resulting data were smoothened with SigmaPlot v12 (SYSTAT) with the median method (0.01 sampling).

For in vivo experiments, spine distance was calculated as the euclidean distance as

$$d = \sqrt{(x_1 - x_2)^2 + (y_1 - y_2)^2 + (z_1 - z_2)^2},$$

where (*x*,*y*,*z*) are the spine coordinates in microns. Distances were calculated for each SA-Ch positive spine to all other SA-Ch positive spines and all SA-Ch negative spines with a custom made program in R (version 3.3.1) (R core team, 2013). Distance to first potentiated neighbour and to first non-potentiated neighbour are defined as the minima of the two sets, respectively. The distances to first potentiated and first non-potentiated neighbour were also calculated for randomly shuffled data by using the "sample" module in R to randomly assign the identity of spines to the (*x*,*y*,*z*)

positions; for every dendrite, five shuffled datasets were considered.

Probability data were calculated as follows with a custom made program in R: for each SA-Ch positive spine we considered the first 20 neighbour spines (both directions along the dendrite were considered). For each dendrite, this gave a set of *N* sequences of 20 spines that could be aligned from position 1 to position 20 generating a *N* x 20 matrix. For each *i*-th column, we counted the number of positive spines, and divided it by the number of rows N. The resulting value is the probability of finding a potentiated spine in position *i*. To calculate the increase in probability, for each dendrite probability data were divided by the expected probability of finding a potentiated spine in the corresponding position if they were randomly arranged. Thus, calculated values were divided by $\frac{p-1}{T-1}$, where *p* and *T* are the number of potentiated spines and the total number of spines in each dendrite, respectively.

Clusters of SA-Ch positive spines were calculated with the "Hierarchical cluster analysis" function in R (contributed to STATLIB by F.Murtagh) with the "single linkage" method with a 2μm threshold. Thus, two spines belong to a cluster if their distance (calculated as above) is lower than 2μm.

Cluster dimension was calculated as the number of members for each cluster.

To calculate the Separation Index (SI), the average fraction of potentiated spines (*f*) was calculated for each slice as the sum of SA-Ch positive spines in dendrites belonging to the slice divided by the total number of spines. Then, for each dendrite, the expected number of potentiated spine p^* was calculated as f x T, where T is the number of spines in the dendrite. SI was calculated as the absolute value of $\frac{p-p^*}{p^*}$, where p is the number of potentiated spines in the dendrite.

The cluster extension was defined calculating all Euclidean distances between spines in a cluster, and taking the maximum distance. The distance along the axis of the molecular layer in the DG was defined as the distance of the centroid of the cluster (which is equivalent to the mean of the relative positions of the spines in the cluster). Scripts are available in Appendix C.

Statistics.

Image analysis was performed using ImageJ. Statistical analysis was performed with OriginPro v9.0 or GraphPad Prism 6. Differences between two groups were evaluated with two-tailed Student's t-test. Residues distributions were compared with Kolmogorov-Smirnov test. Multiple

comparisons were made by one-way ANOVA followed by post-hoc Bonferroni test, unless otherwise stated. Significance was set at α=0.05. 126 neurons were analyzed for spine classification; 106 dendrites from 35 neurons were analyzed in for sNMDAR/sAMPAR calculation. 756 frames (21564 spines) were used for ChETA constructs expression calculation. A total of 1493 spines was analysed for EI calculation. For PSD95/ChETA-Cherry co-localization, a total of 2251 spines from 44 neurons were analyzed. For Homer1c-EGFP/SA-Ch correlation, 302 spines from 27 neurons were analysed; for SEP-GluA1 experiments, 487 spines from 66 different neurons were analysed.

For two-photon uncaging experiments, a total of 48 samples were analysed, and a total of 118 spines were considered. For the time course experiments in two-photon uncaging, we considered the following number of spines: uncaging, 18 stimulated and 24 nearby spines; uncaging with anisomycin, 15 stimulated and 21 nearby spines; without MNI-caged glutamate, 8 stimulated and 8 nearby spines.

For GCaMP6s imaging, 55 spines were stimulated, out of which 17 in presence of VGCC inhibitors, and 17 in presence of TTX. For in vivo analysis, the following number of dendrites (spines/slices/animals) were considered: CA1 home cage 93 (6703/8/4), DG home cage 52 (4157/9/4),

CA1 novel context 111 (10223/8/3), DG novel context 58 (4865/8/3). 13 dendrites were excluded from the calculation of the increase in probability because (i) the fraction of positive spine was below the defined threshold of 0.05, or (ii) it was not possible to define a whole set of 20 neighbours. Comparison between groups were distributions were not assumed as normal was performed with Kruskal-Wallis test, followed by Dunn's test for pairwise comparison.

All statistical information is provided in Appendix B.

SynActive Generation and Validation

The SynActive approach

In order to tag potentiated synapses, the reporter should recapitulate the processes that take place at synapses during long-term potentiation. As seen in the previous sections, local translation is associated with the potentiation of synaptic transmission, and blockade of translation with anisomycin impairs LTP formation. When synapses are stimulated above threshold, translation of genes encoded in dendritic transcripts take place. Thus, any effector or reporter for potentiation should also be translated locally after LTP induction. This property is conferred by RNA sequences that mediate the localization and the translational regulation of the transcript (Figure 20). After local translation, protein-protein interaction may hold the new protein in place; hence, I reasoned that adding a short peptide would help improving retention and specificity.

In this section, I will describe the generation and characterization of a SynActive reporter, starting from the comparison of candidate RNA sequences to regulate translation in an activity-dependent manner, and the test of the impact of the peptide tag on the localization of the reporter. Then, I will describe the response of SynActive translation to neuron treatments and focal LTP induction.

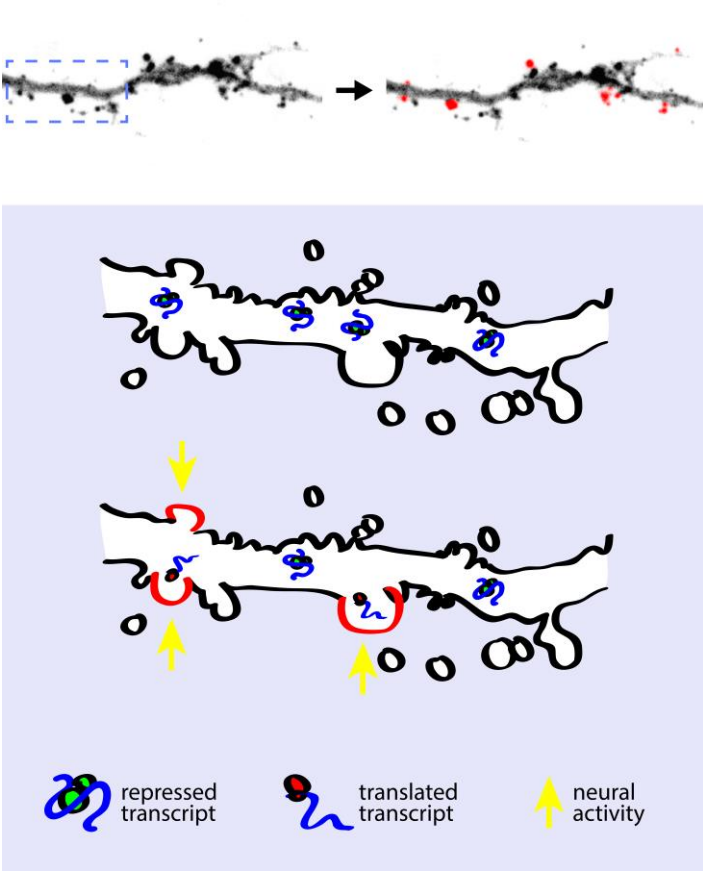

Figure 20 Experimental scheme for the SynActive approach. SynActive transcript is present in dendrites in a repressed state and, when neural activity induces synaptic potentiation, the reporter is translated locally, and hence expressed to selected synapses.

The SynActive reporter that is the object of this thesis is a Channelrhodospin variant (see Introduction), so the last part

of this section will be dedicated to the characterization of its functionality.

RNA candidates

The number of dendritic RNAs is vast and include transcripts as different as coding and non coding RNAs (Doyle and Kiebler, 2011). Among the most dendritically enriched RNAs there are αCaMKII, MAP2 and Arc (Cajigas et al., 2012). An ideal RNA candidate would have low expression under resting condition, and drive translation after synaptic activation. I therefore developed a dual reporter to visualize the RNA localization and the protein product; as shown in Figure 20a, the cDNA of the fast-maturating red fluorescent reporter mCherry (Shaner et al., 2004) was fused to 12 *ms2* stem loops after the Stop codon. *ms2* sequences are recognised by the MS2 protein which I fused to green fluorescent protein EGFP (Fusco et al., 2003). Downstream the *ms2* sequences I inserted candidate DTEs to test their effect on RNA targeting and translation; mCherry was fused to a palmitoylation sequence to anchor the protein to the plasma membrane and slow diffusion (Aakalu et al., 2001; Zacharias et al., 2002).

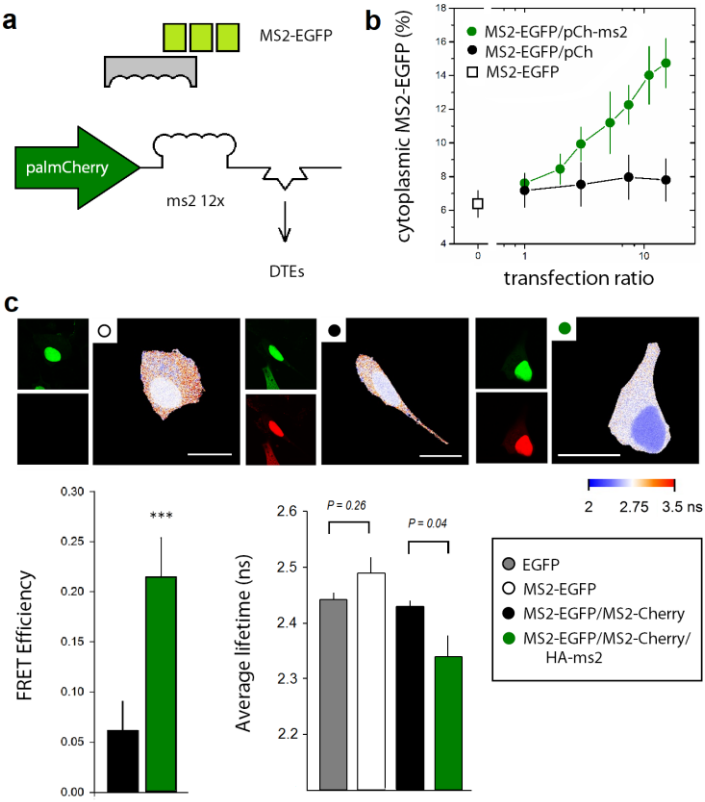

Figure 21 **a** schema of RNA/translation reporter system **b** Fraction of cytoplasmic MS2-EGFP signal at varying levels of palmCherry-ms2 (green) or palmCherry (black) **c** HA-ms2 RNA increases FRET between MS2-EGFP and MS2-Cherry in the cytoplasm. FRET efficiency and EGFP lifetime. Scale bar 20 µm. ***p<0.001, two-tailed Student's t-test. Data are mean±sem

MS2-EGFP is fused to an NLS (as commonly done, e.g. in Fusco et al. (2003)) so in the absence of bound RNA it is retained in the nucleus. The population of cytoplasmic MS2-EGFP increases with the transfection ratio of

palmitoylCherry-*ms2*:MS2-EGFP plasmids, but not when *ms2* RNA sequences are absent (Figure 21b). The presence of transcripts with *ms2* sequences causes the export of bound MS2 protein, as demonstrated by FRET detection between MS2-EGFP and sister MS2-Cherry, evaluated with both a higher FRET efficiency and a reduced EGFP fluorescence lifetime (Figure 21c).

Comparison of dendritic RNAs

To compare the relative expression of palmitoylCherry (palmCherry) reporter when various DTEs are inserted in the 3'UTR (see Figure 20a), I transfected primary cortical neurons with plasmids encoding palmCherry-*ms2*-DTE and soluble EGFP. I then compared the enrichment of palmCherry dendritic pool expressed as the ratio of the dendritic intensity per length divided by the axonal intensity per length (DAR, or dendrite-to-axon ratio) (Figure 22a).

EGFP DAR was evaluated as internal control; EGFP is translated in the soma and the calculated DAR assumes values close to one, indicating that there is no preferential enrichment in dendrites or in axons (Figure 22b). Conversely, IMPA1 axonal targeting element (ATE) drives axonal translation and $\log_{10}$(DAR) assumes negative values.

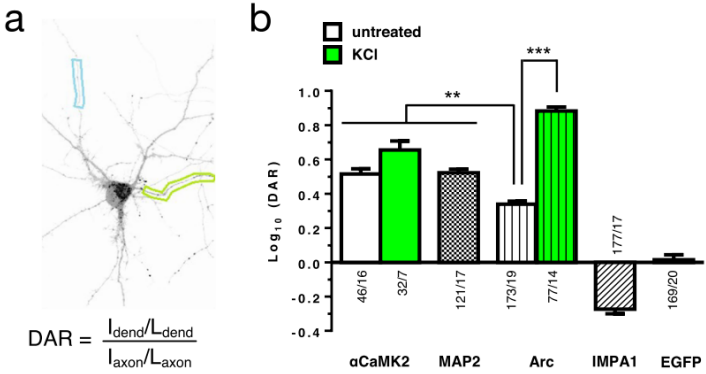

Figure 22 a schema exemplifying DAR calculation. Two typical regions are highlighted in green (dendrite) and light blue (axon). **b** Results of DAR calculation for various DTEs and ATE. Below are represented the number of dendrites/neurons used in the analysis. **P<0.01 and ***P<0.001 one-way ANOVA, Bonferroni comparison of means. Bars are mean±s.e.m

I focused on three prototypical dendritic RNAs, which are reported to exhibit a strong dendritic pattern (Cajigas et al., 2012): I compared the DTEs from αCamKII (Blichenberg et al., 2001), MAP2 (Cristofanilli et al., 2004) and Arc (Kobayashi et al., 2005) (see Appendix A). In unstimulated neurons, palmCherry was highly enriched in dendrites when αCamKII or MAP2 DTEs were present in the 3'UTR of the transcript. Arc DTE significantly enriched dendritic palmCherry pool, although at lower levels compared to αCamKII and MAP2 (Figure 21b). However, treating neurons with 10 mM KCl for 60 minutes dramatically

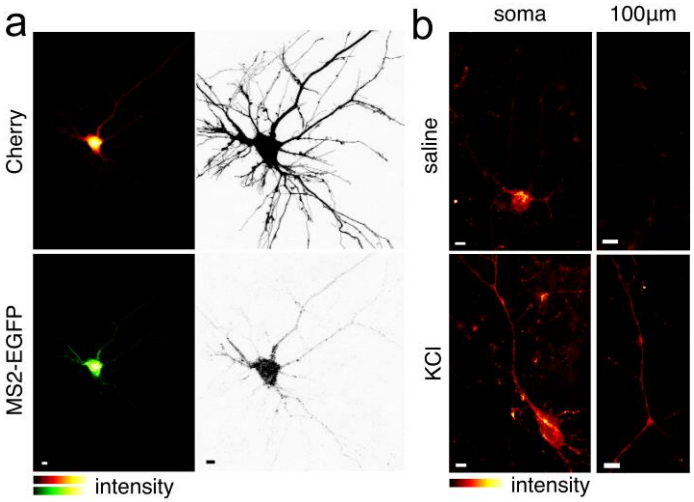

Figure 23 a Under resting conditions, palmCherry-*ms2*-Arc DTE/MS2-EGFP is present in neurons in granular form (see inset). **b** Unstimulated neurons express palmCherry at low levels in dendrites. 60 minutes KCl stimulation increases reporter levels in dendrites close to the soma and as distal as 100µm away from the soma. Scale bar, 5µm.

increased DAR for Arc DTE reporter, while the effect observed for αCaMKII DTE reporter was comparatively smaller (Figure 22b).

Arc DTE in the 3'UTR contributed both localization and regulation to the reporter RNA in neurons. Under resting conditions, palmCherry-*ms2*-Arc DTE bound to MS2-EGFP was mostly present in dendrites in the form of bright spots, indicating the RNA is present in granules, which are generally associated with translation repression (Figure

23a). Consistently, dendritic levels of palmCherry protein were rather low in unstimulated neurons; when neuron were stimulated with 10mM KCl, 60 minutes were sufficient to observe palmCherry expression both in proximal and distal dendrites (Figure 23b).

Cooperative protein/RNA sequences

While 3'UTR sequences usually contain targeting sequences, 5'UTR, and other parts of 3'UTR, may contain regulatory sequences that have permissive or instructive roles in translation (Kindler et al., 2005). Arc 5′-UTR has IRES-like activity (Pinkstaff et al., 2001), a property shared by other RNAs whose synaptic translation is associated to long-term potentiation (LTP) (Kindler and Kreienkamp, 2012; Kindler et al., 2005). I therefore cloned the cDNA of the fast-spiking ChR2 variant ChETA (Gunaydin et al., 2010) fused to the fluorescent protein mCherry between Arc 5' and 3' UTRs.

As ribosomes typically lie at the dendrite-spine junction (Ostroff et al., 2002; Steward and Schuman, 2001), I reasoned that a protein tag interacting with postsynaptic components would improve spine retention and enrichment

of the newly synthesized protein. I therefore fused a short bipartite tag (AAAASIESDVAAAAETQV, hereafter SYN tag) to the C-terminus of ChETA-Cherry. This tag is composed of the N-methyl-D-aspartate receptor (NMDAR) C terminus SIESDV and the PSD95-PDZ-binding consensus ETQV (Figure 24) (Kornau et al., 1995). ETQV sequence has been previously reported to enrich ChR2 localization at postsynaptic densities (Gradinaru et al., 2007). To compare the distinct contributions of the protein and RNA instructive signals, I generated three constructs and expressed them in primary neurons: (i) Arc 5′-ChETA-Cherry-*ms2*-Arc 3′-UTR (hereafter A-Ch); (ii) ChETA-Cherry-SYN tag-*ms2* (S-Ch), and (iii) Arc 5′-ChETA-Cherry-SYN tag-*ms2*-Arc 3′-UTR (SA-Ch) (Figure 25). Nor the SYN tag nor Arc RNA sequences appeared to alter neuron physiology: neurons

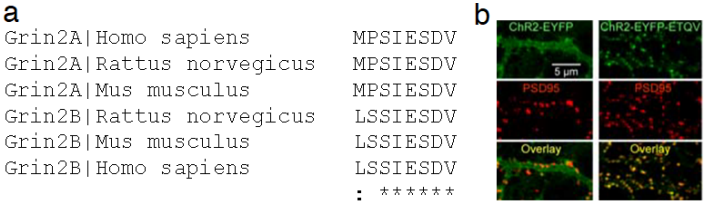

Figure 24 **a** Alignment of NMDAR2A and NMDAR2B sequences from primates and rodents identifies SIESDV consensus. Alignment was performed with ClustalΩ from EMBL-EBI. **b** PDZ-binding sequence ETQV enriches ChR2 at postsynsptic sites. From Gradinaru et al. (2007).

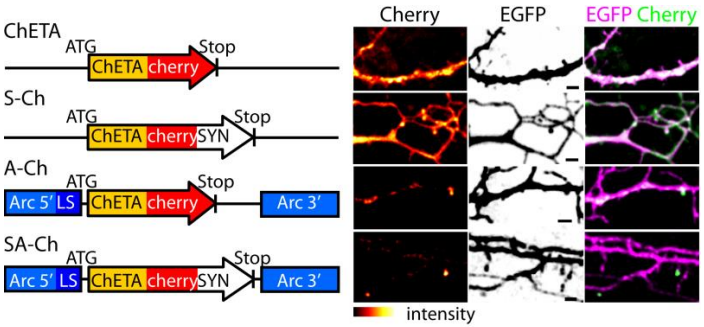

Figure 25 Schematic representation of the construct used in this thesis. On the right, representative images of neurons expressing the four constructs. Scale bar, 2µm

expressing S-Ch or SA-Ch were not morphologically different from neurons transfected with plamids encoding ChETA-Cherry and EGFP, or EGFP alone (Figure 26a). Furthermore, no change in spine density due to S-Ch or SA-Ch with respect to control neurons (EGFP and ChETA/EGFP) was observed ($P>0.999$, one-way ANOVA). There was no difference in spine class distribution, either (Two-way ANOVA, Factor A Construct DF=3 $P>0.999$, Factor B Spine type DF=2 $P<0.0001$) (Figure 26c). I also checked whether SA-Ch expression competed with endogenous receptors on the postsynaptic sites. I evaluated AMPAR and NMDAR expression by performing immunofluorescence on the two receptors' surface pool in

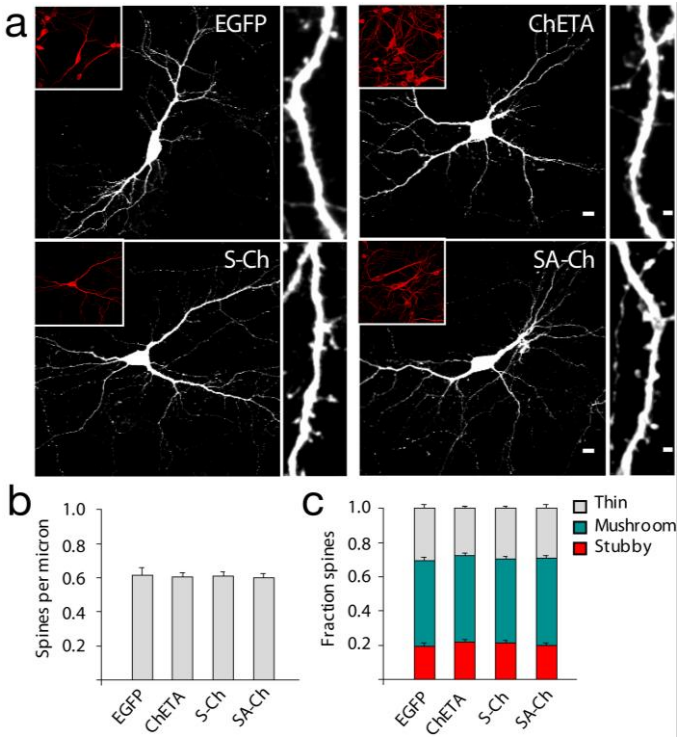

Figure 26 SA-Ch expression does not alter neuron morphology and spine density. **a** Representative neurons transfected with plasmids coding for EGFP alone, ChETA and EGFP, S-Ch and EGFP, and SA-Ch and EGFP. Inset (red) MAP2 immunofluorescence. On the right of each neuron, a magnification of the dendritic arbour. Scale bars: main image 10 µm, magnification 2 µm. **b** Quantification of average number of dendritic spines per micron. Results are not significantly different at the 0.05 level, one-way ANOVA, Bonferroni comparison of means. **c** SA-Ch does not alter spine morphology. Quantification of spine class frequency (stubby, mushroom, thin) for the four groups. Results are not significantly different at the 0.05 level, two-way ANOVA.

neurons expressing SA-Ch/palmitoylTurquoise2 or palmitoylTurquoise only (Figure 27a). I calculated the

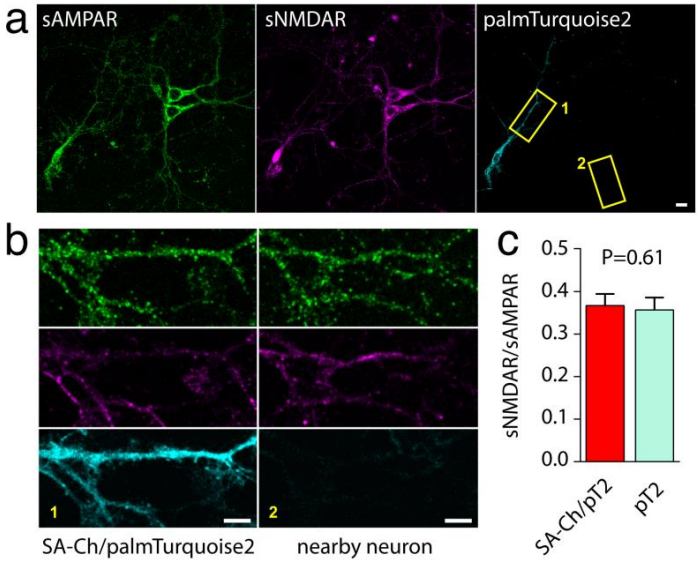

Figure 27 a Detection of surface pools of AMPAR and NMDAR in neurons expressing SA-Ch/palmotoylTurquoise2. No difference between transfected neurons (region 1) and non-transfected neurons (region 2) is evident. **b** Magnification of insets in (**a**.) **c** Quantification of sNMDAR/sAMPAR expression in neurons transfected with plasmids encoding SA-Ch/palmitoylTurquoise2 (SA-Ch/pT2) or palmitoylTurquoise2 (pT2) only. Results are not significative at the α=0.05 level, Student's t-test. Scale bars: main image 10 μm, magnifications 5 μm

relative proportion of the two glutamate receptors (sNMDAR/sAMPAR) and no significant difference between the two samples (P=0.62, Student's t-test) was found.

To evaluate the translation response of the three constructs, as well as that of the parental unmodified

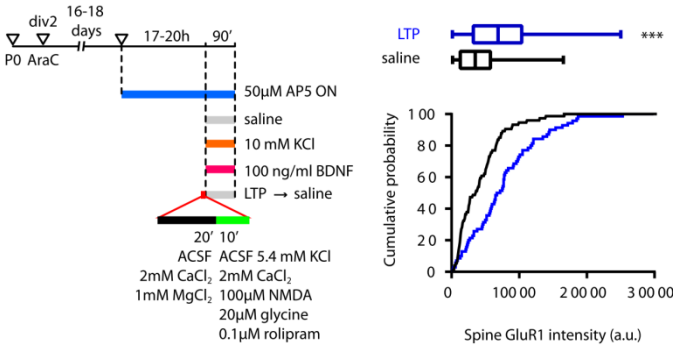

Figure 28 Schema of treatments used in this thesis. Mature cortical or hippocampal neuron cultures were used to evaluate the response to treatments increasing or decreasing activity. Chemical LTP was induced for 10 minutes, then neurons were put back in culture medium as in Palida et al. (2015). This induced NMDAR-dependent potentiation of spines, as confirmed by increased AMPAR syanptic content in hippocampal neuron (right). ***P<0.001 Kruskal-Wallis.

ChETA, I expressed them in cultured neurons with soluble EGFP, and neurons underwent treatments that increased their activity or induced LTP, or to block NMDAR receptor (Figure 28). I observed sparse synapse labelling in neurons expressing SA-Ch or A-Ch, while most spines were labelled by S-Ch or ChETA (Figure 25). Increasing neuron activity with KCl, inducing chemical LTP or treating neurons with BDNF, which induces a slow-rising, translation-dependent form of L-LTP (Panja and Bramham, 2014; Ying et al., 2002), increased the number of spines expressing

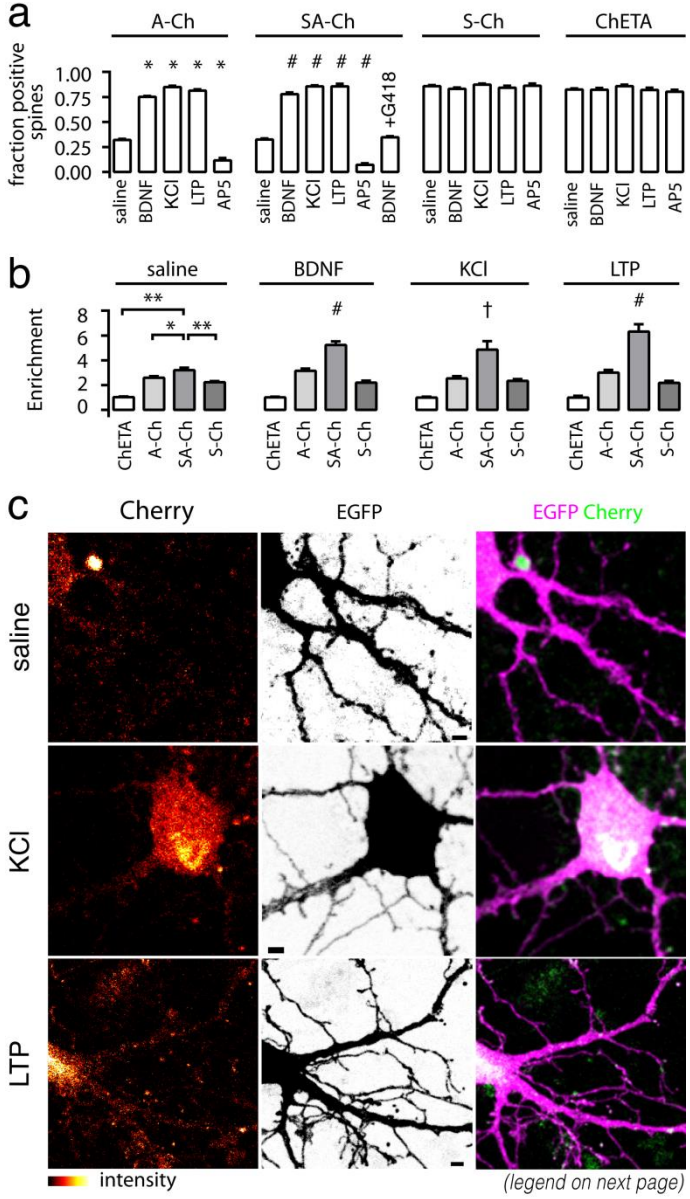
a
A-Ch
SA-Ch
S-Ch
ChETA
fraction positive spines
1.00
0.75
0.50
0.25
0.00
saline
BDNF
KCl
LTP
AP5
+G418
b
saline
BDNF
KCl
LTP
Enrichment
ChETA
A-Ch
SA-Ch
S-Ch
c
Cherry
EGFP
EGFP Cherry
saline
KCl
LTP
intensity
(legend on next page)

← **Figure 29 a** Fraction of ChETA-Cherry-expressing spines under different stimulation conditions, grouped for construct. *P<0.001 to A-Ch saline and #P<0.001 to SA-Ch saline, one-way ANOVA, Bonferroni comparison of means. Differences within and between S-Ch and ChETA values are not significant at the 0.05 level. **b** Enrichment Index for the three constructs and unmodified ChETA-Cherry under different stimulation conditions (see Methods). *P<0.01 and **P<0.001, one-way ANOVA, Bonferroni comparison of means, within group. †P<0.05 and #P<0.001 to SA-Ch, saline treated, one-way ANOVA, Bonferroni comparison of means. **c** Representative neurons expressing SA-Ch in unstimulated cultures, or cultures treated with KCl or chemical LTP. Note the increase in the number of expressing spines. Scale bar, 2μm.

SA-Ch or A-Ch. Importantly, the increased number of expressing spines due to BDNF was abolished by concomitant inhibition of new protein synthesis with geneticin (G418), which targets ribosome elongation (Lai et al., 2004). Blocking NMDAR receptor had the opposite effect, decreasing the number of SA-Ch or A-Ch –positive spines. Conversely, the fraction of spines expressing S-Ch and ChETA was unaffected by any treatment (one-way ANOVA, P>0.05) (Figure 29). In many cases, A-Ch marked more intensely the base of the spine, rather than the head, and Cherry fluorescence was also prominent on the dendritic shaft (Figure 25). Adding the SYN tag increased the synaptic enrichment of the resulting protein, and S-Ch Enrichment was higher than unmodified ChETA. SA-Ch Enrichment was higher that both A-Ch and S-Ch (Figure 29b). Inducing

SA-Ch translation with KCl, BDNF or chemical LTP increased its Enrichment, while A-Ch Enrichment was only modestly sensitive. The observed somatic SA-Ch protein (Figure 29c) can probably be ascribed to the global level of the stimulations, which can signal the overexpressed transcript to be de-repressed also in the soma. In fact, in non-stimulated neurons somatic expression is much lower (Figure 29c, first row) and can be further reduced by controlling promoter strength and localizing stimulation (see section “In vivo synaptic mapping with SA-Ch”).

It can be concluded that, while the SYN tag helps anchoring the newly translated protein at the PSD level, Arc RNA sequences are responsible for the regulation of translation and the response to stimuli. In fact, the behaviour of SA-Ch and A-Ch is almost identical in terms of number of expressing spines. Consistently, BDNF induced dendritic expression of A-Ch: following BDNF treatment, normalized A-Ch protein signal in dendrites was significantly higher than that of EGFP, which lacks DTEs and is translated in the soma only. Conversely, dendritic S-Ch protein distribution was quite similar to that of EGFP (Figure 30). This is consistent with previous observations that BDNF activates the translation of transcripts bearing alphaCaMKII 3′-UTR, increasing the protein levels along dendrites as compared to

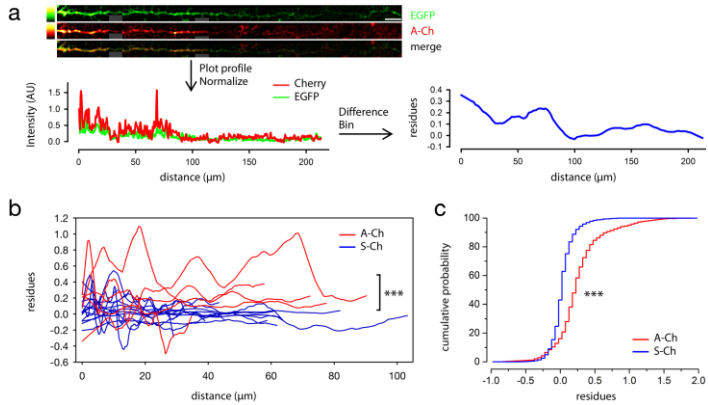

Figure 30 Arc sequences increase dendritic ChETA-Cherry following BDNF-dependent L-LTP and activation of translation. **a** Outline of the analysis: EGFP and Cherry intensities along dendrites are plotted and normalized to the value 10 µm away from the centre of soma; the difference is plotted as difference of single values ("residues") for each distance point and smoothed every ten points to improve readability. As example, one dendrite of a EGFP/A-Ch expressing neurons treated with BDNF is straightened for clarity. Gray boxes represent areas of the figure that could not be reconstructed due to the original curvature of the dendrite. Scale bar, 10 µm. **b** Traces for A-Ch and S-Ch constructs following BDNF treatment. The residues for A-Ch are significantly higher than those calculated for S-Ch. Each trace is a single dendrite. **c** Plot values of residues for the two constructs as cumulative probability. Residues were sampled every 0.12µm along dendrites. ***P<0.001, Kolmogorov-Smirnov.

the soma (Aakalu et al., 2001). The transcript state also confirms that Arc RNA sequences are responsible for the regulation of translation: in unstimulated neurons, SA-Ch/MS2-EGFP signal was present in the somatodendritic compartment in a granular form, indicating that the transcript is likely sequestered in RNPs (Figure 31). RNA

granules were predominantly associated with spines (Figure 31b) and were absent from axons. Stimulating neurons with KCl caused the MS2-EGFP signal to broaden and become more diffuse along dendrites (Figure 31b,d), which was accompanied by translation de-repression and SA-Ch protein expression (Figure 31c).

BDNF sequences

Besides Arc RNA sequences, I tested the ability of trascripts with BDNF-derived sequences to be translated at synapses in an activity-dependent manner. BDNF RNA is found in dendrites (An et al., 2008) and is transported following neuron activation (Tongiorgi et al., 1997). BDNF mediates a form of L-LTP via its receptors TrkB, which is also transported in activity- dependent way; for this reason, the autocrine BDNF/TrkB loop has been proposed as a possible synaptic tag (Bramham and Messaoudi, 2005). I therefore compared the expression pattern of ChETA-Cherry when BDNF 5' and 3'UTR flank its cDNA. BDNF has two alternative 3'UTR, and the long 3'UTR has been implicated in dendritic transport and plasticity (An et al., 2008). Of the 11 alternative 5'UTR isoforms (in the rat), those derived from exon II and exon VI are the most enriched in dendrites;

isoforms derived from the

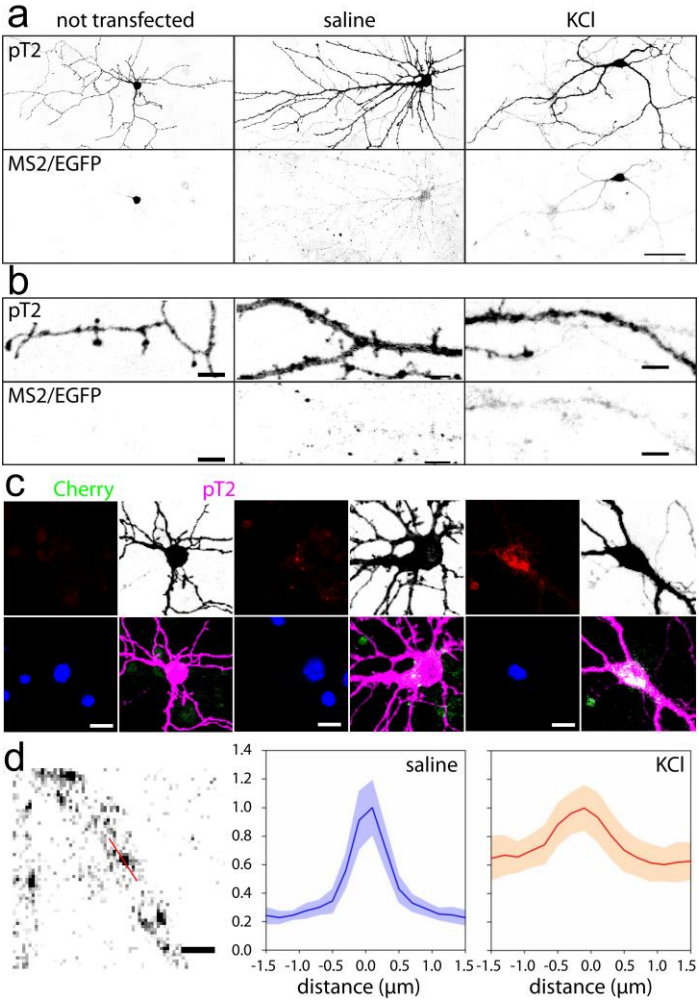

Figure 31 SA-Ch transcript is present in granules in unstimulated neurons. **a** Representative neurons expressing MS2-EGFP only, or MS2-EGFP/SA-Ch(*ms2*) an treated with saline or 10 mM KCl for 90 minutes. **b** magnification of **a**. **c** Corresponding SA-Ch expression. **d** Profile of RNA granules in saline-treated or KCl-treated cultures. Mean±95%CI. Scale bar (**a**) 50µm, (**b**) 5µm, (**c**) 10µm, (**d**) 2µm.

other exons are mostly confined to the proximal part of dendrites (Baj et al., 2013). Notably, exon VI isoform is the variant that traffics more reliably into distal dendrites, followed by exon II isoforms (which include IIa, IIb and IIc, which use different 5' splice sites) (Baj et al., 2011).

I tested three combinations of BDNF sequences, i.e. exon IIa, exon IIc and exon VI as 5'UTR variants, and I cloned the long (BDNF-B) isoform of the 3'UTR in the corresponding position, and I expressed them in neurons treated as Arc sequences. I found that, overall, the response of IIa and IIc variants was less sensitive to the neuron status: while KCl treatment, chemical LTP or BDNF application all increased the number of expressing spines (Figure 32a,b), the response was less prominent than what observed with Arc RNA (see Figure 29 for comparison). This was also due to the high number of tagged spines in resting conditions; also, blocking NMDAR with AP5 during IIa/c-ChETA-Cherry-*ms2*-BDNF B expression only slightly reduced their number (Figure 32a,b). This was probably due to the prominent somatic translation of these BDNF isoforms (Figure 32b). In contrast, isoform VI was almost undetectable in all neurons analysed, and translated protein levels were so low that quantification was impossible. Nor KCl, nor chemical LTP, nor BNDF application changed the

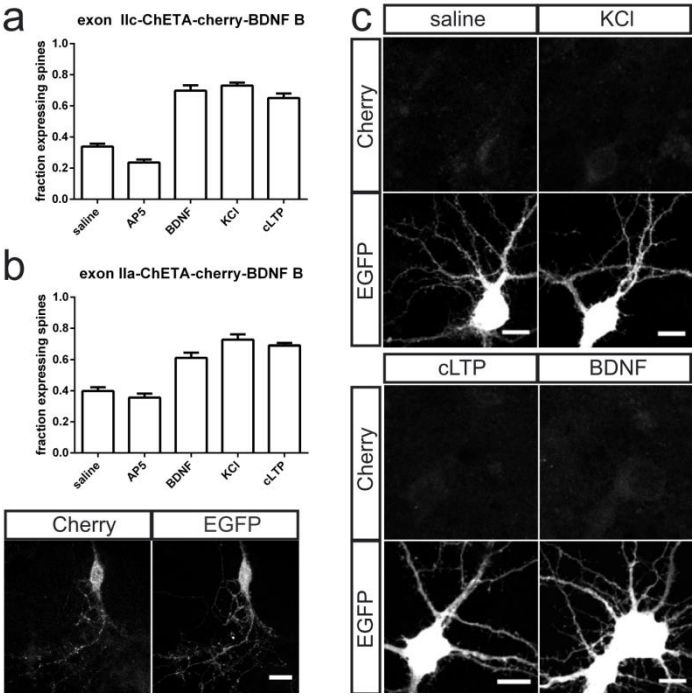

Figure 32 Response of BDNF IIc-ChETA Cherry-*ms2*-BDNF B (**a**) and BDNF IIa-ChETA Cherry-*ms2*-BDNF (**b**) to various treatments as in Figure 27. The response of both was not as strong as Arc RNA, and basal translation was prominent also in neurons were NMDAR receptor was silenced. **c** Expression of BDNF VI-ChETA Cherry-ms2-BDNF was almost undetectable both in unstimulated cultures and in neurons stimulated with KCL, BDNF or chemical LTP. Scale bar, 10µm.

expression levels of isoform VI. This perplexing result would be consistent with the observation that translation of a luciferase reporter in immortalized cells is almost undetectable when isoform VI precedes the start codon

(Vaghi et al., 2014). This is somewhat perplexing, given that it is supposedly the most distally localized BDNF isoform (Baj et al., 2011), and it is only weakly responsive to norepinephrine (Vaghi et al., 2014), suggesting the intriguing possibility that it may act as an *in trans* regulator/activator of other BDNF isoforms by sequestering miRNA or RBP (but that is another story).

SA-Ch localizes to postsynaptic densities

In the previous section, I showed that SA-Ch enrichment to spines was higher than for A-Ch, an effect that can be ascribed to the presence of the SYN tag. Consistently, I

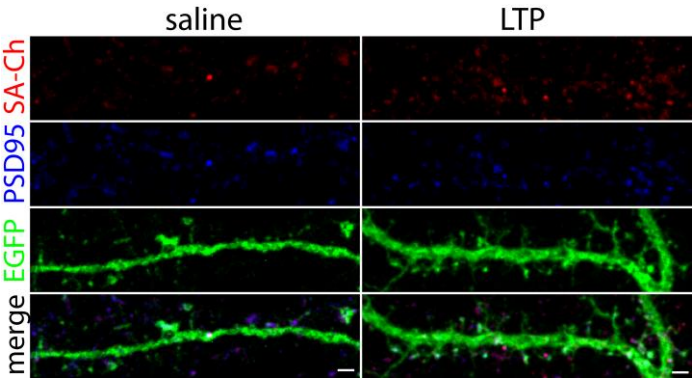

Figure 33 SA-Ch (red) co-localizes with PSD95 (blue) in transfected hippocampal neurons after chemical LTP induction (right) or saline treatment (left). Spine size also increases after LTP induction, as it can be seen in the PSD95 or EGFP channel. Scale bar 2µm.

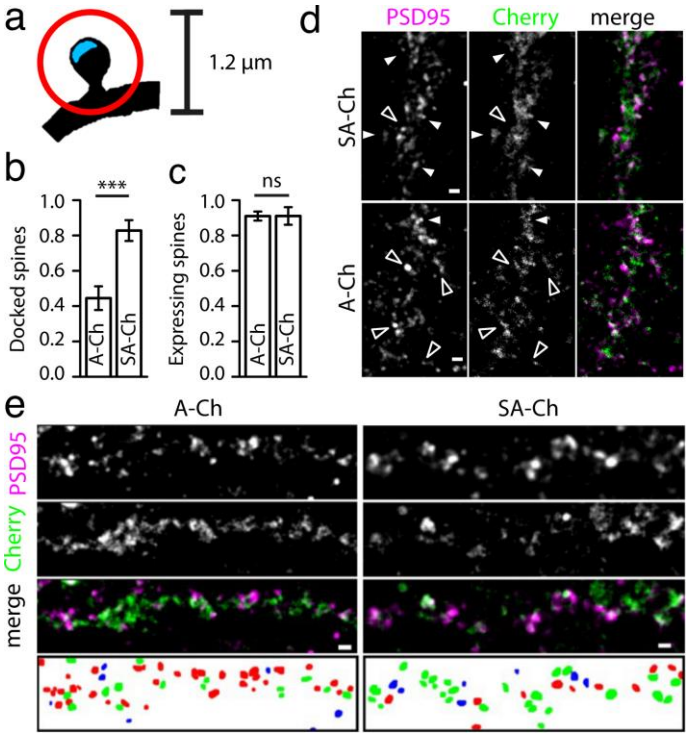

Figure 34 Schematic drawing for "docked" vs. positive but non-"docked" spines. Cherry fluorescence peaks within a circle of 1.2µm diameter (red circle) centered on the postsynaptic density (PSD - blue area) for positive spines, and on the PSD for "docked" spines. Quantification of "docked" **b** and total positive spines following cLTP for A-Ch and SA-Ch. Bars are mean ±SEM. ***P<0.001 two-tailed Student's t-test. ns, not significant at the α=0.05 level. **d** Representative dendrites of neurons expressing the two constructs. White arrowheads indicate "docked" spines, empty arrowheads positive, non-"docked" spines. **e** Another example of SA-Ch and A-Ch expressing neurons stained for PSD95 (magenta in merge) and Cherry (green in merge) IF. Bottom panel: docked synapses (green), positive, non-docked synapses (red), Cherry-negative synapses (blue). Scale bar 1µm

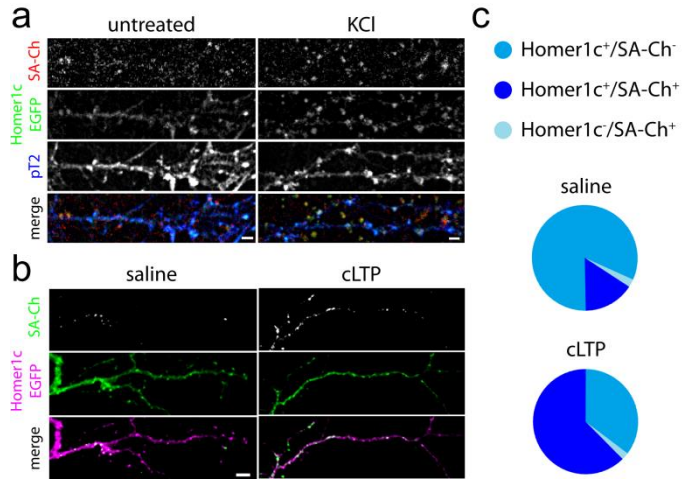

Figure 35 Cortical (**a**) and hippocampal (**b**) neurons expressing SA-Ch, Homer1c-EGFP and palmitoyl-Turquoise2 (pT2). **a** SA-Ch colocalizes with Homer1c-EGFP both in untreated and KCl-stimulated neurons. Scale bar, 2µm. **b** SA-Ch in saline neurons were chemical LTP is induced and control cultures. Scale bar, 5µm. **c** Quantification of data in **b**.

found that SA-Ch protein co-localizes with the postsynaptic marker PSD95 both in untreated cultures and in stimulated neurons (Figure 33). I then compared SA-Ch and A-Ch colocalization with PSD95 after LTP induction by detecting Cherry protein and PSD95 with immunofluorescence. I considered "docked" any spine where the Cherry signal peaked in correspondence with the PSD, evaluated with PSD95 signal. A positive, non-docked, spine was considered if Cherry signal peaked outside the PSD, but within a circle

of 1.2μm. As shown in Figure 34, about half of the spines expressing A-Ch were "docked" (44±7%), whereas these constituted the majority (83±6%) of SA-Ch$^+$ spines. The total number of positive spines was the same for both constructs (Figure 34c).

SA-Ch protein also colocalized with Homer1c. Homer1c is one of the main components of the post-synaptic density (Constals et al., 2015), and the fusion protein to EGFP allows the visualization of the PSDs in live neurons without additional staining. SA-Ch signal overlapped with Homer1c-EGFP in cortical (Figure 35a) and hippocampal (Figure 35b) neurons. Stimulating neurons with KCl or chemical LTP increased the number of Homer1c-EGFP puncta expressing SA-Ch (Figure 35c).

SA-Ch marks potentiated spines

Data presented so far demonstrate the strong dependence of SA-Ch expression on neural activity. This suggests that, in untreated cultures, positive spines received a sustained stimulation from the spontaneous activity of the culture, which could amplify basal NMDAR activation (Espinosa and Kavalali, 2009). Consistently, blocking NMDAR

activity with AP5 drastically reduces SA-Ch expression (Figure 29).

SA-Ch –expressing spines look bigger on average (Figure 36a), and LTP induction caused an increase in spine size (Figure 33) correlated with GluR1 intensity (Figure 28). This is important, as spine enlargement strongly correlates with functional potentiation (Matsuzaki et al., 2004). To express this relationship quantitatively, I correlated Homer1c-EGFP content with the Enrichment of SA-Ch protein; Homer1c has been previously shown to be a reliable indicator of spine volume (Meyer et al., 2014). As shown in

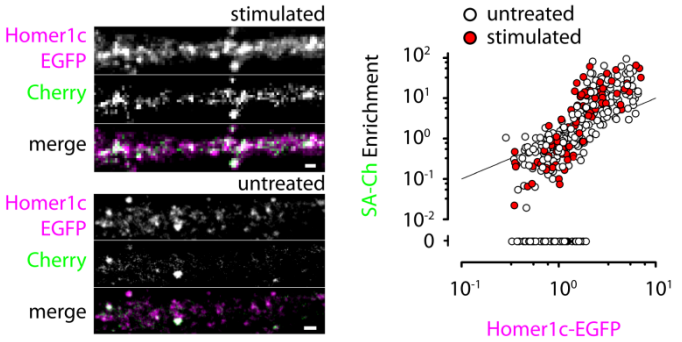

Figure 36 Homer1c-EGFP/SA-Ch expressing neurons in unstimulated and stimulated cultures. Scale bar 1µm. On the right, quantification of SA-Ch enrichment as a function of Homer1c-EGFp spine content. The correlation is supralinear; the line is the diagonal and corresponds to a linear dependence with unitary slope.

Figure 36, SA-Ch seems to preferentially tag larger spines; indeed, spines with higher Homer1c-EGFP content had larger Enrichment values for SA-Ch. Although larger PSDs could accommodate more SA-Ch, yielding higher Enrichment values, it is unlikely that this is the only explanation, as the correlation between the two values was not linear. Indeed, a significant proportion of spines with lower Homer1c content were devoid of SA-Ch signal in non-stimulated neurons, and those spines were assigned a valued of zero for SA-Ch Enrichment (Figure 36).

I next compared the expression of SA-Ch with SEP-GluA1, a marker of functional potentiation (Makino and Malinow, 2011). This receptor bears Superecliptic pHluorine (a pH-sensitive EGFP variant whose fluorescence is quenched by the acidic pH inside vesicles) at the N-terminus of AMPAR-subunit 1 (Kopec et al., 2006; Miesenböck et al., 1998). SEP-GluA1 recapitulates the properties and dynamics of wt GluR1 (Zhang et al., 2015), and stimulating synapses leads to the exposure of SEP-GluA1 from endocytic vesicles and fluorescence recovery (Ashby et al., 2004; Kopec et al., 2006). In neurons expressing SA-Ch and SEP-GluA1 along with cell marker palmitoyl-Turquoise2, SA-Ch –positive spines were 63±3% of SEP-GluA1-positive spines, and 6±2% of SEP-GluA1-

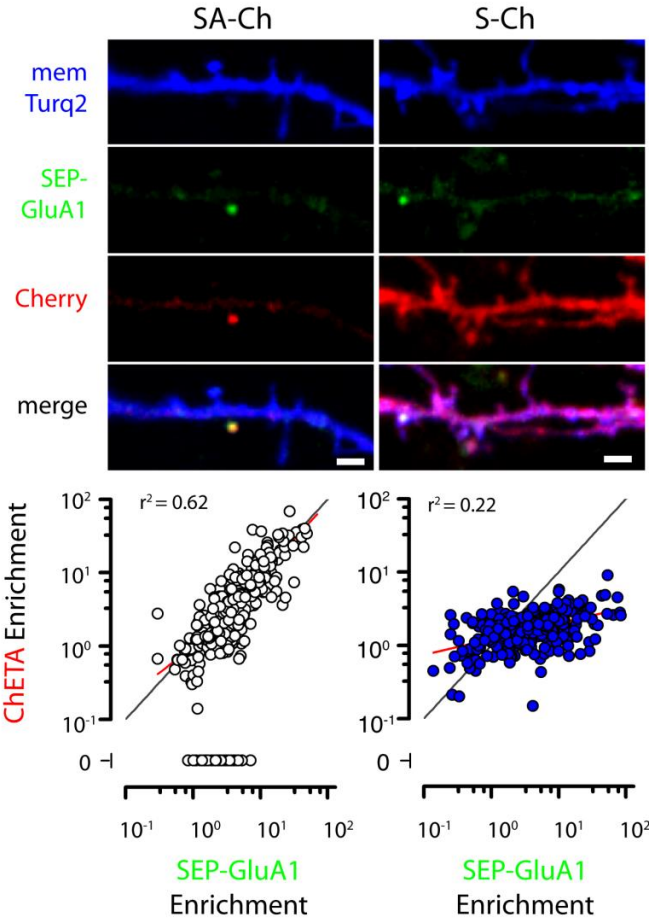

Figure 37 Comparison of SEP-GluA1 and ChETA-cherry expression for S-Ch (which only has SYN tag) and SA-Ch (which has SYN tag and Arc sequences). Scale bar, 2µm. Below, plot of SA-Ch (or S-Ch) vs SEP-GluA1 enrichment reveals a linear dependence for SA-Ch, but not for S-Ch. Red lines represent the linear fit for the two sets of data, and the corresponding adjusted r^2 is reported in the inset. Spines with no detectable SA-Ch signal were assigned the value of zero Enrichment, and correspond to spines with lower SEP-GluA1 values.

negative spines, ($P<0.001$, χ^2-test). The relationship between SA-Ch and SEP-GluA1 enrichment was linear (Figure 37), indicating that SA-Ch is expressed at potentiated synapses. Some of the spines with lower SEP-GluA1 enrichment did not express SA-Ch; these synapses likely received a weaker stimulation that did not activate translation-dependent L-LTP, which is sometimes referred to as LTP2 (Park et al., 2014; Reymann and Frey, 2007). In fact, AMPAR exocytosis takes place during E-LTP phase, which has a lower threshold than translation-dependent L-LTP (Kelleher III et al., 2004; Reymann and Frey, 2007). On the contrary, S-Ch marked all spines regardless of the fact that they expressed SEP-GluA1 or not. S-Ch enrichment only showed a modest dependence on SEP-GluA1, which is likely due to the larger PSDs that spines exposing AMPAR are likely to have (Figure 37).

Focal LTP induction drives SA-Ch expression

Above data demonstrate the correlation of SA-Ch expression with hallmarks of synapse potentiation. I next induced LTP on selected spines by means of two-photon glutamate uncaging. I employed a protocol of stimulation that relies on repetitive laser flashes of 720 nm, thereby

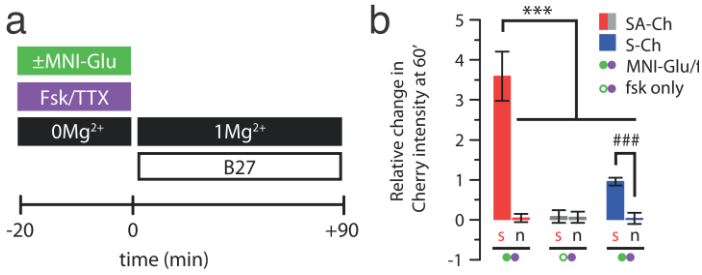

Figure 38 a Outline of the experiment. Time = 0 marks the time of two-photon stimulation. **b** Relative changes in Cherry intensity 60 minutes after stimulation. Uncaging increased SA-Ch expression at stimulated (s) but not at nearby (n) spines; the effect was not seen when MNI-glutamate was absent. The fold change observed for S-Ch was much smaller. Bars are mean±sem. ***P<0.001, one-way ANOVA, Bonferroni comparison of means. ### P<0.001 unpaired samples Student's t-test, two-tailed.

releasing free glutamate in close proximity to spines, in a Mg^{2+}-free bath solution of MNI-caged glutamate and protein kinase A (PKA) activator forskoline (Hill and Zito, 2013; Matsuzaki et al., 2004); spontaneous activity was prevented with TTX during pre-treatment and focal stimulation (Figure 38a).

SA-Ch RNA was translated at potentiated spines, but not at nearby spines: 60 minutes after stimulation, SA-Ch levels in spines close to the uncaging spot were greatly increased relative to pre-stimulation situation (Figure 38b), while no significant difference was observed for other spines

of the same dendrite (Figure 38). When MNI-caged glutamate was absent from bath, no change was observed. This increase is probably due to local translation, as no evident change in neighbour spines and dendrite shaft was evident that could suggest protein relocalization. Furthermore, when I stimulated S-Ch expressing neurons, the observed change was much smaller; as S-Ch transcript is translated at the soma level only, this is likely a result of the PSD expansion following potentiation (Matsuzaki et al., 2004).

To confirm this interpretation, I followed in real time the changes in Cherry intensity following the focal stimulation. After potentiation, the spine volume rapidly increased, and remained stable for at least the whole duration of the experiment. This was paralleled by a slower rise of Cherry fluorescence, which reached a plateau around 60 minutes after stimulation (Figure 39). This increase was dependent on novel protein synthesis, since translation inhibition with anisomycin during the experiment, including the 20 minutes pre-treatment (see Figure 38a), abolished the increase in SA-Ch intensity. When the stimulation was performed in presence of anisomycin, the initial increase in volume was not persistent, and declined to pre-stimulation levels between 60 and 90 minutes (Figure 38). Last,

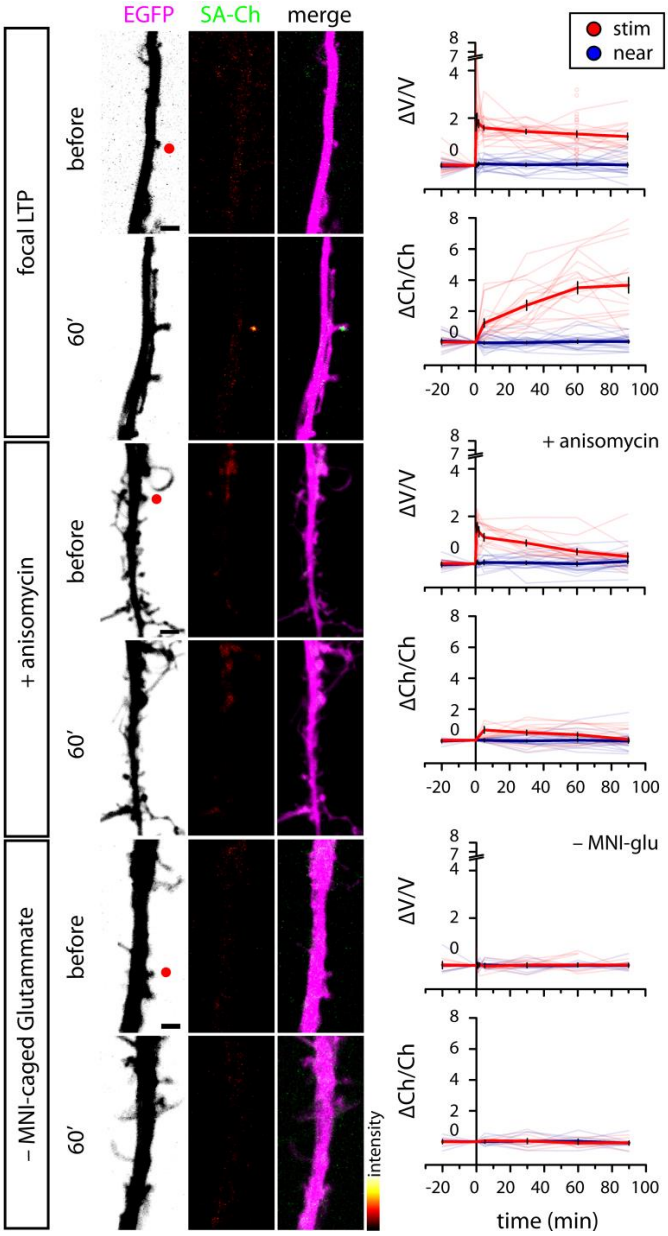
EGFP
SA-Ch
merge
focal LTP
+ anisomycin
– MNI-caged Glutammate
before
60′
before
60′
before
60′
intensity
stim
near
ΔV/V
ΔCh/Ch
+ anisomycin
– MNI-glu
time (min)

← **Figure 39** Translation inhibition with anisomycin blocked SA-Ch accumulation at stimulated synapses. Representative images of stimulated dendrites in neurons transfected with the plasmid encoding SA-Ch before and 60 minutes after stimulation. Red dots in the EGFP channel indicate the location of two-photon uncaging. Experimental conditions are indicated besides of images. Scale bar, 2µm. Next to each pre-post image, time course of relative changes in volume (ΔV/V, top graphs, measured by the EGFP intensity) and SA-Ch intensity (ΔCh/Ch, bottom graphs) of stimulated (red) and near spines (blue). Stimulation induced a long-lasting volume change, paralleled by a slowly rising accumulation of SA-Ch; in the presence of anisomycin, the volume change was transient and no accumulation of SA-Ch was evident. Bold lines represent mean±SEM, whereas narrow lines are single traces for depicted data for stimulated (light red) and nonstimulated (light blue) spines. Open circles are corresponding ΔV/V values at 60min for SA-Ch spines evaluated at 60 minutes only.

uncaging alone had no effect, as focusing the two-photon laser in the absence of MNI-caged glutamate did not influence SA-Ch expression. Thus, I can conclude that synapse potentiation drives local SA-Ch expression in a protein-synthesis-dependent and synapse-specific way.

Synaptic light-evoked calcium transients

Calcium influx is an established indicator of spine activation, both *in vitro* and *in vivo* (Chen et al., 2013; Lee et al., 2016b; Winnubst et al., 2015). I therefore expressed the highly sensitive GCaMP6s indicator (Chen et al., 2013) in cultured neurons along with SA-Ch, and asked if illuminating SA-Ch$^+$ spines would determine the onset of

calcium transients. As single-photon absorption spectra of GCaMP6s and ChETA overlap, GCaMP6s imaging illumination itself determined the activation of the Channelrhodopsin, and calcium entry (Figure 40).

To be able to image calcium changes with minimal Channelrhodopsin cross-excitation, I decided to excite GCaMP6s at 990 nm; in fact, the two-photon absorption spectra are better separated than the single photon ones (Paluch-Siegler et al., 2015). I therefore imaged calcium transients in a region encompassing the base of the spine and the dendrite below at 50Hz; after recording 50 frames to evaluate the baseline, I stimulated the selected SA-Ch^{+} spine with 10ms 488nm laser illumination, in accordance with Schoenenberger et al. (2008). Most spines responded to light illumination generating calcium transients across multiple trials (Figure 41a). GCaMP6s recording without 488nm stimulation did not result in significant calcium transients (Figure 41b). Channelrhodopsins are weakly permeable to calcium (Schneider et al., 2013), but their stimulation could lead to the opening of voltage-gated calcium channels (VGCCs). Accordingly, the response to blue light stimulation was markedly reduced in the presence of VGCC inhibitors nifedipine, Ni^{2+}, and Zn^{2+} (Figure 41a,b). Importantly, TTX in bath did not impair the recording of

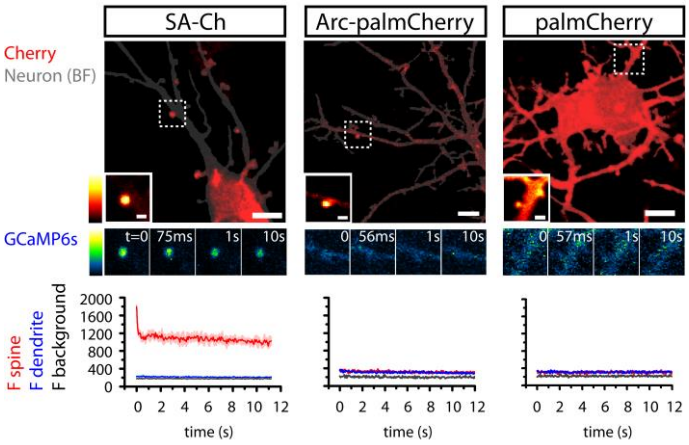

Figure 40 488 nm imaging of GCaMP6s fluorescence also activates SA-Ch making it impossible to record a stable baseline. Note the persisten calcium signal during steady illumination; the peak at initial times is probably due to the channelrhodospin kynetics, that rapidly inactivate yielding a smaller steady photocurrent than at peak (Gunaydin et al., 2010). This was not seen when we imaged GCaMP6s expressing neurons transfected plasmids encoding palmitoylCherry or Arc 5'UTR-palmitoylCherry-*ms2*-Arc 3'UTR. Scale bar 5µm, inset 1µm.

these light-evoked calcium (Figure 41c), confirming the postsynaptic origin of the stimulation.

I then compared the excitability of spines and dendrites of SA-Ch –expressing neurons compared to untargeted ChETA-Cherry (Figure 41c). I stimulated neurons as above and, for every recording session, some traces were performed setting the stimulation region of the

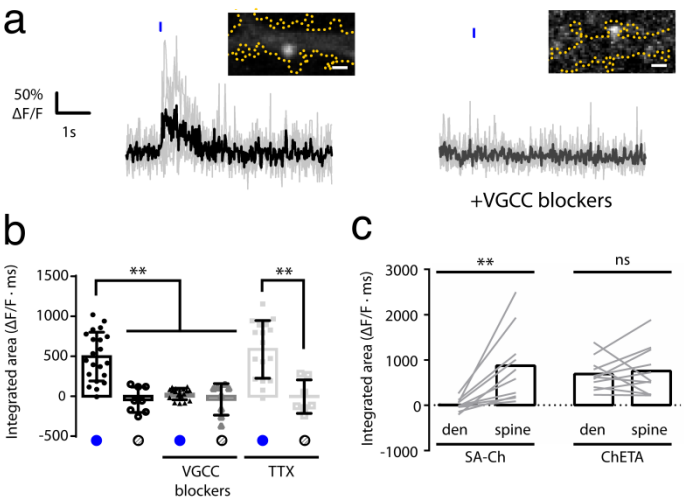

Figure 41 Two-photon GCaMP6s imaging allows recording of calcium transients without significant ChETA activation. **a** Calcium transients evoked after 10ms 488nm illumination (blue dot on top of trace). On the right, transients are abolished in presence of VGCC inhibitors. Single traces are in light gray, the average is in bolds. Inset, SA-Ch expression in the spine excites in shown traces. The yellow dotted profile is the neuron area as evaluated by the GCaMP6s channel. Scale bar, 1µm. **b** Quantification of the integrated area of the calcium transients in neurons expressing SA-Ch when 488nm stimulation was performed (blue circles; filled symbols) or not (white/gray circles; empty symbols). Light-evoked transients were blocked by VGCC inhibitors, but not by TTX. Bars are mean±SD. **P<0.01, Kruskal–Wallis test, Dunn's post-hoc comparisons. **c** Calcium transients when illumination was performed on spines or on dendrites. In SA-Ch neurons, only spine illumination drove calcium influx, while in ChETA expressing neurons both spines and dendrites were excitabile. Lines connect excitation of the same cell. Lines connect single paired data points, bars are mean. **P<0.01 paired Student's t-test, two-tailed. ns, not significant at the α=0.05 level.

spine, and others were performed moving it onto the dendrite. In ChETA-Cherry –expressing neurons the

dendritic region was as excitable as the spines, consistently with Packer et al. (2012), who found that the focusing of 940 nm light on either spines or dendrites of neurons expressing red-shifted C1V1 Channelrhodopsin induced comparable photocurrents. On the other hand, focusing the illumination spot on dendrites from SA-Ch$^+$ neurons did not induce detectable calcium transients, and only SA-Ch$^+$ spines were responsive to light stimulation.

I then compared the spontaneous ΔF/F calcium events that could be sometimes recorded from SA-Ch$^+$ spines with those from control neurons expressing palmitoylCherry (Figure 42). Spontaneous events did not differ in amplitude between the two sets, further suggesting that SA-Ch expression does not alter the normal synaptic transmission. Light-evoked responses were in general smaller than spontaneous events, which could be due to the fact that

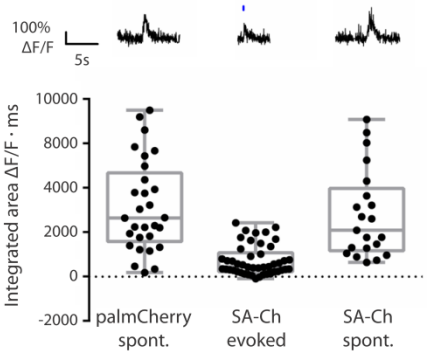

Figure 42 Integrated area of spontaneous calcium transients from SA-Ch$^+$ neurons and control neurons expressing palmitoyl-Cherry, and light-evoked response in SA-Ch$^+$ cells. Each dot is a single trial. Above each boxplot, representative traces are shown.

Channelrhodopsins usually need a high channel density (Baker et al., 2016; Nagel et al., 1995) and ChETA itself does not have the highest photocurrents among the Channelrhodopsin variants (Gunaydin et al., 2010; Mattis et al., 2011) (see Discussion in this section).

Optogenetic activation of SA-Ch neurons

I next asked if the optogenetic activation of SA-Ch$^+$ spines could mimic a physiological response. Sustained synaptic transmission induces the rapid phosphorylation of αCaMKII; this signal lasts for minutes thanks to the self-sustained activity of the enzyme, which is able to phosphorylate itself (Lisman et al., 2012). I stimulated hippocampal neurons expressing SA-Ch and EGFP with an optical protocol similar to theta-burst, a commonly used paradigm used in electrophysiology (Stepan et al., 2015) – i.e. 10 trains of 13 pulses at 100Hz, separated by 2s each, repeated four times. To lower the basal phosphorylation status of intracellular kinases, we pre-treated neurons with CNQX, AP5 and TTX for three hours before the stimulation (Ivanov et al., 2006) (Figure 43a). After the stimulation, I fixed neurons and I detected phospho-CaMKII signal by IF.

After light stimulation, αCaMKII was phosphorylated in SA-Ch –expressing, but not control neurons (Figure 43b). SA-Ch expression in cultures maintained in the dark did not induce αCaMKII phosphorylation and the signal was not different from control cultures (Figure 43b,c). αCaMKII activation is specific to spines expressing SA-Ch, as phosphoCaMKII levels in SA-Ch^{-} spines in light-stimulated neurons were not different from the baseline (Figure 43c). The optical stimulation of ChETA-Cherry also induced αCaMKII phosphorylation; however, the phospho-staining was also evident in the dendrites (Figure 43b). It is possible that, upon generalized neuron activation by ChETA, part of the CaMKII pool fails to translocate from the shaft into the spine due to concomitant extrasynaptic depolarization – conversely, localized SA-Ch activation could more readily induce CamKII phosphorylation and mobilization. This could also explain why the levels of phospho-CaMKII in light-stimulated ChETA-Cherry^{+} spines, while significantly different from the unstimulated ones, are lower than stimulated SA-Ch^{+} spines. Indeed, neurotransmitter-mediated synapse stimulation mobilizes CaMKII from the dendritic shaft and accumulates it at the spine head (Otmakhov et al., 2004; Zhang et al., 2008). Thus, large-field optical stimulation of synaptic SA-Ch is able to simulate an

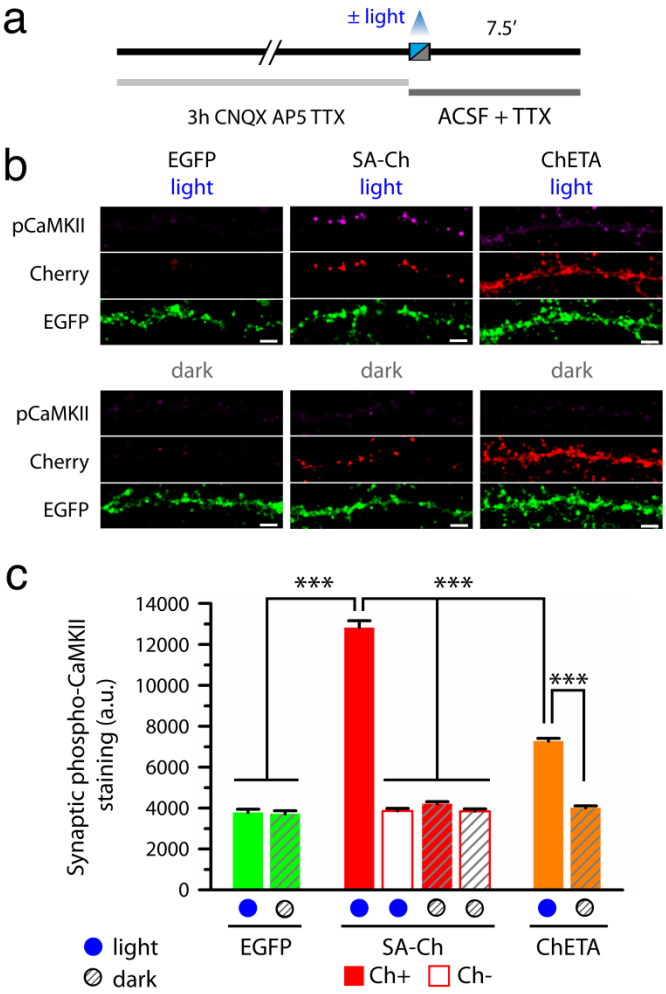

Figure 43 Optical stimulation of SA-Ch spines increases synaptic phospho-CaMKII population. **a** Timeline of experiment. **b** Neurons expressing EGFP, EGFP/SA-Ch or EGFP/ChETA-Cherry stained for phospho-CaMKII after light stimulation or maintained in the dark. Scale bar, 5µm. **c** Quantification of synaptoc phospho-CamKII ***P<0.001, one-way ANOVA, Bonferroni comparison of means. Bars are mean±SEM.

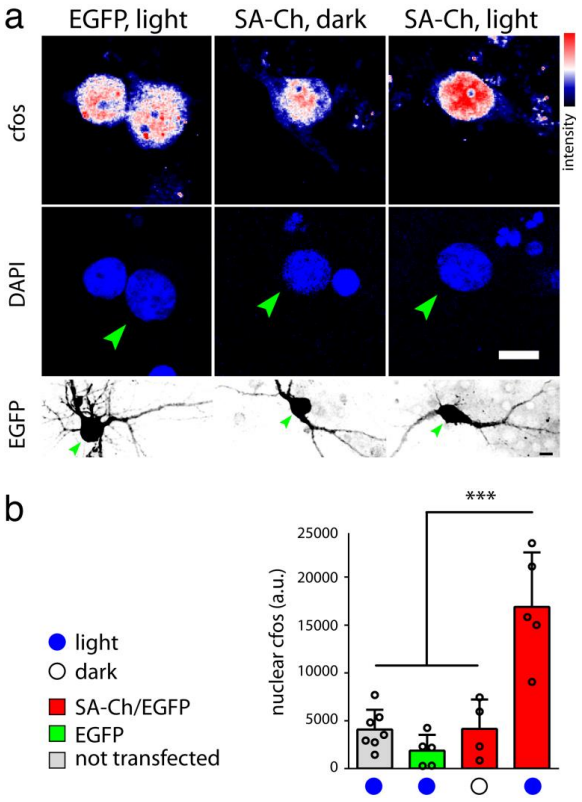

Figure 44 a c-fos and DAPI staining of cells expressing EGFP (left) or SA-Ch and EGFP (middle and right). Cells were illuminated or maintained in the dark as indicated. Green arrowheads indicate corresponding positions in the EGFP channel below. Scale bar, 5 µm. **b** Nuclear c-fos staining for illuminated, EGFP expressing neurons, and SA-Ch/EGFP neurons maintained in the dark is comparable to untransfected cells. Optical stimulation of SA-Ch/EGFP neurons increases c-fos expression in the nucleus. ***P<0.001, one-way ANOVA, Bonferroni comparison of means. Bars are mean±s.d.

input-specific excitation onto the postsynaptic neuron.

Then, I asked whether SA-Ch activation could also activate the whole neuron. I therefore applied the same optogenetic activation protocol as before – without pharmacological inhibition – and we stained neurons for c-fos expression after one hour. Nuclear c-fos levels in SA-Ch$^+$ neurons were increased after illumination (Figure 44), relatively to control neurons that were not transfected or transfected with EGFP only. SA-Ch expression alone was not responsible for the increased levels of c-fos because in cultures transfected with SA-Ch/EGFP that were kept in the dark the c-fos levels were comparable to control neurons. Together, these experiments confirm that SA-Ch is correctly present at synapses and its illumination is capable of driving neuronal responses both locally (αCaMKII activation) and globally (c-fos expression).

Discussion

A marker for potentiated synapses

As we have seen in this section, SynActive expression increases with treatments that increase neuronal activity and is dependent on NMDAR activation and novel protein synthesis (Figure 29). Focal LTP induction demonstrates selective SA-Ch accumulation at potentiated synapses, and

anisomycin administration prevented its expression. Thus, SynActive is expressed at synapses that underwent potentiation, making it possible to recognize and reactivate them.

Traditionally, LTP is detected either with electrophysiological recordings or biochemical assays. These methodologies limit either the spatial or temporal resolution with which biological processes can be observed and manipulated. For example, the electrophysiological standard for LTP – an increase in the amplitude of evoked postsynaptic potentials – often represents a collective change in transmission efficacy across a population of synapses rather than a direct characterization of plasticity at single sites. Optical imaging methods to visualise LTP at such resolution has mostly relied in live imaging of changes at single spines, either in changes of calcium imaging response, volume or signalling activity (Padamesey and Emptage, 2011). Stable tagging with an enduring reporter has been achieved in a constitutive way, and with the exposure of AMPAR subunits coupled to pH-sensitive fluorescent proteins (SEP-GluA1) (Lee et al., 2016a). This is currently the most promising way to mark active synapses as AMPAR are exposed during E-LTP, which makes it likely that the population of tagged synapses corresponds to

the subset where LTP1 is induced (Reymann and Frey, 2007). Given the translation-dependence of the SynActive system, SA-reporters mark synapses where LTP2 is induced (in the notation of Racine et al. (1983), also in Raymond (2007)). Indeed, this subset is generally believed to be more directly involved in memory storage (Martin and Morris, 2002; Raymond, 2007). Indeed, I found that anisomycin treatment blocks SA-Ch expression, also inducing a decaying form of LTP, as estimated by the spine volume change (Figure 39). In addition, a proportion of SEP-GluA1 spines does not express SA-Ch (Figure 37); the subset of SEP-GluA1^{+}/SA-Ch^{-} spines has a lower SEP-GluA1 Enrichment index, suggesting that this set experienced a weaker stimulation.

Protein permanence after translation

After stimulation, SA-Ch RNA is rapidly translated and the protein is translocated in correspondence to stimulated spines, with fluorescence reaching a pleateu at around 60-90 minutes, a compatible time scale with local translation of pre-existing mRNAs, as well as Cherry maturation (Balleza et al., 2018; Shaner et al., 2004) (Figure 39). LTP induction is generally believed to be a one-time event (Frey and Morris, 1997), so in order to perform the memory recall SA-Ch should stay in place long enough not to require

significant distortions to the timetable of established protocol for memory tasks (Liu et al., 2012; Ramirez et al., 2013). A careful evaluation of protein persistence after translation would provide useful information; however, a direct estimation is not a trivial task, especially *in vivo*. Anyway, I followed the newly synthesized SA-Ch for 90 minutes without any indication of fluorescence loss (Figure 39). Synaptic proteins have an average half-life of ~20hours (Alvarez-Castelao and Schuman, 2015; Ehlers, 2003), and exogenous proteins generally persist longer, as they lack physiological degradation sequences, their persistency primarily depending on their stability (Corish and Tyler-Smith, 1999). Indeed, exogenously expressed SEP-GluA1 at specific synapses has been reported an exceptionally long persistence time, with some spines being still tagged after 28 days (Zhang et al., 2015). For these reasons, we expect SA-Ch tag to be long-lived enough to perform recall experiments (Liu et al., 2012) and possibly, reinstate LTP after memory decay (Takeuchi et al., 2014).

Synaptic translation

LTP induction with focal glutamate uncaging caused SA-Ch expression at selected spines only, while no change was observed at nearby spines (Figure 39). This, and its

anisomycin sensitivity, confirm that SynActive reporters are locally translated in dendrites, consistently with most reports for Arc gene, which is transcribed after neuron activation; its transcript is localised to stimulated dendritic regions and translated after LTP induction (Bramham et al., 2010; Gruart and Delgado-García, 2007; Panja et al., 2009).

Although sometimes somatic expression of the reporter was observed, in most unstimulated neurons SA-Ch presence in the cell body was very low (Figure 29, Figure 31). While it is possible that any residual somatic expression is hard to be eliminated altogether (Tushev et al., 2018), the significant signal at the soma level is likely due to the lack of spatial selectivity of the treatments performed in culture, therefore signalling de-repression of SA-Ch transcripts also in the cell body (Figure 31). In addition, strong expression from a constitutive promoter cools also contribute to background expression and, as we shall see in the next section, the use of an inducible promoter can help increase synaptic enrichment and reduce the somatic signal.

Thus, while it is possible that specificity can be further improved, Arc sequences turned out to give the best dendritic localization (Figure 22), consistently with unbiased *in vivo* comparison of dendritic RNAs (de Solis et

al., 2017). In addition, BDNF sequences, which represented another strong candidate for synaptic tagging, proved not to be suitable to drive selective expression of reporters at potentiated synapses (Figure 32).

SA-Ch functionality

As seen in Figures 43 and 44, SA-Ch stimulation in culture activates neuronal biological responses in a light-dependent manner. I also recorded incoming calcium transients in response to the optical stimulation of SA-Ch$^+$ spines, while dendrites were not responsive to light, confirming the synaptic selectivity of SA-Ch. However, light-induced responses were smaller in amplitude than the spontaneous events. It must be noted that ChETA itself does not have the greatest photocurrents in the Channelrhodopsin family (Gunaydin et al., 2010; Mattis et al., 2011) and a number of ChR2 variants now exists with larger photocurrents (Dawydow et al., 2014; Mattis et al., 2011). The majority of these variants differ from the parental ChR2 by a few point mutations (Mattis et al., 2011), so we expect that changing the encoded ChETA sequence into an opsin with a higher photoconductance would replicate the key expression features of SA-Ch in tagging potentiated synapses. In addition, changing the fluorescent proteins attached to SA-

Ch could also increase photocurrents, since Cherry-fused ChR2s have been sometimes reported to have a reduced trafficking to the plasma membrane than fusion proteins of the GFP family (Asrican et al., 2013). Indeed, multiple Channelrhodopsins could be compared to match photocurrents to synaptic currents due to gliotransmission, and single-channel chemogenetic receptors now exist that do not require a second effector as DREADDs do (Roth, 2016), and could provide strong depolarizing (or hyperpolarizing) currents even in a limiting number of molecules at one synapse (Magnus et al., 2011).

In vivo mapping of potentiated synapses

In vivo delivery for synaptic tagging

The data presented in the previous section demonstrate that SA-Ch transcript is translated at potentiated spines in cortical and hippocampal neurons in culture. I next sought to express in the hippocampus of living mice the construct that I described and validated *in vitro*. In this set of experiments, I made use of the properties of SA-Ch as a reporter of potentiation to identify and map potentiated synapses in this brain region. The hippocampus is in fact involved in the processing of spatial information and plays a critical role in the formation of memories. To restrict the expression of SA-Ch to a defined time window, I employed the TetON system – the transcription factor rtTA activates transcription when tetracycline (or its analogue doxycycline) is present (Gossen et al., 1995). I therefore placed the SA-Ch sequence under the third-generation TRE promoter (Tetracycline responsive elements) with minimal background (Loew et al., 2010; Sato et al., 2013). As a control for transgene induction, and to mark transfected neurons, soluble EGFP was also put under the TRE promoter, while rtTA expression was constitutive from the CAG promoter (Figure 45 and 46a). Plasmids bearing the transgenes were delivered into pyramidal neurons of the mouse hippocampus by means of triple-electrode in utero electroporation at embryonic stage E15.5

(Szczurkowska et al., 2016). On postnatal day 20, animals received doxycycline in solution injected intraperitoneally at 1mg per 30g of body weight to induce expression, opening the window for synaptic tagging with SA-Ch (Sato et al., 2013; Zhu et al., 2007) (Figure 46b). Animals were then perfused for imaging SA-Ch expression (Figure 46b,c).

SA-Ch expression pattern in vivo

After two days of doxycycline administration, EGFP expression was evident in transfected neurons (Figure 47); a series of SA-Ch –expressing spines was detected along dendrites of transfected neurons (arrows in Figure 47), but, remarkably, no significant expression was seen in

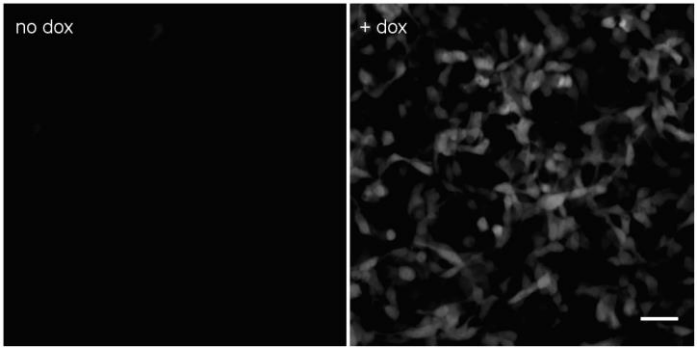

Figure 45 Responsiveness of TetON system. rtTA was cloned after CAG promoter, and followed by TRE::EGFP. HEK293T cells were transfected with the plasmid without doxyxycline (left) or with 1μg/ml doxycycline (right). Scale bar, 50μm.

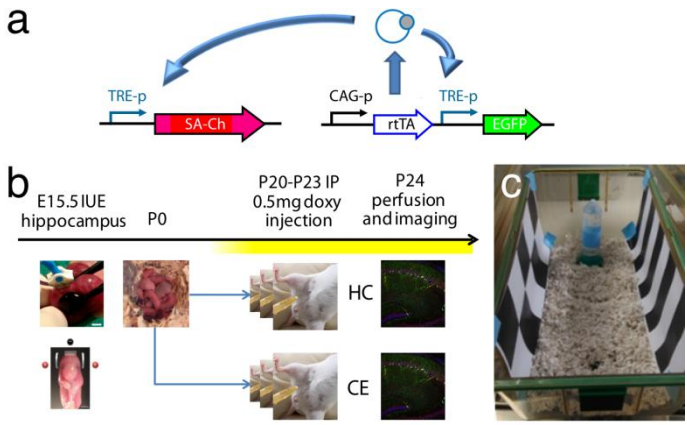

Figure 46 a Schematic representation of constructs used in vivo. Constitutively expressed rtTA activates expression of SA-Ch and soluble EGFP when doxyxycline is present. **b** Timeline of experiment. Pregnant mice were electroporated in utero in the hippocampus at E15.5. On postnatal day 20 expression was induced with intraperitonal injection of doxycycline. Animals were maintained in the home cage (HC group) or let exploring a new context (CE group), then pefused and sliced for imaging. **c** The new context that animals explored.

correspondence of the somas (asterisks in Figure 47). Consistently, most of the fluorescence was detected in the dendritic layers (Figure 48). I compared this expression pattern with that of untargeted ChR2-EYFP expressed in Thy1-ChR2-YFP (line 8) mice; I compared the profile of SA-Ch and ChR2-YFP in the CA1 region after normalizing

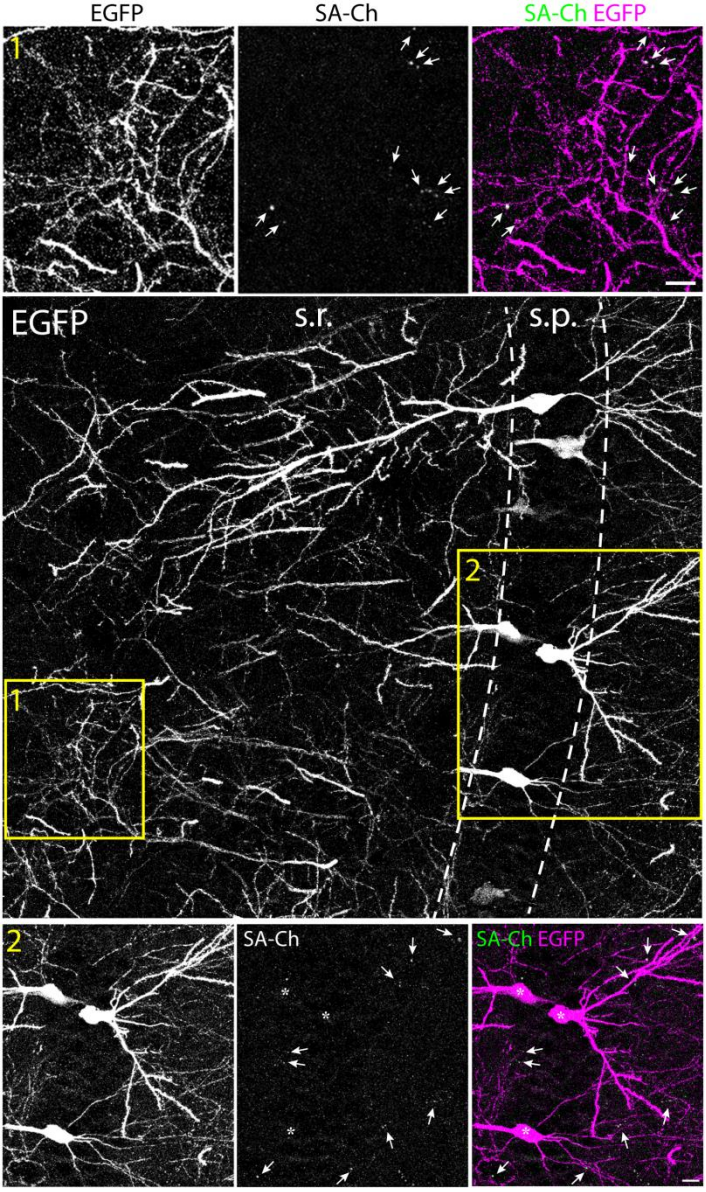
EGFP
SA-Ch
SA-Ch EGFP
1
EGFP
s.r.
s.p.
2
1
2
SA-Ch
SA-Ch EGFP

← **Figure 47** Expression of SA-Ch and EGFP in CA1 neurons after 2 days of doxycyline. We observe transgene expression in pyramidal neurons. Regions 1 and 2 representing dendritic and somatic regions, respectively, are magnified above and below the large field image. Dashed lines represent the limits of the stratum pyramidale (s.p.) containing the somas. Arrows indicate SA-Ch⁺ spines in the dendritic layers straum radiatum (s.r.), stratum lacunosum moleculare and stratum oriens. Asterisks mark soma positions in the various channels. Scale bars, 10μm.

for the peak value (Figure 48). Thy1-ChR2-YFP profile showed a prominent expression in the pyramidal layer, too – note that this value may also be slightly underestimated since, although in this line ChR2 expression is mostly confined to CA1, sparse neurons in CA3 and CA2 also express the transgene, and the projection axons can contribute to the signal calculated in the dendrites of CA1 pyramidal neurons.

In vivo *SA-Ch expression does not alter neuron physiology*

To confirm that *in vivo* SA-Ch expression does not alter neuron physiology, by possibly interfering with glutamate receptor occupancy of postsynaptic sites, AMPAR and

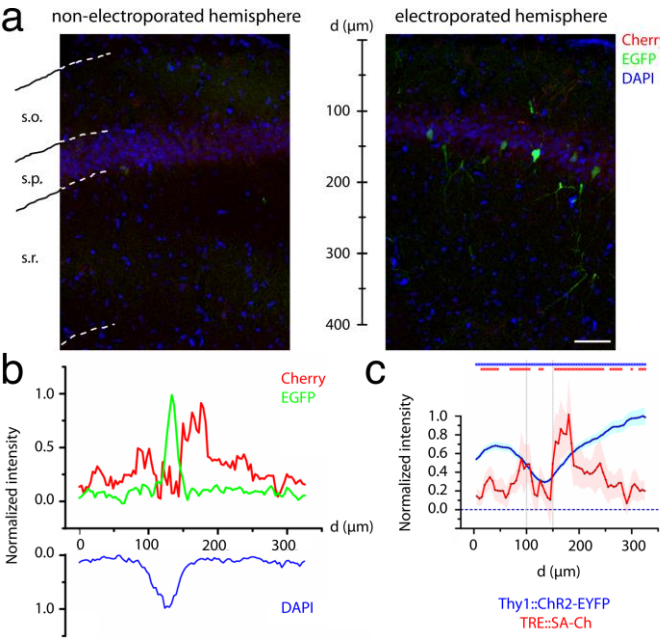

Figure 48 Expression of SA-Ch in mouse hippocampus. **a** CA1 region comprising the stratum oriens (s.o.), the stratum pyramidale (s.p.) and the stratum radiatum (s.r.) from a mouse unilaterally electroporated with TRE:SA-Ch and TRE:EGFP. Electroporated and non electroporated hemispheres are from the same slice. Scale bar 50µm. **b** Profiles were plotted along radial lines starting from the s.o., and averaged (24 profiles from 4 animals) after subtracting the baseline from the non-electroporated hemispheres. The majority of EGFP signal (green line) is concentrated in the soma, while most SA-Ch is dendritic. **c** Profile of SA-Ch expression (red) compared to untargeted ChR2 from Thy1:ChR2-YFP mice (blue). For every trace, values were averaged every 5µm starting from the beginning; for each construct, we plot the average of the corresponding profiles (line and cross)±s.e.m. (shadowed areas). The two constructs are significantly different at the α=0.001 level (two-way ANOVA). Asterisks on the top indicate distance points that are significantly different from zero (dashed line) for SA-Ch (red) and ChR2-YFP (blue). Untargeted ChR2-YFP, but not SA-Ch, is significantly different from zero in the 100-150µm range (z-test, α=0.05).

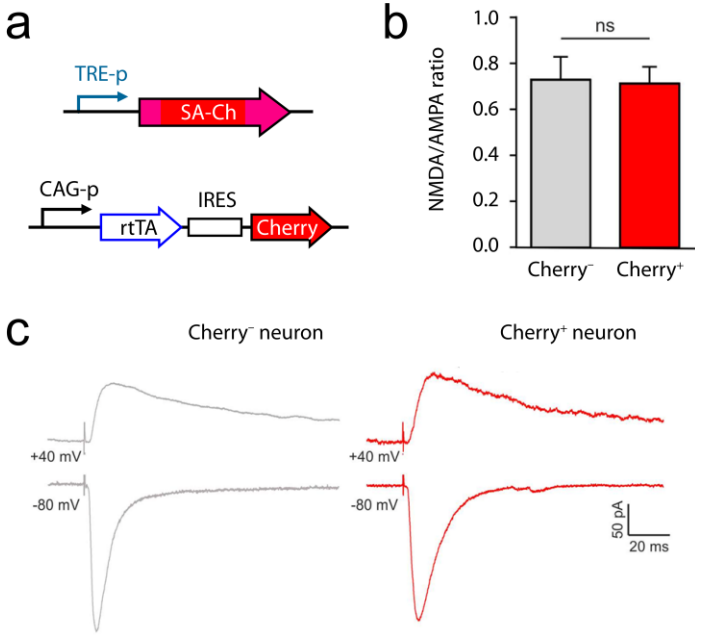

Figure 49 SA-Ch expression does not affect the NMDA/AMPA ratio at CA3-CA1 synapses. **a** Schema of costructs used. **b** NMDA/AMPA ratio for Cherry-negative and Cherry-positive neurons. Average values are expressed as mean±s.e.m. P = 0.52. ns (non-significant), Mann-Whitney test. **c** Representative traces of isolated AMPA- (bottom) and NMDA- (top) EPSCs evoked by Schaffer collateral stimulation in one Cherry-negative CA1 cell (grey traces) and one Cherry-positive CA1 neuron (red traces). The average of ten traces is shown. Stimulation artefacts have been truncated for presentation purposes.

NMDAR components of currents were registered from SA-Ch$^+$ neurons. Mice were electroporated unilaterally with

TRE::SA-Ch and CAG::rtTA-IRES-mCherry to facilitate neuron recognition during electrophysiological recording (Figure 49a). After inducing SA-Ch for 4 days, evoked responses from CA3→CA1 Schaffer collateral stimulation were recorded in patched CA1 pyramidal neurons in whole-cell voltage clamp configuration. The excitation stimulus was calibrated to obtain a half-maximum response, as evaluated with a calibration curve for each neuron. AMPA-EPSCs were recorded at V_m= −80mV, while NMDA-EPSCs were recorded at V_m =+40mV in the presence of AMPAR inhibitor NBQX.

The ratio of NMDA-EPSCs/AMPA-EPSCs was measured from recorded SA-Ch$^+$/Cherry$^+$ neurons; as control, Cherry$^-$ neurons in the non electroporated hippocampus in the other hemisphere were recorded. As it can be seen in Figure 49, SA-Ch expression did not significantly alter the ratio of recorded NMDA/AMPA EPSCs, confirming that also *in vivo*, the expression of SA-Ch did not alter neuron physiology.

Mapping synapses potentiated by context exploration

Next, I sought to map potentiated synapses by a behavioural task as the exploration of a new context by looking at spines expressing SA-Ch. Mice were given doxycycline for 3 days to activate SA-Ch RNA transcription; this was enough for SA-Ch to be expressed at synapses (Figure 50). On the fourth day, an additional dose of doxycycline was given, and mice were let exploring a new environment for three hours (see Figure 46). This paradigm is known to induce IEG expression in the hippocampus of mice and rats was given, and mice were let exploring a new environment like c-fos

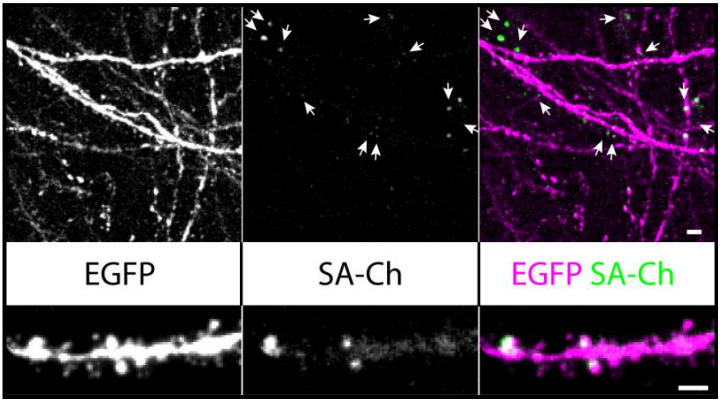

Figure 50 SA-Ch expression after 3.5 dayd of doxycycline administration. Arrowheads indicated spines expressing SA-Ch. Scale bar, 2μm.

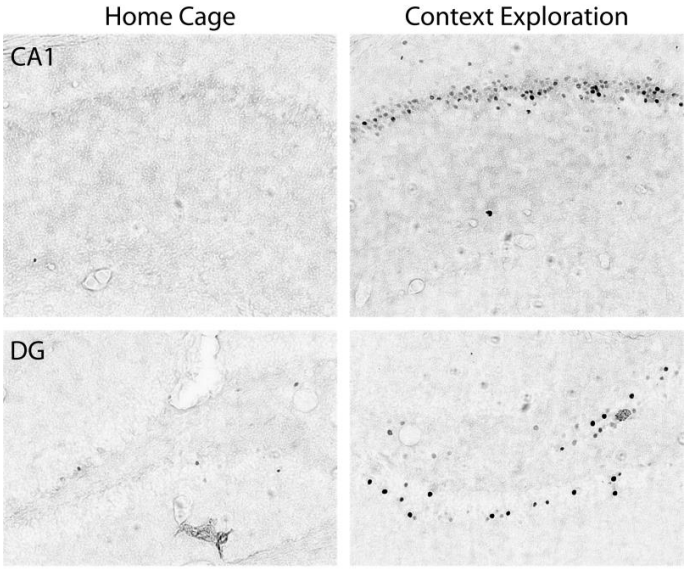

Figure 51 A new context exploration increases the nuber of c-fos$^+$ neurons in the hippocampal regions CA1 (Top row) and DG (Bottom row). Immunohystochemistry againt c-fos on sections from home caged or context exploration mice.

and Arc (Guzowski, 2002; Rinaldi et al., 2010). Indeed, mice sacrificed after one hour from being put in the new context showed robust c-fos expression in CA1 and in the DG, while in home caged mice a much lower number of c-fos$^+$ cells was found (Figure 51).

I then compared the expression of SA-Ch at potentiated synapses in animals that explored the new context for three hours, and compared it with animals that

remained in their home cage for an equal amount of time. This gives a baseline that accounts for potentiated spines during the time doxycycline was present in the organism. The exploration of a novel context increased the number of SA-Ch –expressing spines (Figure 52a); this was true both for pyramidal neurons in the CA1 region and for granule cells in the dentate gyrus (Figure 52b).

Potentiated synapses form clusters *in vivo*

Observing the distribution of potentiated spines along dendrites, I noted a tendency to be in close proximity to other potentiated spines[†] (see Figure 50 or Figure 52a). This suggests that potentiated synapses cluster together; indeed, clustering has been proposed in models for cooperative integration of synaptic activity in neuron computation, sensory integration, and memory formation (Govindarajan et al., 2006; Kastellakis et al., 2015; Knierim and Neunuebel, 2016). For example, a cooperative model for LTP induction

[†] I will use the term "potentiated spine" and "potentiated synapse" rather interchangeably, although the term is not strictly correct since potentiation is the change in response of a synapse. By that locution I mean "a spine being part of a potentiated synapse", for the reason that potentiated synapses are detected by the post-synaptic expression of SA-Ch. Given that a spine is virtually always associated to a presynaptic teminal – thus forming a synapse – I hope the reader will excuse the extension of the concept for the sake of fluency. Note that a similar use can be found for example in Govindarajan et al. (2011).

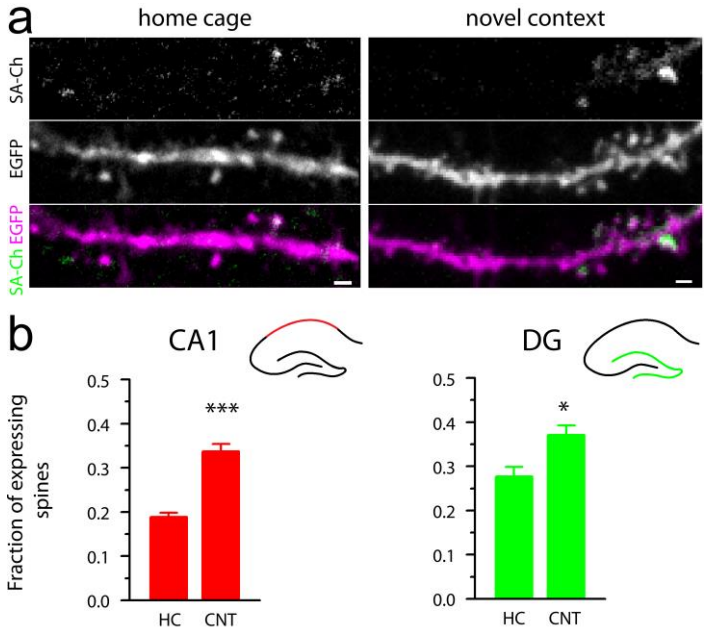

Figure 52 The exploration of a novel context increases the number of SA-Ch –expressing spines **a** Representative images of SA-Ch/EGFP CA1 pyramidal neurons from home cage or novel context animals. Scale bar, 1μm **b** Quantification of SA-Ch$^+$ spines in CA1 and DG for the home cage (HC) and novel context (CNT) groups. *P<0.05 and ***P<0.001 Student's t-test, two-tailed. Bars are means±s.e.m.

proposes clustering of incoming activity as a facilitator of plasticity (Govindarajan et al., 2006), which in turn could facilitate the reactivation of the neuron after stimulation of the cluster of potentiated spines during memory recall (Kastellakis et al., 2015). I therefore calculated the reciprocal distances between all spines to see whether

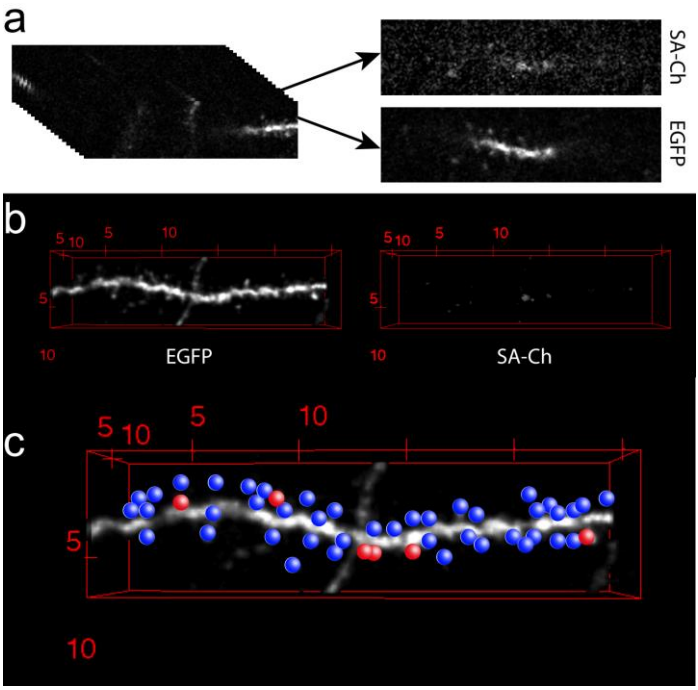

Figure 53 Calculation of inter-spine distance. **a** Slices of the stack encompassing the dendrite of interest were considered and each slice was analyzed in the two channels (EGFP and SA-Ch). The (x,y,z) position of each spine was therfore annotated in the 3D plane. **b** 3D rendering of the two channels of the same dendrite in (**a**). Axes are in red and units are in µm. **c** The procedure gave a map of the spines in the three axes for SA-Ch^{+} (red) and SA-Ch^{-} spines (blue). 3D rendering was performed with ImageJ plugin 3D viewer.

potentiated spines are actually closer to each other than it would occur by chance. As dendrites extend in the three-dimensional space, I first annotated the spatial positions of each spine in the three coordinates, and I assigned different

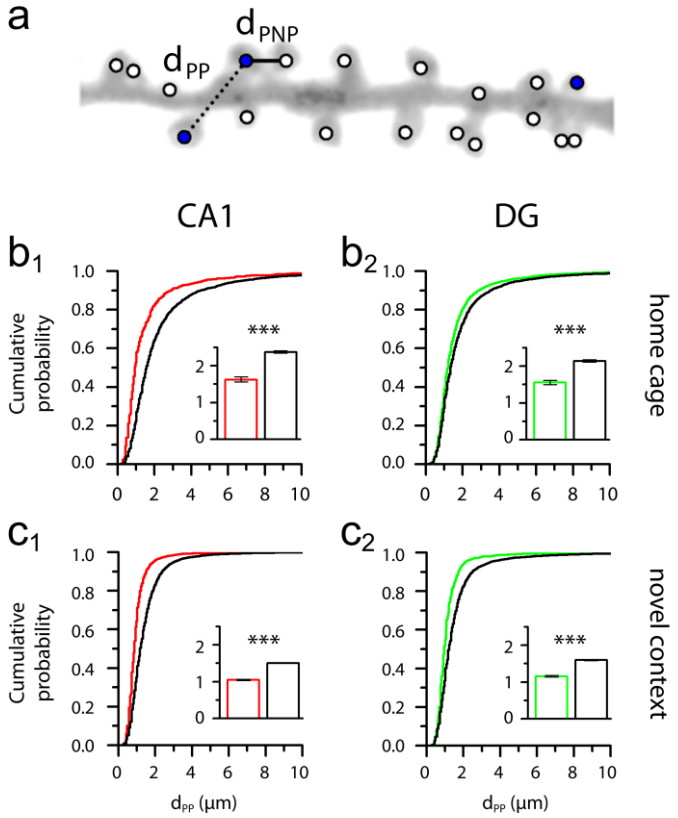

Figure 54 a Schematic representation for d_{PP} and d_{PNP} description. SA-Ch$^+$ spine (potentiated) are in blue, SA-Ch$^-$ are in white. **$b_{1\text{-}2}$** Cumulative distribution of d_{PP} in CA1 (**b_1**) and DG (**b_2**) dendrites of home caged animals. **$c_{1\text{-}2}$** Cumulative distribution of d_{PP} in CA1 (**c_1**) and DG (**c_2**) dendrites on animals exploring a novel context. Coloured lines represent the calculated distribution, black lines the distributions calculated after randomizing positions. Inset, mean±sem of the populations in corresponding graphs. ***P<0.001 Kruskal–Wallis test, followed by Dunn's comparison.

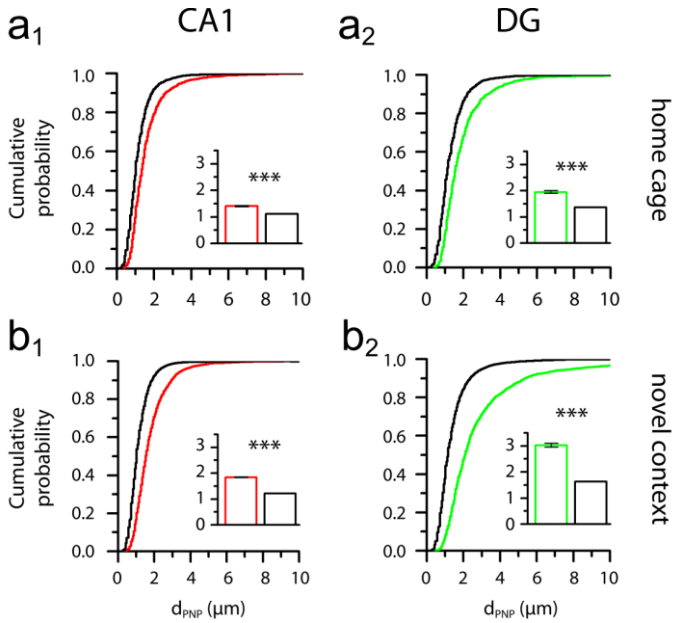

Figure 55 **a$_{1\text{-}2}$** Cumulative distribution of d_{PNP} in CA1 (**a$_1$**) and DG (**a$_2$**) dendrites of home caged animals. **b$_{1\text{-}2}$** Cumulative distribution of d_{PNP} in CA1 (**b$_1$**) and DG (**b$_2$**) dendrites on animals exploring a novel context. Coloured lines represent the calculated distribution, black lines the distributions calculated after randomizing positions. Inset, mean±sem of the populations in corresponding graphs. ***P<0.001 Kruskal–Wallis test, followed by Dunn's comparison.

labels whether they are expressing SA-Ch or not (Figure 53). Then, I calculated the Euclidean distance for each pair of spines. I called d_{PP} the distance between a potentiated spine and its nearest SA-Ch$^+$ neighbour, and d_{PNP} the distance a potentiated spine and the closest SA-Ch$^-$ spine (Figure 54a).

Potentiated synapses could be in close proximity as a consequence of chance distribution alone; however, if this would be the case, one would observe no difference after random swapping the positions of the annotated spines (SA-Ch^+/SA-Ch^-).

I found that the measured d_{PP} distances for CA1 and DG neurons were significantly smaller than what would happen by chance alone (Figure 54b). This was true for both animals of the home cage group and of the novel context group (Figure 54c). Consistently, measured d_{PNP} distances were higher than d_{PNP} calculated after randomly reassigning positions to SA-Ch^+ spines (Figure 55). Thus, potentiated spines have a marked propensity to be close to another potentiated spine. To evaluate the extent of cluster I calculated the likelihood of a spine at varying distances from a potentiated spine to have undergone potentiation during the tagging time. I therefore ordinated spines according to their linear distribution along dendrites and considered a 20-spines window starting from a SA-Ch^+ spine (Figure 56). I found that spines closer to a potentiated synapse were more likely to express SA-Ch^+, and the probability of being potentiated significantly deviated from the chance level up to the third or fifth neighbour (Figure 56). The behaviour was similar in CA1 and DG neurons; context exploration

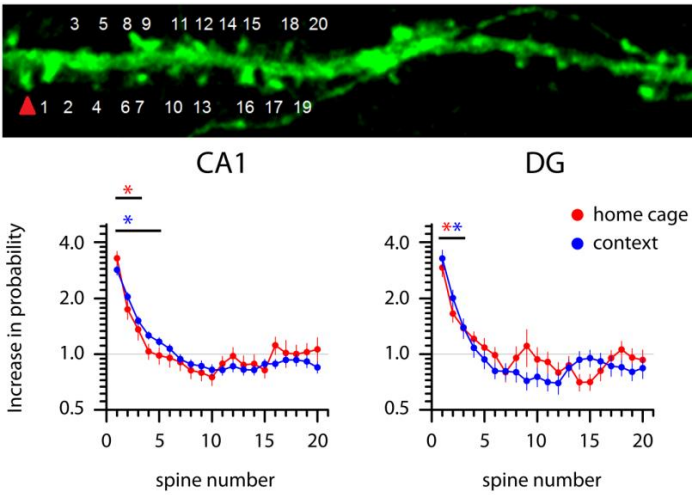

Figure 56 Top, schematic representation of cardinal numbering from a potentiated spine (red arrowhead). Bottom, fold-increase in the probability of the i-th spine from a potentiated one to be potentiated itself. The value is calculated for the first 20 neighbors of a potentiated spines in CA1 (left panel) and DG (right panel) neurons. Under the assumption of random distribution of potentiated spines, this value should be 1 uniformly. *P<0.01, z-test from the reference value of 1. Points are mean±SEM.

further increased the probability of close spines to undergo potentiation together. I therefore defined as cluster a set of potentiated synapses as a set of SA-Ch synapses comprising at least two spines separated by no more than 2μm, i.e., two spines belong to the same cluster if their interdistance is less than 2μm. Although arbitrary, this threshold seems a reasonable value when taken into account the physical

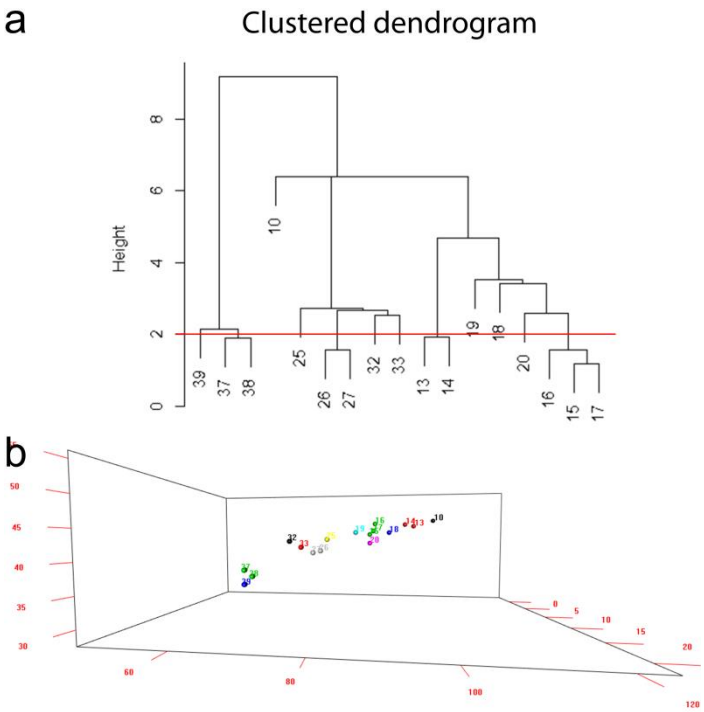

Figure 57 Linear clustering algorithm. **a** The algorithm sorts potentiated (SA-Ch+) spines according to their euclidean distance in microns (height) **b** Resulting sorting of potentiated spines into sets (represented with different colours). For example, the distance between spines #15 and #17 is lower than 2μm and belong to a set (green in **b**); spine #16 is further away than 2μm from #15, but not from #17, therefore spines #15, #16 and #17 form a cluster. Spine #10 does not have any potentiated spine within 2μm, so it forms a set of unitary dimension.

dimensions of spines and their interdistance. I used a so-called "linear" clustering algorithm, which reflects the physical disposition of spines along dendrites, where one

spatial component predominate over the other two (Figure 57a). Furthermore, this confers the property of "adding up" spines if they satisfy the condition of being within 2μm of a spine that already belongs to a spine set. This gave us a series of sets of potentiated synapses for each dendrite of the various samples (Figure 57b). Of course, these spine sets could be represented either by a single potentiated synapse or by a number of potentiated synapses in close proximity (clusters).

Both in CA1 and in the DG, the exposure to a novel context increased the dimension of the sets of potentiated synapses (Figure 57a). After exposure to the new context, a larger number of potentiated spines was in a cluster: in home-caged animals, 86% and 85% of spines in CA1 and DG, respectively, belonged to a cluster and the exposure to a novel context increased this proportion to 95% and 94%, respectively. In addition, clusters were larger in the dendrites of animals that were exposed to the new context (Figure 57b-d). It is therefore possible that the presentation of the new context potentiates new synapses and forms new clusters, or that pre-existing clusters (or single potentiated spines) expand incorporating nearby spines, facilitating their potentiation. While the first possibility would probably sound more consistent with a model with fixed neuron-to-

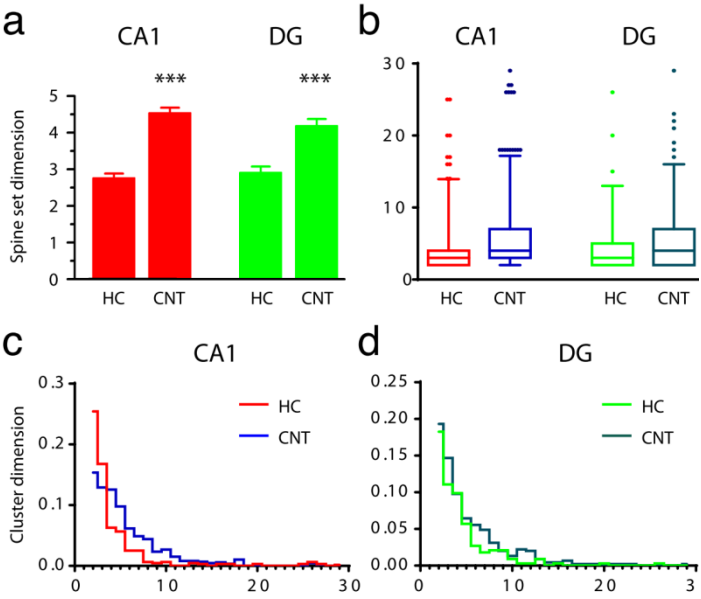

Figure 58 a Dimension of spine sets after clustering in CA1 neurons (red) and DG (green). In the new context groups (CNT) spine sets are bigger and contain a larger number of spines than in the corresponding home cage goups (HC). ***P<0.001 Kruskal–Wallis test, Dunn's comparison. Bars are mean±s.e.m. **b** Distribution of dimension of clusters of potentiated synapses (sets with at least 2 spines). Box is 25-75 percentile, whiskers are 2.5-97.5%. **c,d** Frequency distribution of cluster dimensions for CA1 (**c**) and DG (**d**) groups.

neuron connections, it would not be too surprising if also cluster expansion would contribute to the encoding of a mental representation. Indeed, at the neuronal level, it has been demonstrated that, in the amygdala, neurons that are artificially made more excitable, by means of CREB overexpression, are preferentially recruited in the encoding

and storage of memories (Han et al., 2007, 2009; Zhou et al., 2009). Then, it was found that DG cells with a higher firing rate before the exposure to a new environment are preferentially activated during the exploration, further increasing their firing (Kirschen et al., 2017). In other words, neurons with higher activity or propensity to be activated at the time of the stimulus presentation are more likely to become part of the new engram. Thus, an analogous mechanism might be working at synapses: the presence of a synapse giving a stronger response upon (re)stimulation could facilitate the induction of potentiation in close synapses during neuron activity, and the new set of spines could be more likely to be recruited into an engram.

Discussion – Clustering in LTP and memory encoding

Within the framework of synaptic plasticity, two main possible patterns of distribution have been proposed (Govindarajan et al., 2006): a clustered plasticity model, in which the synaptic engrams of given learning paradigm are clustered in a close proximity on a dendrite and a dispersed plasticity model where the synaptic engrams are randomly distributed within the dendritic arborisation (Figure 59). Indeed multiple possible mechanisms could explain

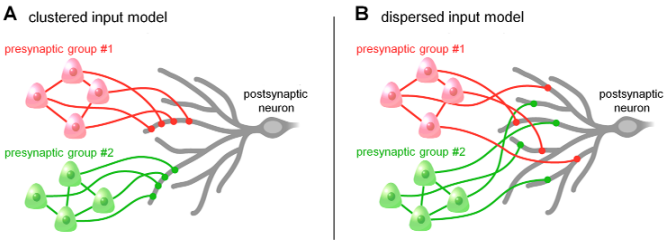

Figure 59 Two working hypotheses for the spatial patterns of dendritic inputs from presynaptic cell assemblies. In the clustered input model (**A**), afferents from synchronous neuron group 1 (or 2) converge onto a small segment of a postsynaptic neuronal dendrite; in the dispersed input model (**B**), the afferent terminals diverge over the dendritic trees. Reproduced from Takahashi et al. (2012).

clustering of potentiated spines. First, they could be due to multiple innervation from the same axon in close proximity. Indeed, McBride et al. (2008) showed that axons projections in the barn owl auditory system form multiple contacts to the same postsynaptic neuron within a few tens of microns. Although tonotopy in this system may facilitate this particular disposition, a recent report showed the presence of hotspots of spine turnover in the dendrites of the mouse retrosplenial cortex (Frank et al., 2018). Training increases the number of potentiated spines in cluster, and the fraction of clustered spines over the total gained positively correlated with the memory performance in a slow variant of contextual fear conditioning with a slow learning curve. It is likely that these newly added spines correspond to potentiated

synapses, as NMDAR inhibitor MK801 impairs this clustering, and it has been shown that newly formed spines are stabilized by individual LTP induction (Hill and Zito, 2013). Thus, although they employ a looser definition of cluster than ours (5μm), the results of Frank et al. (2018) are in substantial agreement with ours. It can be speculated that newly formed spines are stabilised when they come in contact with the axons of the neurons that formed previously potentiated synapses.

A second explanation could be that synchronous activity of spatially close spines could facilitate local depolarization and LTP induction. Clustering of co-active synapses has been demonstrated in CA3 (Kleindienst et al., 2011) and CA1 (Takahashi et al., 2012) dendrites of acute hippocampal slices by means of calcium imaging. Similarly, coactive synapses were found in cortical neurons both in ex vivo preparation of V1 area in the basal dendrites of layer 5 neurons (Gökçe et al., 2016) and in layer 2/3 pyramidal neurons in the somatosensory cortex (Takahashi et al., 2012). Indeed, the distance between co-active spines was smaller than what it would be expected by chance; vice-versa, close spines are more probable than chance to be active (Figure 60). Potentiation is likely to be involved in this phenomenon, as spines that participate in this assemblies

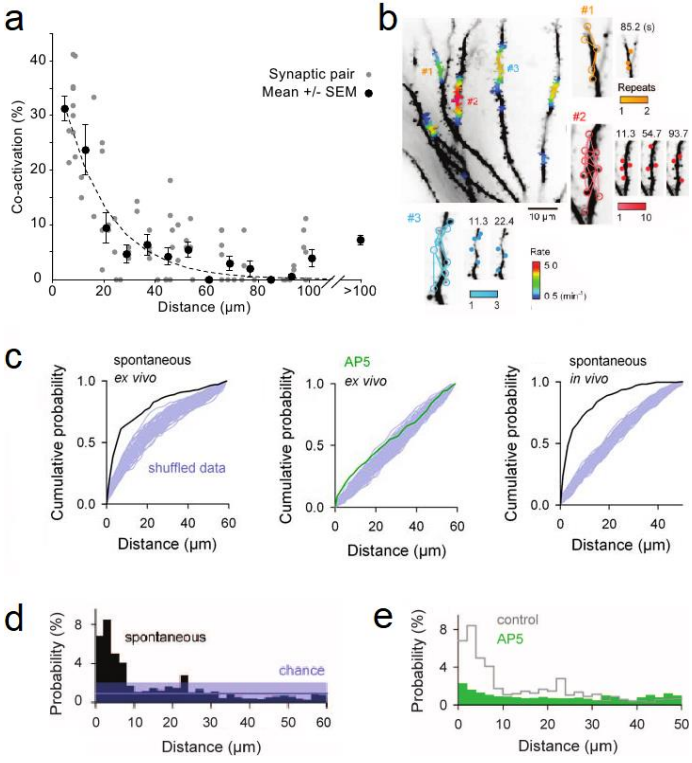

Figure 60 Clustering of co-activity between synapses of the same dendrite. **a** Relationship between intersynaptic distance and co-activation for all synapse pairs in a CA3 neuron from an acute hippocampal slice. Modified fromKleindienst et al. (2011). **b** A heat map of the frequency of assemblets in dendrites of a CA1 neuron (acute hippocampal slice). Assemblet dynamics in hot zones 1, 2, and 3. **c** Distribution of the distance between two coactivated spines was compared to that in stimulations after reshuffling. In vivo data in from layer 2/3 neurons in the somatosensory cortex. **d** The probability of observing spines coactivated within 100 ms as a function of the distance from a given spine in CA1 neurons from an acute hippocampal slice. The chance level and its 95% confidence intervals were estimated from the distribution of distances of more than 10 µm. e Probability of spine coactivation in presence of 100µM AP5. **b,c,d** are modified from Takahashi et al. (2012).

(or functional clusters) are bigger in volume than the rest of them (Takahashi et al., 2012). Also, NMDAR plays a role in the formation of these functional clusters, as treatment with AP5 impairs their preferential distance (Figure 60e). By looking at changes in volume, a correlate of synapse potentiation, Harvey and Svoboda (2007) demonstrated that LTP induction on one spine could facilitate LTP in spines within 10μm, producing long-lasting changes by a subthreshold protocol that would normally not.

Third, the diffusion of intracellular signalling molecules (or, less likely, of extracellular glutamate) could explain the emergence of clusters of potentiated synapses. After LTP induction, MAPK and mTOR signalling can exert an effect over a stretch of dendrite (Govindarajan et al., 2006), and active effector like Ras can diffuse within 10μm of the stimulated synapse (Harvey et al., 2008a). Analogously, PRPs may also be confined in a spatial frame of several microns (Rangaraju et al., 2017; Winnubst and Lohmann, 2012). In support of this, synaptic capture (STC) has been shown to be facilitated if the synapse receiving the subthreshold stimulation is on the same dendrite as the synapse receiving the suprathreshold tetanus; furthermore, efficient STC on the same dendrite of hippocampal organotipic slices can take place within 30μm of the

tetanized synapse, and STC efficiency drops to zero when the distance between the two spines is 70μm (Govindarajan et al., 2011). Similar results were obtained by Harvey and Svoboda (2007) in acute hippocampal slices, albeit they found a smaller distance threshold (around 10μm) for efficient STC to take place.

The aspects I discussed above do not necessarily exclude each other. Indeed they focus on different aspects of the induction of clustered potentiation. Co-active spines (i.e. functional clusters) may facilitate the induction of a clustered form of plasticity, which relies on the local activation of a dendrite stretch via the sharing of PRPs – vice versa, PRPs diffusion may establish clusters of potentiated synapses, which posses the functional property of being coactive. Although no evidence for multiple boutons from the same axon has been found in Takahashi et al. (2012) and Kleindienst et al. (2011), their data still do not rule out the possibility that new spines can form and be stabilized on axons that established a previously potentiated synapses in close proximity. By looking at the connectivity between CA3 and CA1 neurons with matched birth time, Druckmann et al. (2014) then found that the distribution of the CA3-CA1 synapses is clustered on CA1 dendrites; when read with the hindsight of the data I summarized here, it can be speculated

that a pre-existing structured connectivity could underlie, at least to a certain degree, to the emergence of clusters of potentiated spines.

Regardless of the mechanism, clustering can have a profound impact on memory encoding (Routtenberg, 2008). Clustering of activity can determine nonlinear integration of synaptic inputs (Häusser and Mel, 2003), facilitating the response to a given stimulus or the encoding of a unitary piece of representation from converging inputs (Govindarajan et al., 2006; Kastellakis et al., 2015). By imaging the formation of spines in motor cortex dendrites, Fu et al. (2012) analyzed the spine changes that occur during the learning of a motor task that was repeated over multiple days. During this learning protocol, the majority of new spines in the dendrite were more clustered than control spines (<5 μm), and the process was dependent on the activation of NMDA receptors. Newly formed spines, are highly likely to be added to the existing clusters and clustered spines are more stable, thus contributing to the refinement or reinforcement of motor learning, given the correlation between the extent of motor learning and the clustering of new. Increased anatomical clustering of potentiated synapses, detected with the incorporation of fluoresent falloidin, has also been observed in an *in vitro*

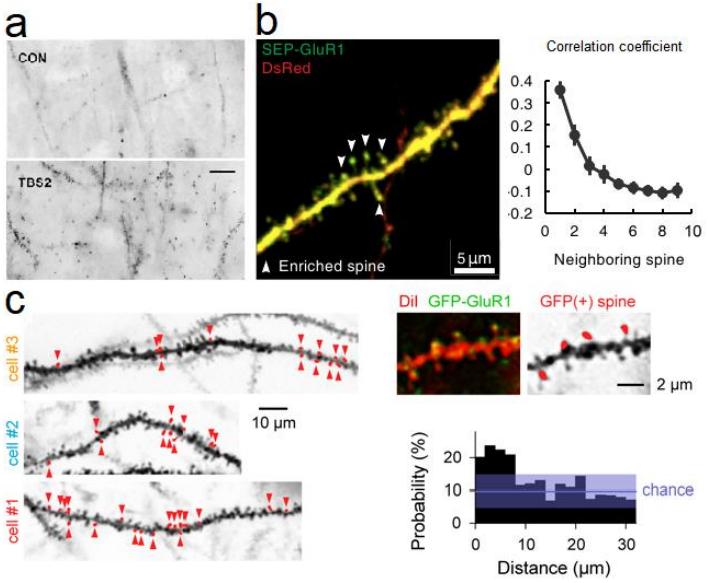

Figure 61 Detection of cluster of activated spines **a** fluorescent falloidin incorporation after theta burst stimulation of hippocampal slices. From Kramár et al. (2012). **b** Clustering of spines incorporating fluorescent SEP-GluA1 after whisker stimulation in the barrel cortex. Modified from Makino and Malinow (2011) **c** Clustering of GFP-GluA1 incorpoating spines after 500s of novel context exploration. Modified from Takahashi et al. (2012).

study which simulated spatial learning in the hippocampus (Kramár et al. 2012) (Figure 61a). Last, the incorporation of fluorescently tagged GluA1 subunits has been used to mark spines that expose AMPA receptors in the barrel cortex in response to whisker stimulation (Figure 61b) (Makino and Malinow, 2011; Zhang et al., 2015). Similarly, GFP-GluA1 was expressed in c-fos^{+} CA1 neurons and tagged spines during a novel context presentation were identified by green

Reference	No. of spines	Physical dimension	Method
Kleindienst et al. (2011)	ND	< 16µm	Calcium imaging of CA3 neurons
Takahashi et al. (2012)	2-12 (3.6±0.7)	4.7 ±3.3 µm[‡]	Calcium imaging of CA1 neurons
Takahashi et al. (2012)	ND	< 28µm (7.7±6.7µm)	Calcium imaging in L2/3 in the somatosensory cortex
Gökçe et al. (2016)	4-14	< 30µm	Calcium imaging if L5 V1 cortical neurons
Makino and Malinow (2011)	ND	ND	SEP-GluA1 incorporation in L2/3 in the barrel cortex
Takahashi et al. (2012)	ND	< 8µm	GFP-GluA1 incorporation in CA1
Harvey and Svoboda (2007)	ND	< 10µm	Crosstalk in LTP (change in volume)
Fu et al. (2012)	ND	ND	New spines L5 Motor cortex
Druckmann et al. (2014)	ND	ND	CA3-CA1 GRASP connectivity
Kramár et al. (2012)	ND	ND	Phalloidin incorporation in CA1 neurons after TBS LTP
this work	2-13[§]	ND	CA1, home cage
this work	2-14[**]	ND	CA1, novel context
this work	2-10[**]	< 6.06 µm[**] 2.1±1.9 µm[††]	DG, home cage
this work	2-13[**]	< 8.33 µm[††] 2.8±3.5 µm[‡‡]	DG, novel context

Table 1 List of works demonstrating clustering of spines and provide an estimate for cluster dimensions. Works employing different criteria in their definition of clusters are included, and the employed method is reported in the table.

[‡] A threshold of 10µm is set as maximum distance in the authors' definition of assemblets.
[§] 5th-95th percentiles
[**] 95th percentile
[††] mean ± standard deviation

AMPAR enrichment (Figure 60c). This confirmed the functional clustering of correlated activity observed in acute hippocampal slices (Takahashi et al., 2012). In this section, I described the employment of SynActive to label synapses that underwent translational-dependent potentiation in the hippocampus of live mice exploring a novel context. The data demonstrate the presence of clusters of potentiatated synapses by local translation of SA-Ch and extend the existing knowledge on the long-lasting synaptic changes such as translation-dependent LTP.

SynActive, as discussed in the previous section, tags synapses that underwent translational-dependent L-LTP. Imaging correlated activity, GFP-AMPAR–expressing spines and SA-Ch$^+$ spines therefore detect different aspects of synaptic activity. The fact that the use of these three unrelated reporters give substantially consistent estimates in terms of number of spines and physical distance (Table 1) strongly suggests that these phenomena are not independent one from the other. It would be interesting then to directly compare these aspects at least in a pairwise way (i.e. compare SEP-GluA1$^+$ and SynActive$^+$ spines / co-active spines and SynActive$^+$ spines, and so on) to evaluate the overlap of these clusters definitions. Also, it would be helpful to define how two aspects of spine physiology are

related to clustering of potentiated spines, i.e. spine enlargement and new spine formation.

Uneven distribution of spines in DG dendrites

Looking at dendrites of granule cells in the molecular layer, I noticed that SA-Ch –expressing spines were distributed unevenly along the radial axis of the molecular layer comprising the non-hilar dendrites of DG cells (Figure 62). I found that potentiated spines were preferentially localized in the most proximal part of dendrites (<40μm) and in the distal part (70-120μm). On the contrary, the middle molecular layer had fewer potentiated spines in the home cage group. Vice versa, after the exploration of the novel environment, spines became potentiated also in the 40-70μm region; an apparent increase in the most distal part, corresponding to the end of dendrites, was also observed in these animals. Consistently, different mechanisms for synaptic integration seem to exist in proximal and distal portions of DG dendrites (Krueppel et al., 2011). This may be due to a lower threshold for potentiation in more distal dendrites, as suggested by Häusser (2001), or could reflect the segregation of incoming inputs (Amaral et al., 2007).

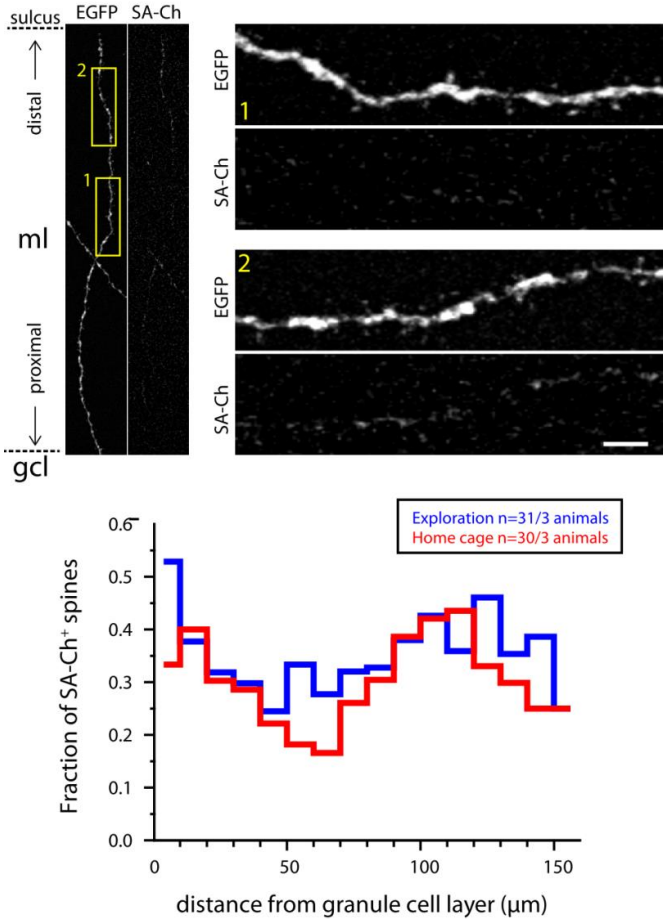

Figure 62 Uneven distribution of SA-Ch+ spines in the molecular layer (ml). The soma layer is on the bottom (gcl), and the outer molecular layer terminating at the sulcus level is oriented on the top. On the rght, magnification of regions 1 and 2 as indicated on the right. Scale bar, 10µm. Below, distibution of SA-Ch$^+$ spines along the radial axis encompassing the molecular layer for the home cage (red) and novel context (blue) groups. Zero pos indicates the end of the granule cell layer.

When looking at single dendrites, I found that in the home cage group the 40-70μm region was anticorrelated with the more distal 90-120μm in terms of fraction of potentiated synapses (Figure 63). Conversely, the 70-90μm region was positively correlated with the 70-90μm region. After the new context exploration, all regions were positively correlated with each other. This is probably due to the fact that, in the home cage group, a population of neurons exists with a higher proportion of potentiated spines and a lower fraction in the proximal part of the dendrites. In the new context group, this population is less represented, and dendrites with a higher number of potentiated synapses in the distal dendrite tend to have a high number of potentiated synapses in the whole dendrite. This is supported by the observation that the electrical activity of the distal portion of the dendrite can propagate to whole dendrite (H.Beck and T.Kelly, personal communication).

I next sought to see whether there are differences in clustering along the dendrites of dentate granule cells. Two parameters were considered, i.e. the cluster dimension (the number of SA-Ch$^+$ spines in a cluster) and the cluster extension (the distance, in μm, between the two most distant spines in a cluster). In home caged animals, there was no significant trend moving distally along dendrites, and we

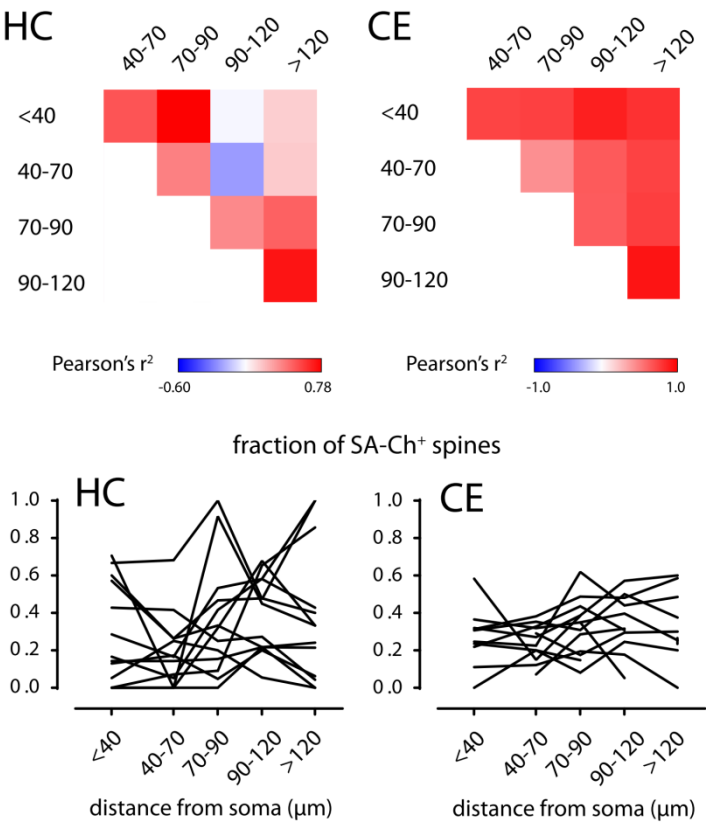

Figure 63 Pearson's r^2 coefficient between the regions <40 µm, 40-70 µm, 70-90 µm, 90-120 µm and >120 µm in home cage (HC) and context exposure (CE) group. Below, traces of single dendrites reporting the number of potentiated synapses in each interval.

identified a small population of larger cluster between approximately 70 and 120µm, consistently with the

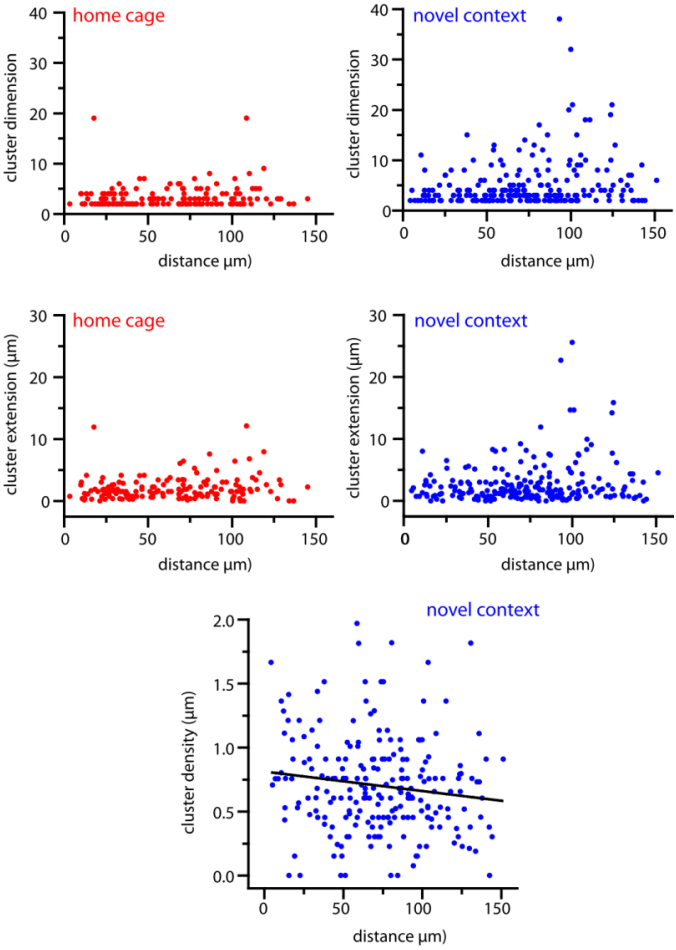

Figure 64 Cluster dimension (number of spines) and extension (distance between the most distant spines in a cluster) for home cage (red) and novel context (blue) groups at varying distance from the granule cell layer. Below, cluster density (extension divided by dimension) displays a significant negative trend at increasing distancs moving distally along the dendrite.

distribution of potentiated spines (Figure 64). Context exploration determined an increase in large clusters along the whole dendrite, and an enlargement of clusters in the 70-120μm region.

I calculated the ratio of the cluster extension divided by the cluster dimension and I called it "cluster density"; the more closely spines in a cluster are packed, the lower the cluster density value is. A significant negative trend was observed moving distally along the dendrites of granule cells, meaning that clusters of potentiated spines are denser in the distal region. It has been shown that synaptic activation in dentate granule cells is characterised by a very strong dendritic attenuation (Kelly and Beck, 2017; Krueppel et al., 2011). Thus, an intriguing possibility is that, in order for a relevant signal to be able to reach the soma, distally located cluster need to recruit a large number of closely packed synapses to efficiently transmit their information content. This could be the source for a more global activation of the dendrite, extending the number of potentiated synapses also in more proximal portions of the dendrite.

Uneven distribution of potentiated spines across neurons

When I compared the disposition of SA-Ch$^+$ spines across neurons in single slices, I noticed that they were not equally represented in different neurons. Some neurons had a higher density of potentiated synapses than nearby dendrites, while some had less. This segregation appeared to be more marked in dentate granule cells than in the CA1 region, where the distribution of potentiated spines looked more uniform, as evidenced in Figure 65a. To quantitatively express this observation, I calculated the absolute deviation of the observed number of potentiated spines from the expected number, normalized on the expected number (Separation Index). For each dendrite, the expected number was estimated by considering the average fraction of potentiated spines in all dendrites analysed in the same slice, multiplied by the number of spines (both SA-Ch$^+$ and SA-Ch$^-$).

When I calculated the Separation Index for the dendrites in our dataset, I found confirmation that dendrites in the DG assumed a greater value than in the CA1 (Figure 65b). This was even more striking when looking at the distribution of the Separation Index (Figure 65c): in the new context group, the majority of dentate granule cells assumed

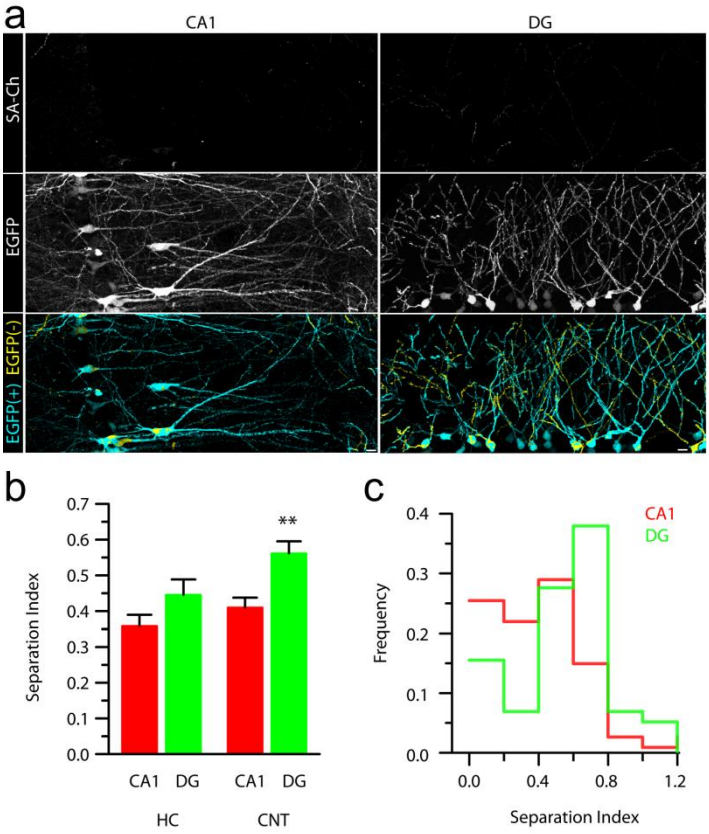

Figure 65 a Localization of SA-Ch⁺ regions (yellow) and SA-Ch⁻ negative region (cyan). The SA-Ch and EGFP channels are shown above. Scale bar, 10μm **b** Separation index for the home cage (HC) and new context (CNT) groups in CA1 and DG. A large separation index value indicates that the number of .potentiated spine in the dendrite strongly deviates from the expected value if potentiated spines were equally distributed in neurons from the same slice. **P<0.01 Kruskal–Wallis test, Dunn's comparison. **c** Separation index distribution of dendrites in CA1 and the DG in context-exposed animals.

a large value for the index. On the contrary, the distribution was shallower and broader for the dendrites of CA1 pyramidal neurons. Thus, DG cells are separated in two distinct groups with either a large or a low fraction of potentiated synapses.

Discussion – Uneven distribution of potentiated synapses

The results presented above indicates that dendrites of granule cells behave more like a homogeneous unit, as also our correlation analysis on different dendritic regions in the DG suggested. Indeed, it has been shown that DG cells are characterised by a very strong dendritic voltage attenuation, so the impact of individual synapses on granule cell output is low. At the same time, integration is linearized by voltage-dependent boosting mechanisms (Krueppel et al., 2011). This could contribute to the sparseness of the activity of granule cells in vivo. In fact, the observed pattern indicates that a coherent set of presynaptic inputs (a "representation") converges onto few neurons in the DG (while it is more dispersed in CA1), while having little or no effect on the nearby granule cells. Thus, the data support a model where the dentate gyrus acts as a pattern separator, discriminating

different contexts. In this model, DG cells encode highly orthogonal contextual information, whereas downstream CA3 and CA1 complete and process this information (Knierim and Neunuebel, 2016; Rebola et al., 2017).

Concluding remarks

Tagging potentiated synapses

The possibility to identify and map activated neurons thanks to the use of activity-dependent promoters (Reijmers et al., 2007) opened new possibilities for experiments unfeasible before (Kawashima et al., 2014), allowing the rapid accumulation of new information regarding populations of cells involved in many types of memory in less than a decade (Kitamura et al., 2017). A similar methodology to map potentiated synapses has been lagging behind, with the exception of the important results that I mentioned in the previous sections (see the Discussion section in the chapter "SynActive Generation and Validation"). Although much effort has been dedicated in establishing a methodology to image synaptic plasticity (Padamesey and Emptage, 2011), to date none of the proposed solutions has apparently met all the expectations of the scientific community (Lee et al., 2016a). First attempts to identify synaptic plasticity focused on imaging synaptic vesicle fusion or postsynaptic activation with fluorescent calcium indicators (Gambino et al., 2014), or with FRET-based sensors of activity of effectors like CaMKII (Lee et al., 2009), ERK (Harvey et al., 2008b), Ras (Yasuda et al., 2006), Cdc42 and RhoA (Murakoshi et al., 2011). However, activity alone does not imply the involvement in the storage of a defined status and

not all active synapses become potentiated (Cichon and Gan, 2015; Winnubst et al., 2015).

The identification of active synapses has been tried with activity-dependent forms of methods based on pre-post synaptic complementation of split florescent protein, i.e. GRASP or Neurexin-Neuroligin mediated complementation (SynView, IdPrime). For example, activity-dependent promoters have been used (A. Nykjaer, personal communication) or the fusion of the presynaptic component to vesicle-localised proteins, so that complementation occurs only after neurotransmitter release (Lee et al., 2016a). Although employed in Drosophila neurons, the system has found limited application; furthermore, it only detects active rather than just potentiated synapses. An interesting study that appeared at the time of writing combined the GRASP system with the TetTAG technology to map the connections for the four possible pre/postsynaptic neuron couples (engram-nonengram/engram-nonengram) between CA3 and the contralateral CA1 region (Choi et al., 2018). An extension of the GRASP system by locally expressing the postsynaptic component can be envisaged in order to detect potentiated synapses (a "SA-GRASP"), with the possibility to map their input provenience by restricting the expression of the presynaptic component to specific projecting areas.

Indeed, the pool of newly translated proteins can be detected with the TimeStamp technology for fluorescence and electron microscopy. While this in principle allows the identification of novel translation after LTP induction, mapping potentiated synapses is probably beyond the scopes of Butko et al. (2012). In fact, it was not shown that potentiation necessarily results in expression at labelled synapses, nor that this translation allows for the unique identification of potentiated synapses.

Among the proposed solutions to image synaptic plasticity, the use of GluR1 subunits coupled to the pH-sensitive fluorescent protein family of pHluorins – which now exists in the green and red versions – is to date the most promising indicator to map potentiated synapses (Makino and Malinow, 2011; Tanaka and Hirano, 2012). Indeed, SEP-GluA1 has been successfully used in the motor cortex to map the activation of synapses after whisker stimulation (Makino and Malinow, 2011; Zhang et al., 2015). However, usable imaging of SEP-GluA1 exposure is only possible in live animals, as fixation disrupts the membrane impermeability and uniforms pH, making it impossible to distinguish the surface-exposed GluR1 pool from the total one (Kopec et al., 2006). This poses severe limitations to the dimension of the area that can be imaged, and to the duration

of the experiment. Also, this limits the applicability to the accessible brain areas by means of two-photon microscopy – essentially, a subset of cortical areas, like the somatosensory, the motor or the visual cortex – or with the use of endoscopes, although the technically challenging live spines imaging of basal CA1 dendrites has just been recently performed (Attardo et al., 2015).

One possible caveat, then, is that, while AMPA receptors are indeed rapidly exposed on the surface of spines that undergo sustained stimulation (Tanaka and Hirano, 2012) – which is generally accepted to be responsible for the increased currents following potentiation – nevertheless potentiation comprises dissociable events and phenomena (Park et al., 2014). Some do not last indefinitely and AMPA receptors incorporation may be transient (Constals et al., 2015). Instead, our strategy can act as reporter of a late-phase, translation-dependent LTP (L-LTP) and can be used to map potentiated synapses across a population of neurons in memory tasks, thus enabling to identify candidate "synaptic engrams". Indeed, SA-Ch significantly correlates with SEP-GluA1 accumulation on postsynaptic sites; however, spines with lower SEP-GluA1 enrichment were also in many cases devoid of SA-Ch, suggesting that SA proteins would tag the subpopulation of SEP-GluA1-

expressing spines that undergo L-LTP, a likely candidate for memory storage unit in the brain (Neves et al., 2008).

Work in acute hippocampal slices identified potentiated spines in CA1 with the incorporation of fluorescent phalloidin (Kramár et al., 2012). Indeed, LTP induces the rapid formation accumulation of F-actin (Okamoto et al., 2004), which is preferentially bound by phalloidin. Recently then, the incorporation of fluorescently tagged AMPA receptors has been observed *in vivo* in the mouse barrel cortex following whisker stimulation (Zhang et al., 2015), and in the hippocampus of context-exposed animals (Takahashi et al., 2012) providing the first observation of potentiated spines in vivo. The reporter that I developed provides a new way to identify potentiated synapses *in vivo* and identify spines undergoing late-phase, translation-dependent LTP (Reymann and Frey, 2007). In this work, I made use of the expression of SA-Ch to map potentiated synapses in the hippocampus following the exploration of a new context. Currently, I am employing fluorescent reporter variants of SynActive to map potentiated synapses in the motor cortex (Figure 66) and the hippocampus after fear conditioning (Figure 67). This will allow mapping of the localization and distribution of potentiated spines during memory encoding and maturation;

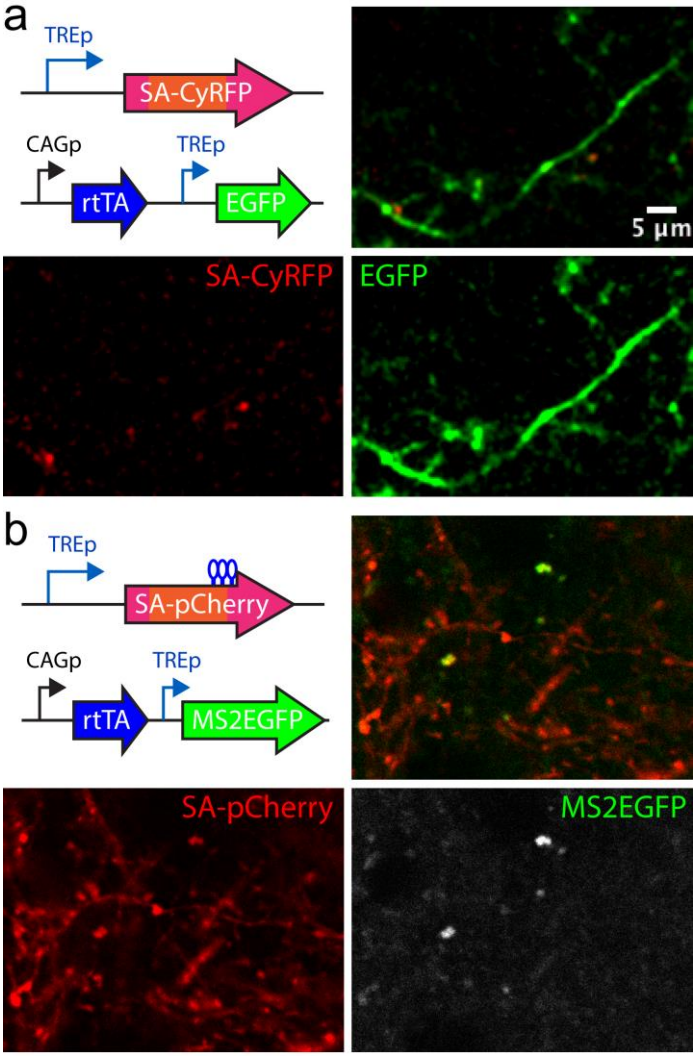

Figure 66 a Expression of SA-CyRFP, a red fluorescent reporter whose expression is regulated by SynActive and a tetracycline reporter, in the mouse motor cortex via in utero electroporation. **b** Dual color visualization of SA-palmCherry-*ms2* expression and of the transcript with MS2-EGFP. Image courtesy of Erez Geron and Wenbiao Gan, New York University.

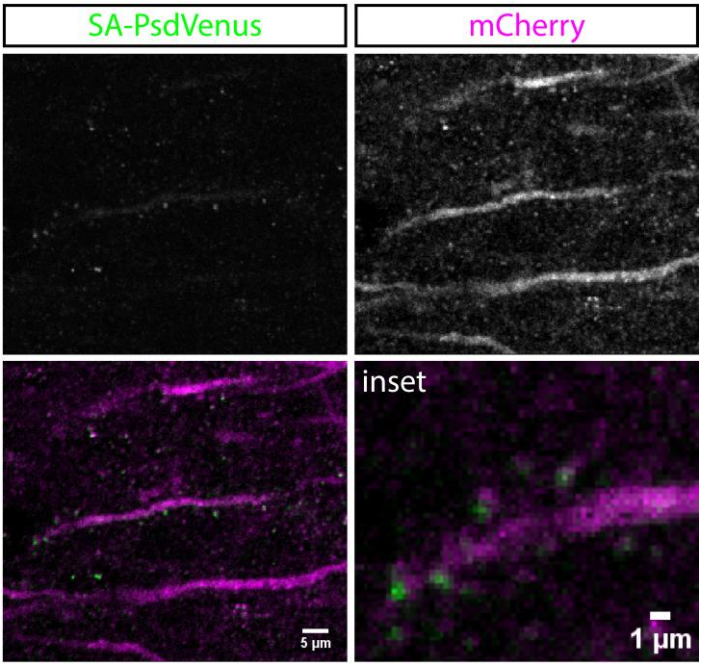

Figure 67 Identification of potentiated synapses after contextual fear conditioning. Mice were electroporated in utero in the hippocampal region CA1 with plasmids encoding TRE::SA-PsdVenus-HA and CAGG::rtTA-IRES-mCherry (thus expressing mCherry as filler); on P30, transgene expression was induced with doxycycline, and animals were fear conditioned in a new context the next day. After 90 minutes, animals were perfused and coronal slices were taken. Potentiated syanpses are identified with the expression of SA-PsdVenus-HA, a green/yellow fluorescent SynActive reporter, while mCherry was used as filler. The image is a single confocal slice from the stratum radiatum. Ongoing experiments in collaboration with Bruno Pinto and Laura Cancedda, Istituto Italiano di Tecnologia in Genova, Italy.

since it is known that ribosomes associated with dendritic spines re-localize during neuron activation, SA-reporters open the possibility to see how ribosomes relocalize with

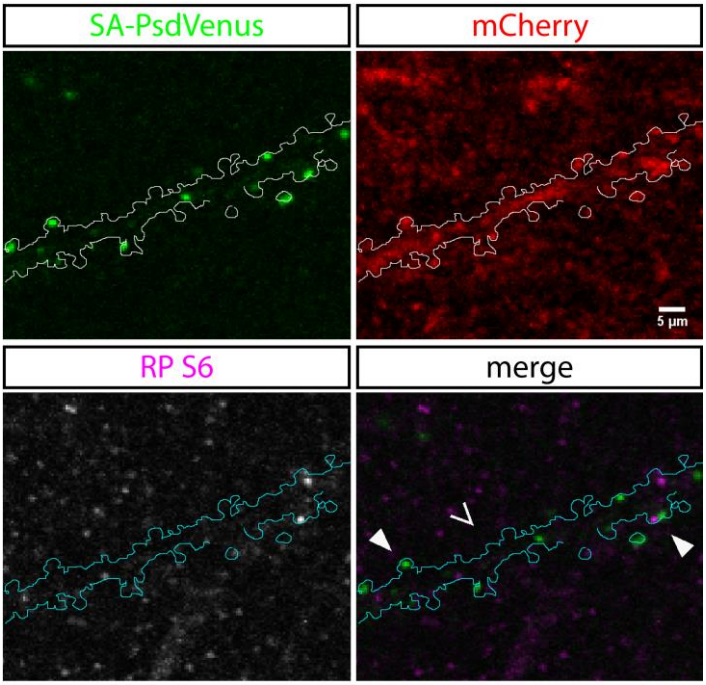

Figure 68 Observation of ribosome localization, detected with immunofluorescence against ribosomal protein S6, after fear memory recall of a contextual fear conditioned mouse. Animals were electroporated in CA1 and expression was induced with doxicyclyne on P30 (div 0) as in Figure 67. Potentiated synapses during memory formation and consolidation during day 1 are tagged by SA-PsdVenus-HA, and animals were fixed on day 2 90 minutes after re-exposure to conditioned context. Images are a single confocal slice, and line corresponds to a dendrite profile in the stratum radiatum. From a very preliminary analysis, it seems that during memory recall ribosomes are preferentially recruited in regions close to synapses potentiated during memory acquisition (filled arrowheads).

respect to potentiated synapses during memory formation and reactivation (Figure 68).

A tool for synapse reactivation

In order to highlight the role of potentiated synapses in a memory recall framework, it is necessary to envisage an experimental strategy to selectively act on them, but cell-wide neuron activation also recruits other learning-related mechanisms at the cellular level (Josselyn et al., 2015). Although subcellular optogenetic stimulation can be achieved by restricting the illumination pattern down to single spines (Packer et al., 2012), this requires a priori knowledge of the sites to be stimulated, which are not always known. Moreover, the feasible number and sparseness of distinct illumination spots heavily depend on technological aspects. On the other hand, the biologically achieved spatial restriction of Channelrhodopsin expression presented here, would allow unbiased excitation of recently activated synapses with standard experimental setups for wide-field illumination. In this scenario, light power should be adjusted so that the effect of the optical stimulation is similar to that of physiological synaptic events; from our results in culture, we have found that although blue light reactivation of the locally expressed SA-Ch is able to elicit calcium transients in a specific manner, these evoked calcium signals look somewhat smaller than calcium events occurring in the same spines spontaneously. However, as I discussed at the end of

the Section “SynActive generation and validation”, the coding sequence could to be changed into any ChR2 variants with larger photocurrents without interfering with the pattern of expression. For instance, the SynActive framework has proven quite flexible in allocating different reporters, as it has been shown in this section. Indeed, I have already cloned in the SynActive vectors two of the most sensitive Channelrhodopsin2 variants available at the time of writing, i.e. CheRiff (Hochbaum et al., 2014), and an improved, soon-to-be published version of the ChR-2-XXL (Dawydow et al., 2014), which has the largest photocurrents described so far, with a faster closing kinetics (a kind communication by Georg Nagel).

SA-Ch application (or any of its relatives) could help clarifying the role of synaptic potentiation in the formation and recall of encoded memories. Synapse re-excitation could be performed more physiologically than what existing technologies used to tag and reactivate whole neurons can achieve. For instance, the work presented in this paper lays the ground for the use of SA-Ch to test the hypothesis of a “synaptic engram,” parallel to the identified “population engram” (Neves et al., 2008; Poo et al., 2016; Rogerson et al., 2014). It is likely that the two activity-tagging approaches (cellular vs. synaptic) would give similar results

where there is large identity overlap between the unit of plasticity and the single neuron, as in the DG (Chavlis et al., 2017; Govindarajan et al., 2011; Rebola et al., 2017). On the other hand, CA1 neurons receive multiple converging inputs whose crosstalk, following activation by current whole-cell optogenetic protocols, is likely to result in memory occlusion (Ramirez et al., 2013). Taking advantage of Arc RNA regulatory sequences, we were able to express a Channelrhodopsin variant at synapses undergoing potentiation, establishing a novel tool to map and reactivate these sites.

While at work in the so far described project, a novel approach towards the development of "synaptic optogenetic" strategies was proposed by Hayashi-Takagi et al. (2015). By expressing a photoactivable form of Rac1 in the motor cortex, Kasai and colleagues demonstrated that the light-induced shrinkage of recently potentiated spines severely impairs motor learning. The light-responsive Rac1 (AS-PaRac1) was fused to a deletion mutant of the rat PSD95 that do not bind receptor partners (Arnold and Clapham, 1999), and a portion of the Arc RNA corresponding to the DTE identified by Kobayashi et al. (2005). After learning a motor task, the motor cortex of the animals was illuminated with an optical protocol that

resulted in a dramatic reduction of transmission efficiency; when later tested for the acquired motor task, the performance of the mice was severely impaired.

Consistently with the data I collected, Kasai and collaborators found specific accumulation of AS-PaRac1 at potentiated synapses that was sensitive to translation inhibitors; as in our case, increasing neuronal activity determined a higher number of expressing spines, while TTX only had a minor effect on AS-PaRac1 expression (Hayashi-Takagi et al., 2015). Unlike SA-Ch, AS-PaRac1 control of expression relies more heavily on the proteic moiety to reduce background expression, as they only employ a portion of the 3'UTR; in some cases, the resulting AS-PaRac1 transcript also bears the 5'UTR due to the employment of SARE promoter (Kawashima et al., 2009). This could explain why the shrinkage effect was more pronounced when they employed the SARE rather than the constitutive CAG promoter – a difference that the authors highlighted themselves but without further speculation about the underlying reasons. Consistently, they showed that the synaptic enrichment of AS-PaRac1 is dependent of active protein degradation by the proteasome, and inhibiting its proteolytic activity dramatically reduced its synaptic localization (Hayashi-Takagi et al., 2015).

The work by Hayashi-Takagi et al. (2015) demonstrate the necessity of a subset of synapses for the efficient recall of a (motor) memory trace, rather than of a selected population of neurons. However, by dramatically altering actin dynamics, such approach determined a drastic alteration of the spine structure; therefore, the interference with the memory trace could not be reverted. Accordingly, it was not possible to perform a memory recall task, as the intervention was purely destructive. This establishes a first demonstration of synaptic engram in the motor cortex. An application in the hippocampus would provide evidence of the existence of synaptic engrams in memories where the spatial component is involved. In fact, in this Thesis I identified a subset of synapses that become potentiated after the exploration of a new context, providing a possible substrate for an engram.

Reactivation of this subset of SA-Ch^{+} spines could test the sufficiency of potentiated synaptic inputs for memory: if these synapses become potentiated during the association of a context with a noxious stimulus (contextual fear conditioning), their optical reactivation is expected to elicit a coherent fear response (Figure 69). In the brain regions where the potentiated synapses are preferentially located on a subset of neurons in a skewed fashion, it is

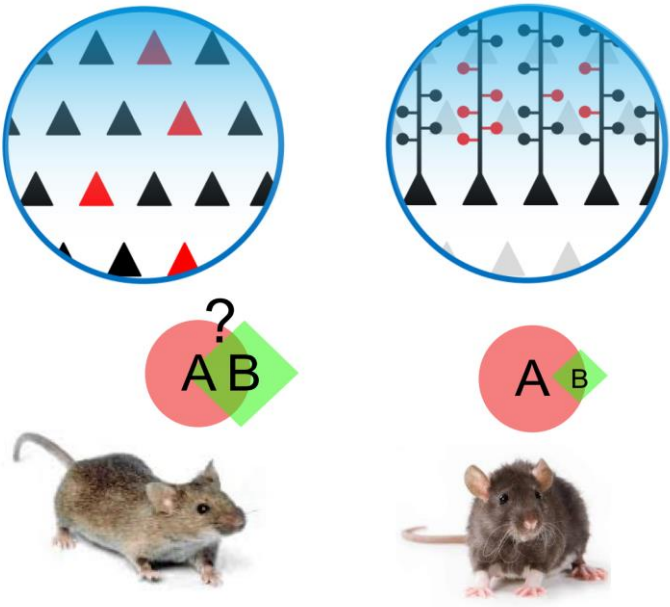

Figure 69 Effect of tagging and reactivating cells (left) or synapses (right) potentiated during the context exposure. When there is large overlap between the cellular engrams for two differnt contexts, reactivation is expected to form a mixed representation. Conversely, the reactivation of potentiation synapses only is expected to more trustfully reevoke the memory of the tagged context only.

expected that the cellular engram is a good representation of the synaptic engram, as in the DG. Therefore, re-exciting the active cells would recapitulate the original activity and, hence, the associated experience. Where two contexts activate two overlapping sets of cells, as in the CA1 region,

re-exciting the cells forms a mixed representation, as reported in Garner et al. (2012). In this situation, it is expected that re-activate the subset of potentiated synapse would represent a more similar stimulation to the original one, and more trustfully reactivate the contextual memory

A SynActive approach to study the proteome

The system I developed allows the expression of a diverse class of proteins at potentiated synapses, as the expression is regulated by the presence of Arc sequences (see Figure 29 and Figure 40). Among the possible applications, a particularly intriguing one is the possibility to profile potentiated synapses at the molecular level by expressing suitable reporters. This would provide invaluable information to define the changes in protein content after potentiation in a behavioural task. While lots of information has been accumulating with time, much is still unknown regarding all the events that take place at synapses after potentiation (Kandel et al., 2014). Furthermore, this could provide new information about how potentiation changes are altered in situations where memory is notoriously affected, such as aging (Ris and Godaux, 2007) and Alzheimer's disease (Sheng et al., 2012). I therefore started employing a

biochemical approach to pulldown (i) PSD95 interactors and (ii) synaptosomes derived from potentiated synapses after fear conditioning, and compared the results with control synapses by means of proteomic analysis.

I injected in the mouse hippocampus AAVs expressing the SynActive version of PSD95 fused to a tag for affinity purification containing the FLAG tag (TAP) within Arc 5' and 3' UTRs (Figure 70). Fear conditioned animals express PSD95-TAP at potentiated synapses, as confirmed by immunohistochemistry against FLAG epitope (Figure 70c). After 90', mice were sacrificed and the interactors of PSD95 from potentiated synapses (SA-PSD95-TAP) or control synapses (PSD95-TAP) were purified using a protocol similar to Fernández et al. (2009). I analysed the samples, confirming the pulldown of PSD95-TAP with anti-FLAG antibodies, along with interactors as NMDAR subunit 2 (Figure 71). Interestingly, I detected CaMKII isoforms in pulldown from samples SA-PSD95-TAP, while they were clearly less represented in PSD95-TAP samples (Figure 71). Consistently when I analysed the sample by mass spectrometry, the pulldown fraction from SA-PSD95-TAP samples containing PSD95 interactors clustered together, while the lysate contents from all samples were very similar

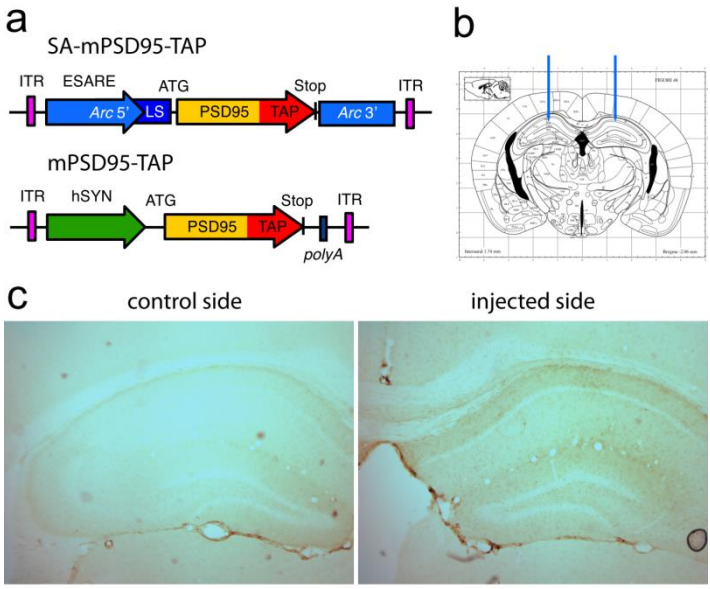

Figure 70 Expression of SynActive PSD95 at potentiated synapses for interactomics analysis. **a** Vectors used: SA-mouse PSD95-TAP tag is cloned within Arc 5′ and 3′UTR, and the costruct is expressed by activity-dependent ESARE promoter, which encompasses part of the 5′UTR. As control, mouse PSD95-TAP is expressed constitutively from the hSYN promoter. The two contructs are expressed by a serotype 2/5 AAV. **b** Bilateral injection in the hippocampus. **c** Control animal unilaterally injected with AAV2/5:ESARE::SA-mPSD95-TAP and subjected to contextual fear conditioning. After 90 minutes, the animal was perfused and stained for FLAG expression, detected by DAP staining. The residual expression on the medial end of the hippocampus of the non injected hemisphere is most probably due to a spillover and diffusion of the AAV solution from the injected hippocampus.xx

to each other. From a preliminary analysis, we found that proteins known to be upregulated in synapse potentiation have indeed a higher enrichment value in the potentiated

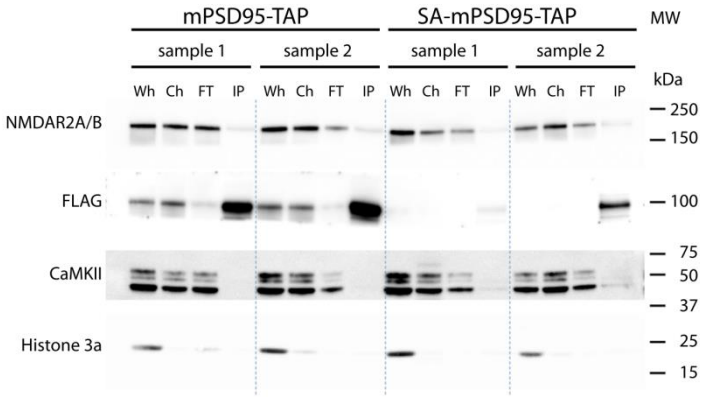

Figure 71 Western blot (WB) analysis of the 2 independent samples for each construct. The analysis confirms efficient pulldown of the mPSD95-TAP protein (FLAG blot) and its interactor NMDAR2A/B, while Histone 3a was notably depleted in the IP fraction. In pulldowns from potentiated spines (SA-mPSD95-TAP), but not in controls (mPSD95-TAP), CaMKII isoforms were co-immunoprecipitated with tagged PSD95. The WB shows immunodetection using the antibodies listed on the left, analyzing different fractions for each sample: Wh, whole homogenate; Ch, clarified homogenate; FT, flowthrough; IP, immunoprecipitated samples with anti-FLAG beads. On the right, reference molecular weigth markers.

→**Figure 72** Proteomic analysis of two biological samples for the interators of PSD95 in potentiated synapses (SA-mPSD95) and control synapses (mPSD95). Peptides optained from anti-FLAG pulldown were precipitated, digested with tripsin and processed for label-free mass spectrometry analysis. **a** Correlation analysis of the crude homogenate (Ch, black) fraction and the anti-FLAG IP (IP, red) for each sample. While the Ch fractions from all samples are very close to each other, the IP samples from potentiated synapses were more correlated to each other than the IP samples from control synapses. **b** A non exaustive list of partners detected in our samples. Values are Log fold-change of the IP with respect to the Ch fraction. Compared to control synapses, in potentiated synapses we found an apparent increase of AMPA receptor subunits, kinases like αCaMKII and PKC, as well as structural protein (actin, Shank3). Ongoing experiments in collaboration with Alessandro Ori, Franz-Lipmann Insitut, Jena.

a

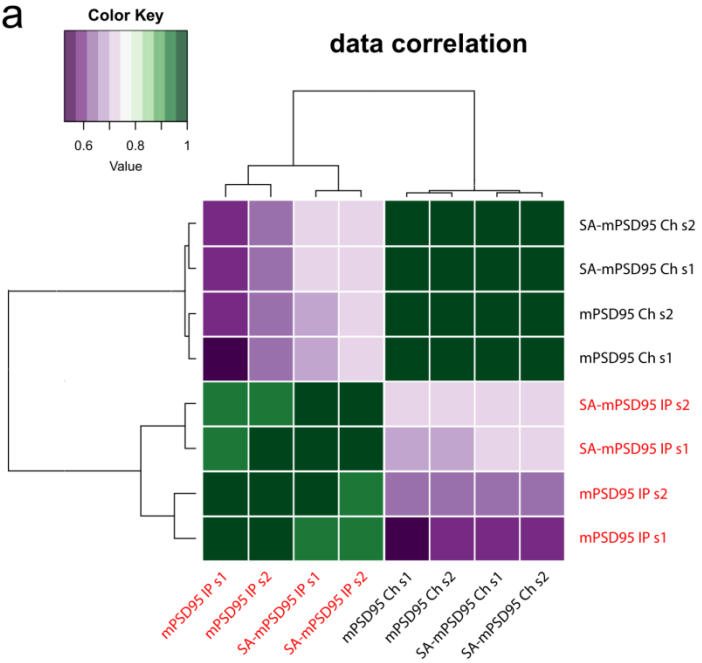

b

		mPSD95-TAP	SA-mPSD95-TAP
NMDAR 2B	↓	2.540546691	1.678538872
NMDAR 2A	↓	2.984315355	1.223803495
NMDAR 1	↓	2.946832657	2.453668752
AMPAR 2	↑	0.934588154	1.245171538
AMPAR 1	↑	0.864520038	1.44156191
mGluR5	↑	-0.122186942	1.289257208
αCaMKII	↑	0.075509494	0.507416736
Shank 3	↑	0.572080809	0.945625493
PKC-A	↑	3.199462684	4.86808808
PKC-ε	↑	2.123591695	2.911350926
FMRP	↑	ND	1.386229944
actin	↑	-3.897016469	-2.685555417

synapse samples (Figure 72b). Among them, we found for example AMPAR subunits 1 and 2, structural proteins Shank3 and actin, and several kinases like αCaMKII and PKC. FMRP and other RNA binding proteins, and mGluR5, which has been previously involved in LTP at CA3-CA1 synapses and spatial learning (Lu et al., 1997) were also detected. It is worth elucidating then the apparent decrease in enrichment for the NMDAR subunits (which looks more marked for subunits 2A and 2B), as this could only reflect a smaller proportion of its reads at mass spectrometry (due to the presence of more interactors in potentiated spines), or highlight a physiological response. In conclusion, this demonstrates that it is possible to purify samples from potentiated synapses, which will lead to an unbiased analysis of the protein content of this particular subset of synapse, and could make it possible to identify targets in early stages of neurodegenerative pathologies that may be causally linked to the disruption of memory.

Final conclusions

In conclusion, I developed a versatile technology to vehicle the expression of reporter constructs and effectors at potentiated synapses. I make use of this property to identify

and map potentiated synapses in the brain, demonstrating the presence of cluster of potentiated synapses in the hippocampus, and providing experimental evidences to theoretical models for information processing in the hippocampus.

The employment of SynActive will enable to map, purify and control the activity of potentiated synapses in the brain. I hope this would help deepen the knowledge of one of the most elusive aspects of the mind in one of its most fundamental mechanisms.

References

Aakalu, G., Smith, W.B., Nguyen, N., Jiang, C., and Schuman, E.M. (2001). Dynamic visualization of local protein synthesis in hippocampal neurons. Neuron *30*, 489–502.

Alvarez-Castelao, B., and Schuman, E.M. (2015). The regulation of synaptic protein turnover. Journal of Biological Chemistry *290*, 28623–28630.

Amaral, D.G., Scharfman, H.E., and Lavenex, P. (2007). The dentate gyrus: fundamental neuroanatomical organization (dentate gyrus for dummies). Prog. Brain Res. *163*, 3–22.

An, J.J., Gharami, K., Liao, G.-Y., Woo, N.H., Lau, A.G., Vanevski, F., Torre, E.R., Jones, K.R., Feng, Y., Lu, B., et al. (2008). Distinct role of long 3′ UTR BDNF mRNA in spine morphology and synaptic plasticity in hippocampal neurons. Cell *134*, 175–187.

Anagnostaras, S.G., Gale, G.D., Fanselow, M.S., and others (2001). Hippocampus and contextual fear conditioning: recent controversies and advances. Hippocampus *11*, 8–17.

Andersen, P., Morris, R., Amaral, D., Bliss, T., and O'Keefe, J. (2007). The Hippocampus Book (Oxford University Press).

Andreassi, C., Zimmermann, C., Mitter, R., Fusco, S., De Vita, S., Saiardi, A., and Riccio, A. (2010). An NGF-responsive element targets myo-inositol monophosphatase-1 mRNA to sympathetic neuron axons. Nature Neuroscience *13*, 291–301.

Aristoteles On Memory. In Parva Naturalia, (Retrieved on January 27 2018, from https://www.gutenberg.org/files/27895),.

Arnold, D.B., and Clapham, D.E. (1999). Molecular determinants for subcellular localization of PSD-95 with an interacting K+ channel. Neuron *23*, 149–157.

Ashby, M.C., Sarah, A., Ralph, G.S., Uney, J., Collingridge, G.L., and Henley, J.M. (2004). Removal of AMPA receptors (AMPARs) from synapses is preceded by transient endocytosis of extrasynaptic AMPARs. The Journal of Neuroscience *24*, 5172–5176.

Asrican, B., Augustine, G.J., Berglund, K., Chen, S., Chow, N., Deisseroth, K., Feng, G., Gloss, B., Hira, R., Hoffmann, C., et al. (2013). Next-generation transgenic mice for optogenetic analysis of neural

circuits. Front Neural Circuits *7*, 160.

Attardo, A., Fitzgerald, J.E., and Schnitzer, M.J. (2015). Impermanence of dendritic spines in live adult CA1 hippocampus. Nature *523*, 592.

Baj, G., Leone, E., Chao, M.V., and Tongiorgi, E. (2011). Spatial segregation of BDNF transcripts enables BDNF to differentially shape distinct dendritic compartments. Proceedings of the National Academy of Sciences *108*, 16813–16818.

Baj, G., Del Turco, D., Schlaudraff, J., Torelli, L., Deller, T., and Tongiorgi, E. (2013). Regulation of the spatial code for BDNF mRNA isoforms in the rat hippocampus following pilocarpine-treatment: A systematic analysis using laser microdissection and quantitative real-time PCR. Hippocampus *23*, 413–423.

Baker, C.A., Elyada, Y.M., Parra, A., and Bolton, M.M. (2016). Cellular resolution circuit mapping with temporal-focused excitation of soma-targeted channelrhodopsin. eLife *5*, e14193.

Balleza, E., Kim, J.M., and Cluzel, P. (2018). Systematic characterization of maturation time of fluorescent proteins in living cells. Nature Methods *15*, 47.

Barad, M., Bourtchouladze, R., Winder, D.G., Golan, H., and Kandel, E. (1998). Rolipram, a type IV-specific phosphodiesterase inhibitor, facilitates the establishment of long-lasting long-term potentiation and improves memory. Proc. Natl. Acad. Sci. U.S.A. *95*, 15020–15025.

Barco, A., Lopez de Armentia, M., and Alarcon, J.M. (2008). Synapse-specific stabilization of plasticity processes: the synaptic tagging and capture hypothesis revisited 10 years later. Neuroscience \& Biobehavioral Reviews *32*, 831–851.

Barde, I., Zanta-Boussif, M.A., Paisant, S., Leboeuf, M., Rameau, P., Delenda, C., and Danos, O. (2006). Efficient control of gene expression in the hematopoietic system using a single Tet-on inducible lentiviral vector. Molecular Therapy *13*, 382–390.

Barrientos, S.A., and Tiznado, V. (2016). Hippocampal CA1 Subregion as a Context Decoder. J. Neurosci. *36*, 6602–6604.

Barrientos, R.M., O'Reilly, R.C., and Rudy, J.W. (2002). Memory for context is impaired by injecting anisomycin into dorsal hippocampus

following context exploration. Behavioural Brain Research *134*, 299–306.

Barth, A.L., Gerkin, R.C., and Dean, K.L. (2004). Alteration of neuronal firing properties after in vivo experience in a FosGFP transgenic mouse. The Journal of Neuroscience *24*, 6466–6475.

Basu, J., and Siegelbaum, S.A. (2015). The corticohippocampal circuit, synaptic plasticity, and memory. Cold Spring Harbor Perspectives in Biology *7*, a021733.

Batish, M., van den Bogaard, P., Kramer, F.R., and Tyagi, S. (2012). Neuronal mRNAs travel singly into dendrites. Proceedings of the National Academy of Sciences *109*, 4645–4650.

Beaudoin III, G.M., Lee, S.-H., Singh, D., Yuan, Y., Ng, Y.-G., Reichardt, L.F., and Arikkath, J. (2012). Culturing pyramidal neurons from the early postnatal mouse hippocampus and cortex. Nature Protocols *7*, 1741–1754.

Blichenberg, A., Schwanke, B., Rehbein, M., Garner, C.C., Richter, D., and Kindler, S. (1999). Identification of a cis-acting dendritic targeting element in MAP2 mRNAs. J. Neurosci. *19*, 8818–8829.

Blichenberg, A., Rehbein, M., Müller, R., Garner, C.C., Richter, D., and Kindler, S. (2001). Identification of a cis-acting dendritic targeting element in the mRNA encoding the alpha subunit of Ca2+/calmodulin-dependent protein kinase II. European Journal of Neuroscience *13*, 1881–1888.

Bliss, T.V., and Collingridge, G.L. (1993). A synaptic model of memory: long-term potentiation in the hippocampus. Nature *361*, 31.

Bliss, T.V., and Lømo, T. (1973). Long-lasting potentiation of synaptic transmission in the dentate area of the anaesthetized rabbit following stimulation of the perforant path. The Journal of Physiology *232*, 331–356.

Bosch, M., Castro, J., Saneyoshi, T., Matsuno, H., Sur, M., and Hayashi, Y. (2014). Structural and Molecular Remodeling of Dendritic Spine Substructures during Long-Term Potentiation . Neuron *82*, 444 – 459.

Bramham, C.R., and Messaoudi, E. (2005). BDNF function in adult synaptic plasticity: the synaptic consolidation hypothesis. Progress in

Neurobiology *76*, 99–125.

Bramham, C.R., and Wells, D.G. (2007). Dendritic mRNA: transport, translation and function. Nature Reviews Neuroscience *8*, 776–789.

Bramham, C.R., Worley, P.F., Moore, M.J., and Guzowski, J.F. (2008). The immediate early gene arc/arg3. 1: regulation, mechanisms, and function. The Journal of Neuroscience *28*, 11760–11767.

Bramham, C.R., Alme, M.N., Bittins, M., Kuipers, S.D., Nair, R.R., Pai, B., Panja, D., Schubert, M., Soule, J., Tiron, A., et al. (2010). The Arc of synaptic memory. Exp Brain Res *200*, 125–140.

Brun, V.H., Ytterbo, K., Morris, R.G., Moser, M.B., and Moser, E.I. (2001). Retrograde amnesia for spatial memory induced by NMDA receptor-mediated long-term potentiation. J. Neurosci. *21*, 356–362.

Buckley, P.T., Lee, M.T., Sul, J.-Y., Miyashiro, K.Y., Bell, T.J., Fisher, S.A., Kim, J., and Eberwine, J. (2011). Cytoplasmic intron sequence-retaining transcripts can be dendritically targeted via ID element retrotransposons. Neuron *69*, 877–884.

Büsselberg, D., Michael, D., Evans, M.L., Carpenter, D.O., and Haas, H.L. (1992). Zinc (Zn 2+) blocks voltage gated calcium channels in cultured rat dorsal root ganglion cells. Brain Research *593*, 77–81.

Butko, M.T., Yang, J., Geng, Y., Kim, H.J., Jeon, N.L., Shu, X., Mackey, M.R., Ellisman, M.H., Tsien, R.Y., and Lin, M.Z. (2012). Fluorescent and photo-oxidizing TimeSTAMP tags track protein fates in light and electron microscopy. Nature Neuroscience *15*, 1742–1751.

Cajigas, I.J., Tushev, G., Will, T.J., Fuerst, N., Schuman, E.M., and others (2012). The local transcriptome in the synaptic neuropil revealed by deep sequencing and high-resolution imaging. Neuron *74*, 453–466.

Castillo, P.E. (2012). Presynaptic LTP and LTD of excitatory and inhibitory synapses. Cold Spring Harbor Perspectives in Biology *4*, a005728.

Cenquizca, L.A., and Swanson, L.W. (2007). Spatial organization of direct hippocampal field CA1 axonal projections to the rest of the cerebral cortex. Brain Research Reviews *56*, 1–26.

Chavlis, S., Petrantonakis, P.C., and Poirazi, P. (2017). Dendrites of dentate gyrus granule cells contribute to pattern separation by controlling sparsity. Hippocampus.

Chen, T.-W., Wardill, T.J., Sun, Y., Pulver, S.R., Renninger, S.L., Baohan, A., Schreiter, E.R., Kerr, R.A., Orger, M.B., Jayaraman, V., et al. (2013). Ultrasensitive fluorescent proteins for imaging neuronal activity. Nature *499*, 295–300.

Chen, X., Leischner, U., Rochefort, N.L., Nelken, I., and Konnerth, A. (2011). Functional mapping of single spines in cortical neurons in vivo. Nature *475*, 501–505.

Chiaruttini, C., Vicario, A., Li, Z., Baj, G., Braiuca, P., Wu, Y., Lee, F., Gardossi, L., Baraban, J., and Tongiorgi, E. (2009). Dendritic trafficking of BDNF mRNA is mediated by translin and blocked by the G196A (Val66Met) mutation. Proceedings of the National Academy of Sciences *106*, 16481–16486.

Choi, J.-H., Sim, S.-E., Kim, J.-I., Choi, D.I., Oh, J., Ye, S., Lee, J., Kim, T., Ko, H.-G., Lim, C.-S., et al. (2018). Interregional synaptic maps among engram cells underlie memory formation. Science *360*, 430–435.

Cichon, J., and Gan, W.-B. (2015). Branch-specific dendritic Ca2+ spikes cause persistent synaptic plasticity. Nature *520*, 180–185.

Constals, A., Penn, A.C., Compans, B., Toulmé, E., Phillipat, A., Marais, S., Retailleau, N., Hafner, A.-S., Coussen, F., Hosy, E., et al. (2015). Glutamate-induced AMPA receptor desensitization increases their mobility and modulates short-term plasticity through unbinding from stargazin. Neuron *85*, 787–803.

Corish, P., and Tyler-Smith, C. (1999). Attenuation of green fluorescent protein half-life in mammalian cells. Protein Engineering *12*, 1035–1040.

Cowansage, K.K., Shuman, T., Dillingham, B.C., Chang, A., Golshani, P., and Mayford, M. (2014). Direct reactivation of a coherent neocortical memory of context. Neuron *84*, 432–441.

Cristofanilli, M., Thanos, S., Brosius, J., Kindler, S., and Tiedge, H. (2004). Neuronal MAP2 mRNA: species-dependent differential dendritic targeting competence. Journal of Molecular Biology *341*, 927–

934.

Dawydow, A., Gueta, R., Ljaschenko, D., Ullrich, S., Hermann, M., Ehmann, N., Gao, S., Fiala, A., Langenhan, T., Nagel, G., et al. (2014). Channelrhodopsin-2-XXL, a powerful optogenetic tool for low-light applications. Proc. Natl. Acad. Sci. U.S.A. *111*, 13972–13977.

Deng, W., Mayford, M., and Gage, F.H. (2013). Selection of distinct populations of dentate granule cells in response to inputs as a mechanism for pattern separation in mice. Elife *2*.

Denny, C.A., Kheirbek, M.A., Alba, E.L., Tanaka, K.F., Brachman, R.A., Laughman, K.B., Tomm, N.K., Turi, G.F., Losonczy, A., and Hen, R. (2014). Hippocampal Memory Traces Are Differentially Modulated by Experience, Time, and Adult Neurogenesis. Neuron *83*, 189–201.

Doyle, M., and Kiebler, M.A. (2011). Mechanisms of dendritic mRNA transport and its role in synaptic tagging. The EMBO Journal *30*, 3540–3552.

Druckmann, S., Feng, L., Lee, B., Yook, C., Zhao, T., Magee, J.C., and Kim, J. (2014). Structured Synaptic Connectivity between Hippocampal Regions. Neuron *3*, 629–640.

Dynes, J.L., and Steward, O. (2012). Arc mRNA docks precisely at the base of individual dendritic spines indicating the existence of a specialized microdomain for synapse-specific mRNA translation. Journal of Comparative Neurology *520*, 3105–3119.

Ehlers, M.D. (2003). Activity level controls postsynaptic composition and signaling via the ubiquitin-proteasome system. Nat. Neurosci. *6*, 231–242.

Espinosa, F., and Kavalali, E.T. (2009). NMDA receptor activation by spontaneous glutamatergic neurotransmission. J. Neurophysiol. *101*, 2290–2296.

Fernández, E., Collins, M.O., Uren, R.T., Kopanitsa, M.V., Komiyama, N.H., Croning, M.D., Zografos, L., Armstrong, J.D., Choudhary, J.S., and Grant, S.G. (2009). Targeted tandem affinity purification of PSD-95 recovers core postsynaptic complexes and schizophrenia susceptibility proteins. Molecular Systems Biology *5*, 269.

Fernández, E., Collins, M.O., Frank, R.A., Zhu, F., Kopanitsa, M.V., Nithianantharajah, J., Lemprière, S.A., Fricker, D., Elsegood, K.A., McLaughlin, C.L., et al. (2017). Arc requires PSD95 for assembly into postsynaptic complexes involved with neural dysfunction and intelligence. Cell Reports *21*, 679–691.

Fonseca, R., Nägerl, U.V., Morris, R.G.M., and Bonhoeffer, T. (2004). Competing for memory: hippocampal LTP under regimes of reduced protein synthesis. Neuron *44*, 1011–1020.

Fonseca, R., Vabulas, R.M., Hartl, F.U., Bonhoeffer, T., and Nägerl, U.V. (2006a). A balance of protein synthesis and proteasome-dependent degradation determines the maintenance of LTP. Neuron *52*, 239–245.

Fonseca, R., Nägerl, U.V., and Bonhoeffer, T. (2006b). Neuronal activity determines the protein synthesis dependence of long-term potentiation. Nat. Neurosci. *9*, 478–480.

Frank, A.C., Huang, S., Zhou, M., Gdalyahu, A., Kastellakis, G., Silva, T.K., Lu, E., Wen, X., Poirazi, P., Trachtenberg, J.T., et al. (2018). Hotspots of dendritic spine turnover facilitate clustered spine addition and learning and memory. Nature Communications *9*, 422.

Frey, U., and Morris, R.G. (1997). Synaptic tagging and long-term potentiation. Nature *385*, 533–536.

Fritzsche, R., Karra, D., Bennett, K.L., Ang, F.Y., Heraud-Farlow, J.E., Tolino, M., Doyle, M., Bauer, K.E., Thomas, S., Planyavsky, M., et al. (2013). Interactome of two diverse RNA granules links mRNA localization to translational repression in neurons. Cell Rep *5*, 1749–1762.

Fu, M., Yu, X., Lu, J., and Zuo, Y. (2012). Repetitive motor learning induces coordinated formation of clustered dendritic spines in vivo. Nature *483*, 92.

Fusco, D., Accornero, N., Lavoie, B., Shenoy, S.M., Blanchard, J.-M., Singer, R.H., and Bertrand, E. (2003). Single mRNA molecules demonstrate probabilistic movement in living mammalian cells. Current Biology *13*, 161–167.

Gambino, F., Pagès, S., Kehayas, V., Baptista, D., Tatti, R., Carleton, A., and Holtmaat, A. (2014). Sensory-evoked LTP driven by dendritic

plateau potentials in vivo. Nature *515*, 116–119.

Gao, Y., Tatavarty, V., Korza, G., Levin, M.K., and Carson, J.H. (2008). Multiplexed dendritic targeting of α calcium calmodulin-dependent protein kinase II, neurogranin, and activity-regulated cytoskeleton-associated protein RNAs by the A2 pathway. Molecular Biology of the Cell *19*, 2311–2327.

Garner, A.R., Rowland, D.C., Hwang, S.Y., Baumgaertel, K., Roth, B.L., Kentros, C., and Mayford, M. (2012). Generation of a synthetic memory trace. Science *335*, 1513–1516.

Genzel, L., Rossato, J.I., Jacobse, J., Grieves, R.M., Spooner, P.A., Battaglia, F.P., Fernández, G., and Morris, R.G. (2017). The yin and yang of memory consolidation: Hippocampal and neocortical. PLoS Biology *15*, e2000531.

Giorgi, C., and Moore, M.J. (2007). The nuclear nurture and cytoplasmic nature of localized mRNPs. In Seminars in Cell \& Developmental Biology, pp. 186–193.

Giorgi, C., Yeo, G.W., Stone, M.E., Katz, D.B., Burge, C., Turrigiano, G., and Moore, M.J. (2007). The EJC factor eIF4AIII modulates synaptic strength and neuronal protein expression. Cell *130*, 179–191.

Glanzer, J., Miyashiro, K., Sul, J.-Y., Barrett, L., Belt, B., Haydon, P., and Eberwine, J. (2005). RNA splicing capability of live neuronal dendrites. Proceedings of the National Academy of Sciences of the United States of America *102*, 16859–16864.

Gold, P.E. (2008). Protein synthesis inhibition and memory: formation vs amnesia. Neurobiol Learn Mem *89*, 201–211.

Gore, F., Schwartz, E.C., and Salzman, C.D. (2015). Manipulating neural activity in physiologically classified neurons: triumphs and challenges. Philos. Trans. R. Soc. Lond., B, Biol. Sci. *370*.

Goshen, I., Brodsky, M., Prakash, R., Wallace, J., Gradinaru, V., Ramakrishnan, C., and Deisseroth, K. (2011). Dynamics of retrieval strategies for remote memories. Cell *147*, 678–689.

Gossen, M., Freundlieb, S., Bender, G., Muller, G., Hillen, W., and Bujard, H. (1995). Transcriptional activation by tetracyclines in

mammalian cells. Science *268*, 1766–1769.

Govindarajan, A., Kelleher, R.J., and Tonegawa, S. (2006). A clustered plasticity model of long-term memory engrams. Nature Reviews Neuroscience *7*, 575–583.

Govindarajan, A., Israely, I., Huang, S.-Y., and Tonegawa, S. (2011). The dendritic branch is the preferred integrative unit for protein synthesis-dependent LTP. Neuron *69*, 132–146.

Gradinaru, V., Thompson, K.R., Zhang, F., Mogri, M., Kay, K., Schneider, M.B., and Deisseroth, K. (2007). Targeting and readout strategies for fast optical neural control in vitro and in vivo. The Journal of Neuroscience *27*, 14231–14238.

Greenberg, K.P., Pham, A., and Werblin, F.S. (2011). Differential targeting of optical neuromodulators to ganglion cell soma and dendrites allows dynamic control of center-surround antagonism. Neuron *69*, 713–720.

Grienberger, C., Chen, X., and Konnerth, A. (2014). Dendritic function< i> in vivo</i>. Trends in Neurosciences.

Gruart, A., and Delgado-García, J.M. (2007). Activity-dependent changes of the hippocampal CA3-CA1 synapse during the acquisition of associative learning in conscious mice. Genes Brain Behav. *6 Suppl 1*, 24–31.

Grubb, M.S., and Burrone, J. (2010). Channelrhodopsin-2 localised to the axon initial segment. PloS One *5*, e13761.

Guenthner, C.J., Miyamichi, K., Yang, H.H., Heller, H.C., and Luo, L. (2013). Permanent genetic access to transiently active neurons via TRAP: targeted recombination in active populations. Neuron *78*, 773–784.

Gunaydin, L.A., Yizhar, O., Berndt, A., Sohal, V.S., Deisseroth, K., and Hegemann, P. (2010). Ultrafast optogenetic control. Nature Neuroscience *13*, 387–392.

Guzowski, J.F. (2002). Insights into immediate-early gene function in hippocampal memory consolidation using antisense oligonucleotide and fluorescent imaging approaches. Hippocampus *12*, 86–104.

Guzowski, J.F., McNaughton, B.L., Barnes, C.A., and Worley, P.F. (1999). Environment-specific expression of the immediate-early gene Arc in hippocampal neuronal ensembles. Nature Neuroscience *2*, 1120–1124.

Guzowski, J.F., Lyford, G.L., Stevenson, G.D., Houston, F.P., McGaugh, J.L., Worley, P.F., and Barnes, C.A. (2000). Inhibition of activity-dependent arc protein expression in the rat hippocampus impairs the maintenance of long-term potentiation and the consolidation of long-term memory. Journal of Neuroscience *20*, 3993–4001.

Guzowski, J.F., Setlow, B., Wagner, E.K., and McGaugh, J.L. (2001). Experience-dependent gene expression in the rat hippocampus after spatial learning: a comparison of the immediate-early genesArc, c-fos, and zif268. The Journal of Neuroscience *21*, 5089–5098.

Gökçe, O., Bonhoeffer, T., and Scheuss, V. (2016). Clusters of synaptic inputs on dendrites of layer 5 pyramidal cells in mouse visual cortex. eLife *5*, e09222.

Hachet, O., and Ephrussi, A. (2004). Splicing of oskar RNA in the nucleus is coupled to its cytoplasmic localization. Nature *428*, 959–963.

Han, J.-H., Kushner, S.A., Yiu, A.P., Cole, C.J., Matynia, A., Brown, R.A., Neve, R.L., Guzowski, J.F., Silva, A.J., and Josselyn, S.A. (2007). Neuronal competition and selection during memory formation. Science *316*, 457–460.

Han, J.-H., Kushner, S.A., Yiu, A.P., Hsiang, H.-L.L., Buch, T., Waisman, A., Bontempi, B., Neve, R.L., Frankland, P.W., and Josselyn, S.A. (2009). Selective erasure of a fear memory. Science *323*, 1492–1496.

Harvey, C.D., and Svoboda, K. (2007). Locally dynamic synaptic learning rules in pyramidal neuron dendrites. Nature *450*, 1195–1200.

Harvey, C.D., Yasuda, R., Zhong, H., and Svoboda, K. (2008a). The spread of Ras activity triggered by activation of a single dendritic spine. Science *321*, 136–140.

Harvey, C.D., Ehrhardt, A.G., Cellurale, C., Zhong, H., Yasuda, R., Davis, R.J., and Svoboda, K. (2008b). A genetically encoded fluorescent sensor of ERK activity. Proceedings of the National Academy of

Sciences *105*, 19264–19269.

Häusser, M. (2001). Synaptic function: dendritic democracy. Current Biology *11*, R10–R12.

Häusser, M., and Mel, B. (2003). Dendrites: bug or feature? Current Opinion in Neurobiology *13*, 372–383.

Havekes, R., and Abel, T. (2009). Genetic dissection of neural circuits and behavior in Mus musculus. Advances in Genetics *65*, 1–38.

Hayashi-Takagi, A., Yagishita, S., Nakamura, M., Shirai, F., Wu, Y.I., Loshbaugh, A.L., Kuhlman, B., Hahn, K.M., and Kasai, H. (2015). Labelling and optical erasure of synaptic memory traces in the motor cortex. Nature *525*, 333–338.

Hill, T.C., and Zito, K. (2013). LTP-induced long-term stabilization of individual nascent dendritic spines. The Journal of Neuroscience *33*, 678–686.

Hochbaum, D.R., Zhao, Y., Farhi, S.L., Klapoetke, N., Werley, C.A., Kapoor, V., Zou, P., Kralj, J.M., Maclaurin, D., Smedemark-Margulies, N., et al. (2014). All-optical electrophysiology in mammalian neurons using engineered microbial rhodopsins. Nature Methods.

Holt, C.E., and Schuman, E.M. (2013). The Central Dogma Decentralized: New Perspectives on RNA Function and Local Translation in Neurons. Neuron *80*, 648–657.

Ifrim, M.F., Williams, K.R., and Bassell, G.J. (2015). Single-Molecule Imaging of PSD-95 mRNA Translation in Dendrites and Its Dysregulation in a Mouse Model of Fragile X Syndrome. The Journal of Neuroscience *35*, 7116–7130.

Ivanov, A., Pellegrino, C., Rama, S., Dumalska, I., Salyha, Y., Ben-Ari, Y., and Medina, I. (2006). Opposing role of synaptic and extrasynaptic NMDA receptors in regulation of the extracellular signal-regulated kinases (ERK) activity in cultured rat hippocampal neurons. The Journal of Physiology *572*, 789–798.

Jakkamsetti, V., Tsai, N.-P., Gross, C., Molinaro, G., Collins, K.A., Nicoletti, F., Wang, K.H., Osten, P., Bassell, G.J., Gibson, J.R., et al. (2013). Experience-induced Arc/Arg3. 1 primes CA1 pyramidal neurons for metabotropic glutamate receptor-dependent long-term synaptic

depression. Neuron *80*, 72–79.

Jeffery, K.J. (2007). Integration of the sensory inputs to place cells: what, where, why, and how? Hippocampus *17*, 775–785.

Josselyn, S.A., Köhler, S., and Frankland, P.W. (2015). Finding the engram. Nat. Rev. Neurosci. *16*, 521–534.

Josselyn, S.A., Köhler, S., and Frankland, P.W. (2017). Heroes of the Engram. Journal of Neuroscience *37*, 4647–4657.

Jung, H., Gkogkas, C.G., Sonenberg, N., and Holt, C.E. (2014). Remote Control of Gene Function by Local Translation . Cell *157*, 26 – 40.

Kaczmarek, L. (1992). Expression of c-fos and other genes encoding transcription factors in long-term potentiation. Behav. Neural Biol. *57*, 263–266.

Kandel, E.R. (2012). The molecular biology of memory: cAMP, PKA, CRE, CREB-1, CREB-2, and CPEB. Molecular Brain *5*, 14.

Kandel, E., Schwartz, J.H., Jessel, T.M., Siegelbaum, S.A., and Hudspeth, A.J. (2013). Principles of Neural Science (5th Edition) (McGraw Hill).

Kandel, E., Dudai, Y., and Mayford, M. (2014). The molecular and systems biology of memory. Cell *157*, 163–186.

Kandel, E.R., Dudai, Y., and Mayford, M.R. (2016). Learning and Memory (Cold Spring Harbor Perspectives in Biology).

Kang, H., and Schuman, E. (1996). A requirement for local protein synthesis in neurotrophin-induced hippocampal synaptic plasticity. Science (New York, NY) *273*, 1402.

Kastellakis, G., Cai, D.J., Mednick, S.C., Silva, A.J., and Poirazi, P. (2015). Synaptic clustering within dendrites: An emerging theory of memory formation. Progress in Neurobiology *126*, 19–35.

Kawashima, T., Okuno, H., Nonaka, M., Adachi-Morishima, A., Kyo, N., Okamura, M., Takemoto-Kimura, S., Worley, P.F., and Bito, H. (2009). Synaptic activity-responsive element in the Arc/Arg3. 1 promoter essential for synapse-to-nucleus signaling in activated neurons.

Proceedings of the National Academy of Sciences *106*, 316–321.

Kawashima, T., Okuno, H., and Bito, H. (2014). A new era for functional labeling of neurons: activity-dependent promoters have come of age. Front Neural Circuits *8*, 37.

Kelleher III, R.J., Govindarajan, A., and Tonegawa, S. (2004). Translational regulatory mechanisms in persistent forms of synaptic plasticity. Neuron *44*, 59–73.

Kelly, T., and Beck, H. (2017). Functional properties of granule cells with hilar basal dendrites in the epileptic dentate gyrus. Epilepsia *58*, 160–171.

Kindler, S., and Kreienkamp, H.-J. (2012). Dendritic mRNA targeting and translation. In Synaptic Plasticity, (Springer), pp. 285–305.

Kindler, S., Wang, H., Richter, D., and Tiedge, H. (2005). RNA transport and local control of translation. Annual Review of Cell and Developmental Biology *21*, 223.

Kirschen, G.W., Shen, J., Tian, M., Schroeder, B., Wang, J., Man, G., Wu, S., and Ge, S. (2017). Active dentate granule cells encode experience to promote the addition of adult-born hippocampal neurons. Journal of Neuroscience *37*, 4661–4678.

Kitamura, T., Sun, C., Martin, J., Kitch, L.J., Schnitzer, M.J., and Tonegawa, S. (2015). Entorhinal Cortical Ocean Cells Encode Specific Contexts and Drive Context-Specific Fear Memory. Neuron *87*, 1317–1331.

Kitamura, T., Ogawa, S.K., Roy, D.S., Okuyama, T., Morrissey, M.D., Smith, L.M., Redondo, R.L., and Tonegawa, S. (2017). Engrams and circuits crucial for systems consolidation of a memory. Science *356*, 73–78.

Klann, E., and Dever, T.E. (2004). Biochemical mechanisms for translational regulation in synaptic plasticity. Nature Reviews Neuroscience *5*, 931–942.

Kleindienst, T., Winnubst, J., Roth-Alpermann, C., Bonhoeffer, T., and Lohmann, C. (2011). Activity-dependent clustering of functional synaptic inputs on developing hippocampal dendrites. Neuron *72*, 1012–

1024.

Knierim, J.J., and Neunuebel, J.P. (2016). Tracking the flow of hippocampal computation: Pattern separation, pattern completion, and attractor dynamics. Neurobiology of Learning and Memory *129*, 38–49.

Kobayashi, H., Yamamoto, S., Maruo, T., and Murakami, F. (2005). Identification of a cis-acting element required for dendritic targeting of activity-regulated cytoskeleton-associated protein mRNA. European Journal of Neuroscience *22*, 2977–2984.

Kopec, C.D., Li, B., Wei, W., Boehm, J., and Malinow, R. (2006). Glutamate receptor exocytosis and spine enlargement during chemically induced long-term potentiation. The Journal of Neuroscience *26*, 2000–2009.

Kornau, H.-C., Schenker, L.T., Kennedy, M.B., and Seeburg, P.H. (1995). Domain interaction between NMDA receptor subunits and the postsynaptic density protein PSD-95. Science *269*, 1737–1740.

Kramár, E.A., Babayan, A.H., Gavin, C.F., Cox, C.D., Jafari, M., Gall, C.M., Rumbaugh, G., and Lynch, G. (2012). Synaptic evidence for the efficacy of spaced learning. Proc. Natl. Acad. Sci. U.S.A. *109*, 5121–5126.

Krucker, T., Siggins, G.R., and Halpain, S. (2000). Dynamic actin filaments are required for stable long-term potentiation (LTP) in area CA1 of the hippocampus. Proceedings of the National Academy of Sciences *97*, 6856–6861.

Krueppel, R., Remy, S., and Beck, H. (2011). Dendritic integration in hippocampal dentate granule cells. Neuron *71*, 512–528.

Kubik, S., Miyashita, T., and Guzowski, J.F. (2007). Using immediate-early genes to map hippocampal subregional functions. Learn. Mem. *14*, 758–770.

Lai, C.-H., Chun, H.H., Nahas, S.A., Mitui, M., Gamo, K.M., Du, L., and Gatti, R.A. (2004). Correction of ATM gene function by aminoglycoside-induced read-through of premature termination codons. Proceedings of the National Academy of Sciences of the United States of America *101*, 15676–15681.

Langston, R.F., Stevenson, C.H., Wilson, C.L., Saunders, I., and Wood, E.R. (2010). The role of hippocampal subregions in memory for stimulus associations. Behav. Brain Res. *215*, 275–291.

Lashley, K.S. (1950). In search of the engram. Society of Experimental Biology Symposium No.4: Physiological Mechanism: In Animal Behaviour.

Lee, Y.-S., and Silva, A. (2009). The molecular and cellular biology of enhanced cognition. Nature Reviews Neuroscience *10*, 126–140.

Lee, D., Hyun, J.H., Jung, K., Hannan, P., and Kwon, H.-B. (2017). A calcium-and light-gated switch to induce gene expression in activated neurons. Nature Biotechnology *35*, 858.

Lee, H., Oh, W.C., Seong, J., and Kim, J. (2016a). Advanced fluorescence protein-based synapse-detectors. Frontiers in Synaptic Neuroscience *8*.

Lee, K.F., Soares, C., Thivierge, J.-P., and Bé"\ique, J.-C. (2016b). Correlated Synaptic Inputs Drive Dendritic Calcium Amplification and Cooperative Plasticity during Clustered Synapse Development. Neuron.

Lee, S.-J.R., Escobedo-Lozoya, Y., Szatmari, E.M., and Yasuda, R. (2009). Activation of CaMKII in single dendritic spines during long-term potentiation. Nature *458*, 299–304.

Lewis, R.A., and Mowry, K.L. (2007). Ribonucleoprotein remodeling during RNA localization. Differentiation *75*, 507–518.

Lewis, T.L.J., Mao, T., Svoboda, K., and Arnold, D.B. (2009). Myosin-dependent targeting of transmembrane proteins to neuronal dendrites. Nature Neuroscience *12*, 568–576.

Lewis, T.L.J., Mao, T., and Arnold, D.B. (2011). A role for myosin VI in the localization of axonal proteins. PLoS Biology *9*, e1001021.

Lin, J.Y., Sann, S.B., Zhou, K., Nabavi, S., Proulx, C.D., Malinow, R., Jin, Y., and Tsien, R.Y. (2013). Optogenetic inhibition of synaptic release with chromophore-assisted light inactivation (CALI). Neuron *79*, 241–253.

Lisman, J., Schulman, H., and Cline, H. (2002). The molecular basis of CaMKII function in synaptic and behavioural memory. Nature Reviews

Neuroscience *3*, 175–190.

Lisman, J., Yasuda, R., and Raghavachari, S. (2012). Mechanisms of CaMKII action in long-term potentiation. Nature Reviews Neuroscience *13*, 169–182.

Liu, X., Ramirez, S., Pang, P.T., Puryear, C.B., Govindarajan, A., Deisseroth, K., and Tonegawa, S. (2012). Optogenetic stimulation of a hippocampal engram activates fear memory recall. Nature *484*, 381–385.

Loew, R., Heinz, N., Hampf, M., Bujard, H., and Gossen, M. (2010). Improved Tet-responsive promoters with minimized background expression. BMC Biotechnol. *10*, 81.

Lu, Y.-M., Jia, Z., Janus, C., Henderson, J.T., Gerlai, R., Wojtowicz, J.M., and Roder, J.C. (1997). Mice lacking metabotropic glutamate receptor 5 show impaired learning and reduced CA1 long-term potentiation (LTP) but normal CA3 LTP. Journal of Neuroscience *17*, 5196–5205.

Lüscher, C., and Malenka, R.C. (2012). NMDA receptor-dependent long-term potentiation and long-term depression (LTP/LTD). Cold Spring Harbor Perspectives in Biology *4*, a005710.

Lyford, G.L., Yamagata, K., Kaufmann, W.E., Barnes, C.A., Sanders, L.K., Copeland, N.G., Gilbert, D.J., Jenkins, N.A., Lanahan, A.A., and Worley, P.F. (1995). < i> Arc</i>, a growth factor and activity-regulated gene, encodes a novel cytoskeleton-associated protein that is enriched in neuronal dendrites. Neuron *14*, 433–445.

Magnus, C.J., Lee, P.H., Atasoy, D., Su, H.H., Looger, L.L., and Sternson, S.M. (2011). Chemical and genetic engineering of selective ion channel-ligand interactions. Science *333*, 1292–1296.

Makino, H., and Malinow, R. (2011). Compartmentalized versus global synaptic plasticity on dendrites controlled by experience. Neuron *72*, 1001–1011.

Mantzur, L., Joels, G., and Lamprecht, R. (2009). Actin polymerization in lateral amygdala is essential for fear memory formation. Neurobiology of Learning and Memory *91*, 85–88.

Martin, S.J., and Morris, R.G.M. (2002). New life in an old idea: the synaptic plasticity and memory hypothesis revisited. Hippocampus *12*,

609–636.

Dal Maschio, M., Ghezzi, D., Bony, G., Alabastri, A., Deidda, G., Brondi, M., Sato, S.S., Zaccaria, R.P., Di Fabrizio, E., Ratto, G.M., et al. (2012). High-performance and site-directed in utero electroporation by a triple-electrode probe. Nature Communications *3*, 960.

Matsuzaki, M., Honkura, N., Ellis-Davies, G.C., and Kasai, H. (2004). Structural basis of long-term potentiation in single dendritic spines. Nature *429*, 761–766.

Mattis, J., Tye, K.M., Ferenczi, E.A., Ramakrishnan, C., O'Shea, D.J., Prakash, R., Gunaydin, L.A., Hyun, M., Fenno, L.E., Gradinaru, V., et al. (2011). Principles for applying optogenetic tools derived from direct comparative analysis of microbial opsins. Nature Methods *9*, 159–172.

Mayford, M., Baranes, D., Podsypanina, K., and Kandel, E.R. (1996). The 3′-untranslated region of CaMKIIα is a cis-acting signal for the localization and translation of mRNA in dendrites. Proceedings of the National Academy of Sciences *93*, 13250–13255.

Mayford, M., Siegelbaum, S.A., and Kandel, E.R. (2012). Synapses and memory storage. Cold Spring Harbor Perspectives in Biology *4*, a005751.

McBride, T.J., Rodriguez-Contreras, A., Trinh, A., Bailey, R., and DeBello, W.M. (2008). Learning drives differential clustering of axodendritic contacts in the barn owl auditory system. Journal of Neuroscience *28*, 6960–6973.

McHugh, T.J., Jones, M.W., Quinn, J.J., Balthasar, N., Coppari, R., Elmquist, J.K., Lowell, B.B., Fanselow, M.S., Wilson, M.A., and Tonegawa, S. (2007). Dentate gyrus NMDA receptors mediate rapid pattern separation in the hippocampal network. Science *317*, 94–99.

McKernan, M., and Shinnick-Gallagher, P. (1997). Fear conditioning induces a lasting potentiation of synaptic currents in vitro. Nature *390*, 607–611.

McNaughton, B.L., Barnes, C.A., Rao, G., Baldwin, J., and Rasmussen, M. (1986). Long-term enhancement of hippocampal synaptic transmission and the acquisition of spatial information. J. Neurosci. *6*, 563–571.

Messaoudi, E., Kanhema, T., Soulé, J., Tiron, A., Dagyte, G., da Silva, B., and Bramham, C.R. (2007). Sustained Arc/Arg3. 1 synthesis controls long-term potentiation consolidation through regulation of local actin polymerization in the dentate gyrus in vivo. The Journal of Neuroscience *27*, 10445–10455.

Meyer, D., Bonhoeffer, T., and Scheuss, V. (2014). Balance and Stability of Synaptic Structures during Synaptic Plasticity . Neuron *82*, 430 – 443.

Miesenböck, G., De Angelis, D.A., and Rothman, J.E. (1998). Visualizing secretion and synaptic transmission with pH-sensitive green fluorescent proteins. Nature *394*, 192–195.

Mikl, M., Vendra, G., and Kiebler, M.A. (2011). Independent localization of MAP2, CaMKIIα and β-actin RNAs in low copy numbers. EMBO Reports *12*, 1077–1084.

Miller, S., Yasuda, M., Coats, J.K., Jones, Y., Martone, M.E., and Mayford, M. (2002). Disruption of dendritic translation of CaMKIIα impairs stabilization of synaptic plasticity and memory consolidation. Neuron *36*, 507–519.

Mori, Y., Imaizumi, K., Katayama, T., Yoneda, T., and Tohyama, M. (2000). Two cis-acting elements in the 3′ untranslated region of α-CaMKII regulate its dendritic targeting. Nature Neuroscience *3*, 1079–1084.

Morris, R., Anderson, E., Lynch, G. a, and Baudry, M. (1986). Selective impairment of learning and blockade of long-term potentiation by an N-methyl-D-aspartate receptor antagonist, AP5. Nature *319*, 774.

Moser, E.I., Krobert, K.A., Moser, M.-B., and Morris, R.G. (1998). Impaired spatial learning after saturation of long-term potentiation. Science *281*, 2038–2042.

Murakoshi, H., Wang, H., and Yasuda, R. (2011). Local, persistent activation of Rho GTPases during plasticity of single dendritic spines. Nature *472*, 100–104.

Murakoshi, H., Shin, M.E., Parra-Bueno, P., Szatmari, E.M., Shibata, A.C., and Yasuda, R. (2017). Kinetics of Endogenous CaMKII Required for Synaptic Plasticity Revealed by Optogenetic Kinase Inhibitor.

Neuron.

Muslimov, I.A., Banker, G., Brosius, J., and Tiedge, H. (1998). Activity-dependent regulation of dendritic BC1 RNA in hippocampal neurons in culture. The Journal of Cell Biology *141*, 1601–1611.

Muslimov, I.A., Nimmrich, V., Hernandez, A.I., Tcherepanov, A., Sacktor, T.C., and Tiedge, H. (2004). Dendritic Transport and Localization of Protein Kinase Mζ mRNA IMPLICATIONS FOR MOLECULAR MEMORY CONSOLIDATION. Journal of Biological Chemistry *279*, 52613–52622.

Muslimov, I.A., Iacoangeli, A., Brosius, J., and Tiedge, H. (2006). Spatial codes in dendritic BC1 RNA. The Journal of Cell Biology *175*, 427–439.

Na, Y., Park, S., Lee, C., Kim, D.-K., Park, J.M., Sockanathan, S., Huganir, R.L., and Worley, P.F. (2016). Real-Time Imaging Reveals Properties of Glutamate-Induced Arc/Arg 3.1 Translation in Neuronal Dendrites. Neuron.

Nabavi, S., Fox, R., Proulx, C., Lin, J., Tsien, R., and Malinow, R. (2014). Engineering a memory with LTD and LTP. Nature *511*, 348–352.

Nadel, L., and Moscovitch, M. (1997). Memory consolidation, retrograde amnesia and the hippocampal complex. Curr. Opin. Neurobiol. *7*, 217–227.

Nagel, G., Möckel, B., Büldt, G., and Bamberg, E. (1995). Functional expression of bacteriorhodopsin in oocytes allows direct measurement of voltage dependence of light induced H+ pumping. FEBS Letters *377*, 263–266.

Nakazawa, K., Quirk, M.C., Chitwood, R. a, Watanabe, M., Yeckel, M.F., Sun, L.D., Kato, A., Carr, C. a, Johnston, D., Wilson, M. a, et al. (2002). Requirement for hippocampal CA3 NMDA receptors in associative memory recall. Science (New York, N.Y.) *297*, 211–218.

Neves, G., Cooke, S.F., and Bliss, T.V. (2008). Synaptic plasticity, memory and the hippocampus: a neural network approach to causality. Nature Reviews Neuroscience *9*, 65–75.

Nicoll, R.A. (2017). A Brief History of Long-Term Potentiation. Neuron *93*, 281–290.

Nomoto, M., Ohkawa, N., Nishizono, H., Yokose, J., Suzuki, A., Matsuo, M., Tsujimura, S., Takahashi, Y., Nagase, M., Watabe, A.M., et al. (2016). Cellular tagging as a neural network mechanism for behavioural tagging. Nature Communications *7*.

Ocampo, A.C., Squire, L.R., and Clark, R.E. (2017). Hippocampal area CA1 and remote memory in rats. Learning \& Memory *24*, 563–568.

Ohkawa, N., Saitoh, Y., Suzuki, A., Tsujimura, S., Murayama, E., Kosugi, S., Nishizono, H., Matsuo, M., Takahashi, Y., Nagase, M., et al. (2015). Artificial association of pre-stored information to generate a qualitatively new memory. Cell Reports *11*, 261–269.

Okamoto, K.-I., Nagai, T., Miyawaki, A., and Hayashi, Y. (2004). Rapid and persistent modulation of actin dynamics regulates postsynaptic reorganization underlying bidirectional plasticity. Nat. Neurosci. *7*, 1104–1112.

Okuno, H., Akashi, K., Ishii, Y., Yagishita-Kyo, N., Suzuki, K., Nonaka, M., Kawashima, T., Fujii, H., Takemoto-Kimura, S., Abe, M., et al. (2012). Inverse synaptic tagging of inactive synapses via dynamic interaction of Arc/Arg3. 1 with CaMKIIβ. Cell *149*, 886–898.

Okuyama, T., Kitamura, T., Roy, D.S., Itohara, S., and Tonegawa, S. (2016). Ventral CA1 neurons store social memory. Science *353*, 1536–1541.

Ostroff, L.E., Fiala, J.C., Allwardt, B., and Harris, K.M. (2002). Polyribosomes redistribute from dendritic shafts into spines with enlarged synapses during LTP in developing rat hippocampal slices. Neuron *35*, 535–545.

Otmakhov, N., Tao-Cheng, J.-H., Carpenter, S., Asrican, B., Dosemeci, A., Reese, T.S., and Lisman, J. (2004). Persistent accumulation of calcium/calmodulin-dependent protein kinase II in dendritic spines after induction of NMDA receptor-dependent chemical long-term potentiation. The Journal of Neuroscience *24*, 9324–9331.

Packer, A.M., Peterka, D.S., Hirtz, J.J., Prakash, R., Deisseroth, K., and Yuste, R. (2012). Two-photon optogenetics of dendritic spines and

neural circuits. Nature Methods *9*, 1202–1205.

Packer, A.M., Roska, B., and Häusser, M. (2013). Targeting neurons and photons for optogenetics. Nature Neuroscience *16*, 805–815.

Padamesey, Z., and Emptage, N.J. (2011). Imaging synaptic plasticity. Molecular Brain *4*.

Palida, S.F., Butko, M.T., Ngo, J.T., Mackey, M.R., Gross, L.A., Ellisman, M.H., and Tsien, R.Y. (2015). PKMζ, But Not PKCλ, Is Rapidly Synthesized and Degraded at the Neuronal Synapse. J. Neurosci. *35*, 7736–7749.

Paluch-Siegler, S., Mayblum, T., Dana, H., Brosh, I., Gefen, I., and Shoham, S. (2015). All-optical bidirectional neural interfacing using hybrid multiphoton holographic optogenetic stimulation. Neurophotonics *2*, 031208–031208.

Panja, D., and Bramham, C.R. (2014). BDNF mechanisms in late LTP formation: a synthesis and breakdown. Neuropharmacology *76*, 664–676.

Panja, D., Dagyte, G., Bidinosti, M., Wibrand, K., Kristiansen, Å.-M., Sonenberg, N., and Bramham, C.R. (2009). Novel translational control in Arc-dependent long term potentiation consolidation in vivo. Journal of Biological Chemistry *284*, 31498–31511.

Papoutsi, A., Kastellakis, G., Psarrou, M., Anastasakis, S., and Poirazi, P. (2014). Coding and decoding with dendrites. J. Physiol. Paris *108*, 18–27.

Paradies, M.A., and Steward, O. (1997). Multiple subcellular mRNA distribution patterns in neurons: a nonisotopic in situ hybridization analysis. Journal of Neurobiology *33*, 473–493.

Park, P., Volianskis, A., Sanderson, T.M., Bortolotto, Z.A., Jane, D.E., Zhuo, M., Kaang, B.-K., and Collingridge, G.L. (2014). NMDA receptor-dependent long-term potentiation comprises a family of temporally overlapping forms of synaptic plasticity that are induced by different patterns of stimulation. Phil. Trans. R. Soc. B *369*, 20130131.

Pastuzyn, E.D., Day, C.E., Kearns, R.B., Kyrke-Smith, M., Taibi, A.V., McCormick, J., Yoder, N., Belnap, D.M., Erlendsson, S., Morado, D.R., et al. (2018). The neuronal gene Arc encodes a repurposed

retrotransposon Gag protein that mediates intercellular RNA transfer. Cell *172*, 275–288.

Paxinos, G. (2015). The Rat Nervous System (Fourth Edition) (Academic Press).

Paxinos, G., and Franklin, K.B. (2001). The Mouse Brain in stereotaxis coordinates (Academic Press).

Pinkstaff, J.K., Chappell, S.A., Mauro, V.P., Edelman, G.M., and Krushel, L.A. (2001). Internal initiation of translation of five dendritically localized neuronal mRNAs. Proceedings of the National Academy of Sciences *98*, 2770–2775.

Pirbhoy, P.S., Farris, S., and Steward, O. (2016). Synaptic activation of ribosomal protein S6 phosphorylation occurs locally in activated dendritic domains. Learning \& Memory *23*, 255–269.

Plath, N., Ohana, O., Dammermann, B., Errington, M.L., Schmitz, D., Gross, C., Mao, X., Engelsberg, A., Mahlke, C., Welzl, H., et al. (2006). Arc/Arg3. 1 is essential for the consolidation of synaptic plasticity and memories. Neuron *52*, 437–444.

Plato Theaetetus (Project Gutemberg, Retrieved January 27 2018, from https://www.gutenberg.org/files/1726).

Poo, M., Pignatelli, M., Ryan, T.J., Tonegawa, S., Bonhoeffer, T., Martin, K.C., Rudenko, A., Tsai, L.-H., Tsien, R.W., Fishell, G., et al. (2016). What is memory? The present state of the engram. BMC Biology *14*, 1.

R core team (2013). R: A language and environment for statistical computing.

Racine, R.J., Milgram, N.W., and Hafner, S. (1983). Long-term potentiation phenomena in the rat limbic forebrain. Brain Res. *260*, 217–231.

Raju, C.S., Fukuda, N., López-Iglesias, C., Göritz, C., Visa, N., and Percipalle, P. (2011). In neurons, activity-dependent association of dendritically transported mRNA transcripts with the transacting factor CBF-A is mediated by A2RE/RTS elements. Molecular Biology of the Cell *22*, 1864–1877.

Ramirez, S., Liu, X., Lin, P.-A., Suh, J., Pignatelli, M., Redondo, R.L., Ryan, T.J., and Tonegawa, S. (2013). Creating a false memory in the hippocampus. Science *341*, 387–391.

Rangaraju, V., tom Dieck, S., and Schuman, E.M. (2017). Local translation in neuronal compartments: how local is local? EMBO Reports *18*, 693–711.

Raymond, C.R. (2007). LTP forms 1, 2 and 3: different mechanisms for the "long"in long-term potentiation. Trends in Neurosciences *30*, 167–175.

Rebola, N., Carta, M., and Mulle, C. (2017). Operation and plasticity of hippocampal CA3 circuits: implications for memory encoding. Nature Reviews Neuroscience.

Redondo, R.L., Kim, J., Arons, A.L., Ramirez, S., Liu, X., and Tonegawa, S. (2014). Bidirectional switch of the valence associated with a hippocampal contextual memory engram. Nature *513*, 426–430.

Reijmers, L.G., Perkins, B.L., Matsuo, N., and Mayford, M. (2007). Localization of a stable neural correlate of associative memory. Science *317*, 1230–1233.

Reymann, K.G., and Frey, J.U. (2007). The late maintenance of hippocampal LTP: requirements, phases, "synaptic tagging", "late-associativity" and implications. Neuropharmacology *52*, 24–40.

Rinaldi, A., Romeo, S., Agust'\in-Pavón, C., Oliverio, A., and Mele, A. (2010). Distinct patterns of Fos immunoreactivity in striatum and hippocampus induced by different kinds of novelty in mice. Neurobiology of Learning and Memory *94*, 373–381.

Ris, L., and Godaux, E. (2007). Synapse specificity of long-term potentiation breaks down with aging. Learn. Mem. *14*, 185–189.

Rogerson, T., Cai, D.J., Frank, A., Sano, Y., Shobe, J., Lopez-Aranda, M.F., and Silva, A.J. (2014). Synaptic tagging during memory allocation. Nat. Rev. Neurosci. *15*, 157–169.

Rossetti, T., Banerjee, S., Kim, C., Leubner, M., Lamar, C., Gupta, P., Lee, B., Neve, R., and Lisman, J. (2017). Memory erasure experiments indicate a critical role of CaMKII in memory storage. Neuron *96*, 207–

216.

Roth, B.L. (2016). DREADDs for Neuroscientists. Neuron *89*, 683–694.

Routtenberg, A. (2008). The substrate for long-lasting memory: if not protein synthesis, then what? Neurobiol Learn Mem *89*, 225–233.

Roy, D.S., Arons, A., Mitchell, T.I., Pignatelli, M., Ryan, T.J., and Tonegawa, S. (2016). Memory retrieval by activating engram cells in mouse models of early Alzheimer's disease. Nature *531*, 508–512.

Roy, D.S., Kitamura, T., Okuyama, T., Ogawa, S.K., Sun, C., Obata, Y., Yoshiki, A., and Tonegawa, S. (2017a). Distinct neural circuits for the formation and retrieval of episodic memories. Cell *170*, 1000–1012.

Roy, D.S., Muralidhar, S., Smith, L.M., and Tonegawa, S. (2017b). Silent memory engrams as the basis for retrograde amnesia. Proceedings of the National Academy of Sciences *114*, E9972–E9979.

Roy, R., Hohng, S., and Ha, T. (2008). A practical guide to single-molecule FRET. Nature Methods *5*, 507–516.

Rudy, J.W. (2008). The Neurobiology of Learning and Memory (Oxford University Press).

Ryan, T.J., Roy, D.S., Pignatelli, M., Arons, A., and Tonegawa, S. (2015). Engram cells retain memory under retrograde amnesia. Science *348*, 1007–1013.

Sacchetti, B., Lorenzini, C.A., Baldi, E., Bucherelli, C., Roberto, M., Tassoni, G., and Brunelli, M. (2001). Long-lasting hippocampal potentiation and contextual memory consolidation. European Journal of Neuroscience *13*, 2291–2298.

Sakaguchi, M., Kim, K., Yu, L.M.Y., Hashikawa, Y., Sekine, Y., Okumura, Y., Kawano, M., Hayashi, M., Kumar, D., Boyden, E.S., et al. (2015). Inhibiting the Activity of CA1 Hippocampal Neurons Prevents the Recall of Contextual Fear Memory in Inducible ArchT Transgenic Mice. PLoS ONE *10*, e0130163.

Sakurai, K., Zhao, S., Takatoh, J., Rodriguez, E., Lu, J., Leavitt, A.D., Fu, M., Han, B.-X., and Wang, F. (2016). Capturing and Manipulating Activated Neuronal Ensembles with CANE Delineates a Hypothalamic

Social-Fear Circuit. Neuron *92*, 739–753.

Sato, T., Muroyama, Y., and Saito, T. (2013). Inducible gene expression in postmitotic neurons by an in vivo electroporation-based tetracycline system. Journal of Neuroscience Methods *214*, 170–176.

Schacter, D.L., Eich, J.E., and Tulving, E. (1978). Richard Semon's theory of memory. Journal of Verbal Learning and Verbal Behavior *17*, 721–743.

Schneider, F., Gradmann, D., and Hegemann, P. (2013). Ion selectivity and competition in channelrhodopsins. Biophys. J. *105*, 91–100.

Schoenenberger, P., Grunditz, Å., Rose, T., and Oertner, T.G. (2008). Optimizing the spatial resolution of Channelrhodopsin-2 activation. Brain Cell Biology *36*, 119–127.

Scoville, W.B., and Milner, B. (1957). Loss of recent memory after bilateral hippocampal lesions. Journal of Neurology, Neurosurgery, and Psychiatry *20*, 11.

Semon, R.W. (1921). The Mneme (George Allen & Unwin).

Semon, R.W. (1923). Mnemic Psychology (George Allen & Unwin).

Shaner, N.C., Campbell, R.E., Steinbach, P.A., Giepmans, B.N.G., Palmer, A.E., and Tsien, R.Y. (2004). Improved monomeric red, orange and yellow fluorescent proteins derived from Discosoma sp. red fluorescent protein. Nat. Biotechnol. *22*, 1567–1572.

Sheng, M., Sabatini, B.L., and Südhof, T.C. (2012). Synapses and Alzheimer's disease. Cold Spring Harbor Perspectives in Biology *4*, a005777.

Shipton, O.A., El-Gaby, M., Apergis-Schoute, J., Deisseroth, K., Bannerman, D.M., Paulsen, O., and Kohl, M.M. (2014). Left-right dissociation of hippocampal memory processes in mice. Proceedings of the National Academy of Sciences *111*, 15238–15243.

Silva, A.J., Stevens, C.F., Tonegawa, S., and Wang, Y. (1992a). Deficient hippocampal long-term potentiation in alpha-calcium-calmodulin kinase II mutant mice. Science *257*, 201–206.

Silva, A.J., Paylor, R., Wehner, J.M., and Tonegawa, S. (1992b). Impaired spatial learning in alpha-calcium-calmodulin kinase II mutant mice. Science *257*, 206–211.

De Solis, C.A., Morales, A.A., Hosek, M.P., Partin, A.C., and Ploski, J.E. (2017). Is Arc mRNA unique: a search for mRNAs that localize to the distal dendrites of dentate gyrus granule cells following neural activity. Frontiers in Molecular Neuroscience *10*, 314.

Sørensen, A.T., Cooper, Y.A., Baratta, M.V., Weng, F.-J., Zhang, Y., Ramamoorthi, K., Fropf, R., LaVerriere, E., Xue, J., Young, A., et al. (2016). A robust activity marking system for exploring active neuronal ensembles. Elife *5*, e13918.

Squire, L.R. (1986). Mechanisms of memory. Science *232*, 1612–1619.

Stepan, J., Dine, J., and Eder, M. (2015). Functional optical probing of the hippocampal trisynaptic circuit in vitro: network dynamics, filter properties, and polysynaptic induction of CA1 LTP. Frontiers in Neuroscience *9*, 160.

Steward, O., and Reeves, T.M. (1988). Protein-synthetic machinery beneath postsynaptic sites on CNS neurons: association between polyribosomes and other organelles at the synaptic site. The Journal of Neuroscience *8*, 176–184.

Steward, O., and Schuman, E.M. (2001). Protein synthesis at synaptic sites on dendrites. In Annual Reviews in Neuroscience, pp. 299–325.

Steward, O., and Worley, P.F. (2001a). A cellular mechanism for targeting newly synthesized mRNAs to synaptic sites on dendrites. Proceedings of the National Academy of Sciences *98*, 7062–7068.

Steward, O., and Worley, P.F. (2001b). Selective targeting of newly synthesized Arc mRNA to active synapses requires NMDA receptor activation. Neuron *30*, 227–240.

Steward, O., Farris, S., Pirbhoy, P.S., Darnell, J., and Driesche, S.J.V. (2015). Localization and local translation of Arc/Arg3.1 mRNA at synapses: some observations and paradoxes. Front Mol Neurosci *7*, 101.

Subramanian, M., Rage, F., Tabet, R., Flatter, E., Mandel, J.-L., and Moine, H. (2011). G-quadruplex RNA structure as a signal for neurite

mRNA targeting. EMBO Reports *12*, 697–704.

Sutton, M.A., and Schuman, E.M. (2006). Dendritic protein synthesis, synaptic plasticity, and memory. Cell *127*, 49–58.

Szczurkowska, J., Cwetsch, A.W., Dal Maschio, M., Ghezzi, D., Ratto, G.M., and Cancedda, L. (2016). Targeted in vivo genetic manipulation of the mouse or rat brain by in utero electroporation with a triple-electrode probe. Nature Protocols *11*, 399–412.

Takahashi, N., Kitamura, K., Matsuo, N., Mayford, M., Kano, M., Matsuki, N., and Ikegaya, Y. (2012). Locally synchronized synaptic inputs. Science *335*, 353–356.

Takeuchi, T., Duszkiewicz, A.J., and Morris, R.G. (2014). The synaptic plasticity and memory hypothesis: encoding, storage and persistence. Phil. Trans. R. Soc. B *369*, 20130288.

Tanaka, H., and Hirano, T. (2012). Visualization of subunit-specific delivery of glutamate receptors to postsynaptic membrane during hippocampal long-term potentiation. Cell Reports *1*, 291–298.

Tanaka, K.Z., Pevzner, A., Hamidi, A.B., Nakazawa, Y., Graham, J., and Wiltgen, B.J. (2014). Cortical representations are reinstated by the hippocampus during memory retrieval. Neuron *84*, 347–354.

Tayler, K.K., Tanaka, K.Z., Reijmers, L.G., and Wiltgen, B.J. (2013). Reactivation of neural ensembles during the retrieval of recent and remote memory. Curr. Biol. *23*, 99–106.

Tonegawa, S., Liu, X., Ramirez, S., and Redondo, R. (2015). Memory engram cells have come of age. Neuron *87*, 918–931.

Tongiorgi, E., Righi, M., and Cattaneo, A. (1997). Activity-dependent dendritic targeting of BDNF and TrkB mRNAs in hippocampal neurons. The Journal of Neuroscience *17*, 9492–9505.

Torre, E., and Steward, O. (1992). Demonstration of local protein synthesis within dendrites using a new cell culture system that permits the isolation of living axons and dendrites from their cell bodies. The Journal of Neuroscience *12*, 762–772.

Tse, D., Langston, R.F., Kakeyama, M., Bethus, I., Spooner, P.A., Wood, E.R., Witter, M.P., and Morris, R.G. (2007). Schemas and

memory consolidation. Science *316*, 76–82.

Tsien, J.Z., Huerta, P.T., and Tonegawa, S. (1996). The essential role of hippocampal CA1 NMDA receptor-dependent synaptic plasticity in spatial memory. Cell *87*, 1327–1338.

Tushev, G., Glock, C., Heumüller, M., Biever, A., Jovanovic, M., and Schuman, E.M. (2018). Alternative 3′ UTRs Modify the Localization, Regulatory Potential, Stability, and Plasticity of mRNAs in Neuronal Compartments. Neuron *98*, 495–511.

Vaghi, V., Polacchini, A., Baj, G., Pinheiro, V.L., Vicario, A., and Tongiorgi, E. (2014). Pharmacological Profile of Brain-derived Neurotrophic Factor (BDNF) Splice Variant Translation Using a Novel Drug Screening Assay A "QUANTITATIVE CODE."Journal of Biological Chemistry *289*, 27702–27713.

Varga, Z., Jia, H., Sakmann, B., and Konnerth, A. (2011). Dendritic coding of multiple sensory inputs in single cortical neurons in vivo. Proceedings of the National Academy of Sciences *108*, 15420–15425.

Vickers, C.A., Dickson, K.S., and Wyllie, D.J.A. (2005). Induction and maintenance of late-phase long-term potentiation in isolated dendrites of rat hippocampal CA1 pyramidal neurones. The Journal of Physiology *568*, 803–813.

Wang, W., Wildes, C.P., Pattarabanjird, T., Sanchez, M.I., Glober, G.F., Matthews, G.A., Tye, K.M., and Ting, A.Y. (2017). A light-and calcium-gated transcription factor for imaging and manipulating activated neurons. Nature Biotechnology *35*, 864.

Wells, D.G. (2006). RNA-binding proteins: a lesson in repression. The Journal of Neuroscience *26*, 7135–7138.

Whitlock, J.R., Heynen, A.J., Shuler, M.G., and Bear, M.F. (2006). Learning induces long-term potentiation in the hippocampus. Science *313*, 1093–1097.

Wigström, H., Gustafsson, B., HUANG, Y.-Y., and Abraham, W. (1986). Hippocampal long-term potentiation is induced by pairing single afferent volleys with intracellularly injected depolarizing current pulses. Acta Physiologica *126*, 317–319.

Will, T.J., Tushev, G., Kochen, L., Nassim-Assir, B., Cajigas, I.J., Tom Dieck, S., and Schuman, E.M. (2013). Deep sequencing and high-resolution imaging reveal compartment-specific localization of Bdnf mRNA in hippocampal neurons. Sci Signal *6*, rs16.

Winnubst, J., and Lohmann, C. (2012). Synaptic clustering during development and learning: the why, when, and how. Front Mol Neurosci *5*, 70.

Winnubst, J., Cheyne, J.E., Niculescu, D., and Lohmann, C. (2015). Spontaneous Activity Drives Local Synaptic Plasticity In Vivo. Neuron *87*, 399–410.

Xu, T., Yu, X., Perlik, A.J., Tobin, W.F., Zweig, J.A., Tennant, K., Jones, T., and Zuo, Y. (2009). Rapid formation and selective stabilization of synapses for enduring motor memories. Nature *462*, 915–919.

Ben-Yakov, A., Dudai, Y., and Mayford, M.R. (2015). Memory Retrieval in Mice and Men. Cold Spring Harbor Perspectives in Biology *7*, a021790.

Yang, G., Pan, F., and Gan, W.-B. (2009). Stably maintained dendritic spines are associated with lifelong memories. Nature *462*, 920–924.

Yang, Y., Liu, D., Huang, W., Deng, J., Sun, Y., Zuo, Y., and Poo, M. (2016). Selective synaptic remodeling of amygdalocortical connections associated with fear memory. Nature Neuroscience *19*, 1348–1355.

Yasuda, R., Harvey, C.D., Zhong, H., Sobczyk, A., van Aelst, L., and Svoboda, K. (2006). Supersensitive Ras activation in dendrites and spines revealed by two-photon fluorescence lifetime imaging. Nat. Neurosci. *9*, 283–291.

Yin, Y., Edelman, G.M., and Vanderklish, P.W. (2002). The brain-derived neurotrophic factor enhances synthesis of Arc in synaptoneurosomes. Proc. Natl. Acad. Sci. U.S.A. *99*, 2368–2373.

Ying, S.-W., Futter, M., Rosenblum, K., Webber, M.J., Hunt, S.P., Bliss, T.V., and Bramham, C.R. (2002). Brain-derived neurotrophic factor induces long-term potentiation in intact adult hippocampus: requirement for ERK activation coupled to CREB and upregulation of Arc synthesis. The Journal of Neuroscience *22*, 1532–1540.

Yizhar, O., Fenno, L.E., Davidson, T.J., Mogri, M., and Deisseroth, K. (2011). Optogenetics in neural systems. Neuron *71*, 9–34.

Yuste, R. (2010). Dendritic spines (MIT Press).

Zacharias, D.A., Violin, J.D., Newton, A.C., and Tsien, R.Y. (2002). Partitioning of lipid-modified monomeric GFPs into membrane microdomains of live cells. Science *296*, 913–916.

Zhang, Y., Cudmore, R.H., Lin, D.-T., Linden, D.J., and Huganir, R.L. (2015). Visualization of NMDA receptor-dependent AMPA receptor synaptic plasticity in vivo. Nat. Neurosci. *18*, 402–407.

Zhang, W., Wu, J., Ward, M.D., Yang, S., Chuang, Y.-A., Xiao, M., Li, R., Leahy, D.J., and Worley, P.F. (2015b). Structural Basis of Arc Binding to Synaptic Proteins: Implications for Cognitive Disease. Neuron *86*, 490–500.

Zhang, Y.-P., Holbro, N., and Oertner, T.G. (2008). Optical induction of plasticity at single synapses reveals input-specific accumulation of alphaCaMKII. Proceedings of the National Academy of Sciences *105*, 12039–12044.

Zhou, Y., Won, J., Karlsson, M.G., Zhou, M., Rogerson, T., Balaji, J., Neve, R., Poirazi, P., and Silva, A.J. (2009). CREB regulates excitability and the allocation of memory to subsets of neurons in the amygdala. Nature Neuroscience *12*, 1438–1443.

Zhu, P., Aller, M.I., Baron, U., Cambridge, S., Bausen, M., Herb, J., Sawinski, J., Cetin, A., Osten, P., Nelson, M.L., et al. (2007). Silencing and un-silencing of tetracycline-controlled genes in neurons. PLoS ONE *2*, e533.

Appendix A

Sequences of constructs used in this thesis (5' to 3')

SA-ChETA-Cherry

AGTGCTCTGGCGAGTAGTCCTCCCTCAGCCGCAGTCTCTGGGCCTCTT
CAGCTTGAGCGGCGGCGAGCCTGCCACACTCGCTAAGCTCCTCCGGCA
CCGCGCACTTGCCACTGCCACTGCCGCTTCGCGCCCGCTGCAGCCGCC
GGCTCTGAATCCTTCTGGCTTCCGCCTCAGAGGAGTTCTTAGCCTGTC
CCGAACCGTAACCCCGGCGAGCAGACGGAGCTGGACCAGCTAGCATGG
ATTATGGAGGCGCTTTGTCTGCCGTCGGACGCGAACTTTTGTTCGTTA
CTAATCCTGTGGTGGTGAACGGGTCCGTCCTGGTCCCTGAGGATCAAT
GTTACTGTGCCGGATGGATTGAATCTCGCGGCACGAACGGCGCTCAGA
CCGCGTCAAATGTCCTGCAGTGGCTTGCAGCAGGATTCAGCATTTTGC
TGCTGATGTTCTATGCCTACCAAACCTGGAAATCTACATGCGGCTGGG
AGGAGATCTATGTGTGCGCCATTGAAATGGTTAAGGTGATTCTCGAGT
TCTTTTTTGAGTTTAAGAATCCCTCTATGCTCTACCTTGCCACAGGAC
ACCGGGTGCAGTGGCTGCGCTATGCAGCCTGGCTGCTCACTTGTCCTG
TCATCCTTATCCACCTGAGCAACCTCACCGGCCTGAGCAACGACTACA
GCAGGAGAACCATGGGACTCCTTGTCTCAGACATCGGGACTATCGTGT
GGGGGGCTACCAGCGCCATGGCAACCGGCTATGTTAAAGTCATCTTCT
TTTGTCTTGGATTGTGCTATGGCGCGAACACATTTTTTCACGCCGCCA
AAGCATATATCGAGGGTTATCATACTGTGCCAAAGGGTCGGTGCCGCC
AGGTCGTGACCGGCATGGCATGGCTGTTTTTCGTGAGCTGGGGTATGT
TCCCAATTCTCTTCATTTTGGGGCCCGAAGGTTTTGGCGTCCTGAGCG
TCTATGGCTCCACCGTAGGTCACACGATTATTGATCTGATGAGTAAAA
ATTGTTGGGGGTTGTTGGGACACTACCTGCGCGTCCTGATCCACGAGC
ACATATTGATTCACGGAGATATCCGCAAAACCACCAAACTGAACATCG
GCGGAACGGAGATCGAGGTCGAGACTCTCGTCGAAGACGAAGCCGAGG
CCGGAGCCGTGCCAGCGGCCGCCGTGAGCAAGGGCGAGGAGGATAACA
TGGCCATCATCAAGGAGTTCATGCGCTTCAAGGTGCACATGGAGGGCT
CCGTGAACGGCCACGAGTTCGAGATCGAGGGCGAGGGCGAGGGCCGCC
CCTACGAGGGCACCCAGACCGCCAAGCTGAAGGTGACCAAGGGTGGCC
CCCTGCCCTTCGCCTGGGACATCCTGTCCCCTCAGTTCATGTACGGCT
CCAAGGCCTACGTGAAGCACCCCGCCGACATCCCCGACTACTTGAAGC
TGTCCTTCCCCGAGGGCTTCAAGTGGGAGCGCGTGATGAACTTCGAGG
ACGGCGGCGTGGTGACCGTGACCCAGGACTCCTCCCTGCAGGACGGCG

AGTTCATCTACAAGGTGAAGCTGCGCGGCACCAACTTCCCCTCCGACG
GCCCCGTAATGCAGAAGAAGACCATGGGCTGGGAGGCCTCCTCCGAGC
GGATGTACCCCGAGGACGGCGCCCTGAAGGGCGAGATCAAGCAGAGGC
TGAAGCTGAAGGACGGCGGCCACTACGACGCTGAGGTCAAGACCACCT
ACAAGGCCAAGAAGCCCGTGCAGCTGCCCGGCGCCTACAACGTCAACA
TCAAGTTGGACATCACCTCCCACAACGAGGACTACACCATCGTGGAAC
AGTACGAACGCGCCGAGGGCCGCCACTCCACCGGCGGCATGGACGAGC
TGTACGCCGCTGCTTCAATTGAAAGTGACGTGGCCGCAGCCGAAACCC
AGGTGTAATAAGTACAAGTAAAGATCCTAAGGTACCTAATTGCCTAGA
AAACATGAGGATCACCCATGTCTGCAGGTCGACTCTAGAAAACATGAG
GATCACCCATGTCTGCAGTATTCCCGGGTTCATTAGATCCTAAGGTAC
CTAATTGCCTAGAAAACATGAGGATCACCCATGTCTGCAGGTCGACTC
TAGAAAACATGAGGATCACCCATGTCTGCAGTATTCCCGGGTTCATTA
GATCCTAAGGTACCTAATTGCCTAGAAAACATGAGGATCACCCATGTC
TGCAGGTCGACTCCAGAAAACATGAGGATCACCCATGTCTGCAGTATT
CCCGGGTTCATTAGATCCTAAGGTACCTAATTGCCTAGAAAACATGAG
GATCACCCATGTCTGCAGGTCGACTCTAGAAAACATGAGGATCACCCA
TGTCTGCAGTATTCCCGGGTTCATTAGATCCTAAGGTACCTAATTGCC
TAGAAAACATGAGGATCACCCATGTCTGCAGGTCGACTCTAGAAAACA
TGAGGATCACCCATGTCTGCAGTATTCCCGGGTTCATTAGATCCTAAG
GTACCTAATTGCCTAGAAAACATGAGGATCACCCATGTCTGCAGGTCG
ACTCCAGAAAACATGAGGATCACCCATGTCTGCAGTATTCCCGGGTTC
ATTAGATCCGAATTCAGGGGCCAGCCCAGGGTCCCCAGCCTGCCTGCC
ACACCCAGTCTGTGGCTTTTGTCAACTAGGACTTGATTGAGCTGGGGC
TGACACCCAAGGGGATGCCCTGTCCAGCCAGACACCTTCTCACCCACT
GGCCTGACTCACAACTGCCACACAACCATGATTCATGGACATCAAGAA
GCCCCTCTCCCATAGGGCTCCCACCTGCCACCTACCCCTCACCTGTCT
GCCCTAGTCCTGGCCCTGTCTCCAGTGGCCTCACCCTCTACACTCTCA
GACCATCACAGAACACCTTTGGCTTCCTCATTCTGCATCAGTGTCCAG
GGCCCTTTGGGTAGTCAAGAAATCAAGTGTCTGAAAGGCAATGAAAAG
TAGGCACCAAACCCAAGGGGCATCCCAGGGCAGATGCTAAAGCAGAAT
CAGAGATGGCCGAAGGAACCTCTACTTCCGGGGATGCAGCCCGCTCCT
ACAGACACAGCAGATCCAGCTGGTGCCCTACCTGCCTCCCAGAGCAAC
TGGCCAGTCTTGGGCAGCATAGCTCCCCTCTCAGGGTGAGCTGAAGCA
GCAGACCTGACGCGCTGGCGCCTCCTGGCCCCCAGCAGTGATTCATAC
CAGTGAAGAAAAGCAGACTTCGGCTCCATGACTCAGCCATGCCAGGCG
GAGGGTCCCAGAGGGGCTGAGTCCTCAGCCCCAGCTGAGGCAGCAGCT
GGAGTCTTCAGAGCCAGGTGAATGACACCAGGTCTCAAGCTGCTGAGA
AGTCTTTCCGGCCATGTCTGGAAGGGGTACCACCCCAGCACCAGCACC
GTCCCCTCCTCTCTTGAAGCTGCCTGCACAGAGGTTCCAAGACACTTT
CAAGGCAGAGAAAATAGGATTACAAAGAGGAGGTGCCTGGCAGAGGGC
AGCACCCAGCTCAGCCTCAGAGCTGAAGGTGAAGACAAGCCAGCGTGA
AACCCCGGGTCTGCCACGAATGCCCGCTCCGCTGGCCACTCACCAGCT
GCCTGCCACAAGCCACTGCAGCTTGAGCAGGGTCTGTGCCCTCTCAGC
ACAGAGCCCAGTTCGCTGCGTGGCCTTTGGCCCCCGCCAGAACCTTGC

AGGAGCCTTAAGGTTCGGGCCCTAGCCCAGCCTGACCTTACCTGCTGT
GCCCTGCCTGCTGGTCAAGTCCAGTCCCAGGAGACCCCATGCCTTGGC
TCCTAGGCTGTTCCAGGCACTTCCCTGACCTGCCGGGTGATTGCCCAG
CTGGAACCTCATCCACACCCCAGCACCAACCACCTCGTGTTGGTAACT
GCTCGTGTCTGTAGTCTGAGTAGGCCATGTTGAGGTTCCTCCATCTGC
CTGGTCCATTGGTGTTCTGAGACCAGTTCCACTGCTGTTCTGACAGAT
CCCCCACCCTGTGCCCCTGCCAGCCCCCACAGGTTTATTTTTGCACAT
AAACCATGACCCATACTAATTTGGCTAGCTCTGGGGACTAGGGAGACC
CTGGAGATCTCAAGAGTGTGGCTATCCCCTATTTTCACCAAGCCTTCA
ATATCCAGCCAGGCCATCTGCCCACACCATCTTACCTCAAAGACAGAC
ATATATATATATATACATATATATGATTTTGTTAATAAAACTATGAAA
TTTAAA

Arc 5’UTR

Arc Leader Sequence

ChETA

Cherry

SYN tag

12X MS2

Arc 3’UTR

Translation:

MDYGGALSAVGRELLFVTNPVVVNGSVLVPEDQCYCAGWIESRGTNGA
QTASNVLQWLAAGFSILLLMFYAYQTWKSTCGWEEIYVCAIEMVKVIL
EFFFEFKNPSMLYLATGHRVQWLRYAAWLLTCPVILIHLSNLTGLSND
YSRRTMGLLVSDIGTIVWGATSAMATGYVKVIFFCLGLCYGANTFFHA
AKAYIEGYHTVPKGRCRQVVTGMAWLFFVSWGMFPILFILGPEGFGVL
SVYGSTVGHTIIDLMSKNCWGLLGHYLRVLIHEHILIHGDIRKTTKLN
IGGTEIEVETLVEDEAEAGAVPAAAVSKGEEDNMAIIKEFMRFKVHME
GSVNGHEFEIEGEGEGRPYEGTQTAKLKVTKGGPLPFAWDILSPQFMY
GSKAYVKHPADIPDYLKLSFPEGFKWERVMNFEDGGVVTVTQDSSLQD
GEFIYKVKLRGTNFPSDGPVMQKKTMGWEASSERMYPEDGALKGEIKQ
RLKLKDGGHYDAEVKTTYKAKKPVQLPGAYNVNIKLDITSHNEDYTIV
EQYERAEGRHSTGGMDELYAAASIESDVAAAETQV*

A-ChETA-Cherry

AGTGCTCTGGCGAGTAGTCCTCCCTCAGCCGCAGTCTCTGGGCCTCTT
CAGCTTGAGCGGCGGCGAGCCTGCCACACTCGCTAAGCTCCTCCGGCA
CCGCGCACTTGCCACTGCCACTGCCGCTTCGCGCCCGCTGCAGCCGCC
GGCTCTGAATCCTTCTGGCTTCCGCCTCAGAGGAGTTCTTAGCCTGTC
CCGAACCGTAACCCCGGCGAGCAGACGGAGCTGGACCAGCTAGCATGG
ATTATGGAGGCGCTTTGTCTGCCGTCGGACGCGAACTTTTGTTCGTTA
CTAATCCTGTGGTGGTGAACGGGTCCGTCCTGGTCCCTGAGGATCAAT
GTTACTGTGCCGGATGGATTGAATCTCGCGGCACGAACGGCGCTCAGA
CCGCGTCAAATGTCCTGCAGTGGCTTGCAGCAGGATTCAGCATTTTGC
TGCTGATGTTCTATGCCTACCAAACCTGGAAATCTACATGCGGCTGGG
AGGAGATCTATGTGTGCGCCATTGAAATGGTTAAGGTGATTCTCGAGT
TCTTTTTTGAGTTTAAGAATCCCTCTATGCTCTACCTTGCCACAGGAC
ACCGGGTGCAGTGGCTGCGCTATGCAGCCTGGCTGCTCACTTGTCCTG
TCATCCTTATCCACCTGAGCAACCTCACCGGCCTGAGCAACGACTACA
GCAGGAGAACCATGGGACTCCTTGTCTCAGACATCGGGACTATCGTGT
GGGGGGCTACCAGCGCCATGGCAACCGGCTATGTTAAAGTCATCTTCT
TTTGTCTTGGATTGTGCTATGGCGCGAACACATTTTTTCACGCCGCCA
AAGCATATATCGAGGGTTATCATACTGTGCCAAAGGGTCGGTGCCGCC
AGGTCGTGACCGGCATGGCATGGCTGtttttcgtgagctggggtatgt
tcccaattctcttcattttggggcccgaaggttttggcgtcctgagcg
tctatggctccaccgtaggtcacacgattattgatctgatgagtaaaa
attgttgggggttgttgggacactacctgcgcgtcctgatccacgagc
acatattgattcacggagatatccgcaaaaccaccaaactgaacatcg
gcggaacggagatcgaggtcgagactctcgtcgaagacgaagccgagg
ccggagccgtgccagcggccgccgtgagcaagggcgaggaggataaca
tggccatcatcaaggagttcatgcgcttcaaggtgcacatggagggct
ccgtgaacggccacgagttcgagatcgagggcgagggcgagggccgcc
cctacgagggcacccagaccgccaagctgaaggtgaccaagggtggcc
ccctgcccttcgcctgggacatcctgtcccctcagttcatgtacggct
ccaaggcctacgtgaagcaccccgccgacatccccgactacttgaagc
tgtccttccccgagggcttcaagtgggagcgcgtgatgaacttcgagg
acggcggcgtggtgaccgtgacccaggactcctccctgcaggacggcg
agttcatctacaaggtgaagctgcgcggcaccaacttcccctccgacg
gccccgtaatgcagaagaagaccatgggctgggaggcctcctccgagc
ggatgtaccccgaggacggcgccctgaagggcgagatcaagcagaggc
tgaagctgaaggacggcggccactacgacgctgaggtcaagaccacct
acaaggccaagaagcccgtgcagctgcccggcgcctacaacgtcaaca
tcaagttggacatcacctcccacaacgaggactacaccatcgtggaac
agtacgaacgcgccgagggccgccactccaccggcggcatgGACGAGC
TGTACAAGTAAAGATCCTAAGGTACCTAATTGCCTAGAAAACATGAGG
ATCACCCATGTCTGCAGGTCGACTCTAGAAAACATGAGGATCACCCAT
GTCTGCAGTATTCCCGGGTTCATTAGATCCTAAGGTACCTAATTGCCT

AGAAAACATGAGGATCACCCATGTCTGCAGGTCGACTCTAGAAAACAT
GAGGATCACCCATGTCTGCAGTATTCCCGGGTTCATTAGATCCTAAGG
TACCTAATTGCCTAGAAAACATGAGGATCACCCATGTCTGCAGGTCGA
CTCCAGAAAACATGAGGATCACCCATGTCTGCAGTATTCCCGGGTTCA
TTAGATCCTAAGGTACCTAATTGCCTAGAAAACATGAGGATCACCCAT
GTCTGCAGGTCGACTCTAGAAAACATGAGGATCACCCATGTCTGCAGT
ATTCCCGGGTTCATTAGATCCTAAGGTACCTAATTGCCTAGAAAACAT
GAGGATCACCCATGTCTGCAGGTCGACTCTAGAAAACATGAGGATCAC
CCATGTCTGCAGTATTCCCGGGTTCATTAGATCCTAAGGTACCTAATT
GCCTAGAAAACATGAGGATCACCCATGTCTGCAGGTCGACTCCAGAAA
ACATGAGGATCACCCATGTCTGCAGTATTCCCGGGTTCATTAGATCCg
aattcAGGGGCCAGCCCAGGGTCCCCAGCCTGCCTGCCACACCCAGTC
TGTGGCTTTTGTCAACTAGGACTTGATTGAGCTGGGGCTGACACCCAA
GGGGATGCCCTGTCCAGCCAGACACCTTCTCACCCACTGGCCTGACTC
ACAACTGCCACACAACCATGATTCATGGACATCAAGAAGCCCCTCTCC
CATAGGGCTCCCACCTGCCACCTACCCCTCACCTGTCTGCCCTAGTCC
TGGCCCTGTCTCCAGTGGCCTCACCCTCTACACTCTCAGACCATCACA
GAACACCTTTGGCTTCCTCATTCTGCATCAGTGTCCAGGGCCCTTTGG
GTAGTCAAGAAATCAAGTGTCTGAAAGGCAATGAAAAGTAGGCACCAA
ACCCAAGGGGCATCCCAGGGCAGATGCTAAAGCAGAATCAGAGATGGC
CGAAGGAACCTCTACTTCCGGGGATGCAGCCCGCTCCTACAGACACAG
CAGATCCAGCTGGTGCCCTACCTGCCTCCCAGAGCAACTGGCCAGTCT
TGGGCAGCATAGCTCCCCTCTCAGGGTGAGCTGAAGCAGCAGACCTGA
CGCGCTGGCGCCTCCTGGCCCCCAGCAGTGATTCATACCAGTGAAGAA
AAGCAGACTTCGGCTCCATGACTCAGCCATGCCAGGCGGAGGGTCCCA
GAGGGGCTGAGTCCTCAGCCCCAGCTGAGGCAGCAGCTGGAGTCTTCA
GAGCCAGGTGAATGACACCAGGTCTCAAGCTGCTGAGAAGTCTTTCCG
GCCATGTCTGGAAGGGGTACCACCCCAGCACCAGCACCGTCCCCTCCT
CTCTTGAAGCTGCCTGCACAGAGGTTCCAAGACACTTTCAAGGCAGAG
AAAATAGGATTACAAAGAGGAGGTGCCTGGCAGAGGGCAGCACCCAGC
TCAGCCTCAGAGCTGAAGGTGAAGACAAGCCAGCGTGAAACCCCGGGT
CTGCCACGAATGCCCGCTCCGCTGGCCACTCACCAGCTGCCTGCCACA
AGCCACTGCAGCTTGAGCAGGGTCTGTGCCCTCTCAGCACAGAGCCCA
GTTCGCTGCGTGGCCTTTGGCCCCCGCCAGAACCTTGCAGGAGCCTTA
AGGTTCGGGCCCTAGCCCAGCCTGACCTTACCTGCTGTGCCCTGCCTG
CTGGTCAAGTCCAGTCCCAGGAGACCCCATGCCTTGGCTCCTAGGCTG
TTCCAGGCACTTCCCTGACCTGCCGGGTGATTGCCCAGCTGGAACCTC
ATCCACACCCCAGCACCAACCACCTCGTGTTGGTAACTGCTCGTGTCT
GTAGTCTGAGTAGGCCATGTTGAGGTTCCTCCATCTGCCTGGTCCATT
GGTGTTCTGAGACCAGTTCCACTGCTGTTCTGACAGATCCCCCACCCT
GTGCCCCTGCCAGCCCCCACAGGTTTATTTTTGCACATAAACCATGAC
CCATACTAATTTGGCTAGCTCTGGGGACTAGGGAGACCCTGGAGATCT
CAAGAGTGTGGCTATCCCCTATTTTCACCAAGCCTTCAATATCCAGCC
AGGCCATCTGCCCACACCATCTTACCTCAAAGACAGACATATATATAT
ATATACATATATATGATTTTGTTAATAAAACTATGAAATTTAAA

Arc 5’UTR

Arc Leader Sequence

ChETA

Cherry

12X MS2

Arc 3’UTR

S-ChETA-Cherry

atggattatggaggcgctttgtctgccgtcggacgcgaacttttgttc
gttactaatcctgtggtggtgaacgggtccgtcctggtccctgaggat
caatgttactgtgccggatggattgaatctcgcggcacgaacggcgct
cagaccgcgtcaaatgtcctgcagtggcttgcagcaggattcagcatt
ttgctgctgatgttctatgcctaccaaacctggaaatctacatgcggc
tgggaggagatctatgtgtgcgccattgaaatggttaaggtgattctc
gagttctttttgagtttaagaatccctctatgctctaccttgccaca
ggacaccgggtgcagtggctgcgctatgcagcctggctgctcacttgt
cctgtcatccttatccacctgagcaacctcaccggcctgagcaacgac
tacagcaggagaaccatgggactccttgtctcagacatcgggactatc
gtgtgggggctaccagcgccatggcaaccggctatgttaaagtcatc
ttcttttgtcttggattgtgctatggcgcgaacacatttttcacgcc
gccaaagcatatatcgagggttatcatactgtgccaaagggtcggtgc
cgccaggtcgtgaccggcatggcatggctgtttttcgtgagctggggt
atgttcccaattctcttcattttggggcccgaaggttttggcgtcctg
agcgtctatggctccaccgtaggtcacacgattattgatctgatgagt
aaaaattgttgggggttgttgggacactacctgcgcgtcctgatccac
gagcacatattgattcacggagatatccgcaaaaccaccaaactgaac
atcggcggaacggagatcgaggtcgagactctcgtcgaagacgaagcc
gaggccggagccgtgccagcggccgccGTGAGCAAGGGCGAGGAGGAT
AACATGGCCATCATCAAGGAGTTCATGCGCTTCAAGGTGCACATGGAG
GGCTCCGTGAACGGCCACGAGTTCGAGATCGAGGGCGAGGGCGAGGGC
CGCCCCTACGAGGGCACCCAGACCGCCAAGCTGAAGGTGACCAAGGGT
GGCCCCCTGCCCTTCGCCTGGGACATCCTGTCCCCTCAGTTCATGTAC
GGCTCCAAGGCCTACGTGAAGCACCCCGCCGACATCCCCGACTACTTG
AAGCTGTCCTTCCCCGAGGGCTTCAAGTGGGAGCGCGTGATGAACTTC
GAGGACGGCGGCGTGGTGACCGTGACCCAGGACTCCTCCCTGCAGGAC
GGCGAGTTCATCTACAAGGTGAAGCTGCGCGGCACCAACTTCCCCTCC
GACGGCCCCGTAATGCAGAAGAAGACCATGGGCTGGGAGGCCTCCTCC
GAGCGGATGTACCCCGAGGACGGCGCCCTGAAGGGCGAGATCAAGCAG
AGGCTGAAGCTGAAGGACGGCGGCCACTACGACGCTGAGGTCAAGACC

ACCTACAAGGCCAAGAAGCCCGTGCAGCTGCCCGGCGCCTACAACGTC
AACATCAAGTTGGACATCACCTCCCACAACGAGGACTACACCATCGTG
GAACAGTACGAACGCGCCGAGGGCCGCCACTCCACCGGCGGCATGGAC
GAGCTGTACGCCGCTGCTTCAATTGAAAGTGACGTGGCCGCAGCCGAA
ACCCAGGTGTATAAGTAAAGATCCTAAGGTACCTAATTGCCTAGAAAA
CATGAGGATCACCCATGTCTGCAGGTCGACTCTAGAAAACATGAGGAT
CACCCATGTCTGCAGTATTCCCGGGTTCATTAGATCCTAAGGTACCTA
ATTGCCTAGAAAACATGAGGATCACCCATGTCTGCAGGTCGACTCTAG
AAAACATGAGGATCACCCATGTCTGCAGTATTCCCGGGTTCATTAGAT
CCTAAGGTACCTAATTGCCTAGAAAACATGAGGATCACCCATGTCTGC
AGGTCGACTCCAGAAAACATGAGGATCACCCATGTCTGCAGTATTCCC
GGGTTCATTAGATCCTAAGGTACCTAATTGCCTAGAAAACATGAGGAT
CACCCATGTCTGCAGGTCGACTCTAGAAAACATGAGGATCACCCATGT
CTGCAGTATTCCCGGGTTCATTAGATCCTAAGGTACCTAATTGCCTAG
AAAACATGAGGATCACCCATGTCTGCAGGTCGACTCTAGAAAACATGA
GGATCACCCATGTCTGCAGTATTCCCGGGTTCATTAGATCCTAAGGTA
CCTAATTGCCTAGAAAACATGAGGATCACCCATGTCTGCAGGTCGACT
CCAGAAAACATGAGGATCACCCATGTCTGCAGTATTCCCGGGTTCATT

ChETA

Cherry

SYN tag

12X MS2

CAG::rtTA-TRE::EGFP

actagttattaatagtaatcaattacggggtcattagttcatagccca
tatatggagttccgcgttacataacttacggtaaatggcccgcctggc
tgaccgcccaacgacccccgcccattgacgtcaataatgacgtatgtt
cccatagtaacgccaatagggactttccattgacgtcaatgggtggac
tatttacggtaaactgcccacttggcagtac
atcaagtgtatcatatgccaagtacgccccctattgacgtcaatgacg
gtaaatggcccgcctggcattatgcccagtacatgaccttatgggact
ttcctacttggcagtacatctacgtattagtcatcgctattaccatgg
gtcgaggtgagccccacgttctgcttcactctccccatctccccccc
tccccacccccaattttgtatttatttatttttttaattattttgtgca
gcgatgggggcgggggggggggggcgcgcgccaggcggggcggggcg
gggcgaggggcggggcggggcgaggcggagaggtgcggcggcagccaa
tcagagcggcgcgctccgaaagtttccttttatggcgaggcggcggcg
gcggcggccctataaaaagcgaagcgcgcggcgggcgggagtcgctgc

gttgccttcgccccgtgccccgctccgcgccgcctcgcgccgcccgcc
ccggctctgactgaccgcgttactcccacaggtgagcgggcgggacgg
ccctttctcctccgggctgtaattagcgcttggtttaatgacggctcgt
ttctttttctgtggctgcgtgaaagccttaaagggctccgggagggccc
tttgtgcgggggggagcggctcgggggtgcgtgcgtgtgtgtgtgcg
tggggagcgccgcgtgcggcccgcgctgcccgggcggctgtgagcgctg
cgggcgcggcgcgggctttgtgcgctccgcgtgtgcgcgaggggagc
gcggccgggggcggtgccccgcggtgcgggggggctgcgaggggaaca
aaggctgcgtgcggggtgtgtgcgtgggggggtgagcagggggtgtgg
gcgcggcggtcgggctgtaacccccccctgcacccccctccccgagtt
gctgagcacggcccggcttcgggtgcggggctccgtgcggggcgtggc
gcgggggctcgccgtgccgggcgggggggtggcggcaggtgggggtgccg
ggcggggcggggccgcctcgggccggggagggctcgggggaggggcgc
ggcggccccggagcgccggcggctgtcgaggcgcggcgagccgcagcc
attgccttttatggtaatcgtgcgagagggcgcagggacttcctttgt
cccaaatctggcggagccgaaatctgggaggcgccgccgcaccccctc
tagcgggcgcgggcgaagcggtgcggcgccggcaggaaggaaatgggc
ggggagggccttcgtgcgtcgccgcgccgccgtcccctttctccatctc
cagcctcggggctgccgcaggggacggctgccttcgggggggacggg
gcagggcggggttcggcttctggcgtgtgaccggcggctctagagcct
ctgctaaccatgttcatgccttcttctttttcctacagctcctgggca
acgtgctggttgttgtgctgtctcatcattttggcaaagaattcGATT
GCCGCCATGTCTAGACTGGACAAGAGCAAAGTCATAAACGGCGCTCTG
GAATTACTCAATGGAGTCGGTATCGAAGGCCTGACGACAAGGAAACTC
GCTCAAAAGCTGGGAGTTGAGCAGCCTACCCTGTACTGGCACGTGAAG
AACAAGCGGGCCCTGCTCGATGCCCTGCCAATCGAGATGCTGGACAGG
CATCATACCCACTTCTGCCCCCTGGAAGGCGAGTCATGGCAAGACTTT
CTGCGGAACAACGCCAAGTCATTCCGCTGTGCTCTCCTCTCACATCGC
GACGGGGCTAAAGTGCATCTCGGCACCCGCCCAACAGAGAAACAGTAC
GAAACCCTGGAAAATCAGCTCGCGTTCCTGTGTCAGCAAGGCTTCTCC
CTGGAGAACGCACTGTACGCTCTGTCCGCCGTGGGCCACTTTACACTG
GGCTGCGTATTGGAGGAACAGGAGCATCAAGTAGCAAAAGAGGAAAGA
GAGACACCTACCACCGATTCTATGCCCCCACTTCTGAGACAAGCAATT
GAGCTGTTCGACCGGCAGGGAGCCGAACCTGCCTTCCTTTTCGGCCTG
GAACTAATCATATGTGGCCTGGAGAAACAGCTAAAGTGCGAAAGCGGC
GGGCCGGCCGACGCCCTTGACGATTTTGACTTAGACATGCTCCCAGCC
GATGCCCTTGACGACTTTGACCTTGATATGCTGCCTGCTGACGCTCTT
GACGATTTTGACCTTGACATGCTCCCCGGGTAAGCGGCCGCAATAAAA
TATCTTTTTTTTCATTACATCTGTGTGTTGGTTTTTTGTGTGTCgtcg
acCAAAATTTTATCGATCACGAGACTAGCCtcgagtttaccactccct
atcagtgatagagaaaagtgaaagtcgagtttaccactccctatcagt
gatagagaaaagtgaaagtcgagtttaccactccctatcagtgataga
gaaaagtgaaagtcgagtttaccactccctatcagtgatagagaaaagt
gaaagtcgagtttaccactccctatcagtgatagagaaaagtgaaag

tcgagtttaccactccctatcagtgatagagaaaagtgaaagtcgagt
ttaccactccctatcagtgatagagaaaagtgaaagtcgagctcggta
cccgggtcgagtaggcgtgtacggtgggaggcctatataagcagagct
cgtttagtgaaccgtcagatcgcctggagacgccatccacgctgtttt
gacctccatagaagacaccgggaccgatccagcctccgcggccccgaa
ttcgagctcggtacccggggatcctctagtcagctgacgcgtATGGTG
AGCAAGGGCGAGGAGCTGTTCACCGGGGTGGTGCCCATCCTGGTCGAG
CTGGACGGCGACGTAAACGGCCACAAGTTCAGCGTGTCCGGCGAGGGC
GAGGGCGATGCCACCTACGGCAAGCTGACCCTGAAGTTCATCTGCACC
ACCGGCAAGCTGCCCGTGCCCTGGCCCACCCTCGTGACCACCCTGACC
TACGGCGTGCAGTGCTTCAGCCGCTACCCCGACCACATGAAGCAGCAC
GACTTCTTCAAGTCCGCCATGCCCGAAGGCTACGTCCAGGAGCGCACC
ATCTTCTTCAAGGACGACGGCAACTACAAGACCCGCGCCGAGGTGAAG
TTCGAGGGCGACACCCTGGTGAACCGCATCGAGCTGAAGGGCATCGAC
TTCAAGGAGGACGGCAACATCCTGGGGCACAAGCTGGAGTACAACTAC
AACAGCCACAACGTCTATATCATGGCCGACAAGCAGAAGAACGGCATC
AAGGTGAACTTCAAGATCCGCCACAACATCGAGGACGGCAGCGTGCAG
CTCGCCGACCACTACCAGCAGAACACCCCCATCGGCGACGGCCCCGTG
CTGCTGCCCGACAACCACTACCTGAGCACCCAGTCCGCCCTGAGCAAA
GACCCCAACGAGAAGCGCGATCACATGGTCCTGCTGGAGTTCGTGACC
GCCGCCGGGATCACTCTCGGCATGGACGAGCTGTACAAGTAA

tetO
rtTA
EGFP
CAG promoter
synthetic polyA

TRE3g::SA-Ch-pCK0.4::rtTA

CCCGAAGGACTTCCAGGGGAACGCCTGGTTCTTTTAGTCCGTCGGGTT
CGCCACTTTGACTGGAGGTCGATTTTGGGATGTTGTCAGGGGGCGGAG
CCTATGGAAAACGCCAGCAACGCGGCCTTTTTACGGTTCCTGGCCTTT
TGCTGGCCTTTTGCTCATTAGGCACCCCAGGCTTTACCCGAACGACCG
AGCGCAGCGAGTCAGTGAGCGAGGAAGCGGAGAGCGCCCAATACGCAA
GGAAACAGCTATGACCATGTTAATGCAGCTGGCACGACAGGTTTCCCG
ACTGGAAAGCGGGCAGTGAAAGGAAGGCCCATGAGGCCAGTTAATTAA
TCGGTCCGTTTACTCCCTATCAGTGATAGAGAACGTATGAAGAGTTTA

CTCCCTATCAGTGATAGAGAACGTATGCAGACTTTACTCCCTATCAGT
GATAGAGAACGTATAAGGAGTTTACTCCCTATCAGTGATAGAGAACGT
ATGACCAGTTTACTCCCTATCAGTGATAGAGAACGTATCTACAGTTTA
CTCCCTATCAGTGATAGAGAACGTATATCCAGTTTACTCCCTATCAGT
GATAGAGAACGTATAAGCTTTAGGCGTGTACGGTGGGCGCCTATAAAA
GCAGAGCTCGTTTAGTGAACCGTCAGATCGCCTGGAGCAATTCCACAA
CACTTTTGTCTTATACCAACTTTCCGTACCACTTCCTACCCTCGTAAA
AGCCTCCGCGGCCCCGAATTCGAGCTCGGTACCCGGGGATCCTCTAGT
CAGCTGACGCGTAGTGCTCTGGCGAGTAGTCCTCCCTCAGCCGCAGTC
TCTGGGCCTCTTCAGCTTGAGCGGCGGCGAGCCTGCCACACTCGCTAA
GCTCCTCCGGCACCGCGCACTTGCCACTGCCACTGCCGCTTCGCGCCC
GCTGCAGCCGCCGGCTCTGAATCCTTCTGGCTTCCGCCTCAGAGGAGT
TCTTAGCCTGTCCCGAACCGTAACCCCGGCGAGCAGACGGAGCTGGAC
CAGCTAGCATGGATTATGGAGGCGCTTTGTCTGCCGTCGGACGCGAAC
TTTTGTTCGTTACTAATCCTGTGGTGGTGAACGGGTCCGTCCTGGTCC
CTGAGGATCAATGTTACTGTGCCGGATGGATTGAATCTCGCGGCACGA
ACGGCGCTCAGACCGCGTCAAATGTCCTGCAGTGGCTTGCAGCAGGAT
TCAGCATTTTGCTGCTGATGTTCTATGCCTACCAAACCTGGAAATCTA
CATGCGGCTGGGAGGAGATCTATGTGTGCGCCATTGAAATGGTTAAGG
TGATTCTCGAGTTCTTTTTTGAGTTTAAGAATCCCTCTATGCTCTACC
TTGCCACAGGACACCGGGTGCAGTGGCTGCGCTATGCAGCCTGGCTGC
TCACTTGTCCTGTCATCCTTATCCACCTGAGCAACCTCACCGGCCTGA
GCAACGACTACAGCAGGAGAACCATGGGACTCCTTGTCTCAGACATCG
GGACTATCGTGTGGGGGGCTACCAGCGCCATGGCAACCGGCTATGTTA
AAGTCATCTTCTTTTGTCTTGGATTGTGCTATGGCGCGAACACATTTT
TTCACGCCGCCAAAGCATATATCGAGGGTTATCATACTGTGCCAAAGG
GTCGGTGCCGCCAGGTCGTGACCGGCATGGCATGGCTGttttttcgtga
gctggggtatgttcccaattctcttcattttggggcccgaaggttttg
gcgtcctgagcgtctatggctccaccgtaggtcacacgattattgatc
tgatgagtaaaaattgttgggggttgttgggacactacctgcgcgtcc
tgatccacgagcacatattgattcacggagatatccgcaaaaccacca
aactgaacatcggcggaacggagatcgaggtcgagactctcgtcgaag
acgaagccgaggccggagccgtgccagcggccgccgtgagcaagggcg
aggaggataacatggccatcatcaaggagttcatgcgcttcaaggtgc
acatggagggctccgtgaacggccacgagttcgagatcgagggcgagg
gcgagggccgcccctacgagggcacccagaccgccaagctgaaggtga
ccaagggtggcccccctgcccttcgcctgggacatcctgtcccctcagt
tcatgtacggctccaaggcctacgtgaagcaccccgccgacatccccg
actacttgaagctgtccttccccgagggcttcaagtgggagcgcgtga
tgaacttcgaggacggcggcgtggtgaccgtgacccaggactcctccc
tgcaggacggcgagttcatctacaaggtgaagctgcgcggcaccaact
tcccctccgacggccccgtaatgcagaagaagaccatgggctgggagg
cctcctccgagcggatgtaccccgaggacggcgccctgaagggcgaga
tcaagcagaggctgaagctgaaggacggcggccactacgacgctgagg
tcaagaccacctacaaggccaAGAAGCCCGTGCAGCTGCCCGGCGCCT

ACAACGTCAACATCAAGTTGGACATCACCTCCCACAACGAGGACTACA
CCATCGTGGAACAGTACGAACGCGCCGAGGGCCGCCACTCCACCGGCG
GCATGGACGAGCTGTACGCCGCTGCTTCAATTGAAAGTGACGTGGCCG
CAGCCGAAACCCAGGTGTAATAAGTACAAGTAAAGATCCTAAGGTACC
TAATTGCCTAGAAAACATGAGGATCACCCATGTCTGCAGGTCGACTCT
AGAAAACATGAGGATCACCCATGTCTGCAGTATTCCCGGGTTCATTAG
ATCCTAAGGTACCTAATTGCCTAGAAAACATGAGGATCACCCATGTCT
GCAGGTCGACTCTAGAAAACATGAGGATCACCCATGTCTGCAGTATTC
CCGGGTTCATTAGATCCTAAGGTACCTAATTGCCTAGAAAACATGAGG
ATCACCCATGTCTGCAGGTCGACTCCAGAAAACATGAGGATCACCCAT
GTCTGCAGTATTCCCGGGTTCATTAGATCCTAAGGTACCTAATTGCCT
AGAAAACATGAGGATCACCCATGTCTGCAGGTCGACTCTAGAAAACAT
GAGGATCACCCATGTCTGCAGTATTCCCGGGTTCATTAGATCCTAAGG
TACCTAATTGCCTAGAAAACATGAGGATCACCCATGTCTGCAGGTCGA
CTCTAGAAAACATGAGGATCACCCATGTCTGCAGTATTCCCGGGTTCA
TTAGATCCTAAGGTACCTAATTGCCTAGAAAACATGAGGATCACCCAT
GTCTGCAGGTCGACTCCAGAAAACATGAGGATCACCCATGTCTGCAGT
ATTCCCGGGTTCATTAGATCCGAATTCAGGGGCCAGCCCAGGGTCCCC
AGCCTGCCTGCCACACCCAGTCTGTGGCTTTTGTCAACTAGGACTTGA
TTGAGCTGGGGCTGACACCCAAGGGGATGCCCTGTCCAGCCAGACACC
TTCTCACCCACTGGCCTGACTCACAACTGCCACACAACCATGATTCAT
GGACATCAAGAAGCCCCTCTCCCATAGGGCTCCCACCTGCCACCTACC
CCTCACCTGTCTGCCCTAGTCCTGGCCCTGTCTCCAGTGGCCTCACCC
TCTACACTCTCAGACCATCACAGAACACCTTTGGCTTCCTCATTCTGC
ATCAGTGTCCAGGGCCCTTTGGGTAGTCAAGAAATCAAGTGTCTGAAA
GGCAATGAAAAGTAGGCACCAAACCCAAGGGGCATCCCAGGGCAGATG
CTAAAGCAGAATCAGAGATGGCCGAAGGAACCTCTACTTCCGGGGATG
CAGCCCGCTCCTACAGACACAGCAGATCCAGCTGGTGCCCTACCTGCC
TCCCAGAGCAACTGGCCAGTCTTGGGCAGCATAGCTCCCCTCTCAGGG
TGAGCTGAAGCAGCAGACCTGACGCGCTGGCGCCTCCTGGCCCCCAGC
AGTGATTCATACCAGTGAAGAAAAGCAGACTTCGGCTCCATGACTCAG
CCATGCCAGGCGGAGGGTCCCAGAGGGGCTGAGTCCTCAGCCCCAGCT
GAGGCAGCAGCTGGAGTCTTCAGAGCCAGGTGAATGACACCAGGTCTC
AAGCTGCTGAGAAGTCTTTCCGGCCATGTCTGGAAGGGGTACCACCCC
AGCACCAGCACCGTCCCCTCCTCTCTTGAAGCTGCCTGCACAGAGGTT
CCAAGACACTTTCAAGGCAGAGAAAATAGGATTACAAAGAGGAGGTGC
CTGGCAGAGGGCAGCACCCAGCTCAGCCTCAGAGCTGAAGGTGAAGAC
AAGCCAGCGTGAAACCCCGGGTCTGCCACGAATGCCCGCTCCGCTGGC
CACTCACCAGCTGCCTGCCACAAGCCACTGCAGCTTGAGCAGGGTCTG
TGCCCTCTCAGCACAGAGCCCAGTTCGCTGCGTGGCCTTTGGCCCCCG
CCAGAACCTTGCAGGAGCCTTAAGGTTCGGGCCCTAGCCCAGCCTGAC
CTTACCTGCTGTGCCCTGCCTGCTGGTCAAGTCCAGTCCCAGGAGACC
CCATGCCTTGGCTCCTAGGCTGTTCCAGGCACTTCCCTGACCTGCCGG
GTGATTGCCCAGCTGGAACCTCATCCACACCCCAGCACCAACCACCTC
GTGTTGGTAACTGCTCGTGTCTGTAGTCTGAGTAGGCCATGTTGAGGT

TCCTCCATCTGCCTGGTCCATTGGTGTTCTGAGACCAGTTCCACTGCT
GTTCTGACAGATCCCCCACCCTGTGCCCCTGCCAGCCCCCACAGGTTT
ATTTTTGCACATAAACCATGACCCATACTAATTTGGCTAGCTCTGGGG
ACTAGGGAGACCCTGGAGATCTCAAGAGTGTGGCTATCCCCTATTTTC
ACCAAGCCTTCAATATCCAGCCAGGCCATCTGCCCACACCATCTTACC
TCAAAGACAGACATATATATATATATACATATATATGATTTTGTTAAT
AAAACTATGAAATTTAAAACGCGTgctagcgtttaaacGGCGCGCCCG
ACTGTGCCTTCTAGTTGCCAGCCATCTGTTGTTTGCCCCTCCCCCGTG
CCTTCCTTGACCCTGGAAGGTGCCACTCCCACTGTCCTTTCCTAATAA
AATGAGGAAATTGCATCGCATTGTCTGAGTAGGTGTCATTCTATTCTG
GGGGGTGGGGTGGGGCAGGACAGCAAGGGGGAGGATTGGGAAGACAAT
AGCAGGCATGCTGGGGATGCGGTGGGCTCTATGGCTAGGCGGCCGCAT
CGATAAGCTTGTCGACGATaccaggtCGGACAtaacttgtggactaag
tttgttcacatCCCCTTCTCCAACCCCCTCAGTACATCACCCTGGGgG
AACAgGGTCCACTTGCTcCTGGGCCCACACAGTCCTGCAGTATTGTGT
ATATAAGGCCAGGGCAAAGAGGAGCAGGTTTTAAAGTGAAAGGCAGGC
AGGTGTTGGGGAGGCAGTTACCGGGGCAACGGGAACAGGGCGTTTCGG
AGGTGGTTGCCATGGGGACCTGGATGCTGACGAAGGCTCGCGAGGCTG
TGAGCAGCCACAGTGCCCTGCTCAGAAGCCCCAAGCTCGTCAGTCAAG
CCGGTTCTCCGTTTGCACTCAGGAGCACGGGCAGGCGAGTGGCCCCTA
GTTCTGGGGGCAGCtctagagcGGGGATCCGTTTATCTGCAGAATTCG
CCCgatccgcgcggacttgaTTGCCGCCATGTCTAGACTGGACAAGAG
CAAAGTCATAAACGGCGCTCTGGAATTACTCAATGGAGTCGGTATCGA
AGGCCTGACGACAAGGAAACTCGCTCAAAAGCTGGGAGTTGAGCAGCC
TACCCTGTACTGGCACGTGAAGAACAAGCGGGCCCTGCTCGATGCCCT
GCCAATCGAGATGCTGGACAGGCATCATACCCACTTCTGCCCCCTGGA
AGGCGAGTCATGGCAAGACTTTCTGCGGAACAACGCCAAGTCATTCCG
CTGTGCTCTCCTCTCACATCGCGACGGGGCTAAAGTGCATCTCGGCAC
CCGCCCAACAGAGAAACAGTACGAAACCCTGGAAAATCAGCTCGCGTT
CCTGTGTCAGCAAGGCTTCTCCCTGGAGAACGCACTGTACGCTCTGTC
CGCCGTGGGCCACTTTACACTGGGCTGCGTATTGGAGGAACAGGAGCA
TCAAGTAGCAAAAGAGGAAAGAGAGACACCTACCACCGATTCTATGCC
CCCACTTCTGAGACAAGCAATTGAGCTGTTCGACCGGCAGGGAGCCGA
ACCTGCCTTCCTTTTCGGCCTGGAACTAATCATATGTGGCCTGGAGAA
ACAGCTAAAGTGCGAAAGCGGCGGGCCGGCCGACGCCCTTGACGATTT
TGACTTAGACATGCTCCCAGCCGATGCCCTTGACGACTTTGACCTTGA
TATGCTGCCTGCTGACGCTCTTGACGATTTTGACCTTGACATGCTCCC
CGGGTAAGCGGCCGCAATAAAATATCTTTTTTTTCATTACATCTGTGT
GTTGGTTTTTTGTGTGTCaccaggt

Arc 5’UTR
Arc Leader Sequence
ChETA

Cherry
SYN tag
12X MS2
Arc 3'UTR
bGH polyA
CaMKII04 core promoter
tetO
rtTA
synthetic polyA

DTEs and ATE used in the study

Arc DTE
Arc DTE maps nucleotides 2035-2702 of Author's sequence (Kobayashi et al, Eur J Neurosc, 2005). See as reference NCBI entry NM_019361.1 [Rattus norvegicus activity-regulated cytoskeleton-associated protein (Arc), mRNA] with T2130A mismatch and T2293Δ deletion, as reported by the Authors (H.Kobayashi, personal communication)

TTCGGCTCCATGACTCAGCCATGCCAGGCGGAGGGTCCCAGAGGGGCT
GAGTCCTCAGCCCCAGCTGAGGCAGCAGCTGGAGTCTTCAGAGCCAGG
AGAATGACACCAGGTCTCAAGCTGCTGAGAAGTCTTTCCGGCCATGTC
TGGAAGGGGTACCACCCCAGCACCAGCACCGTCCCCTCCTCTCTTGAA
GCTGCCTGCACAGAGGTTCCAAGACACTTTCAAGGCAGAGAAAATAGG
ATTACAAAGAGGAGGTGCCTGGCAGAGGGCAGCACCCAGCTCAGCCTC
AGAGCTGAAGGTGAAGACAAGCCAGCGTGAAACCCCGGGTCTGCCACG
AATGCCCGCTCCGCTGGCCACTCACCAGCTGCCTGCCACAAGCCACTG
CAGCTTGAGCAGGGTCTGTGCCCTCTCAGCACAGAGCCCAGTTCGCTG
CGTGGCCTTTGGCCCCCGCCAGAACCTTGCAGGAGCCTTAAGGTTCGG
GCCCTAGCCCAGCCTGACCTTACCTGCTGTGCCCTGCCTGCTGGTCAA
GTCCAGTCCCAGGAGACCCCATGCCTTGGCTCCTAGGCTGTTCCAGGC
ACTTCCCTGACCTGCCGGGTGATTGCCCAGCTGGAACCTCATCCACAC
CCCAGCACCAACCACCTCGTGTTGGTAACTGCTCGTGTCTGTA

CaMKII DTE
Sequence cloned in pNECKu1481-2708 in (Blichenberg et al, Eur J Neurosc, 2001).

GATCCCTTGTCTGCACTGTTTTCTTTGCATGACTTTATATGCAGTAAG
TATGTTGAGAAAAAAAAGAGCAAAGACAAAAAAGAAGAAAAACACTCA
GCAAAATCAAACGACACGTTTTGGACAAAAAATATAATAATAACATTC
AAGGTTATATTCTCAGTGTCCAACTTGGAATTACGTTGCTGCCTCTCT
GTGCTTTTGGTCTCTGTGTGGCTGTGTTTTGCCAGCATGAGACCCTGT
CCCCTCTGGAGGTTTCTAGGGGAGGAAGAGCCGTGTGTCGGGGGGGGG
GGTTGGAGACAGCTTTGTCCTCTCAGCTTTTTGGGGGGGTTGATTGGA
GCAGAAGTGGAAGGGGATGTTTAATCCAGAACTTTCTGGTATTTCCCT
TTCTCCCACGCAGTGAGCTATACGCTGGGCTCTTCTCTCAAATCCTGC
TGCCCAGGGACAAGTATAGGGTAGAAGGGTGGCCCTATTGTCTAAGCC
ACTCCACTGTAGCCCTCTGCCTTTGGTAGAGACACTGCTACCCAGACC
CAAGAATGGGCCCTTGTCCCACCCCAGATCTAGGCTTCTTCATAAGGC
TCAGCAAACTCATTGTCCCCAGCCATTCCCCCACTAAAGGTAAAAGAA
GGTGTGGCCTTTACCAGGGGACACTGCGATTATCAATCAAGCCCTCTT
CAAGCCTCAGTTTCACCACCAATGTTCCTACCCAGACTGATGGAAGGT
CAAACTAAATGATGTCACAAGTGCACACCATCTTTGAGAACTTGCTGG
GTTTGTCACTGGCTGGCCTTCTTATGCACCAGGCCCGGCCAATTCCCA
TCTTTTCCCCTGTGTGCCCCCTCATTTTCCTATTTGGTGCCAGTCTGT
TGAAGACCAGCAACAAATGCAGGGGAAAGAAGTGTCTGGGGGCTTTGG
TAGGCTTTGACCCCCCGTTCTGATCAGAAGGGCTGTGTGGCTTTGGGT
GAGTCCTGTGCCCTCCTGGGGCCTTAGTTTCCTCAGCCAGAAGATGCC
TATGCCCTGCCTTCTGTTGGCTAACATGCCCCTGTCCACTGTGTGCCT
GTCCACATGTGGAGAAGTGGAGGCAGGTCCCTGCCCCAGTCTGAGACG
GCCCGCTCTGCAGAGGCCGCTCCTGTGGGTGGGCAGCCAACTCATGTA
GACCTTGGGACACTACAATGGCCCCAAGGTAGCAGGCAGGGGAACTGG
CAGAAAAACTGCCCTCCTCAGACAAGCT

MAP2 DTE

Sequence cloned in pNEu2432-3071 in (Blichenberg et al, *J Neurosc*, 1999).

AGCGGCCGCGATCTAGCACTAAAATATCATTTTTCTAATGTTAATACA
ATTATAATGGATACAAGTCCTTGTTTTATGTGAAAATGTGATTCACAC
ATGAATGTAAAGTCAACACAAGAAGGACCTGAATTTTTTGTACCAGAC
AGAGACAGAGAAATGCACAGGCTAAAATTCACTTCCTTATGGGAATGT
GGGATGGATCCCACCTTACCTACTTAAGATAATGACTCAAATTAAGCT
TTTTGGACACCACTTTTGTGGGGATACACATACGCTGATCTAGAAATG
AAAGGCGCACAGCTACATTTCTAGATCCACTAATGCCAGTTTCTCTTT
GGCTTCAGCCTTTGAGAACCTGTTCAAGAATACGTAAGTATCCAGAGC
TCTGAAGAGTTCGAAGGCCAACTTTTTCAGTGAACTCACACACTCTGG
GTCTCCTGCAACTGACAATTGGGTACCTTGCAACAATGCGGGAAGGAT
CCGAGTTTATGATGAGTTTCAAAGGCCGTGTTCACTTAGGAACTGACT
CTCTCTGGATCTGCCTGCTGCGTTCCAGCAGGATGACGGGCTGAAATC

CCACCCATAGGGAAGACACCTGTGCAATTCCAGCTCAGTTTGGCTGAA
GGTAACTAAAGAAGAAGGTCCAGTAA

IMPA1 ATE

Sequence cloned in pSC-A IMPA1L (Andreassi et al, *Nat Neurosc*, **13**, 291--301, 2010) corresponding to IMPA1 nts 2044-2165. Sequence maps nts 1126-1249 of NCBI entry GU441530.1 [Rattus norvegicus strain Sprague-Dawley inositol (myo)-1(or 4)-monophosphatase 1 (Impa1-L) mRNA, 3' UTR]

CTGTATTTATGCTGCTAATTACATGCATTTAAAACATCAGGAACCATG
TAAATCCTATTACAAGACAGGTTGCTTTTGCAATTAAATTTATTTACT
TACAAGC

BDNF exon IIa

GCTTTGGCAAAGCCATCCGCACGTGACAAAACGTAAGGAAGTGGAAGA
AACCGTCTAGAGCAATATCAAGTACCACTTAATTAGAGAATATTTTTT
TAACCTTTTCCTCCTGCTGCGCCGGGTGTGTGATCCGGGCGAGCAGAG
TCCATTCAGCACCTTGGACAGAGCCAGCGGATTTGTCCGAGGTGGTAG
TACTTCATCCAGATGACATCATTGGCTGACACTTTCGAACACGTGA

BDNF exon IIc

GCTTTGGCAAAGCCATCCGCACGTGACAAAACGTAAGGAAGTGGAAGA
AACCGTCTAGAGCAATATCAAGTACCACTTAATTAGAGAATATTTTTT
TAACCTTTTCCTCCTGCTGCGCCGGGTGTGTGATCCGGGCGAGCAGAG
TCCATTCAGCACCTTGGACAGAGCCAGCGGATTTGTCCGAGGTGGTAG
TACTTCATCCAGGTATTCTTTTCCTCGCTGTCAAGCCAACCCGGTGTC
GCCCTTAAAAAGCGTCTTTTCCGAGGTTCGGCTCACACTGAGATCGGG
GCTGGAGAGAGAGTCAGATTTTGGAGCGGAGCGTTTGGAGAGCCAGCC
CCAGTTTGGTCCCCTCATTGAGCTCGCTGAAGTTGGCTTCCTAGCGGT
GTAGGCTGGAATAGACTCTTGGCAAGCTCCGGGTTGGTATACTGGGTT
AACTTTGGGAAATGCAAGTGTTTATCTCCAGGATCTAGCCACCGGGGT
GGTGTAAGCCGCAAAGAAGATGACATCATTGGCTGACACTTTCGAACA
CGTGA

BDNF exon VI

CCAATCGAAGCTCAACCGAAGAGCTAAATAATGTCTGACCCCAGTGCC
TGGCGCTGGCTGAGCTCTGGGTGCCCGCCGCTGCCGCCGCGCCGGGGC
GCACCCGCTGGCTGGCTGTCGCACGGTCCCCATTGCGCCCGGGACTCC
CCGGCTTGGAGAAGGAAACCGCCTGGGGCGGCGCGCCACCTCCGCCTG
GCAGGCTTTGATGAGACCGGGTTCCCTCAGCTCGCCACCGCTGCTTTG
GGGCAGACGAGAAAGCGCACGGGGCCCAGGGCAGGGCGCAGGGACCAG

GAGCGTGACAACAATGTGACTCCACTGCCGGGGATCCGAGAGCTTTGT
GTGGACCCTGAG

BDNF B 3'UTR

ACTGTCCCTCTTTCAGAAAACAGACAAAAAAACAAAAAACAAAAAAAA
GCAAAAACAAAAATTTGAACCAAAACATTCCGTTTACATTTTAGACAC
TAAGTATCTTCGTTCTTGTTAGTACTCTGTTCTACTGCTTTCAACTTC
TCATAGCGTTGGAATTAAAACTTGTCAAGGTGCTGTTGTCATTGCTTT
ACTGGCTTAGGGGATGGGGAACGGGAGGGGTAGATTTCTGTTTGTTTT
GTGTTTTATTTCGTTTGTTTGTTTGTTTTGTTTTTTAGTTCCACCCGG
AGTAGGGATGGAGAAAATTTCTTCACTCTCCATTCTGGTTGATAAAGC
GTTACATTTGTATGTTGTAAAAAATGTTTGCAAAATCCAATCAGATGA
CTGGAAAACGAATAAAAATTAAGGCAACTGAATAAAATGCTCACACAA
CACTGCCCATGATGTATCTCCCTGGTCCCCCAGGTCACTCTTCTGGCA
TGGGTCAGGGAAAGCTGCTTTTATTGGAAAGACCAGCATTTGTTTAAA
GCACATTCTTTCCCTCCCTCCTCCCATTTTGGTCCCTTTCTTTTTTGT
TTTGTTTTAAGAAAGAAAATTAAGTTGCGCGCTTTGAAATATTTTATC
ACTGCTGTGAACAGATGAACAATGTGTGTCATTTCATGACACTCGTGG
AAAACAGTGATTTTTTTTTTATTTTTTGCCCTAAGGAGAAACAAGTAA
GAATAACCGAAAATGTTCTTTTTTTTTTAAAGGCATAAACAGTGGATAA
GTTATAATATGGCCTAACAATGTTTGCAGATAAAAGATATTGCATACA
GCCAGATACTAGAGCAGGGATCCACACTGCCACTGAAATGCGACTGAA
TGGCCCTGTGGAGGCTAAGTGGAGCTGACATACTATTTCCTGGCAGAG
CAGGAGGAATTTCTGAGTGGCCATCCTGAGGTCTAGATGGAGGTGGGG
AATGGTACTTGAGACATTCCTAAAGGAAGGCTCGGAAGCACCCTTCAG
AGCAGGCTCTGGAATGATGTGTCAAGTTTCTTAGGCCTTCTGCTTTAA
GTGCCTACGTTACCTAACAGTGCTCAAGAGGTTCTCAATTGGAGAACC
ACACTCAAATCCATTTATGGCCTCCATCCCATTTTAAATAATTATGGA
TAAAGTTGGATTAACCTGGAGCAGCTTTGGATCCAAATATGGCATAGC
AGTGATGCTATCAGTGCAGCATGATGGGAAATGTTTGCTGTGAAGAGA
CTTAACTTTCTTTGCGCTTAGACTTCAGGAAGCCTAGGTTTTATTTAT
TTATTTTTTTGAGACATTTTGGTGAAAGGAAAAAAGAAAGAAGAAAAC
AAACAAACAAAACCAGAAAAAGCACCAAAACTTAGGCAGAATGAGCAA
TGTCTGTCTGTAAGGGCTAGAATGACAAGGCATAGGAAGGTGCTTTCA
CTGTGAAAGAGACAAGAACACAGGAGGAAATACTGCTTAAGTGAAGAG
CACAGAAAGCTCCTGATAGTTCTGTCCATTCAGCACAAGGGTCCCTTC
TACACTTTACCTCTTGGGGTTAGGAGAAGTCAAGCTGGAAGCCTGAAT
GAATGGCCCCAATGAGAACTAGTGTTAAGCCCATTTCCCTAGTGAGGT
TTTCCGCCAGCGCGAATGTGTTAGTGGTTACCTGACTGGGCTCCTGGG
CATCAGAAAAAGAGGCAAACAATTGCTTCATCTTAGGAGTGGAAAGGG
TGAAACAAAGTGGCTGTCCACTGTGACTCAGGGAGTGAAGATACCATC
AGCAAATAGTTTCTTTTTGTTCAACTGTTCCTTTAGAACTAGTCTGTC
TTCTGGAGTCCCACTGAATCCCCTGTTTTTGGAAGACTTCACGTAGCC
TAGATTGTTTTGTGCCGTTTGACAACATTAATCTCTGTCATCATTTCT
AACCTATTAAGGAATGCTTTGAATATCTGCTATATGCTAACTTTTTGC

AGCTTCATTCTGAGAGACGTTAGTCAAACAAATAAAAGGAGCCCCATC
ACAATCTCACGGTATTCGAAGGGCCAGGTCGATTAGGTGGCTTCATAG
GAGACCCTCCGCAACTGTGTGGTCAGTGGCTGGCTCTCATACCCACTA
AGATACATCATAGCTCCATGTCGGTGGTTTATGTTGACCTGAGATTGA
TTTGTTAAAATCTCTCCTCTGTTTCTGTTCGTTCTGTTTCCGTCCTGT
TCTGTTCTGTTCTGTTCTGAAAGTCTTGCTGTGGTCTCTTTTTGGCAG
AAGTGTTTCATGCATGGCAGCAGGCCTGATGCTTTTTATAGTGATTCC
CATTGAAACTGTAAGTAAATGTCTGTGGCCTTGTTCTCTCTATGGTAA
AGATATTATTCACCATGTAAAACAAGAAAAATATTTATTGTATTTTAG
TATATTTATATAATTATGTTATTGAAAAAAATTGGCATTAAAACTTAA
CCACATCAGAAGCCTATTGTAAGTTAACTTGTTTATTGCAGCTTATAA
TGGTTACAAATAAAGCAATAACGCGT

Appendix B

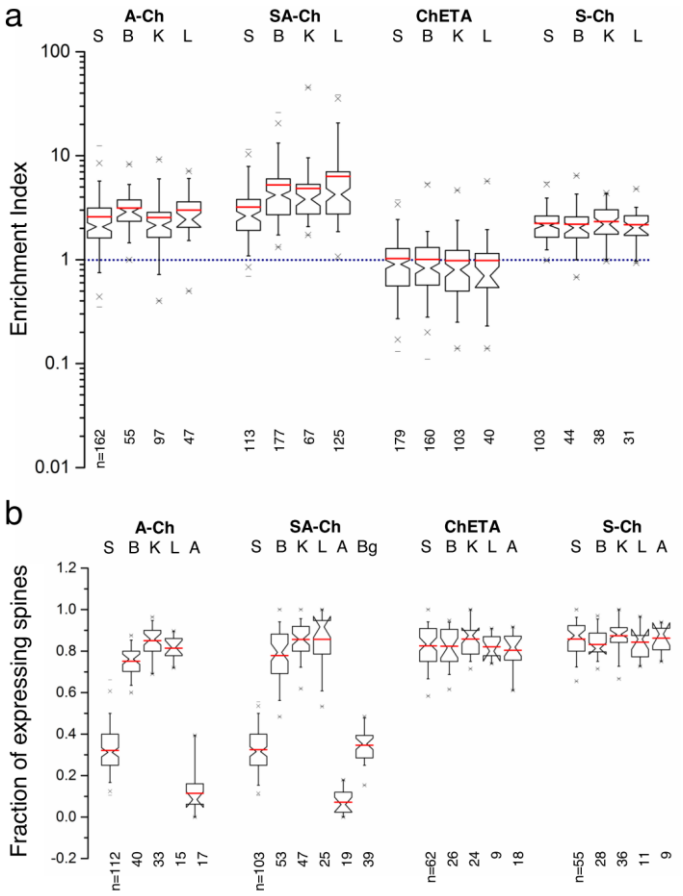

Figure B Notched boxplots of data presented in Figure 28a and 28b in the main text. Notch is median ± 95% confidence interval of the median. Red

line is mean, crosses are 1% and 99% of the distribution, horizontal lines are the corresponding extremes (minimum and maximum). Legend S:saline, B:BDNF, K:KCl, L:cLTP, A:AP5, Bg;BDNF+G418. Data are from 2 to 5 replicates each

Table B Statistical information for data presented in the main text and in the Supporting Information. NA = not applicable

Figure	Sample	Min/25%/median/50%/Max	n	replicates	P value
21	CaMKII	0.021/0.408/0.531/0.685/0.805	46	2	One-way ANOVA, Bonferroni comparison of means Arc vs. CaMKII 0.00694 Arc vs. CaMKII KCl 7.50859E-7 Arc vs. MAP2 4.35833E-6 Arc vs. Arc KCl 8.16394E-36 Arc vs. EGFP 1.97554E-21 Arc KCl vs. CaMKII KCl 0.00588
	CaMKII KCl	0.045/0.47/0.631/0.828/1.308	32	2	
	MAP2	0.086/0.371/0.525/0.675/1.056	121	2	
	Arc	-0.271/0.189/0.335/0.497/0.906	173	2	
	Arc KCl	0.37/0.72/0.924/1.001/.415	77	2	
	IMPA1	-1.925/-0.473/-0.236/-0.428/0.459	177	2	
	EGFP	-1.67/-0.165/0.045/0.267/0.909	169	2	
25b	EGFP	0.31/0.486/0.575/0.66/1.789	33	2	One-way ANOVA, Bonferroni comparison of means P>0.999 for all pairwise comparisons
	ChETA	0.269/0.495/0.624/0.686/0.948	36	2	
	S-Ch	0.413/0.518/0.603/0.648/0.951	34	2	
	SA-Ch	0.384/0.535/0.595/0.641/0.825	27	2	
25c	EGFP s	0.075/0.125/0.186/0.241/0.556	33	2	Two-way ANOVA, Factor A Construct DF=3 P<0.0001 Factor B Spine type DF =2 P>0.999 Interaction DF=6 P=0.6605
	EGFP m	0.267/0.417/0.522/0.562/0.678			
	EGFP t	0.111/0.205/0.314/0.393/0.489			
	ChETA s	0.071/0.150/0.227/0.286/0.412	36	2	
	ChETA m	0.344/0.422/0.491/0.593/0.688			
	ChETA t	0.125/0.234/0.28/0.323/0.438			
	S-Ch s	0.079/0.178/0.218/0.267/0.378	34	2	

	S-Ch m	0.216/0.425/0.509/ 0.556/0.681			
	S-Ch t	0.191/0.244/0.289/ 0.336/0.448			
	SA-Ch s	0.115/.159/0.209/ 0.243/0.3	27	2	
	SA-Ch m	0.324/0.423/0.514/ 0.577/0.667			
	SA-Ch t	0.133/0.226/0.281/ 0.367/0.467			
26	SA-Ch	0.0531/0.2212/0.3542/ 0.5169/0.7574	52	3	Unpaired Student's t-test two-tailed, P=0.609
	pTurquoise 2	0.0939/0.1921/0.2943/ 0.4946/1.046	54	4	
28	see Figure B				
31a	saline	0.214/0.316/0.425/ 0.488/0.621	22	2	One-way ANOVA, Tukey's comparisons of means S vs BDNF P=7.1E-6 S vs KCl P=8E-6 S vs LTP P=8E-6 S vs AP5 P=0.499
	BDNF	0.428/0.571/0.607/ 0.679/0.813	11	1	
	KCl	0.571/0.62/0.732/ 0.842/0.857	10	1	
	cLTP	0.5/0.621/0.679/ 0.732/0.875	32	2	
	AP5	0.1/0.263/0.333/ 0.425/0.611	23	1	
31b	saline	0.133/0.25/0.333/ 0.385/0.652	33	2	One-way ANOVA, Tukey's comparisons of means S vs BDNF P=9E-6 S vs KCl P=8E-6 S vs LTP P=8E-6 S vs AP5 P=0.005
	BDNF	0.6/0.643/0.68/0.75/ 0.833	6	1	
	KCl	0.6/0.7/0.75/0.769/ 0.857	13	1	
	cLTP	0.434/0.588/0.673/ 0.712/0.818	12	2	
	AP5	0.125/0.167/0.222/0.3/ 0.364	17	1	
33b	A-Ch	0.302/0.426/0.447/ 0.488/0.547	11	2	A-Ch vs. SA.Ch unpaired Student's t-test, two-tailed 2.36365E-21
	SA-Ch	0.677/0.786/0.833/ 0.867/0.935	33	2	
33c	A-Ch	0.863/0.901/0.914/ 0.931/0.953	11	2	A-Ch vs. SA.Ch unpaired Student's t-test, two-tailed 0.97014354
	SA-Ch	0.8/0.891/0.92/0.943/ 0.987	33	2	
34	Saline	NA	28	2	NA
	LTP	NA	20	2	
35	SA-Ch untreated	NA	290 (27 neurons)	5	Linear regression of Log(values) untreated slope 1.892±0.086 df_r=1 df_c=228 (without SA-Ch EI = 0 points)

	SA-Ch stimulated	NA	79 (10 neurons)	2	untreated slope 2.642±0.137 df_n=1 df_d=286 (Log(SA-Ch EI) was assigned value -2 for SA-Ch EI=0 points) stimulated slope 2.290±0.167 df_n=1 df_d=77
36	SA-Ch	NA	468 (71 neurons)	6	Linear regression of Log(values) SA-Ch slope 0.9749±0.03459 df_n=1 df_d=396 (without SA-Ch EI = 0 points) S-Ch slope 0.2150±0.02447 df_n=1 df_d=267
	S-Ch	NA	269 (37 neurons)	3	
37	SA-Ch, MNI+fsk; s	0.365/1.029/3.047/ 4.558/11.35	25	9	One-way ANOVA 2.09832E-14, Bonferroni comparison of means: SA MNI+fsk s vs. SA MNI+fsk n 5.48E-15 SA MNI+fsk s vs. SA fsk s 1.20761E-9 SA MNI+fsk s vs. SA fsk n 1.23116E-10 SA MNI+fsk s vs. S MNI+fsk s 4.81463E-4 SA MNI+fsk s vs. S MNI+fsk n 1.20215E-5 S MNI+fsk s vs. S MNI+fsk n : unpaired Student's t-test, two-tailed, Welch's correction 3.78818E-4
	SA-Ch, MNI+fsk; n	-0.834/.0.46/-0.105 /0.523/2.128	46		
	SA-Ch, fsk; s	-0.69/-0.358/-0.11 /0.417/1.821	15	4	
	SA-Ch, fsk; n	-0.738/-0.35/0.096/ 0.349/1.583	18		
	S-Ch, MNI+fsk; s	0.496/0.728/1.044/ 1.181/1.268	8	3	
	S-Ch, MNI+fsk; n	-0.366/-0.348 /0.072/0.362/ 0.436	6		
38 ΔV/V	MNI+fsk; s	NA	22	8	NA
	MNI+fsk; n	NA	24		
	MNI+fsk+ anys; s	NA	15	4	
	MNI+fsk+ anys; n	NA	21		
	MNI; s	NA	11	4	
	MNI; n	NA	8		
38 ΔCh/ Ch	MNI+fsk; s	NA	18	6	NA
	MNI+fsk; n	NA	24		
	MNI+fsk+ anys; s	NA	15	4	

	MNI+fsk+ anys; n	NA	21		
	MNI; s	NA	8	3	
	MNI; n	NA	8		
40b	ACSF	-6.563/261.088/ 446.831/744.326/ 1018.398	21	7	Kruskall-Wallis test of one-way ANOVA, Dunn's test ACSF vs. ACSF no stim 0.0036 ACSF vs. VGCC inh 0.0003 ACSF vs. VGCC inh no stim 0.0064 ACSF vs. TTX >0.999 TTX vs. TTX no stim 0.0053
	ACSF no stim	-255.74/-185.019/ -8.183 /119.138/ 149.746	8	3	
	VGCC inh	-91.493/-19.504 /57.271/82.74/117.5	17	4	
	VGCC inh no stim	-368.323/-210.356 /53.643/103.581/ 152.094	8	2	
	TTX	-26.478/214.382/ 670.663/889.896/ 1154.409	17	4	
	TTX no stim	-243.011/-147.721/ -116.593/267.253/ 282.191	7	3	
40c	SA-Ch spine	86.987/200.365/690.2 25/1139.499/2501.239	10	4	Paired Student's t-test, two-tailed SA-Ch spine vs. dendrite t=3.686 df=9 P=0.005 ChETA spine vs. dendrite t=0.4454 df=10 P=0.6655
	SA-Ch dendrite	-205.586/-38.087/ -4.111/63.192/261.866			
	ChETA spine	216.865/242.926/ 534.5/1236/1887.415	11	4	
	ChETA dendrite	231.715/400.722/ 624.056/883.32/ 1391.364			
41	pCherry spont	181/1578/2638/4670/7 494	29	2	Kruskal-Wallis test, Dunn's comparison SA-Ch evoked vs. pCherry spont P<0.001 SA-Ch spont vs. pCherry spont P>0.999
	SA-Ch evoked	-96.66/224/435.9/ 1072/2423	46	7	
	SA-Ch spont	641.3/1163/2086/3970 /7082	21	3	
42	EGFP light	45.792/1806.92/2951. 662/4627.827/ 21196.312	364	2	One-way ANOVA, Bonferroni comparison of means SA-Ch light Ch^+ vs. EGFP light 2.63728E-143 SA-Ch light Ch^+ vs. EGFP dark 2.10596E-140
	EGFP dark	53.092/1747.77/3088. 081/4913.416/ 27877.427	347	2	
	SA-Ch light Ch+	34.134/5676.424/9672 .529/15828.503/ 91633.554	1051	2	

	SA-Ch light Ch-	-111.551/1931.315/ 3200.99/4871.958/ 27607.742	539		SA-Ch light Ch^+ vs. SA-Ch light Ch^- 2.39868E-182 SA-Ch light Ch^+ vs. SA-Ch dark Ch^+ 3.53488E-205 SA-Ch light Ch^+ vs. SA-Ch dark Ch^- 2.05879E-186 SA-Ch light Ch^+ vs. ChETA light 2.42246E-104 SA-Ch light Ch^+ vs. ChETA dark 6.02358E-233 SA-Ch light Ch- vs. EGFP light >0.999 SA-Ch dark Ch^+ vs. EGFP dark >0.999 ChETA light vs. ChETA dark 3.77679E-34
	SA-Ch dark Ch+	-5.994/2007.332/ 3432.829/5711.051/ 23357.363	751	2	
	SA-Ch dark Ch-	21.232/2049.816/3319 .291/5116.423/ 19137.313	557		
	ChETA light	530.912/4155.527/628 5.748/9236.164/ 36990.65	1002	2	
	ChETA dark	10.808/2088.084/3329 .345/5109.629/ 20177.826	890	2	
43	EGFP light	NA	5	2	One-way ANOVA, Bonferroni comparison of means SA-Ch light vs. EGFP light 1.13809E-5 SA-Ch light vs. NT light 3.19138E-5 SA-Ch light vs. SA-Ch dark 1.716E-4
	NT dark	NA	7	2	
	SA-Ch dark	NA	4	2	
	SA-Ch light	NA	5	2	
47c	SA-Ch	NA	24	4	Two-way ANOVA Factor A construct DF=1 P<0.0001 Factor B distance DF=64 P<0.0001
	Thy1-ChR2	NA	44	2	
48	$Cherry^+$	50/53.5/67/80/120	9	5	Mann-Whitey test, two tailed P=0.5163
	$Cherry^-$	30/51/78/87/112	7	4	
51	CA1 hc	0.0476/0.1277/0.1702/ 0.2167/0.573	93	3	Unpaired Student's t-test, two-tailed, Welch's correction CA1 hc vs. CA1 cnt 8.06341E-13 DG hc vs. DG cnt 0.02098
	CA1 cnt	0.037/0.2055/0.3107/ 0.48/0.8529	111	3	
	DG hc	0.037/0.139/0.2623/ 0.3869/0.6415	52	3	
	DG cnt	0.0588/0.1346/0.2705/ 0.5636/0.9074	58	3	
53-54	CA1 hc d_{PP}	0.214/0.688/0.999/1.7 11/32.181	1172	3	Kruskal-Wallis test, Dunn's comparisons mean rank differences: CA1 hc d_{PP} vs. CA1 hc d_{PP} shuffled -2875 CA1 hc d_{PNP} vs. CA1 hc d_{PNP} shuffled 1711 CA1 cnt d_{PP} vs. CA1 cnt d_{PP} shuffled -8137 CA1 cnt d_{PNP} vs. CA1 cnt d_{PNP} shuffled 9785
	CA1 hc d_{PNP}	0.329/0.955/1.236/1.6 08/8.747	1172		
	CA1 cnt d_{PP}	0.214/0.688/0.906/1.1 79/15.7	3474	3	
	CA1 cnt d_{PNP}	0.392/1.179/1.596/2.1 88/11.2	3474		

	DG hc d_{PP}	0.151/0.755/1.068/1.604/26.6	1211	3	DG hc d_{PP} vs. DG hc d_{PP} shuffled -2796 DG hc d_{PNP} vs. DG hc d_{PNP} shuffled 2244 DG cnt d_{PP} vs. DG cnt d_{PP} shuffled -9048 DG cnt d_{PNP} vs. DG cnt d_{PNP} shuffled 4923
	DG hc d_{PNP}	0.338/1.117/1.546/2.218/28.03	1211		
	DG cnt d_{PP}	0.302/0.755/0.967/1.281/19.54	1886	3	
	DG cnt d_{PNP}	0.338/1.478/2.092/3.276/25.91	1886		
55	CA1 hc	NA	91	4	NA
	CA1 cnt	NA	108	3	
	DG hc	NA	49	4	
	DG cnt	NA	53	3	
57	CA1 hc	1/1/2/3/25	630	4	Kruskal-Wallis test, Dunn's comparisons mean rank differences CA1 hc vs. CA1 cnt -360 DG hc vs. DG cnt -275.9
	CA1 cnt	1/2/3/6/29	859	3	
	DG hc	1/1/2/4/26	334	4	
	DG cnt	1/2/3/6/29	450	3	
61	DG hc	NA	31	3	NA
	DG cnt	NA	30	3	
63	DG hc	NA	155	3	ANOVA on model (df=1,218), Prob>F =0.03825
	DG cnt	NA	220	3	
64	CA1 hc	0/0.13/0.297/0.527/1.822	93	4	Kruskal-Wallis test, Dunn's comparisons mean rank differences CA1 hc vs. DG hc -28.21 CA1 cnt vs. DG cnt – 52.6
	CA1 cnt	0.001/0.178/0.412/0.587/1.257	111	3	
	DG hc	0.038/0.196/0.42/0.643/1.288	52	4	
	DG cnt	0.015/0.415/0.6/0.736/1.19	58	3	

Appendix C

Scripts in R used in this thesis

C.1 Distances between potentiated spines (d_{PP} and d_{PNP})

Input data is provided as tabulated file as follows

```
Type    Slice   X       Y
3       108     16      20      #SA-Ch-
3       108     21      16      #SA-Ch-
3       109     32      24      #SA-Ch-
4       109     41      30      #SA-Ch+
4       109     42      36      #SA-Ch+
4       109     51      34      #SA-Ch+
3       110     10      5       #SA-Ch-
3       110     9       12      #SA-Ch-
3       110     20      11      #SA-Ch-
3       110     19      13      #SA-Ch-
3       110     11      20      #SA-Ch-
3       110     8       18      #SA-Ch-
...

in_filepath="C:/XXX.txt"
                                        #input data
out_filepath="C:/YYY.csv"
                                       #output data
spinedata= read.table(in_filepath, header= TRUE)
                        #reading data from the file
spinedata=transform(spinedata,
X=X*0.378,Y=Y*0.378,Slice=Slice*0.25)
                  #scaling the values by pizel size

dis=function(x,y){
   #distance function [coordinates of two spines]
```

```
      d=sqrt((x[1]-y[1])^2+(x[2]-y[2])^2+(x[3]-
y[3])^2)
          #eucledean distance between two spines,
                        (x1,x2,x3) and (y1,y2,y3)
return (d)}
         #function returns the eucledean distance

spine_p=which(spinedata$Type %in% 4)
                           #ID of potentiated spines
spine_np=which(spinedata$Type %in% 3)
                     #ID of non-potentiated spines
near_neigh_p=c()
near_neigh_np=c()

for (i in spine_p){
                       #loop for potentiated spines
    neigh_dis_p=c()
    for (j in spine_p){
   #loop considering all potentiated spines other
                                        than itself
          if (i!=j){

neigh_dis_p=c(neigh_dis_p,dis(spinedata[i,c(2:4)
],spinedata[j,c(2:4)]))}}

  #calculating distance to all potentiated spines
   other than itself and adding the values to the
                       potentiated neighbour list
near_neigh_p=c(near_neigh_p,min(neigh_dis_p))
  #takes the min value and adds it to the nearest
                       potentiated neighbour list
      neigh_dis_np=c()
      for (k in spine_np){
     #loop considering all non potentiated spines

neigh_dis_np=c(neigh_dis_np,dis(spinedata[i,c(2:
4)],spinedata[k,c(2:4)]))}
```

```
     #calculating distance to all non potentiated
          spines and adding the values to the non
               potentiated neighbour list
       near_neigh_np=c(near_neigh_np,min(neigh_di
s_np))}
                                  #calculating the
    minumum of the distances and adding it to the
           nearest non potentiated neighbour list

out=data.frame(near_neigh_p,near_neigh_np)
print (out)

write.table
(out,file=out_filepath,row.names=FALSE,col.names
=c("near_neigh_pot","near_neigh_non_pot"),sep=",
")
                          #writing the output data
```

C.2 Distances between potentiated spines (d_{PP} and d_{PNP}) after random shuffling

```
in_filepath="C:/XXX.txt"
                               #input data file_path
spinedata= read.table(in_filepath, header= TRUE)
                       #reading data from the file
spinedata=transform(spinedata,
X=X*0.378,Y=Y*0.378,Slice=Slice*0.25)
                                      #pixel size

dis=function(x,y){
       d=sqrt((x[1]-y[1])^2+(x[2]-y[2])^2+(x[3]-
       y[3])^2)
       return (d)}
         #function returns the eucledean distance

neigh=function(spinedata){
```

```
spine_p=which(spinedata$Type %in% 4)
spine_np=which(spinedata$Type %in% 3)
near_neigh_p=c()
near_neigh_np=c()

for (i in spine_p){
    for (j in spine_p){
           if (i!=j){

neigh_dis_p=c(neigh_dis_p,dis(spinedata[i,c(2:4)
],spinedata[j,c(2:4)]))}}

       near_neigh_p=c(near_neigh_p,min(neigh_dis_
p))

       neigh_dis_np=c()
       for (k in spine_np){

neigh_dis_np=c(neigh_dis_np,dis(spinedata[i,c(2:
4)],spinedata[k,c(2:4)]))}

       near_neigh_np=c(near_neigh_np,min(neigh_di
s_np))}

       return(data.frame(near_neigh_p,near_neigh_
np))}
                        #nearest neighbour function


plot.new()
par(mfrow=c(1,5))
for (m in c(1:5)){
   #loop that shuffles the spine identity 5 times
    Type=sample(spinedata$Type)
                      #shuffling the spine identity

spine_shuf=data.frame(Type,spinedata[,c(2:5)])
```

```
        out_filepath=sprintf("C:/YYYshuf.csv", m)
                                #output data file_path
        out=neigh(spine_shuf)
                                 #calling the function
                                          print (out)
    write.table
(out,file=out_filepath,row.names=FALSE,col.names
=c("near_neigh_pot","near_neigh_non_pot"),sep=",
")
                                          #writing the
                                         output data (
```

C.3 Cluster dimension

Input data is provided as tabulated file as follows

```
Type    Slice   X       Y
3       108     16      20              #SA-Ch-
3       108     21      16              #SA-Ch-
3       109     32      24              #SA-Ch-
4       109     41      30              #SA-Ch+
4       109     42      36              #SA-Ch+
4       109     51      34              #SA-Ch+
3       110     10      5               #SA-Ch-
3       110     9       12              #SA-Ch-
3       110     20      11              #SA-Ch-
3       110     19      13              #SA-Ch-
3       110     11      20              #SA-Ch-
3       110     8       18              #SA-Ch-
...


in_filepath="C:/XXX.txt"
                                  #input data file_path
out_filepath="C:/YYY.txt"
                                #output data file_path
spinedata= read.table(in_filepath, header= TRUE)
                                          #reading data
```

```
spinedata=transform(spinedata,
X=X*0.378,Y=Y*0.378,Slice=Slice*0.25)
                #scaling the values by pizel size
spine_p=spinedata[which(spinedata$Type %in%
4),c(2:4)]
                        #potentiated spines subset
library(rgl)
Plot=function(spines,ncolor){
    rgl.open()
       rgl.bg(color = "white")
       rgl.spheres(spines$X, spines$Y,
spines$Slice, r=0.3, color = ncolor)
       axes3d(edges='bbox', labels= TRUE, tick=
TRUE, nticks=5, box= FALSE, expand=2)
       text3d(spines$X+1,spines$Y+1,spines$Slice+
1,text=rownames(spines))}
                    #display the 3dplot of spines

Hier=function(spines){
       #hierarchical clustering using coordinates
    dis=dist(spines, method='euclidean')
                        #euclidean distance matrix
    fit_hclust=hclust(dis, method="single")
                               #create a dendogram
    plot(fit_hclust)
                                #display dendogram
       groups= cutree(fit_hclust, h=2)
           #clustering interspine threshold = 2µm
       print("Hierarchical_Agglomerative")
       print(groups)
            #display the spines for each clusters
       Plot(spines,groups)
                              #display the 3d plot
       freq_tab=data.frame(table(groups))
                    #cluter ID and no.of elements
       return (freq_tab$Freq)}
       #return the no.of elements in the clusters

clust_freq= Hier(spine_p)
```

```
write.table(clust_freq,file=out_filepath,col.nam
e="clust_freq",row.names=F)
                    #write the output data to file
```

C.4 Cluster dimension in the DG vs X-coordinate

```
in_filepath="C:/XXX.txt"
                                #input data file_path
out_filepath="C:/YYY.txt"
                               #output data file_path
spinedata= read.table(in_filepath, header= TRUE)
                                   #reading data
spinedata=transform(spinedata,
X=X*0.378,Y=Y*0.378,Slice=Slice*0.25)
                 #scaling the values by pizel size
spine_p=spinedata[which(spinedata$Type %in%
4),c(2:4)]
                          #potentiated spines subset

Hier=function(spines){
                             #hierarchical clustering
    dis=dist(spines, method='euclidean')
                           #euclidean distance matrix
    fit_hclust=hclust(dis, method="single")
                              #creating a dendogram
       groups= cutree(fit_hclust, h=2)
           #clustering interspine threshold = 2µm
       return (data.frame(groups))}
      #return spine ID and the cluster it belongs

groups= Hier(spine_p)
                    #clustering potentiated spines
clus=groups[,1]
spine_p_n=data.frame(spine_p,clus)
       #vector with potentiated spine coordinates
                               and the cluster number
freq_tab=data.frame(table(groups))
```

```
    #table containing the cluter number and no.of
                                        elements in it
dimension=freq_tab$Freq
                    #no.of spines in each cluster
xmean=c()
ymean=c()
zmean=c()
x_dis=c()
for (i in (1:max(spine_p_n$clus))){
         subs=subset(spine_p_n,spine_p_n$clus==i)
              #coordinates of spines in a cluster
         xmean=c(xmean,mean(subs$X))
         ymean=c(ymean,mean(subs$Y))
         zmean=c(zmean,mean(subs$Slice))
              #cluster centroid x,y,z-coordinates
         x_dis=c(x_dis,max(dist(subs$X)))
                              #cluster x-extension
}

x_dis=ifelse(x_dis=='-Inf','Not enough
data',x_dis)
data_out=data.frame(xmean,ymean,zmean,dimension,
x_dis)
     #output data - cluster, centroid, dimension,
                                          extension
print (data_out)
write.table
(data_out,file=out_filepath,row.names=TRUE,col.n
ames=NA,sep=",")
                    #write the output data to file
```

C.5 Probability of i-th spine to be potentiated

Input data is a set of strings each corresponding to a dendrite (d1, d2 etc) in a slice, where 1=potentiated and

0=non potentiated. Spines are ordered moving unidirectionally along the dendrite.

```
       1       2       3       4       5       6       7 …
d1     0       0       1       1       0       1       1 …
d2     1       1       1       0       1       1       0 …
d3     0       1       0       0       0       0       1 …
...
```

```
spinedata= read.table("XXX.txt", sep="\t")
                                #input data file_path
r=nrow(spinedata)
             #number of dendrites in the slice +1
n=20
                                #number of neighbours
prob_data=c()
nor_prob_data=c()

for (i in (2:r)){
     #loop considering all dendrites in the slice
    print (i-1)

l=length(spinedata[i,][!is.na(spinedata[i,])])
             #number of spines in the dendrite +1
       mat=c()
    for (j in 2:l){
     #loop considering all spines in the dendrite
          if (spinedata[i,j]==1){
         #checks whether the spine is potentiated
              if (j<(l-n)){
   #checks whether the spine have n neighbours on
                                      the right side

mat=c(mat,as.numeric(spinedata[i,c((j+1):(j+n))]
))}
    #adding the string of n right neighbours to a
                                                list
                  if (j>(n+1)){
```

```
   #checks whether the spine have n neighbours on
                                    the left side

mat=c(mat,as.numeric(spinedata[i,c((j-1):(j-
n))]))}}}
     #adding the string of n left neighbours to a
                                              list
       datalist=as.data.frame(matrix(mat,ncol=n,b
yrow=TRUE))
   #convert the list into a matrix with n columns
     NOTE:the i-th column corresponds to the i-th
    neighbour from the potentiated spine in first
                                          position
       print (datalist)
       prob=c()
       for (k in (1:n))
prob[k]=sum(datalist[k])/nrow(datalist)
      # probability of potentiated spines in each
                              column of the matrix
       prob_data=c(prob_data,prob)
    #adds to a list containing the probability of
                                potentiated spines
       nor_prob=prob/((sum(spinedata[i,c(2:l)])-
1)/(l-2))
                      #normalising the probability
       nor_prob_data=c(nor_prob_data,nor_prob)}
        #adds to a list containing the normalised
                probability of potentiated spines

prob_data=as.data.frame(matrix(prob_data,ncol=n,
byrow=TRUE))
        #converting the list into a matrix with n
                                              columns
rownames(prob_data)=sprintf("d%d",1:(r-1))
colnames(prob_data)=sprintf("n%d",1:n)
print (prob_data)

nor_prob_data=as.data.frame(matrix(nor_prob_data
,ncol=n,byrow=TRUE))
```

```
        #converting the list into a matrix with n
                                                columns
rownames(nor_prob_data)=sprintf("d%d",1:(r-1))
colnames(nor_prob_data)=sprintf("n%d",1:n)
print (nor_prob_data)

out_filepath="C:/YYYp.csv"
                              #output data file_path1
out_filepath_n="C:/YYYp_n.csv"
                              #output data file_path2
write.table
(prob_data,file=out_filepath,sep=",",row.names=T
,col.names=NA)
 #writing the output data (probability) to a file
write.table
(nor_prob_data,file=out_filepath_n,sep=",",row.n
ames=T,col.names=NA)
             #writing the output data (normalised
                               probability) to a file
```

C.6 Count potentiated spines

```
spinedata= read.table("C:/XXX.txt", sep="\t")
                                #input data file_path
r=nrow(spinedata)
             #number of dendrites in the slice +1
tot_sp=c()
pot_sp=c()

for (i in (2:r)){
     #loop considering all dendrites in the slice

st=length(spinedata[i,][!is.na(spinedata[i,])])-
1
                 #number of spines in the dendrite
       sp=sum(spinedata[i,c(2:(st+1))])
    #number of potentiated spines in the dendrite
       tot_sp=c(tot_sp,st)
```

```
                        #list with the ID of spines
      pot_sp=c(pot_sp,sp)}
         #list with the ID of potentiated spines

out=data.frame(tot_sp,pot_sp)
print (out)
out_filepath="C:/YYY.csv"
                                                #output
data file_path
write.table
(out,file=out_filepath,row.names=sprintf("d%d",1
:(r-1)),col.names=NA,sep=",")
                           #writing the output data
```

Publications

Part of this thesis was published in Nature Communications as:

Gobbo, F., Marchetti, L., Jacob, A., Pinto, B., Binini, N., Pecoraro Bisogni, F., Alia, C., Luin, S., Caleo, M., Fellin, T., et al. (2017). *Activity-dependent expression of Channelrhodopsin at neuronal synapses*. Nature Communications *8*, 1629.

During the PhD course I took part in parallel projects that were published as:

Gobbo, F., Bonsignore, F., Amodeo, R., Cattaneo, A., and Marchetti, L. (2018). *Site-Specific Direct Labeling of Neurotrophins and Their Receptors: From Biochemistry to Advanced Imaging Applications. In Neurotrophic Factors*, (Springer), pp. 295–314.

Rizzi, C., Tiberi, A., Giustizieri, M., Marrone, M.C., Gobbo, F., Carucci, N.M., Meli, G., Arisi, I., D'Onofrio, M., Marinelli, S., et al. (2018). *NGF steers microglia toward a neuroprotective phenotype*. Glia.

Colla, E., Panattoni, G., Ricci, A., Rizzi, C., Rota, L., Carucci, N., Valvano, V., Gobbo, F., Capsoni, S., Lee, M.K., et al. (2018). *Toxic properties of microsome-associated alpha-synuclein species in mouse primary neurons*. Neurobiology of Disease *111*, 36–47.

De Nadai, T., Marchetti, L., Di Rienzo, C., Calvello, M., Signore, G., Di Matteo, P., Gobbo, F., Turturro, S., Meucci, S., Viegi, A., et al. (2016). *Precursor and mature NGF live tracking: one versus many at a time in the axons*. Scientific Reports *6*, 20272.

These include the following papers in preparation or in submission:

Yan R, Yalinca H, Paoletti F, Gobbo F, Marchetti L, Kuzmanic A, Lamba D, Luigi F, Gervasio F, Konarev PV, Cattaneo A, Pastore A, *The structure of the Pro-domain of mouse proNGF in contact with the NGF domain* (available at bioRxiv https://doi.org/10.1101/333070)

Carucci NM, Testa G, Gobbo F, Galli-Resta L, Capsoni S, Cattaneo A, *Astrocytes sense, and respond to, a reduction of extracellular Nerve Growth Factor levels by a phosphorylation of TrkA in the endoplasmic reticulum* (in preparation)

Marchetti L*, Bonsignore F* Gobbo F*, Amodeo R, Signore G, Calvello MA, Porciani D, Beltram F, Cattaneo A, Luin S. *A lonely dance of p75NTR monomers regulates neurotrophin signalling* (in preparation)
*authors contributed equally

Acknowledgments

I wish to thank all the people that made this work possible by contributing with their work, competence and passion. I am truly grateful to Laura Marchetti for her constant support and help. I wish to thank Bruno Pinto and Laura Cancedda for their invaluable work with in utero electroporation, and Noemi Binini, Federico Pecoraro Bisogni and Tommaso Fellin for the electrophysiology help and useful discussion. Thank you to Ajesh Jacob for the help in R scripts and data analysis. Thank you to Claudia Alia and Matteo Caleo for the support during in vitro stimulation and Thy1-ChR2 mice. Thanks to Stefano Luin for his help with microscopy during these years. A special thank you to my supervisor, Antonino Cattaneo, for constant mentoring and useful discussion.

We thank Stefan Kindler, Antonella Riccio, Alessandro Marcello, Daniel Choquet, Georg Nagel and Karl Deisseroth for providing cDNA clones and constructs. We thank Giovanna Testa (Scuola Normale Superiore, Pisa) for help with animal perfusion and slice preparation for IF. I wish to thank Marco Mainardi (Scuola Normale Superiore, Pisa), for getting involved in the project and performing joint experiments in extending SynActive, providing invaluable skills for its application. We thank Caterina

Rizzi and Nicola Maria Carucci (Scuola Normale Superiore, Pisa) for the help with cortex and hippocampus dissections.

I would also like to thank our current collaborators for the useful discussion and the amazing experiments we are conducting. Thanks to the precious work by Bruno Pinto and Laura Cancedda at the Istituto Italiano di Tecnologia in Genova we are mapping potentiated synapses in the various stages of memory acquitition (encoding, maturation and recall). With Erez Geron and Wenbiao Gan at the Skyrball Institute at New York University we are applying the SA-reporters to the motor cortex for live of potentiation with two-photon imaging. In collaboration with Tony Kelly and Heinz Beck at University of Bonn Medical Center in Germany, along with Bruno Pinto and Laura Cancedda, we are further studying the distribution of potentiated synapses in the demtate gyrus. Last, with Alessandro Ori at Franz-Lipmann Institut in Jena (Germany), Cinzia Caterino and Alessandro Cellerino (Scuola Normale Superiore, Pisa) and Lorena Zentilin at ICGEB in Trieste, we are applying the SynActive tools to profile the proteome of potentiated synapses.

⁘ ⁘ ⁘

I would like to thank all the people that are part of my life and support me everyday with their love and help, even from the other side of the world. Thank you to Federico, Viola, Elisabetta, Raffaella, Enrico, Marco, Luca, Andrea, Marco, Vincenzo, Mattia,

Federico, Mariah, Luca, Pierpaolo, Silvia, Francesca, Martina, Annachiara, Raffaele, Bruno, Rosy, Fulvio, Giovanna, Marco, Caterina, Barbara, Laura, Melissa, Paola, Gianmarco, Cecilia, Frenk, Sebastian, Marco, David, Alessandra, Gemma, and all the people that supported me during these years.

Thank you to my wonderful parents, Anny and Enzo, and to my brother Davide for always supporting me. Wherever my life will take me, I know I will always be able to call it home.

[this page intentionally left blank]